UILU-ENG-81-2014

CIVIL ENGINEERING STUDIES
STRUCTURAL RESEARCH SERIES NO. 495
Illinois Cooperative Highway and Transportation Research
Program Series No. 192

TIME-DEPENDENT DEFORMATIONS IN SEGMENTAL PRESTRESSED CONCRETE BRIDGES

By
VERNON MARSHALL
WILLIAM L. GAMBLE

Issued as Documentation of Progress Report on
the Study of
Time-Dependent Behavior of Segmental
Cantilever Concrete Bridges
Project IHR-307
Illinois Cooperative Highway and Transportation Research Program
Phase 3

Conducted by
THE STRUCTURAL RESEARCH LABORATORY
DEPARTMENT OF CIVIL ENGINEERING
ENGINEERING EXPERIMENT STATION
UNIVERSITY OF ILLINOIS
AT URBANA-CHAMPAIGN

in cooperation with
THE PORTLAND CEMENT ASSOCIATION
SKOKIE, ILLINOIS
and
THE STATE OF ILLINOIS
DEPARTMENT OF TRANSPORTATION
and
THE U.S. DEPARTMENT OF TRANSPORTATION
FEDERAL HIGHWAY ADMINISTRATION

UNIVERSITY OF ILLINOIS
AT URBANA-CHAMPAIGN
URBANA, ILLINOIS
OCTOBER 1981

TECHNICAL REPORT STANDARD TITLE PAGE

1. Report No.	2. Government Accession No.	3. Recipient's Catalog No.
FHWA/IL/UI-192		

4. Title and Subtitle	5. Report Date
Time-Dependent Deformations in Segmental Prestressed Concrete Bridges	October 1981
	6. Performing Organization Code

7. Author(s)	8. Performing Organization Report No.
Vernon Marshall William L. Gamble	UILU-ENG-81-2014 SRS-495

9. Performing Organization Name and Address	10. Work Unit No.
University of Illinois at Urbana-Champaign Engineering Experiment Station Department of Civil Engineering Urbana, Illinois 61801	11. Contract or Grant No. IHR-307
	13. Type of Report and Period Covered Interim June 1978-January 1981
12. Sponsoring Agency Name and Address Illinois Department of Transportation Bureau of Materials and Physical Research 126 East Ash Street Springfield, Illinois 62706	14. Sponsoring Agency Code

15. Supplementary Notes

Study was conducted for the Portland Cement Association and was sponsored by the Illinois Department of Transportation in cooperation with the U.S. Department of Transportation, Federal Highway Administration.

16. Abstract

A rational analytical procedure for estimating the time-dependent behavior of segmental prestressed concrete bridges built by the cantilever method is presented. It is based on a step-by-step numerical procedure which attempts to account for most of the important parameters that influence the time-dependent behavior of such structures, and the procedure was incorporated in a computer program.

Comparisons were made between computed strains and those measured in the Kishwaukee River Bridge at Rockford, Illinois. Good agreement between the two sets of values was obtained as long as the computations were based on the creep properties of samples of concrete from the bridge, for the particular case where the creep specimens were stored outdoors in the same environment that the structure experienced.

In this particular structure shrinkage strains in the concrete dominated the time-dependent response. Creep deformations were relatively small because most of the precast segments were old when they were erected, and relaxation of steel stress was small because of the type of post-tensioned bar reinforcement used in the structure.

17. Key Words	18. Distribution Statement
Prestressed concrete, Segmental bridges, Time-dependent effects, Creep, Shrinkage, Relaxation	No restrictions. This document is available to the public through the National Technical Information Service, Springfield, Virginia 22161

19. Security Classif. (of this report)	20. Security Classif. (of this page)	21. No. of Pages	22. Price
Unclassified	Unclassified	251	

Form DOT F 1700.7 (8-69)

TABLE OF CONTENTS

Page

LIST OF TABLES

LIST OF FIGURES

Figure | Page

1. INTRODUCTION

1.1 General Remarks

For major highway bridge structures the current trend is to move toward the use of longer spans. Some of the more important reasons that may be quoted are considerations related to safety, economy, function, and aesthetics of the structure. Because of the upper limits that are imposed on the lengths in which precast prestressed girders can be supplied (normally in the 100 ft range), new construction techniques had to be developed. One of the solutions to this problem has been the development of various segmental construction procedures, with the cantilever construction method being widely accepted as the preferred method. In segmental cantilevered bridge construction, which is primarily the progressive construction of a series of double cantilevers from short segments, the adjacent cantilevers may either be made continuous or hinged at midspan. Because of the excessive deflections sometimes exhibited by structures where adjacent double cantilevers are connected by hinges, the tendency has lately been to make cantilevers continuous by providing suitable connections and prestressing details.

Cantilever construction techniques have been used for a very long time by builders of wooden bridges. Furthermore, cantilever construction procedures and prefabrication techniques have been used by designers of long-span steel bridges since the turn of the century. It was in 1948 that Freyssinet made use of a combination of a cantilever construction technique and precast segments to construct a prestressed concrete bridge across the Marne River near Paris. In Germany the construction of the Worms Bridge in 1952 resulted in the acceptance of the cast-in-place cantilever construction procedure in that country (46).* Ever since that time period, the development of segmental prestressed bridge construction procedures has been vigorously pursued in Western Europe. In the U.S.A. the first segmental prestressed

---

* Numbers in parentheses refer to entries in the List of References.

box girder bridge was constructed in 1973 at Corpus Christi, Texas (27). That bridge was constructed by the cantilever method used in conjunction with precast segments. A cast-in-place segmental prestressed concrete bridge was constructed across the Pine Valley, near San Diego, in 1974. Subsequently a number of segmental prestressed concrete bridges have been built in the U.S.A.

One of the major problems associated with prestressed concrete structures is the time-dependent loss of prestressing force due to creep and shrinkage of the concrete as well as relaxation of the prestressing steel reinforcement. These phenomena can lead to time-dependent deformations greatly in excess of the initial instantaneous elastic deformation of the structure. It should thus be clear that for long span prestressed concrete bridges built by the segmental cantilevered construction procedure, these deformations may be very important, especially when consideration is given to the fact that for these bridges the ends of adjacent cantilevers should meet at the correct grade and alignment. Furthermore, excessive deflection of such structures can lead to violations of certain serviceability requirements as well as an objectionable structure from an aesthetic point of view.

At the present time the Portland Cement Association is conducting an experimental research program aimed at recording time-dependent concrete strains as well as deflections on the Kishwaukee River Bridge near Rockford, Illinois. The bridge is a continuous five span structure built by the segmental cantilevered method. The segments were precast. In addition to monitoring the deflections and concrete strains of the bridge itself, the shrinkage and creep properties of the concrete used in the bridge are being determined on specimens stored outdoors in Skokie, Illinois, as well as on laboratory stored specimens. The availability of this experimental data in addition to a detailed description of the construction sequence of the bridge therefore provided an excellent opportunity to conduct an analytical study of the time-dependent behavior of the Kishwaukee River Bridge.

1.2 Previous Work

The publications that deal with the topic of the long-time behavior of segmentally constructed prestressed concrete bridges are limited in number. In what follows most of the available literature that has a direct bearing on this topic is briefly discussed. Furthermore, some of the more important publications that deal with the design and construction of segmentally constructed prestressed concrete bridges are mentioned.

In the literature several state of the art papers exist. Of special interest are two publications by Muller (46,47) and one by Libby (41). Construction techniques as well as design considerations were discussed. What is of interest, however, was the emphasis on the time-dependent redistribution of longitudinal bending moments due to the time-dependent properties of concrete and steel, as a design consideration. A report by Lacey and Breen (38) summarized the state of the art of prestressed segmental long-span bridges as of 1969, and in a further report by Ballinger et al. (5) a state of the art survey covering segmental prestressed concrete bridges actually constructed in Western Europe, was given. The latter report covered design and construction practices up to the year 1977.

In his book on the limit state design of prestressed concrete structures, Guyon (25) described and discussed the design considerations involved in the design of cantilevered prestressed concrete bridges built in segments. A design example was given.

The long-time behavior of four prestressed concrete bridges, built by the cantilever method in conjunction with a cast-in-situ technique, was studied by Keijer (34). For all these bridges, adjacent cantilevers were connected at midspan by means of hinges. Comparison of the results of an extensive parametric study with measurements of the vertical deflections of these structures yielded the following conclusion: Concrete creep had a dominating influence on the deformations of this type of bridge. Consequently the creep coefficient as well as the functional form expressing the creep-time relationship was of prime importance in predicting the long-time

deformations. A logarithmic creep-time relationship yielded satisfactory agreement between the calculated and the observed deflections.

Measurements of creep and shrinkage strains as well as deflections were made on a large number of prestressed concrete bridges in Japan (37). The structures thus studied included several bridges built by the cantilever method. These results were used to derive the final value of shrinkage strain as well as the value of the creep coefficient.

The shrinkage and creep strains of a prestressed concrete cantilever bridge over the Oise River, in France, was studied by Belmain and Le Bourdelles (7). According to Danon (12) that work was primarily aimed at assessing the accuracy of the recommendations of the C.E.B.(11) and the French Code in predicting creep and shrinkage.

Ghali et al. (21) presented a step-by-step procedure to calculate prestress loss and deformations in multistage prestressed members. The procedure accounted for the effect of elastic and creep recoveries on the prestress loss, as well as the reduction of intrinsic relaxation of the prestressing steel reinforcement due to varying strain. It was, furthermore, incorporated in a computer program (20).

A comprehensive research program aimed at studying various topics related to segmentally erected precast prestressed concrete box girder bridges was conducted at the University of Texas at Austin (9,10,33,38, 39). During the course of that work a state of the art survey was published, criteria for design procedures were developed and optimization of the cross-section was studied, a computer program that incorporated an incremental analysis procedure used in conjunction with the Finite Segment Method was developed, a scale model of the Corpus Christie Bridge was built and tested, and various construction problems associated with these bridges were investigated. In that work, however, the time-dependent behavior of this type of structure was not studied.

An in-depth study of the various parameters that affect the time-dependent behavior of prestressed concrete bridges built by the cantilever method was conducted by Danon and Gamble (12). That study dealt only with the structural behavior of the cantilevers, which make up this type of

structure, up to the stage just prior to the connection of adjacent cantilevers. During the course of that work a computer program capable of predicting the time-dependent stresses, strains, loss of prestress and deflections of a segmentally constructed prestressed cantilever bridge was developed. The creep behavior of concrete subjected to a varying state of stress was predicted both by the method of superposition as well as the rate of creep method. The present investigation was basically a continuation of that work.

A computer program capable of analyzing curved segmentally erected concrete box girder bridges, was developed by van Zyl (58). In that work the time-dependent properties of concrete and steel were accounted for. The creep function was expressed as a Dirichlet series, a form which greatly reduces the bookkeeping effort necessary, when applying the method of superposition to the prediction of concrete creep in an environment where the concrete stress continually varies. The stiffness method was used, in conjunction with skew-ended finite elements with eight degrees of freedom at each of the two end nodes, to perform the structural analysis. A wide range of operations normally encountered in the construction of segmentally erected prestressed concrete bridges were accounted for in the analytical procedure.

A procedure for the analysis of time-dependent effects in prestressed concrete structures constructed in stages was developed and implemented in a computer program by Khalil (36). Special attention was paid to the analysis of prestressed concrete cable-stayed systems. The creep response of concrete was divided into a recoverable component and an irrecoverable component. Non-linear shrinkage strain distributions across the depth of a member were accounted for. Structural concrete members with up to three different concrete layers, each having different time-dependent properties, were included. The overall structural analysis was performed on the basis of the stiffness method used in conjunction with the tangent stiffness method to account for geometric non-linearities.

It should be noted that none of the last three references mentioned above presented extensive comparisons of generated data with experimental data, for the particular case of the time-dependent behavior of segmentally constructed prestressed concrete bridges.

1.3 Object and Scope

The prime objective of this study is to provide a further insight into the time-dependent behavior of segmental post-tensioned box girder bridges built by the cantilever method. The investigation is specifically aimed at those bridges where segments are precast and adjacent cantilevers are made continuous by means of cast in-situ closure segments together with the provision of suitable continuity prestressing tendons.

The scope of the investigation may be divided into two parts:

1. The development of a rational analytical procedure, suitable for computer programming, for the purpose of predicting the time-dependent behavior of continuous segmental post-tensioned bridges built by the cantilever method.
2. A comparison of measured deformations of the Kishwaukee River Bridge with analytically obtained results. The analytically obtained prestressing force, concrete stresses and bending moments are also discussed.

The analytical procedure for estimating the time-dependent behavior of segmental prestressed concrete bridges is based on a step-by-step numerical procedure which attempts to account for most of the important parameters that influence the time-dependent behavior of these structures. The construction history of the structure is also accounted for as accurately as possible by the analytical procedure. This procedure was incorporated in a computer program.

A procedure for estimating the creep of concrete subjected to a varying state of stress is introduced. This procedure is intended primarily

for use when a limited number of experimentally determined specific creep curves are available, and is based on both the rate of creep method and the method of superposition. The method of superposition is used to predict the creep of concrete subjected to a varying state of stress when the concrete material properties are obtained by following the recommendations of the C.E.B. (11).

In order to gauge the effectiveness of the analytical procedure introduced herein, the Kishwaukee River Bridge was analyzed and the results compared with measured deformations of the actual structure. The structure was analyzed using material properties for concrete as experimentally obtained from outdoor stored and laboratory stored specimens as well as those prescribed by the C.E.B. (11). The prestressing force, concrete stresses and bending moments obtained from these analyses are presented and discussed so that some of the characteristics of the time-dependent behavior of the structure considered herein may be illustrated.

Finally, the effects on the time-dependent behavior of the Kishwaukee River Bridge of actual loads applied during the construction of the structure are investigated.

This work was completed as part of the Illinois Cooperative Highway Research Program, Project IHR-307, "Time-Dependent Behavior of Segmental Cantilever Concrete Bridges," by the Department of Civil Engineering, in the Engineering Experiment Station, University of Illinois at Urbana-Champaign. This report was prepared by the University for the Portland Cement Association, and the work was sponsored by the Illinois Department of Transporation in cooperation with the Federal Highway Administration.

2. BASIC MATERIAL PROPERTIES

2.1 Introduction

Any successful structural analysis basically involves the simultaneous satisfaction of the following three requirements:

a) Equations of equilibrium,

b) Compatibility relations and

c) Constitutive relations.

The equations of equilibrium and the compatibility relations do not involve the material properties. The constitutive relations, on the other hand, relate the stresses to strains and are consequently dependent on the material properties. In addition to exhibiting an instantaneous elastic response to applied stress within the working stress range, the material behavior of concrete is also strongly time dependent. Thus, for the overall structural analysis to be successful it is essential that the rheological properties of concrete and steel be estimated reasonably accurately.

The purpose of this section is to present some of the more important factors that influence the time-dependent behavior of the concrete and steel, as well as the procedures used in this study to predict this behavior. It should be emphasized that this description is very brief and that comprehensive reviews of the theories of creep and shrinkage exist in the literature (45,50).

2.2 Creep and Shrinkage of Concrete

2.2.1 General

When a concrete specimen is subjected to a sustained stress, the resulting strain can be divided into the following three components:

a) Instantaneous Elastic Strain: As the stress is applied to the concrete an instantaneous elastic strain will take place. In this case the applied stress is linearly related to the resulting strain by Young's Modulus.

$$f_c = E_c \varepsilon \qquad (2.1)$$

where: f_c = applied stress,
ε = strain and
E_c = Young's Modulus for concrete.

b) Shrinkage Strain: In the absence of temperature variations, shrinkage will be considered as that part of the time-dependent strain that is stress independent.

c) Creep Strain: Creep strain will be considered as that part of the time-dependent strain that is dependent on the applied stress. Specific creep is defined as the creep due to a unit applied stress.

The definitions of shrinkage and creep given above imply that they are additive when they occur simultaneously. Thus, the assumption made here is that shrinkage and creep of concrete are two independent phenomena. This, however, is not correct because they are known to be dependent on each other, the effect of shrinkage on creep being to increase the magnitude of the latter (50). The above approach, however, has proved to be quite satisfactory in the treatment of most practical applications where creep and shrinkage occur simultaneously. It also has the advantage of simplicity.

2.2.2 Factors that Influence Shrinkage and Creep

In order to facilitate the understanding of the time-dependent behavior of a prestressed concrete structure it is necessary to have some understanding of the more important factors that influence the shrinkage and creep behavior of concrete. Neville (50) groups these factors into two broad categories: Intrinsic factors which deal with the actual composition

of the concrete as well as the influence of stress, and environmental factors which account for the state of the environment to which the concrete is exposed. A number of these factors are discussed in the following paragraphs.

1. Influence of the fineness of the cement: Tests conducted by Davis et al. (14) indicate that for normal portland cement, finer cement led to greater values of creep but for low heat portland cement the reverse was true. Furthermore, creep and shrinkage tests on 1:3 concrete with portland cements of differing fineness demonstrated that the finer cement was associated with increased creep and shrinkage strains only at an early age (8). At greater ages the shrinkage and creep strains tended to approximately the same values. In the light of these tests it would seem that it is not entirely correct to associate very fine cement with increased creep.

2. Influence of air entrainment and admixtures: It appears that air entrainment generally tends to increase creep, but in the normal practical range (i.e. air contents below 5 to 6 percent) this influence is of no importance. Shrinkage seems to be essentially unaffected by air entrainment. It is possible that a substantial increase in creep may result when admixtures are used with normal weight aggregate concrete. Data, however, on the influence of admixtures on creep are limited (50).

3. Influence of aggregate: The aggregate content as well as the mineralogical character of the aggregate each have an influence on creep and shrinkage. As the seat of creep is found to be in the cement paste, the effect of the aggregate is to restrain the deformation of the surrounding paste due to shrinkage and creep. Thus, an increase in the aggregate-cement ratio of the concrete will lead to greater restraint against deformation of the paste and subsequently lead to lower values of creep and shrinkage. Mineralogically, it appears that the modulus of elasticity and the porosity of the aggregate are the most important factors that influence creep and shrinkage. Aggregates that have higher values for the modulus of elasticity are able to offer greater restraint to potential creep and shrinkage of the paste. It is possible that an increase of aggregate

porosity can facilitate transfer of moisture within the concrete so that aggregates with higher porosity are associated with greater creep and shrinkage. It should be noted that aggregates with greater porosity tend to have a lower modulus of elasticity, thus providing less mechanical resistance to creep and shrinkage of the paste (44,50,57).

4. Influence of the water-cement ratio: Experimental evidence indicates that specific creep as well as shrinkage are both increased as the water-cement ratio of the concrete is increased (50,51,57). The water content of a mix is controlled by the water-cement ratio and the aggregate-cement ratio. Of the two, it appears that the water-cement ratio has the stronger influence on creep (49).

5. Influence of the size and shape of the specimen: As far as creep is concerned, it is most probably only drying creep that is affected by a variation of the size and shape of the specimen because basic creep remains unaffected by loss of moisture from the concrete and, as such, is independent of the size and shape of the specimen. The volume to surface ratio can be used as a general parameter to describe the influence of the size and shape of the specimen on creep and shrinkage. Creep and shrinkage reduce with an increase in the volume/surface ratio, i.e. as the specimen becomes larger, with creep approaching the value of basic creep for very large specimens. After a period of several weeks after application of the load the rate of creep is the same for specimens of all sizes, so that it appears as if the size and shape of the specimen has its greatest effect for a relatively short period of time immediately following application of the load. Shrinkage is affected to a greater extent than creep by the size and shape of the specimen. Furthermore, the shape of the specimen only has a secondary effect on creep and shrinkage (26,49,51). Anderson et al. (4) reported that the generally accepted concepts of the influence of the size and shape of a member on shrinkage should be applied to very thin members with caution. Very thin members dry out rapidly and consequently exhibit high initial rates of shrinkage. This drying process may be so complete that the hydration process, which accounts for continued shrinkage in larger specimens, is severely hampered or even halted. The net result is

that the ultimate shrinkage which might be expected to develop in these very thin members cannot be attained.

6. Influence of the magnitude of the applied stress: Even though it has been well established that creep is linearly related to the applied stress, there exists some confusion as to the exact value of the upper limit of proportionality. Values of this limit in the range of 30 to 75 percent of the concrete strength have been proposed. Because severe microcracking at the aggregate-paste interface occurs beyond 40 to 60 percent of the concrete strength it seems reasonable to assume that the nonlinear behavior of creep is due to the onset of microcracking. For most practical structures, creep may be considered to be linearly related to stress within the working stress range (1,49). It is of interest to note that the creep behavior of concrete subjected to a tensile stress is about the same as compressive creep (49).

7. Influence of the age at loading: Evidently the age at which the concrete is loaded has an important influence on the magnitude of creep. The effect is to increase creep with smaller ages at loading. For the first few weeks under load the rate of creep is much greater for concretes loaded at an early age than for older concretes. At later ages the rate of creep is apparently independent of the age at loading. The manner in which the age at loading influences creep seems to be related to the manner in which it affects the development of strength and the degree of hydration. For these very reasons, maturity has been found to correlate well with creep. Furthermore, creep becomes more or less independent of the age at loading when conditions are such that the degree of hydration remains constant (49,50,51).

8. Influence of temperature: Tests by England and Ross (17) indicated that the creep of sealed and unsealed specimens was greatly increased as the concrete temperature was increased. In the range of 68-140^{o}F (20-60^{o}C) the effect of temperature on creep was greater than in the range of 212-284^{o}F (100-140^{o}C). Both the sealed and unsealed specimens behaved similarly. Shrinkage was also found to increase with an increase in temperature.

The general pattern of behavior of specimens stored at different temperatures has been found to be the same (48). Furthermore, the relationship between creep and the stress-strength ratio appears to remain linear at elevated temperatures up to at least 205°F (96°C). It should be noted that these observations were made on specimens that simulate mass concrete conditions, so that only basic creep is under consideration here.

Creep is apparently not a monotonic function of temperature and passes a maximum in the vicinity of 160°F (71°C). It should be mentioned that specimens that are heated just before loading are more severely affected by the influence of temperature than specimens that are kept at sustained elevated temperatures for their whole life. When concrete is pre-dried, temperature has a less important influence on creep (50).

9. Influence of relative humidity: The effect of relative humidity on creep and shrinkage is to increase the magnitude of these phenomena as the relative humidity decreases. As far as creep is concerned it should be noted that relative humidity per se is not the influencing factor, but rather the process of drying while under load. This is confirmed by the fact that creep is not affected by relative humidity if the concrete has already reached hygral equilibrium before loading and, furthermore, that creep is dependent on relative humidity when drying occurs while the concrete is loaded. When concrete is drying under load, the ultimate creep as well as the rate of creep will be higher than concrete that remains either wet or dry (49,50). Under conditions where the relative humidity alternates, creep and shrinkage are not similarly influenced. The shrinkage of concrete subjected to changes of relative humidity may be less than that associated with the average value of relative humidity (18). Furthermore, it appears that the reversible moisture movement in concrete subjected to an increase in relative humidity after a period of drying is not associated with an increase in the final value of shrinkage (45). Creep, on the other hand, is increased when the concrete is subjected to an environment where the relative humidity varies. This increase takes place when moisture is either lost or gained (3,49,50).

2.2.3 Prediction of Creep and Shrinkage

As previously mentioned, an essential requirement for a successful structural analysis involves an accurate assessment of the material properties. It therefore becomes necessary to determine the creep and shrinkage properties of the concrete either by conducting actual creep and shrinkage tests (55), or by predicting these properties by making use of some reliable procedure developed for this purpose.

In the development of procedures for the prediction of creep and shrinkage it appears as if there exist two approaches to the solution of this problem. The first approach has been to define the creep and shrinkage in terms of a number of multiplying factors where each of these factors represents the influence on creep and shrinkage of a specific intrinsic or environmental factor relative to some chosen reference state. It should be noted that in these procedures these factors have generally been assumed to be independent of each other. Examples of this type of procedure may be found in References (2), (11), (40) and (50). The other approach has been to make use of rheological models. In some cases the elements included in these models attempt to model the time-dependent behavior of specific components of the concrete. In other cases the rheological elements included in these models simply serve as a vehicle to predict the overall time-dependent behavior of the concrete with no attempt being made to relate them to any particular physical process. Examples of these rheological models may be found in Reference (50).

Since the former approach tends to relate creep and shrinkage to variables that are more convenient to use from an engineering point of view, an example of the first approach was used. Specifically, the procedure outlined by the C.E.B. (11) has been used. In what follows the details of this procedure are given.

2.2.3.1 Prediction of Creep According to the C.E.B. Recommendations

The procedure recommended by the C.E.B. (11) for the prediction of creep is based on linear creep theory which leads to the conclusion that for

a given concrete under constant environmental conditions and subjected to a constant sustained load, the creep strain is linearly related to the instantaneous elastic strain. This assumption is generally true for the range of stress levels encountered in most structures at working conditions. Thus, the following expression is given for creep strain:

$$\varepsilon_{cr} = \frac{f_c}{E_{b28}} \phi_t \qquad (2.2)$$

where: f_c = constant sustained concrete stress,
E_{b28} = secant modulus of elasticity of the concrete at 28 days and
ϕ_t = creep coefficient.

The tangent modulus of elasticity for normal aggregate concretes at any time, may be calculated as follows:

$$E_c(t) = 66\ 000 \sqrt{f'_c(t)} \qquad (2.3)$$

with: $E_c(t)$ and $f'_c(t)$ both in N/cm^2

or $$E_c(t) = 79\ 400 \sqrt{f'_c(t)} \qquad (2.4)$$

with: $E_c(t)$ and $f'_c(t)$ both in psi.

where: $f'_c(t)$ is the cylinder compressive strength at time t. The ratio of compressive strength at an age of t days to the 28 day compressive strength, as recommended by the C.E.B. for normal aggregate concrete, is presented graphically in Figure 2.1.

The secant modulus of elasticity is taken as being 90 percent of the tangent modulus of elasticity.

The creep coefficient reflects the quality of the concrete as well as the envisaged working conditions. It is given as the product of five partial coefficients:

$$\phi_t = K_c K_d K_b K_e K_t \qquad (2.5)$$

Each of these coefficients is presented in the form of a graph.

K_c: K_c depends on the relative humidity and is thus a reflection of the environment. (See Figure 2.2)

K_d: K_d reflects the degree of hardening of the concrete at first loading. The graph can be used to determine K_d as a function of age at loading, if the concrete hardens at an average concrete temperature of 20^oC and also if sufficient protection against excessive loss of moisture has been provided. If hardening takes place at a temperature other than 20^oC the corresponding degree of hardening may be used to determine K_d. (See Figure 2.3) The degree of hardening is calculated from:

$$D = \Sigma\Delta_t(T+10) \qquad (2.6)$$

where: D = degree of hardening

Δ_t = number of days during which hardening has taken place at T^oC.

K_b: K_b expresses the dependence of creep on the composition of the concrete mix and is given as a function of the water/cement ratio as well as the cement content. (See Figure 2.4)

K_e: The dependence of creep on member size is given by the factor K_e. It is expressed as a function of the theoretical thickness, where the theoretical thickness, given by twice the ratio of the cross-sectional area to the perimeter exposed to

the atmosphere, in turn describes the member size and shape. (See Figure 2.5)

K_t: K_t describes the time-dependence of creep. The effect of member size on the rate of creep is reflected here by presenting K_t as a function of the theoretical thickness as well as time. (See Figure 2.6)

2.2.3.2 Prediction of Shrinkage According to the C.E.B. Recommendations

As for the case of creep, the shrinkage of concrete at constant environmental conditions is expressed by the C.E.B. as the product of five multiplying factors, thus:

$$\varepsilon_{sh} = \varepsilon_c K_b K_e K_p K_t \qquad (2.7)$$

K_b and K_t are taken to be the same as for creep. It is, however, important to realize that in the evaluation of K_t for shrinkage, the time is considered to be the elapsed time since the end of curing.

ε_c: This is the basic shrinkage strain and is given as a function of relative humidity. (See Figure 2.7)

K_e: This factor reflects the dependence of shrinkage on the theoretical thickness of the member. (See Figure 2.8)

K_p: K_p takes account of the restraining effect of the longitudianl steel reinforcement on the shrinkage strain. It is given by the following expression:

$$K_p = \frac{100}{100 + np}$$

where: n = 20 with regard to creep and
p = percentage longitudinal steel.

It is of some importance to note here that these expressions for creep and shrinkage apply to environments where the temperature as well as relative humidity remain constant. Under field conditions, however, these conditions are obviously not met, so that it becomes important to use values of relative humidity, for the evaluation of K_c and ε_c, which will somehow reflect the influence of the variable environmental conditions on creep and shrinkage. This problem was addressed by Mossiossian and Gamble (45), who were led to the conclusion that the C.E.B. could yield a reasonable estimate of creep and shrinkage in the field. For field stored specimens, the upper and lower bounds of creep could be estimated by using the minimum monthly average and the annual average values of the relative humidity in the field. Shrinkage could be estimated by using the average annual relative humidity in the field. For shrinkage it must be realized that seasonal fluctuations, actually encountered in the field, cannot be predicted by the C.E.B. procedure. Hernandez and Gamble (28) pursued this matter further and established that for structures in the Midwest, the expected creep and shrinkage in the field could be estimated rather well by using a combination of creep at 50 percent relative humidity and shrinkage at 80 percent relative humidity in conjunction with the C.E.B. procedure. Comparisons of creep and shrinkage data generated by the above approach with data obtained from specimens stored outdoors in Skokie, Ill. are made in Figures 2.9 and 2.10. The agreements are better for creep than for shrinkage, and the great importance of the variable environment on the shrinkage is readily apparent.

2.3 Relaxation of Steel

Initially, prestressing steel responds to an imposed strain as a linearly elastic material. However, if this strain level is maintained at a constant value a time-dependent loss of stress will occur. This

phenomenon is defined as relaxation. Relaxation and creep are intimately related to the extent that they may be regarded as two consequences of the same phenomenon under different conditions. Even though the prestressing reinforcement in a prestressed concrete beam is subjected to a continuously changing state of strain, it has generally been acknowledged that these conditions approach the conditions to be found in a relaxation test rather than those to be found in a creep test. The ratio of initial stress to yield stress, the type of steel, temperature, and time each appear to have a major effect on the magnitude of the relaxation loss to be expected.

The expression developed by Magura, Sozen and Siess (42) may be used to determine the loss of prestressing force due to relaxation. This expression is based on data that originated from a collection of 501 relaxation tests on cold-drawn wire. It is given by:

$$\frac{f_s(t)}{f_{si}} = 1 - \frac{\log t}{10}\left(\frac{f_{si}}{f_y} - 0.55\right) \qquad (2.8)$$

where: $f_s(t)$ = steel stress at time t,
f_{si} = initial steel stress immediately after stressing,
f_y = yield stress of steel, measured at an offset strain of 0.001,
t = time, in hours, after stressing and
log t = logarithm of time to the base 10.

In the development of this expression the ratio of initial stress to yield stress was of prime importance. It may also be seen that this expression obviously only applies to initial stress/yield stress ratios larger than 0.55, which is reasonable, because below this value the expected relaxation loss is very small and of negligible importance in the practical sense. The effect of the type of steel was not explicitly accounted for in this expression. It was, however, argued by the authors

that part of this effect was implicit in the effect of the initial stress/yield stress ratio. The temperature was excluded as a parameter because for temperature variations encountered under normal working conditions this parameter is of minor importance. It should be pointed out that if the temperature variations are large, the effect on relaxation may be of significant proportions.

For the case that the prestressing strand exhibits an exceptionally low relaxation loss, Eq. 2.8 will tend to overestimate this loss. It has been found (12,18) that for such cases the relaxation losses may successfully be estimated by modifying Eq. 2.8 as follows:

$$\frac{f_s(t)}{f_{si}} = 1 - \frac{\log t}{c}\left(\frac{f_{si}}{f_y} - 0.55\right) \qquad (2.9)$$

where: c = relaxation constant, to be experimentally determined.

Because Dywidag bars, the prestressing reinforcement used in the structure under consideration in this investigation, exhibit rather low relaxation losses, the approach outlined above was followed. By suitably adjusting the value of the relaxation constant, Eq. 2.9 could be fitted to available experimental data (52). It was found that for c = 36, Eq. 2.9 would closely estimate the relaxation losses to be expected for a Dywidag bar. (See Figure 2.11) It should be noted that this value applies to the case where $f_{si}/f_y = 0.875$. The appropriate value for the relaxation constant was found to be c = 56 for $f_{si}/f_y = 0.75$. It would thus appear that the relaxation constant, as defined above, is dependent on the initial stress/yield stress ratio in the case of Dywidag bars. The value of c = 36 was used in conjunction with Eq. 2.9 throughout this study because the bars were initially stressed to a level where $f_{si}/f_y = 0.91$, in the structure that was investigated.

3. ANALYTICAL CONSIDERATIONS

3.1 Introduction

During the lifetime of a prestressed concrete structure the prestressing force continually varies due to the combined effects of creep and shrinkage of the concrete as well as relaxation of the steel. As a result, the concrete stress and steel strain may be expected to vary continually in such members. It therefore becomes necessary to devise procedures whereby creep, under a variable state of stress, and relaxation, under a variable state of strain, may be predicted from creep and relaxation versus time relationships that apply to constant states of stress and strain, respectively.

Any analytical procedure aimed at predicting the time-dependent behavior of segmentally constructed prestressed concrete bridges must be able to account for the time-dependent nature of the construction procedure involved in the erection of such structures. Furthermore, the analysis must take the effects of the complex interaction of creep, shrinkage and relaxation on the time-dependent behavior of the structure into account.

The purpose of this chapter is to present some of the more important procedures available, as well as the actual procedures used in this study for the prediction of creep of concrete and relaxation of steel under variable states of stress and strain, respectively. A step-by-step numerical procedure for the prediction of the time-dependent behavior of a segmentally constructed prestressed concrete bridge is also introduced. This numerical procedure is suited to computer programming.

3.2 Creep of Concrete in a Variable Stress Environment

In the situation where the sustained concrete stress varies with time, there are three generally accepted basic methods of predicting the

creep strain of concrete (43,45, 50, 53):

a) The effective modulus method,
b) The rate of creep method and
c) The method of superposition.

Each of these procedures attempts to predict the creep behavior of concrete subjected to a sustained stress that varies in magnitude, by making use of creep curves that apply to concrete subjected to a constant sustained stress.

3.2.1 Effective Modulus Method

By the effective modulus method the normal procedures of structural mechanics are employed in the analysis of the structure, the only difference being that the conventional modulus of elasticity of the concrete is replaced by an effective modulus that allows for both elastic and creep strains. This reduced effective modulus is thus given by:

$$E_c'(t) = \frac{1}{\varepsilon + C_1(t)} \qquad (3.1)$$

where: $E_c'(t)$ = effective modulus of the concrete at time t,
ε = instantaneous elastic strain due to a unit stress and
$C_1(t)$ = specific creep at time t.

When the concrete is subjected to severe stress variations this method breaks down because it is theoretically unsound. It always predicts complete recovery of strain when the concrete stress is reduced to zero and, moreover, completely ignores the stress history of the concrete. In situations where the concrete stress is continually being reduced, this method tends to underestimate the long-time strain (53). The advantage of this procedure primarily lies in its simplicity.

3.2.2 Rate of Creep Method

The rate of creep method has as its foundation the assumption that the rate of specific creep, given by $dC_1(t)/dt$, is independent of the previous stress history of the concrete. Once this assumption has been accepted, the rate of creep at any time may be written as:

$$\frac{d\varepsilon_{cr}(t)}{dt} = f_c(t) \frac{dC_1(t)}{dt} \tag{3.2}$$

where: $\varepsilon_{cr}(t)$ = total creep strain as a function of time,
$C_1(t)$ = specific creep for concrete loaded at time t_1, as a function of time and
$f_c(t)$ = concrete stress as a function of time.

Furthermore, $f_c(t)$ and $dC_1(t)/dt$ are independent variables, due to the assumption made above.

Thus, the total creep strain that takes place during the time interval t_1 to t may be determined by integrating Eq. 3.2 with respect to time:

$$\varepsilon_{cr}(t) = \int_{t_1}^{t} f_c(t) \frac{dC_1(t)}{dt} dt \tag{3.3}$$

The procedure may be graphically illustrated as follows: Consider a concrete specimen subjected to the stress history given in Figure 3.1a. The specific creep curve for the concrete, initially loaded at age t_1 is given in Figure 3.1b. The creep and elastic response of the concrete to the applied stress are calculated as follows (see Figure 3.1c):

1. At time t_1 the instantaneous elastic strain is given by f_1/E_c.
2. The creep strain during the time interval t_1 to t_2 is given by the product $f_1C_1(t)$.
3. At time t_2 the instantaneous elastic recovery due to the abrupt change in stress from f_1 to f_2 is given by $(f_1-f_2)/E_c$.
4. The subsequent change in creep strain beyond time t_2 is obtained by the product of the change in the specific creep strain beyond t_2, and f_2.

The stress history is, in a sense, ignored by this method, when the assumption that the rate of specific creep is independent of previous stress history, is made. This, of course, implies that only one specific creep curve, corresponding to the age at first loading, is used to predict the creep strain over the entire life of the concrete. The basis of this assumption apparently stems from the experimental observation that for concrete initially loaded at ages greater than approximately 28 days, the rate of creep is independent of the age of loading (50). For the particular case in which concrete initially loaded at an early age is subjected to a severe change of stress at an advanced age, the change of creep predicted by rate of creep method will be less than actually observed (18). This is apparently due to the fact that at this advanced age the rate of specific creep, obtained by making use of the specific creep curve corresponding to the age at first loading, is very small relative to the rate of specific creep that would be predicted by the specific creep curve corresponding to the age at which the severe change of stress actually takes place. Furthermore, when the concrete stress is removed the product $f_c(t)\ [\,dC_1(t)/dt\,]$ reduces to zero, so that Eq. 3.3 does not predict any creep recovery. This is contrary to the observed behavior of concrete (53). In the light of these observations it appears that the rate of creep method will overestimate creep of concrete in an environment where the stress decreases and vice versa (53). However, when stress changes are small the method seems to

predict the creep behavior of concrete quite accurately. It is only in instances of severe stress variations, especially when these variations take place at later concrete ages, where the method tends to break down (12, 18,45).

One of the more important applications of the rate of creep method to the prediction of creep under variable stress was the development of the Dischinger differential equation (45). Derivations of this equation may be found in Refs. (40) and (50). The application of the Dischinger equation to the calculation of creep and shrinkage losses in prestressed concrete members was comprehensively covered by Leonhardt (40).

3.2.3 The Method of Superposition

This method is based on McHenry's hypothesis (43) which states that the creep strain produced in concrete at time t by a particular stress change is independent of the effects of any other stress changes applied prior to time t. This is not a pure application of the principle of superposition but rather a modified version because allowance is made for the change in the creep properties of the concrete under later increments of stress. It is furthermore assumed that concrete creep is the same in tension as in compression so that the time-dependent relation between creep strain and concrete stress may be written thus:

$$\varepsilon_{cr}(t) = f_1 C_1(t) + \sum_{i=2}^{n} \Delta f(t_i)\, C_i(t) \qquad (3.4)$$

where: f_1 = initial stress in the concrete at the time of first loading, t_1,

$C_1(t)$ = specific creep at time t for concrete loaded at age t_1,

$\Delta f(t_i)$ = stress increments or decrements applied at time $t_1 < t_i < t$ and

$C_i(t)$ = specific creep at time t, for concrete loaded at age $t_i > t_1$.

The procedure may be graphically illustrated as follows: Consider a concrete specimen subjected to the stress history given in Figure 3.2a. The specific creep curves for concrete initially loaded at ages t_1 and t_2 are given in Figure 3.2b by $C_1(t)$ and $C_2(t)$, respectively. According to the method of superposition the creep and elastic strains are calculated as follows (see Figure 3.2c):

1. At time t_1 the instantaneous elastic strain is given by f_1/E_c.
2. The creep strain during the time interval t_1 to t_2 is given by $f_1C_1(t)$.
3. At time t_2 the instantaneous elastic recovery due to the abrupt change in stress from f_1 to f_2 is given by $(f_1-f_2)/E_c$.
4. The subsequent strain is computed by considering the stress change as a load applied to the concrete at age t_2. The creep strain due to the stress change is thus computed by using the specific creep curve $C_2(t)$. The strain beyond t_2 is calculated by adding the instantaneous elastic and creep strains due to (f_1-f_2) to the instantaneous elastic and creep strains due to f_1. Due respect is paid to the signs of the stresses and resulting strains.

Even though Eq. 3.4, strictly speaking, only applies to the case where the stress varies in a step-wise manner, continuously varying stress histories may be approximated by dividing the stress into a series of increments that are constant over small time intervals.

This method is superior to the two previously mentioned methods. It predicts creep recovery upon removal of load and, furthermore, accounts for the entire stress history of the concrete. On the other hand, this method presents some practical drawbacks. In the first place, a specific creep curve is required for each stress change to which the concrete is subjected, so that for most practical problems the experimental work involved

may become prohibitive. Secondly, the fact that a record of the stress history must be kept may lead to considerable numerical effort for the solution of any practical problem.

The creep recovery associated with a decrease in concrete stress, as predicted by the method of superposition, is the same as the creep due to a stress of magnitude equal to the stress change applied at the time at which the stress change occurred. There is, however, substantial experimental evidence that the actual creep recovery in such a case would be slightly less than that predicted by the method of superposition (13,45,50). This observation thus leads to the conclusion that in a situation where the stress continually decreases the creep strain will be underestimated by the method of superposition, and the creep strain will be overestimated if the stress continually increases. This trend is confirmed, amongst others, by the results of the tests done by Ross (53).

One approach to the solution of this problem has been to divide creep into recoverable and irrecoverable components (31,36). Even though this approach will model the creep response of a plain concrete specimen subjected to a variable stress state slightly more accurately than the method of superposition, there are some difficulties in its application to the estimation of the creep behavior of structural members. For example, when a prestressed concrete beam is subjected to a change in sustained moment the fibers on one side of the centroid of the section will be loaded while the fibers on the other side will be unloaded. If creep is considered to be divided into recoverable and irrecoverable components, these fibers will now creep at different rates so that the strain distribution through the depth of the section will no longer be linearly distributed. This is a direct violation of the assumption made in beam theory that plane sections remain plane. Thus, the assumption, implicit in the method of superposition, that creep and creep recovery are equal is necessary in order to satisfy the assumptions made in Bernoulli-Euler beam theory.

Dilger et al. (15) accounted for the difference in creep and creep recovery in the application of the method of superposition to the prediction of the creep of prestressed concrete beams. The specific creep recovery

was estimated by multiplying the specific creep by a reduction factor R, defined as the ratio of specific creep recovery to specific creep. For the particular case of a beam subjected to a change in moment, an average reduction factor (1+R)/2 was applied to both specific creep and specific creep recovery. The reason for this was to ensure that all the fibers through the section would creep at the same rate so that the assumptions of beam theory could be satisfied.

The method of superposition was used as the basis for the derivation of the Trost relaxation coefficient method, for the direct calculation of strain under a varying stress. A detailed derivation and discussion of this procedure was given by Neville (50). The effect of aging of the concrete on the final values of creep for stress changes applied after initial loading is accounted for by the relaxation coefficient. Bazant (6) extended the method to include the effect of the variation of the modulus of elasticity with time and also presented values of the aging coefficients (or relaxation coefficients) corresponding to creep curves recommended by the C.E.B. as well as the A.C.I. Committee 209 (2). He referred to this procedure as the age-adjusted effective modulus method due to the similarity of the form of the expression relating the creep strain due to the continuously varying component of stress, to a single elasticity problem with a modulus of elasticity modified appropriately by the aging coefficient.

3.2.4 Procedure Used in the Present Study

As mentioned before (see Section 3.2.2) the rate of creep method will lead to erroneous results when large stress changes occur at later ages. In order to overcome this problem Mossiossian and Gamble (45) introduced the revised rate of creep procedure. That procedure was, in essence, exactly the same as the rate of creep method, the only difference being that a new specific creep curve was used when a large stress change occurred at later ages. The age at loading corresponding to the new

specific creep curve was taken to be the same as the concrete age at which this large change in stress took place. When applied to the prediction of the time-dependent behavior of composite prestressed concrete girder bridges, the revised rate of creep approach yielded acceptable results (18,28,45). It should be pointed out that the revised rate of creep method is ideally suited to the time-dependent analysis of the precast girders in such structures because the girders are, in fact, subjected to a severe change in stress a significant period of time after being initially loaded, when the in-situ deck slab is cast. Danon and Gamble (12) also applied the revised rate of creep method to the time-dependent analysis of concrete bridges built by the cantilever method.

A pure application of the method of superposition to the time-dependent analysis of segmentally erected prestressed concrete bridges would be preferable. However, the construction procedure involved in the erection of these structures is of such a nature that the individual segments are subjected to numerous stress changes during the lifetime of the bridge so that a large number of specific creep curves would be necessary. Furthermore, additional specific creep curves would be required in order to account for the time-dependent change in concrete stress due to the loss of prestressing force. It should thus be clear that the experimental work involved in determining the required specific creep curves would be formidable, thus rendering a pure application of the method of superposition not feasible for the analysis of the type of structure considered in this study when experimentally determined creep properties are to be used.

In order to overcome the problems inherent in both the method of superposition and the rate of creep method, it seemed logical to devise a procedure composed of a combination of these two methods such that the disadvantages of the one would be compensated for, to an extent, by the advantages of the other. This philosophy was followed as far as possible in devising the procedure used in this study for the estimation of the creep of concrete subjected to a varying state of stress, when experimentally determined creep curves were used in the analysis.

The proposed procedure may be divided into three steps as follows:

Step 1: The original stress history to which the concrete is subjected is decomposed into n sub-histories, where n is the total number of specific creep curves available. Each of the sub-histories corresponds to the cumulative changes in stress that occur with time during the time interval defined by the ages at loading of two consecutive specific creep curves. The change in stress at the beginning of the time interval is included in the sub-history, while the change that occurs at the end of the interval is excluded. The final value assumed by a particular sub-history is held constant for times greater than the upper limit of the time interval to which this sub-history applies. When all of these sub-histories are superimposed they must yield the original stress history.

Step 2: The next step is to determine the creep response of the concrete to each of these sub-histories separately. The creep response due to a particular sub-history is determined by making use of the rate of creep method in conjunction with the specific creep curve that applies to this sub-history, that is the specific creep curve whose age at loading coincides with the beginning of the time interval to which this sub-history corresponds. This step will yield a creep response for each sub-history.

Step 3: The total creep response of the concrete to the original stress history is determined by superimposing the individual creep responses determined in Step 2. This step is, in essence an application of the method of superposition.

When three or more specific creep curves are available, the proposed procedure may be expressed as follows:

$$\varepsilon_{cr}(t) = \sum_{t_i=\tau_1}^{(\tau_2-1)} f(t_i)\,[C_1(t_{i+1}) - C_1(t_i)] + f(\tau_2-1)\,[C_1(t) - C_1(\tau_2)]$$

$$+ \sum_{r=2}^{n-1} \sum_{t_i=\tau_r}^{(\tau_{r+1}-1)} [f(t_i) - f(\tau_r-1)]\,[C_r(t_{i+1}) - C_r(t_i)]$$

$$+ \sum_{r=2}^{n-1} [f(\tau_{r+1}-1) - f(\tau_r-1)]\,[C_r(t) - C_r(\tau_{r+1})]$$

$$+ \sum_{t_i=\tau_n}^{t-1} [f(t_i) - f(\tau_n-1)]\,[C_n(t_{i+1}) - C_n(t_i)] \qquad (3.5)$$

where: t_i = concrete age at stress change i,

τ_r = concrete age at loading corresponding to the r'th specific creep curve,

$f(t_i)$ = concrete stress at t_i,

$C_r(t_i)$ = specific creep at t_i for concrete initially loaded at τ_r and

n = total number of specific creep curves.

The notation (τ_r-1) indicates the concrete age at which the stress change just prior to τ_r occurred. Thus if $\tau_r = t_m$, then $(\tau_r-1) = t_{m-1}$.

For the case where two specific creep curves are available, Eq. 3.5 simplifies to:

$$\varepsilon_{cr}(t) = \sum_{t_i=\tau_1}^{(\tau_2-1)} f(t_i)\,[C_1(t_{i+1}) - C_1(t_i)] + f(\tau_2-1)\,[C_1(t) - C_1(\tau_2)]$$

$$+ \sum_{t_i=\tau_2}^{t-1} [f(t_i) - f(\tau_2-1)]\,[C_2(t_{i+1}) - C_2(t_i)] \qquad (3.6)$$

The proposed procedure can be graphically illustrated as follows: Consider a concrete specimen subjected to the stress history given in Figure 3.3a. Two specific creep curves are available for the analysis, $C_1(t)$ corresponding to an age at loading at $\tau_1=t_1$, and $C_2(t)$ corresponding to an age at loading at $\tau_2=t_3$ (see Figure 3.3b). The creep and elastic strains are calculated as follows:

1. Firstly, the stress history is divided into two parts: $\Delta f_1(t)$, which is simply the original stress history up to time t_2, the time at which the stress change just prior to τ_2 occurs, and $\Delta f_2(t)$, which corresponds to the cumulative changes in stress that take place at τ_2 and beyond. The sub-histories $\Delta f_1(t)$ and $\Delta f_2(t)$ are given in Figures 3.3c and 3.3e respectively.

2. The rate of creep method is used in conjunction with specific creep curve $C_1(t)$ to calculate the creep and elastic strains due to $\Delta f_1(t)$, as shown by Figure 3.3d. The creep and elastic strains due to $\Delta f_2(t)$ are also calculated by using the rate of creep method but, in this case, specific creep curve $C_2(t)$ is used (see Figure 3.3f).

3. The total creep and elastic response of the concrete to the original stress history is found by superimposing the creep and elastic response due to sub-history $\Delta f_1(t)$, as determined

in step 2, on that due to sub-history $\Delta f_2(t)$ (see Figure 3.3g). Due respect is paid to the signs of the stresses and strains.

An implicit assumption made in the derivation of this procedure was that the ages at loading corresponding to each specific creep curve coincide with the times at which stress changes occur. The age at which the concrete is initially loaded must also coincide with the age at loading corresponding to the first specific creep curve.

When only one specific creep curve is available, the proposed procedure corresponds exactly to the rate of creep method. On the other hand, if there is a specific creep curve available for each change in stress then this procedure corresponds exactly to the method of superposition. The proposed procedure may, therefore, be expected to exhibit the peculiarities inherent in both the rate of creep method and the method of superposition. Bearing in mind the bias inherent in the creep behavior as predicted by the rate of creep method (see Sect. 3.3.2) and that inherent in the creep behavior as predicted by the method of superposition (see Sect. 3.3.3), as well as the fact that the proposed procedure represents a combination of both methods, it would seem reasonable to expect that the magnitude of the creep strain, as predicted by this procedure, would be bounded by the magnitudes predicted by the aforementioned procedures, when the concrete stress is either continually increasing or continually decreasing. That is, the proposed procedure may be expected to predict creep strains that are less than those predicted by the method of superposition, but are greater than those predicted by the rate of creep method when the stress is continually increasing. For the case in which the stress is continually decreasing, the creep strains predicted by this method may be expected to be less than those predicted by the rate of creep method, but greater than those predicted by the method of superposition.

The creep and elastic responses to a continually increasing as well as a continually decreasing stress history were calculated by using all

three of the above procedures, and are presented in Figures 3.4 and 3.5 respectively. In order to generate the specific creep curves required for these calculations, the recommendations of the C.E.B. (11) were used in conjunction with the material properties of the P.C.A. outdoor creep specimens for segment SB1-N1 (see Appendix B). The proposed procedure was used with two specific creep curves with ages at loading of 28 days and 91 days. The expectation expressed in the previous paragraph is clearly justified by these results, as they show that the magnitude of the creep strains predicted by the proposed procedure is bounded by the magnitude of the creep strains predicted by the rate of creep method and the method of superposition when the stress history continually changes in one direction. It should be noted that for times up to the time at which the first stress change takes place, all three procedures predict creep strains of equal magnitude. Furthermore, the proposed procedure and the rate of creep method predict identical creep responses for times up to the age at which the second specific creep curve is included in the calculations of the proposed procedure (91 days, for these examples). The explanation for this observation lies in the fact that the proposed procedure corresponds exactly to the rate of creep method when only one specific creep curve is included in the computations.

During the course of this investigation the C.E.B. recommendations (11) were also used to generate the creep properties of the concrete. In this instance the creep response of concrete was estimated by applying the method of superposition. In order to facilitate these calculations, expressions were derived for the C.E.B. creep factors K_t and K_d by making use of a curve fitting procedure (see Appendix A).

It should be mentioned here that the specific creep curve can be expressed as a Dirichlet series as follows:

$$C_\tau(t) = \sum_{i=1}^{m} a_i(\tau) \left[1 - e^{-\lambda_i \phi(T)(t-\tau)}\right] \qquad (3.7)$$

where: $C_\tau(t)$ = specific creep for concrete loaded at age τ, as a function of time,

$a_i(\tau)$ = aging parameters, dependent on the age at loading τ,

$\phi(T)$ = temperature shift function,

T = temperature and

λ_i = retardation times.

The particular expression given by Eq. 3.7 is due to Kabir (32). This expression can be fitted to experimental results or to creep curves recommended by any code of practice. Van Zyl (58) and Khalil (36) outlined procedures whereby the coefficients a_i and λ_i may be determined. A new set of a_i's have to be determined for each age at loading. In order to reduce the computational effort involved, it is possible to derive a set of a_i's for particular ages at loading, and then to find the a_i's corresponding to intermediate ages at loading by linear interpolation (58).

The prime advantage of this particular representation of the specific creep curve is that when it is used with the method of superposition, the entire stress history is stored in a set of hidden state variables by keeping the running totals of each of these variables as the calculation progresses. There is such a variable for each term of the Dirichlet series. Detailed derivations of the hidden state variables are given in Refs. (32), (36) and (59). This property substantially reduces the storage requirements involved in the computer solution of practical problems.

Consideration of the form of this representation of specific creep will reveal that it cannot reflect the fluctuations that characterize experimentally obtained specific creep curves, especially when these curves were obtained from specimens that were stored outdoors. These fluctuations may be important in certain cases.

The Dirichlet series representation of specific creep was not used during the course of this study.

3.3 Relaxation of Steel in a Variable Strain Environment

As previously explained, the combined effects of creep and shrinkage of the concrete as well as relaxation of the steel will subject the prestressing steel to a continuously varying state of strain. In addition, instantaneous strain changes may be imposed on the prestressing steel due to the application of additional sustained loads, such as the erection of a new segment or the stressing of additional tendons in the case of segmental cantilever construction. The expression used for the estimation of relaxation losses, Eq. 2.9, is applicable only to steel subjected to a constant sustained strain. It, therefore, becomes necessary to account for the fact that the loss of prestressing force in the steel is not entirely due to pure relaxation in order to improve the estimation of relaxation losses. The procedure employed by Hernandez and Gamble (28) was used in this study to achieve this aim. This procedure may be explained by referring to Figure 3.6 as follows: Curve 1 gives the stress-time behavior of the prestressing steel subjected to an initial stress f_{s1}, as evaluated by using Eq. 2.9. At time t_1 a change in steel stress, Δf_s, occurs due to causes other than relaxation. At this point in time the stress-time relationship for the steel transfers to curve 2, which is based on a hypothetical initial stress, f_{s2}. This hypothetical initial stress (i.e. f_{s2}) is found by solving Eq. 2.9 for f_{si}, using as $f_s(t)$ the known value of the steel stress $f_s(t_1)$ and setting t to the value t_1. The relaxation losses beyond t_2 are found using curve 2, which represents Eq. 2.9 with the initial stress set to the value of the hypothetical initial stress, f_{s2}.

An alternative approach to the solution of this problem has been suggested by Glodowski and Lorenzetti (22). This procedure was also based on a curve transfer procedure. The curve to which the stress-time relationship transferred after a change in strain due to causes other than relaxation, was based on an effective initial stress defined as the algebraic sum of the initial applied stress and any subsequent stress changes due to factors other than relaxation. The starting point on this new curve was

defined by the previous relaxation losses.

An argument that favors the second method when compared to the procedure followed in this study lies in the manner in which the effective initial stress level is determined. This argument was given in Ref. (22) and is repeated here. By the procedure used in this study the hypothetical initial stress is calculated on the basis of the total stress level in the steel, and thus includes changes in stress due to relaxation as well as those due to other causes. By the second procedure the effective initial stress is based on stress changes due to causes other than relaxation. Stress changes due to relaxation are excluded. In the derivation of Eq. 2.9 the initial stress level was assumed to be an independent variable (see Sect. 2.3) so that the initial stress should be independent of prior relaxation losses. Obviously, the second procedure fulfills this requirement while the first procedure does not.

A study aimed at the comparison of these two procedures was carried out by Hernandez and Gamble (28). Those authors concluded that the two procedures yielded results that did not differ significantly. Furthermore, insufficient experimental results are available to comment meaningfully on the relative accuracy of the results predicted by these two procedures. Due to its relative ease of application the first procedure was used in this study.

3.4 Elastic Recovery

In prestressed concrete members the combined effects of creep and shrinkage of the concrete and relaxation of the steel tend to reduce the prestressing force with time. This loss of prestressing force is accompanied by change of concrete stress which, in turn, leads to an elastic rebound of the concrete strain. The change in concrete stress will lead to creep recovery and, in the context of this study, the elastic rebound of the concrete is referred to as elastic recovery. If these recoveries are ignored

in the analytical procedure, then the total prestress loss will be over-estimated. It should be noted that in the case of segmentally erected post-tensioned bridges, elastic recovery will accompany the stress changes induced in the structure by moments due to the self weight of a newly erected segment, or by the increase in prestressing force due to the stressing of a new tendon.

Ghali et al. (19) and Ghali et al. (21) introduced procedures for the estimation of the loss of prestressing force. Both of those procedures accounted for the effects of creep and elastic recoveries on the total loss of prestress.

The approach used in this study to estimate the elastic recovery may best be explained in terms of the assumption that the concrete is perfectly bonded to the steel. It is thus assumed that the strain changes in the concrete at the level of the steel are equal to the strain changes in the steel. When a strain is imposed on the concrete due to, for example, the effects of shrinkage and the concrete is allowed to deform freely, the change in strain in the concrete at the level of the steel will obviously not be equal to the change in steel strain. The problem now reduces to the calculation of the change in steel stress and the subsequent change in concrete stress necessary to reestablish the compatibility of concrete and steel strains, while simultaneously satisfying the equations of equilibrium. This calculation directly yields the elastic recovery of the concrete as well as the change in prestress due to the imposed strain.

A detailed derivation of the procedure used in this study for the estimation of elastic recovery is presented in Appendix A. This procedure can be used to estimate the elastic recovery of the concrete resulting from shrinkage and creep of concrete, relaxation of steel, and the effects of applied loads. It applies to prestressed concrete flexural members and can handle the case where any number of tendons are located at different levels throughout the depth of the member.

For the case where an external moment is applied, the resulting concrete stresses as calculated by using the transformed section properties

will be the same as the result obtained when the concrete stresses, calculated by using the net section properties, are corrected for the effects of elastic recovery.

3.5 Initial Prestressing Force

For post-tensioned prestressing systems, the individual cables are subjected to several sources of instantaneous loss of prestressing force, so that for these systems the initial prestressing force will generally vary along the length of the tendon. There are three possible sources of immediate loss of force: Friction losses, anchor-set losses, and losses due to elastic shortening.

When a cable is stressed, normal forces will be set up between the cable itself and the surrounding material due to the curvature of the cable. The stressing operation will, furthermore, cause the tendon to move relative to the duct, and will, in the presence of these normal forces, give rise to frictional forces that will reduce the tensile force in the cable. This loss in prestressing force increases as the distance of the point, under consideration, from the stressing end increases. There are two major sources of curvature as far as the cable is concerned: Intentional curvature and unintentional curvature (40). The intentional curvature is defined by the cable profile while the unintentional curvatures (wobble) arise from unforseen deviations from the theoretical profile. Expressions for the estimation of the friction losses are given in most textbooks covering the topic of prestressed concrete (see, for example, Refs. 35 and 40). The coefficient of friction, μ, depends on the hardness of the materials sliding over each other, the surface conditions of the sliding faces, the contact pressure between the surfaces, and any lubrication that may be present. The wobble coefficient, k, primarily depends on the standard of workmanship, the particular prestressing system used, the magnitude of the intentional curvatures, and the flexural stiffness of the metal ducts as well as that of the cable itself (40). Obviously the

magnitudes of μ and k vary over a wide range. Some values suitable for design are given in Refs. 35 and 40.

Once a tendon has been stressed it is somehow anchored and the jack removed. Exactly how the tendon is anchored will depend on the particular type of prestressing system being used. What is of importance, however, is that this anchoring operation is accompanied by a small amount of deformation or slip which, in turn, leads to a loss in prestressing force. For long cables this loss is usually small, but for the case of short tendons this loss may be significant. The amount of slip to be expected at the anchors will primarily depend on the prestressing system being used, as well as the quality of workmanship. The amount of slip to be allowed for should be provided by the manufacturers of the prestressing system being used. Some values are to be found in Ref. 40. An iterative procedure for the solution of the problem of the estimation of the prestress loss due to slip at the anchor is given by Leonhardt (40). By approximating the actual cable profile with circular arcs, Huang (29) derived closed-form expressions by which these losses may be estimated.

For practical reasons the tendons in a post-tensioned member are not stressed simultaneously. As a tendon is stressed it will tend to shorten the member due to instantaneous elastic effects. It should thus be clear that the elastic shortening induced by a cable will reduce the prestressing force existing in the cables that have already been stressed and anchored. Various procedures for the estimation of the prestress loss due to the effects of elastic shortening are presented in Refs. 18 and 40.

In the present study, all of the above-mentioned losses are accounted for. The expressions used for the estimation of friction and anchor-set losses are derived in Appendix A. The losses due to elastic shortening are automatically accounted for by including the effects of elastic recovery (see Sect. 3.4) as each tendon is stressed.

3.6 Basic Analytical Assumptions

The basic assumptions of the analysis, as they apply to the material properties as well as to analytical considerations, are listed in what follows.

1. At the stress levels encountered during the course of the analysis, concrete and steel both have linear elastic stress-strain relationships under short-time loading.
2. The strains vary linearly over the depth of the cross-section of the member. This is a direct result of the usual assumption made in beam theory that plane sections remain plane before and after application of the load.
3. The modulus of elasticity of the concrete, expressed as a function of time, is known and may be considered as a step function.
4. Linear creep theory is applicable within the range of stress levels encountered during the course of the analysis.
5. The specific creep of concrete is known as a function of time as well as age at loading and may be considered a step function. When experimental data is used, the number of different specific creep curves will depend on the available data.
6. The strains due to free shrinkage of the concrete are uniformly distributed over the depth of the cross-section of the member.
7. The concrete shrinkage strain, expressed as a function of time, is known and may be considered as a step function.
8. All the time-dependent and instantaneous elastic material properties are taken to be the same for each segment.
9. The modulus of elasticity of steel is known.
10. The loss of steel stress due to relaxation, expressed as a function of time, is known and may be considered as a step function.

11. For the purposes of estimating the change in creep strain that takes place during a particular time interval, the concrete stress is assumed to remain constant at the value that existed at the beginning of the time interval.
12. The change in stress relaxation that takes place during a particular time interval occurs under constant strain. Relaxation during the time interval is based on a hypothetical initial stress evaluated from the stress in the steel at the beginning of the time interval.
13. Prior to erection, each segment is considered to be stress-free.
14. All strains that take place in a segment prior to erection have no structural significance.
15. Within the elastic range the elastic strains, as well as creep and shrinkage strains, are considered to be additive. It is thus assumed that creep and shrinkage are additive phenomena.
16. All the effects of the nontensioned reinforcing steel on the long-time behavior of the structure are ignored.
17. The concrete is assumed to be perfectly bonded to the prestressing steel so that the change of strain of the steel is equal to that of the concrete at the level of the steel.
18. The complete construction history of the structure is known. This requires knowledge of the sequence of casting, curing and erection of each segment. Furthermore, the times at which certain construction activities, such as casting of closure segments, stressing of positive continuity tendons, and release of supports, take place are assumed to be known.
19. An in-situ closure segment is assumed to be free of stress up to the time that the positive continuity tendons passing through it are stressed.

20. The self weight of a side-span end is assumed not to impose any loads on the structure prior to the time that the continuity tendons within that particular side-span are stressed.

3.7 Numerical Procedure

The integral expressing the strains in the structure as a function of time is solved using a step-by-step numerical integration scheme because of the difficulty encountered in expressing the rheological properties of concrete and steel as well as their inter-dependent effects in terms of mathematical functions, which prohibit the development of closed form solutions. The time period over which the time-dependent behavior of the structure is to be determined is divided into a number of short time intervals. Creep, shrinkage and relaxation are converted into step functions in the time domain and are, furthermore, assumed to have independent effects over each time interval.

It is recommended that the time intervals be chosen in such a manner that they are smaller for the time periods immediately following large changes in concrete or steel stress, and become progressively larger for later times. The reason for choosing the time intervals on this basis lies in the fact that most of the expected creep and relaxation takes place in a relatively short period of time immediately following application of stress, and then proceeds at a greatly reduced rate for later times. Furthermore, it should be mentioned that for the period of time immediately following the end of curing, concrete shrinks at a high rate.

The numerical procedure used in this study was incorporated in a computer program, coded in Fortran IV. The program was developed specifically for the time-dependent analysis of the Kishwaukee River bridge and is capable of accounting for the effects of most of the construction activities encountered during the course of the construction of this particular bridge.

Furthermore, the program was designed in such a way that the inclusion of any further construction activities may be accomplished with relative ease.

The double cantilevers and side-span ends are assembled independently of each other. These structures can then be assembled in any specified order into intermediate structures, to eventually yield the completed structure. The analysis proceeds independently for each of the above-mentioned structures so that the actual construction history was used for the analysis. The number of segments and consequently the spans of the double cantilevers and intermediate structures need not be the same. Segments can vary in length as well as cross-sectional properties.

When double cantilevers are joined to each other, or to existing intermediate structures, the moment resisting part of the double cantilever support is usually released. The effects of this operation were accounted for in the program. The application and removal of construction loads were also taken into account. Only point loads were considered.

Since all the tendons in the Kishwaukee River bridge were straight, only straight prestressing tendons were included in the program. Friction as well as anchor-set losses were accounted for.

The time at which any construction activity takes place must coincide with the beginning of a time interval.

The program was set up so that experimentally determined concrete material properties could be directly used. In the absence of experimental data, these properties, as based on the recommendations of the C.E.B. (11), could be automatically generated by the program. When experimentally determined material properties were used, the creep of concrete subjected to variable stresses was estimated by the procedure outlined in Sect. 3.2.4. For the case of specific creep curves generated by using the C.E.B. recommendations, the method of superposition was used for the prediction of creep. The variation of the modulus of elasticity with time was also accounted for in the analysis.

The size of the problem that can be solved by the program depends only on the amount of central memory available on the computer being used. No further restrictions are placed on the number of double cantilevers,

which defines the number of spans in the final structure, the number of segments and the number of different tendons in the structure, and the amount of experimental data.

In what follows, the numerical procedure is summarized in step-by-step form. Sections are automatically taken at the middle of each segment. Unless otherwise indicated, concrete stresses and strains are calculated at the extreme top and bottom fibers of each section in the structure under consideration. The value of each of these quantities at any level on a particular section may be found by linear interpolation. All the indicated summations are algebraic. The details of most of the computations are given in Appendix A.

The assembly of each double cantilever was independently accounted for because it is improbable that the sequence of casting, curing and erection of the segments for each of these structures will be identical in practice. The numerical procedure followed in this study for the analysis of a double cantilever is presented below.

1. If a new segment is to be erected, calculate the concrete stresses and strains due to the self weight of this segment. Correct these stresses and strains for the effects of elastic recovery of the concrete. This calculation will also yield the change in prestressing force due to the self weight of the new segment.
2. If a tendon is to be stressed, calculate the prestressing force taking into account friction losses as well as anchor-set losses.
3. Calculate the concrete stresses and strains due to the prestressing force determined in step 2. Correct these stresses and strains for the effects of elastic recovery of the concrete. This calculation will yield the change in prestressing force due to the stressing of the tendon. This change in prestressing force represents the prestress loss in the already stressed tendons due to elastic shortening of the concrete. It should be

noted that the tendon being stressed is not included in the calculation of elastic recovery of the concrete.

4. Repeat steps 2 and 3 until all the tendons associated with the erection of this segment have been stressed.
5. Repeat steps 1 through 4 until all the segments that are to be erected at the beginning of this time interval have been accounted for.
6. If loads are to be applied or removed, calculate the concrete stresses and strains due to the resulting moments. The concrete stresses and strains are subsequently corrected for the effects of elastic recovery of the concrete and the corresponding change in prestressing force determined.
7. The total changes in concrete stresses and strains as well as the total change in prestressing force due to instantaneous elastic effects at the beginning of this particular time interval are found by keeping the running sums of the corrected concrete stresses and strains as well as the changes in prestressing force as determined in steps 1, 3 and 6. For each time interval these running sums are initialized to zero before executing step 1 for the first time.
8. Update the total concrete stresses and strains by adding the total change in the concrete stresses and strains due to the instantaneous elastic effects at the beginning of the time interval, as determined in step 7, to the total concrete stresses and strains existing at the beginning of the time interval.
9. Update the total prestressing force by adding the change in prestressing force due to the instantaneous elastic effects at the beginning of the time interval, as determined in step 7, to the total prestressing force existing at the beginning of the time interval.

It is understood that if any of the above steps are not applicable for the time step under consideration, then that particular step is skipped. In order to determine the time-dependent effects during a time interval, the following procedure is followed:

10. Calculate the change in creep strains at the extreme top and bottom fibers of each section for this time interval. The procedure to be used will depend on whether experimentally determined specific creep curves, or specific creep curves generated by the C.E.B. recommendations (11) are used (see Sect. 3.2.4). The required stress histories are recorded at the extreme top and bottom fibers of each section. By accounting for the effects of elastic recovery of the concrete, the creep strains may be corrected. This calculation, furthermore, directly yields the change in prestressing force and the associated change in concrete stress due to the change in creep strain.
11. Find the free shrinkage strain of the concrete for this time interval. It is assumed to be uniformly distributed through the cross-section. This shrinkage strain is corrected by accounting for the effects of elastic recovery of the concrete. The change in prestressing force and concrete stress due to the change in shrinkage strain are also determined.
12. Calculate the loss of prestressing force in each tendon due to relaxation. This calculation is based on the steel stress existing at the beginning of the time interval, including the instantaneous elastic effects. By applying this loss of prestressing force as a tensile force acting on the section, the change in concrete stress and strain is corrected for the effects of elastic recovery of the concrete. The change in prestressing force resulting from this calculation must be added to the relaxation loss to yield the total change in

prestressing force due to stress relaxation of the steel, for this time interval.

13. The total change in concrete stresses and strains, as well as the total change in prestressing force due to the time-dependent effects for this time interval are found by summing the corrected changes in concrete stresses and strains as well as the changes in prestressing force due to the effects of creep, shrinkage and relaxation as determined in steps 10 through 12.
14. Update the total concrete stresses and strains by adding the total changes in these quantities due to the time-dependent effects for this time interval, as determined in step 13, to the total values, as determined in step 8.
15. Update the total prestressing force by adding the change in prestressing force due to the time-dependent effects for this time interval, as determined in step 13, to the total prestressing force, as determined in step 9.

The operations described by steps 1 through 15 are executed at each integration point, or section, along the span of each cantilever making up the double cantilever. The number of sections considered will depend on the total number of segments erected at the time corresponding to the beginning of the time interval under consideration.

The deflected shape of each cantilever at the end of the time interval can be calculated by repeating the following steps for each cantilever:

16. Calculate the total curvature at each section along the cantilever by making use of the total concrete strains, as determined in step 14.
17. Using the curvatures found in step 16 in conjunction with the Newmark numerical integration procedure given in Ref. 23, calculate the deflected shape of the cantilever.

The procedure, as defined by steps 1 through 17, is repeated for each time step up to the time that a closure segment is cast. From this time onwards, the calculation proceeds as follows:

18. If the cantilever to which the closure segment applies forms part of a side-span end, skip to step 20. It is assumed that, for this case, the closure segment is cast on false-work, so that its self-weight does not impose any loads on the structure at this stage.
19. Find the bending moment at each section of the cantilever to which the closure segment is added due to half the total weight of the segment. Subsequently calculate the concrete stresses and strains due to these moments. Correct these stresses and strains for the effects of elastic recovery of the concrete and find the resulting change in prestressing force.
20. If loads are to be applied or removed at the beginning of this time interval, calculate the concrete stresses and strains due to the moments resulting from these loads. These stresses and strains are subsequently corrected for the effects of elastic recovery, and the corresponding change in prestressing force determined.
21. Find the total change in the concrete stresses and strains as well as the total change in prestressing force that occurred at the beginning of the time interval by summing the appropriate quantities as determined in steps 19 and 20, when the closure segment is cast at this time. If the closure segment is not cast at this time, then the corrected changes in the concrete stresses and strains as well as the change in prestressing force determined in step 20 represents the total changes in these quantities that occurred at the beginning of the time interval.

22. Update the total concrete stresses and strains as well as the total prestressing force by adding the changes in these quantities, as determined in step 21, to the total values existing at the beginning of the time interval.
23. Find the total changes in concrete stresses and strains as well as the total change in prestressing force that take place during the time interval due to the effects of creep and shrinkage of the concrete, and relaxation of the steel. This step is executed exactly as indicated by steps 10 through 13.
24. Update the total concrete stresses and strains as well as the total prestressing force by adding the changes in these quantities due to the time-dependent effects for this time interval, as determined in step 23, to the total values determined in step 22.
25. Using the total concrete strains determined in step 24, the curvatures at each section are calculated, and subsequently the deflected shape of each cantilever, at the end of the time interval, is computed.

Steps 20 through 25 are repeated for each time interval up to the time that the tendons which establish continuity of this double cantilever with the structure to which it is joined are stressed. It should be noted that steps 18 through 25 are applied only to the first closure segment that applies to this double cantilever. When the closure segment on the opposite cantilever is cast, the structure must be changed from a double cantilever to an intermediate structure.

The procedure defined by steps 1 through 25 is repeated for each double cantilever until all these structures have been accounted for. Subsequently, each of the side-span ends is assembled. The numerical procedure followed is similar to that followed for the assembly of the double cantilevers. There are, however, some differences: It is assumed that no construction loads are imposed on the side-span end, the self-weight of the

closure segment is assumed not to impose any loads on the side-span end, and the boundary conditions for which moments and deflections are calculated correspond to a simply supported beam. All these assumptions are based on the fact that the side-span ends are assembled on false-work.

Once all the double cantilevers and side-span ends have been analyzed up to the point where the tendons that establish continuity between each of these structures and another structure are to be stressed, the numerical procedure is continued as follows for each of the resulting intermediate structures:

26. Find the prestressing force due to the stressing of the tendons that establish continuity of the new intermediate structure, accounting for friction and anchor-set losses. Calculate the concrete stresses and strains due to this force and apply the appropriate corrections due to the effects of elastic recovery of the concrete. The change in prestressing force in the already stressed tendons is also determined. By repeating the above calculations for each of the tendons in the sequence that they are stressed, the loss of prestress due to elastic shortening is correctly accounted for.
27. If the structure is statically determinate, skip to step 29.
28. Find all the elements of the flexibility matrix as it applies to the calculation of the unknown vertical reactions at each interior support. For this calculation the current value of the modulus of elasticity of the concrete for each segment is used, and the effects of elastic recovery of the concrete are properly accounted for. The exact procedure followed in finding the flexibility matrix is presented in Appendix A.5.
29. Calculate the change in deflected shape due to the stressing of the tendons by using the change in concrete strains found in step 26. For a statically determinate intermediate structure use the actual boundary conditions for this computation. If

the structure is statically indeterminate this calculation is based on the boundary conditions corresponding to a beam simply supported at the two outside supports, i.e. the internal supports are removed. This constitutes the equivalent statically determinate structure (see Appendix A.5).

30. If the structure is statically determinate, skip to step 36.
31. Find the vertical reactions at the interior supports by making use of the flexibility matrix and the deflected shape of the equivalent statically determinate structure, as determined in step 29 (see Appendix A.5).
32. Find the moments in the equivalent statically determinate structure due to the vertical reactions determined in step 31. This is done by applying these reactions as point loads on the equivalent statically determinate structure.
33. Find the concrete stresses and strains due to the moments found in step 32. By considering the effects of elastic recovery, these concrete stresses and strains may be corrected and the resulting change in prestressing force found.
34. Find the deflected shape of the equivalent statically determinate structure due to the strains found in step 33.
35. The concrete stresses and strains as well as the change in prestressing force found in step 33, and the deflected shape found in step 34 represent the corrections in these quantities due to the effects of continuity of the structure.
36. Find the total changes in the concrete stresses and strains as well as prestressing force due to stressing of the continuity tendons by summing the appropriate quantities found in steps 26 and 33. For statically determinate structures the total changes are given by the values found in step 26.
37. Find the total change in deflection due to stressing of the continuity tendons by superimposing the deflected shapes

calculated in steps 29 and 34. For statically determinate structures, the total change in deflection is given by the deflected shape found in step 29.

38. Update the total concrete stresses and strains as well as the total prestressing force by adding the changes in these quantities, as determined in step 36, to the values existing at the beginning of the time interval.
39. Update the total deflections by adding the change in deflection, as determined in step 37, to the total deflection existing at the beginning of the time interval.
40. Update the total bending moments by adding the change in bending moment due to the effects of continuity, as found in step 32, to the total bending moments existing at the beginning of the time interval.

If one of the structures forming this new intermediate structure is a side-span end, the effect of the self-weight of this side-span end now, for the first time, imposes loads on the structure. The effect of this weight is taken into account in the next few steps. For the case that neither component structure forming the new intermediate structure is a side-span end, the following steps are skipped and the numerical procedure continued from step 48.

41. Find the change in moments due to the self-weight of the side-span end as well as that of the closure segment. For the case of a statically indeterminate structure this calculation is based on the equivalent statically determinate structure.
42. Calculate the change in concrete stresses and strains due to the change in moments, found in step 41. Correct these concrete stresses and strains for the effects of elastic recovery, and find the associated change in prestressing force.
43. Calculate the change in deflected shape due to the self-weight of the side-span end by using the change in concrete strains,

found in step 42. For a statically indeterminate structure base this calculation on the equivalent statically determinate structure.

44. If the structure is statically determinate, skip to step 46.

45. Find the change in moment, the change in concrete stresses and strains, the change in prestressing force, and the change in deflected shape due to the effects of continuity of the intermediate structure. These operations are performed as indicated by steps 31 through 35, but are based on the deflected shape found in step 43.

46. Find the total change in moments, the total change in concrete stresses and strains as well as prestressing force, and the total change in deflection due to the self-weight of the side-span end by adding the changes in these quantities as found in steps 41, 42 and 43 to the appropriate changes due to the effects of continuity, as found in step 45. It is understood that for a statically determinate structure the changes found in steps 41, 42 and 43 constitute the total changes in the appropriate quantities.

47. Update the total bending moments, the total concrete stresses and strains, the total prestressing force, and the total deflections by adding the total change in these quantities, as found in step 46, to the total values existing after being updated in steps 38, 39 and 40.

For time steps up to the time that a closure segment is cast, the following procedure is followed for each time step:

48. Find the elements of the flexibility matrix. For this calculation use the current value of the modulus of elasticity of the concrete (see also step 28). If the intermediate structure is statically determinate, skip this step.

49. Determine the moments due to any loads that are applied or removed, as well as supports that are released, at the beginning of the time interval. For the case of a statically

indeterminate structure this calculation is based on the equivalent statically determinate structure. If neither of the above-mentioned operations are performed at the beginning of this time interval, ignore this step and skip to step 52.

50. Following the procedures outlined by steps 42 through 46, for the case of accounting for the self-weight of a side-span end, the total change in moments, the total change in concrete stresses and strains as well as prestressing force and the total change in deflection, due to the moments found in step 49, may be determined.

51. Update the total moments, the total concrete stresses and strains, the total prestressing force, and the total deflections, by adding the total change in these quantities, as found in step 50, to the total values existing prior to the execution of step 48.

52. Find the total changes in concrete stresses and strains as well as the total change in prestressing force that take place during the time interval due to the combined effects of creep and shrinkage of the concrete as well as relaxation of the steel. This step is executed exactly as outlined by steps 10 through 13.

53. Calculate the change in deflected shape due to the time-dependent effects for this time interval by using the total change in concrete strains found in step 52. For a statically indeterminate structure base this calculation on the equivalent statically determinate structure.

54. If the structure is statically determinate skip to step 56.

55. Find the change in moments, the change in concrete stresses and strains, the change in prestressing force, and the change in the deflected shape due to the continuity of the intermediate structure. This step is executed as outlined by steps 31 through 35, based on the deflected shape found in step 53.

56. Find the total change in concrete stresses and strains as well as prestressing force, and the total change in deflection due to the time-dependent effects, for this time interval, by adding the changes in these quantities as found in steps 52 and 53, to the appropriate changes due to the effects of continuity, as found in step 55. The change in moment as calculated in step 55 represents the total change in moment due to the time-dependent effects for this time interval. If the intermediate structure is statically determinate the changes found in steps 52 and 53 constitute the total changes in the above-mentioned quantities, and there is no change in moment due to the time-dependent effects.
57. Update the total moments, the total concrete stresses and strains, the total prestressing force, and the total deflections by adding the total change in these quantities, as found in step 56, to the total values existing before execution of step 52.

The procedure outlined by steps 48 through 57 is repeated for each time interval up to the time that the closure segment joining this intermediate structure to another structure, is cast. If the particular intermediate structure being considered is the final structure, the above procedure is repeated until the last time interval has been accounted for. At this point the analysis is halted.

If the next structure to be added to this intermediate structure is a side-span end, the self-weight of the closure segment is assumed not to impose any loads on the intermediate structure up to the time that the continuity tendons, which establish continuity of the intermediate structure and the side-span end, are stressed. In this case the numerical procedure is resumed from step 62. Otherwise, the self-weight of the closure segment must be included from the time of casting, and the numerical procedure is continued as follows:

58. Find the flexibility matrix based on the current value of the modulus of elasticity of the concrete (see also step 28). If the intermediate structure is statically determinate, skip this step.
59. Find the moments in the intermediate structure due to half the self-weight of the closure segment. For the case of a statically indeterminate structure this calculation is based on the equivalent statically determinate structure.
60. Following the procedure as outlined in steps 42 through 46, for the case of the self-weight of a side-span end, the total change in moments, the total change in concrete stresses and strains as well as prestressing force, and the total change in deflection due to the bending moments found in step 59, may be determined.
61. Update the total moments, the total concrete stresses and strains, the total prestressing force, and the total deflected shape by adding the total change in these quantities, as found in step 60, to the total values existing prior to the execution of step 59.
62. Evaluate the behavior of the structure for each time interval up to the time that the next set of continuity tendons, that apply to this intermediate structure, are stressed. This is done by repeating the operations outlined in steps 48 through 57 for each time interval.

Once step 62 has been executed, the next intermediate structure can be analyzed, and the numerical procedure is resumed from step 26. This process is continued until all the intermediate structures, including the final structure, have been analyzed.

4. CALCULATED AND MEASURED DEFORMATIONS OF THE KISHWAUKEE RIVER BRIDGE

4.1 Introduction

It is a recognized fact that the prime contributors to the time-dependent behavior of prestressed concrete structures are the time-dependent material properties of concrete and steel. In the light of the discussions presented in Sections 2 and 3 it should be clear that this behavior will be influenced by numerous factors related to the surrounding environment and the composition of the concrete, as well as the stress history to which the constituent materials making up the structure are subjected. Of particular importance is the effect of the variations of the environmental factors on the time-dependent behavior of the concrete, since most real structures are not subjected to constant environments. It is, furthermore, of importance to note that the complex interaction of the creep and shrinkage of concrete as well as the relaxation of steel will have an influence on the time-dependent behavior of the structure.

It should be realized from the outset that it is virtually impossible to account exactly for the effects of all the above-mentioned contributory factors when conducting an analysis aimed at predicting the time-dependent behavior of a prestressed concrete structure. The difficulties involved in accounting for these effects primarily stem from the present lack of understanding of exactly how these factors affect the creep and shrinkage properties of the concrete as well as the lack of records which exactly describe the variable environmental conditions to which real structures are subjected. Nonetheless, such an analysis should in some measure attempt to account for most of these effects. For the particular case of prestressed concrete bridges built in segments by the cantilever method, the stresses are built up in a complex manner due to the nature of the construction procedure. This construction procedure should be reflected as accurately as possible in the analysis because of the

dependence of creep on the stress history to which the concrete is subjected.

In this work the time-dependent behavior of the Kishwaukee River Bridge was studied. The superstructure of this bridge is a five-span continuous box girder built in segments by the cantilever method. For details of the structure as well as the construction sequence, see Appendix B. This Appendix also provides the prestressing details.

An experimental program aimed at recording concrete strains at three different sections on the bridge itself, as well as determining the material properties of the concrete used in the bridge from laboratory stored specimens as well as specimens stored outdoors was conducted at the Construction Technology Laboratories of the Portland Cement Association (P.C.A.) (54). The locations of the instrumented segments were chosen such that records of concrete strain could be obtained in the support, quarter-span and mid-span regions of a particular span (see Figure 4.1 and B.1 b). These segments are designated SB1-N1, SB1-N9 and SB1-N16, respectively. Longitudinal concrete strains were measured by making use of Whittemore mechanical strain gauges, which measure surface concrete strain, and Carlson strain meters, which measure internal concrete strain. The locations of the Carlson strain meters at a particular section are given in Figure 4.2.

In this section analytically obtained concrete strains are compared to strains obtained from the Carlson strain meters. Three analyses were made, the differences lying in the material properties assigned to the concrete. For Analysis 1 the material properties determined experimentally from the outdoor stored concrete specimens were used. It was felt that these material properties would introduce into the analysis the effects on the time-dependent behavior of the variable environment to which the actual structure was subjected. Analysis 2 was conducted on the basis of concrete material properties determined experimentally from laboratory stored specimens. The procedure as proposed in Sect. 3.2.4 was used to calculate creep strains for the case of Analysis 1 and Analysis 2. For Analysis 3 the recommendations of the C.E.B. (11) were used to generate the concrete

material properties. For this particular analysis the method of superposition was used to estimate the creep of concrete. It was felt that Analysis 3 would represent the basis from which a designer would generally have to approach the solution of the problem at hand. It is very seldom that experimental data related to the creep and shrinkage properties of the concrete to be used in a structure is available at the time of design, so that Analysis 3 would serve as a useful indicator of the level of confidence with which the C.E.B. recommendations may be applied to the estimation of the time-dependent behavior of the type of structure under consideration herein. Following the recommendations of Hernandez and Gamble (28), creep was based on 50 percent relative humidity and shrinkage on 80 percent relative humidity in the case of Analysis 3.

4.2 Measured and Analytically Obtained Concrete Strains

The total concrete strains generated by Analysis 1, Analysis 2 and Analysis 3 are compared with the strains measured by means of the Carlson strain meters at the instrumented segments in Figures 4.3 through 4.11, Figures 4.12 through 4.20, and Figures 4.21 through 4.29, respectively. At each of the instrumented segments, measurements of strain were taken at three different levels through the depth of the segment (See Figure 4.2). It should be mentioned that gauge 1 was located slightly below gauges 2 and 8, and that gauge 5 was located slightly above gauges 4 and 6. The analytically obtained top and bottom fiber strains were reduced to levels 8 in., 56 in. and 131 in. (0.203 m, 1.422 m and 3.327 m) above the bottom fiber of the section so that these strains could directly be compared to the measured strains.

The time scales that apply to each of the above-mentioned plots were chosen such that day zero coincided with the day on which the particular segment being considered was erected. Thus, the origin of the time scales for the different instrumented segments do not fall on the same calendar day. The times at which some of the major construction activities

took place are marked in Figures 4.3, 4.6 and 4.9 for segments SB1-N1, SB1-N9 and SB1-N16, respectively. It should be mentioned that since total strain is being plotted as a function of time, the instantaneous elastic effects of the various construction activities are easily identified by obvious discontinuities in these plots.

For the correct interpretation of the measured strains, it is important to realize that there are no data points available for any of the strain meters for the time period extending from the time at which the continuity tendons for intermediate structure 9 were stressed to the time at which the closure segment for the final structure was cast. This means that the variations in concrete strain that took place during this time period are unknown.

4.2.1 Observations

Analysis 1 (see Figures 4.3 through 4.11): Bearing in mind the scatter inherent in the measured strains, the predicted strains compare very well with measured values. The shapes of the calculated curves as well as the magnitude of the calculated total time-dependent strains compare well with the measured quantities. As far as the shapes of the total concrete strain versus time curves are concerned it appears as if the trends of the measured curves are followed by the calculated curves for the first 250 days. Beyond the first 350 days the trends of the measured curves are not followed by the estimated curves, but it appears that a hint of these trends is present in the calculated curves in the vicinity of 300 days. The fluctuations of the time-dependent strain which characterize the trends referred to above seem to be amplified for segments further away from the pier, especially in the case of the calculated curves.

Analysis 2 (see Figures 4.12 through 4.20): For times beyond 300 days it appears that the magnitude and shape of the generated total concrete strain versus time curves closely

approximate the magnitude and shape of the measured curves. Once again, this comparison should be seen in the light of the scatter of the experimental data. Prior to 300 days the shapes of the generated curves do not agree with those of the measured curves. The time-dependent parts of the generated curves are, relatively speaking, smooth when compared to the experimentally determined curves as well as the curves generated by Analysis 1.

Analysis 3 (see Figures 4.21 through 4.29): The magnitudes of the calculated curves of total concrete strain versus time are consistently smaller than the experimentally determined curves. The time-dependent parts of the generated curves are smooth and do not reflect any of the fluctuations inherent in the curves obtained from the measurements of strain on the bridge.

Compared to the experimentally determined values of total strain it appears that Analysis 1 yielded the best values for total strain and Analysis 3 the worst.

At all stages Analysis 3 yielded values of concrete strain that were significantly lower than the values calculated by either one of the other analyses. A significant contributor to this observation appears to be the very high value of the concrete modulus of elasticity associated with the C.E.B. recommendations. When compared to the concrete modulus of elasticity used for Analysis 1 it is 36 percent higher at 28 days, and 54 percent higher at 360 days. For the case of Analysis 2, a similar comparison shows that the C.E.B. recommendations predict a concrete modulus of elasticity 34 percent higher at 28 days, and 50 percent higher at 360 days. This high value for the concrete modulus of elasticity led to rather low predicted values for instantaneous elastic strains. This point is clearly illustrated by comparing the magnitude of the total concrete strains obtained from Analysis 3 to the corresponding strains obtained from the other two analyses for the time period prior to the time at which the continuity tendons that establish continuity of intermediate structure 9

were stressed. During this time period the concrete strains in the instrumented segments are primarily due to instantaneous elastic effects.

In view of the very high value of the concrete modulus of elasticity predicted by the C.E.B. recommendations, it may be tempting to use the procedure outlined by these recommendations to calculate the creep and shrinkage properties of the concrete with an adjusted lower value for the modulus of elasticity. This would, however, be incorrect because the creep strain calculation is based on the initial instantaneous elastic strain which, in turn, directly involves the modulus of elasticity of the concrete. Consequently the multiplying factors that determine the creep factor (see Sect. 2.2.3.1) will implicitly reflect the high value of the modulus of elasticity prescribed by the C.E.B. recommendations.

The total time-dependent strain predicted by Analysis 3 is substantially lower than that predicted by either of the other two analyses. The difference in the total time-dependent strains predicted by Analysis 1 and Analysis 2 decreases as the section considered is located further from the pier. These trends are illustrated in Table 4.1. It should be noted that the values presented in Table 4.1 are based on the total change in top and bottom fiber concrete strains, excluding elastic effects, for the time period defined by the time at which the tendons that establish continuity of intermediate structure 9 are stressed and the time up to which the analysis is carried. During this time period the majority of the time-dependent deformation takes place.

4.2.2 Discussion

The shapes of the total concrete strain versus time curves for the case of the analysis of the Kishwaukee River Bridge highlight some important points that deserve special attention.

Comparing the shapes of the specific creep curves as well as the shrinkage curves used in Analysis 1 and Analysis 2 (see Figures B.5 through B.10) and bearing in mind that the creep and shrinkage curves as predicted

by the C.E.B. recommendations are smooth, it appears that the greatest differences in the shapes of these curves apply to the case of shrinkage. In particular, the shrinkage curve obtained from the outdoor stored specimens (see Figure B.10) shows a period of swelling (age 100-200 days) followed by a period of shrinkage (age 200-400 days). Since the tests for determining this shrinkage curve was started during the summer, the onset of the period of swelling was marked by the commencement of winter so that this swelling may have been associated with the increase of relative humidity that usually occurs during winter. It also appears as if the onset of another period of swelling is marked by a concrete age in the vicinity of 400 days. Unfortunately, there are no data points between a concrete age of 407 and 792 days to substantiate the above speculation. Bearing in mind that the instrumented segments were erected about 100 days after the end of curing (see Appendix B), the first "dip" in the shrinkage curve, described above, should correspond to the time period defined by the first 250 days after erection of the segments. Inspection of Figures 4.3 through 4.11 clearly indicates the profound influence that the shape of the shrinkage curve has on the time-dependent strains. The second "dip" in the shrinkage curve is also reflected in the results generated by Analysis 1. The implication that the shape of the shrinkage curve is an extremely important factor in establishing the trends followed by the time-dependent concrete strains is substantiated by consideration of the shapes of the total concrete strain versus time curves generated by Analysis 2 (see Figures 4.12 through 4.20). The trends present in the results generated by Analysis 1 are markedly absent in these curves primarily due to the fact that these trends are also absent in the shrinkage curve used for Analysis 2 (see Figure B.8). Furthermore, the "dip" near the end of the shrinkage curve for the laboratory stored specimens is reflected in the results generated by Analysis 2.

The effects of the shape of the shrinkage curve on the trends followed by the total strain appear to be more apparent for sections further away from the pier, especially in the case of Analysis 1. The reason for this most probably lies in the fact that the section close to the pier was

subjected to higher compressive stresses and consequently the component of the time-dependent deformation due to creep was greater in this region, thus offsetting the relative importance of the influence of shrinkage on the time-dependent strains. It is of interest to note that for the results of Analysis 2 the above trend does not really apply, because the slight "dip" in the shrinkage curve for this case takes place about 300 days after the segments were initially loaded. By that time the greatest portion of creep could have been expected to have taken place so that any changes in shrinkage taking place at that time may be expected to have had a major influence on the total time-dependent strain.

In the light of the above discussion it would thus appear that shrinkage has an extremely important influence on the total time-dependent strains to be expected in structures of the type under consideration here, where the segments are old when erected. Specifically, it was only the analysis that incorporated the shrinkage curve obtained experimentally from outdoor stored specimens that could correctly predict the seasonal fluctuations of the total concrete strains. It is quite obvious that these seasonal fluctuations cannot be correctly predicted when the material properties used in the analytical procedure are based either on results experimentally obtained from laboratory stored specimens or on the recommendations of the C.E.B. It should also be mentioned that the data obtained from the outdoor stored specimens inherently reflect the effect of the varying environmental factors, e.g. temperature and relative humidity, to which the structure was subjected on the time-dependent properties of the concrete. These effects cannot be reflected by the data obtained from the laboratory stored specimens or the C.E.B. recommendations. The data obtained from the laboratory stored specimens has the advantage over that obtained from the recommendations of the C.E.B. in that the influence of the intrinsic factors on the rheological properties of the concrete are more correctly determined.

For the particular case where the structure is built out of segments that are old at the time of erection, as is the case for the Kishwaukee River Bridge, the initial part of shrinkage has no structural effect because it takes place prior to erection of the segments. Thus, as

far as the structural analysis of the Kishwaukee River Bridge is concerned, it is only the part of the shrinkage curve beyond a concrete age of about 100 days that is of interest. If these portions of the shrinkage curves for the outdoor and laboratory stored specimens are compared (see Figures B.8 and B.10), it becomes clear that even though a major portion of the shrinkage at 800 days has developed at 100 days for both specimens, the behavior beyond 100 days differs greatly for the two specimens. The effects of these differences in the shrinkage curves on the structural behavior is of great importance, as has been illustrated above. It is thus suggested that when a shrinkage curve is obtained from outdoor specimens for use in an analysis such as that being performed in this study, measurements of shrinkage strain should be taken at time intervals that are short enough to include all the seasonal fluctuations in the shrinkage curve. This procedure should be followed for a time period of at least two years. This stands in opposition to the generally accepted practice employed in determining the shrinkage curve for laboratory stored specimens where the initial part of the curve is carefully determined and the later part determined on the basis of measurements of shrinkage strain taken at successively larger time intervals. The justification for each of the above procedures lies in the difference in shape of the shrinkage curves obtained from outdoor and laboratory stored specimens.

For the present analysis each segment in the entire structure was assigned the same material properties. Bearing in mind the fact that the various double cantilevers were not constructed at the same time of the year and that the segments were not cast at the same time, it becomes clear that for Analysis 1 the seasonal dependence of shrinkage is, strictly speaking, correctly reflected by the analysis only for the case of the instrumented cantilever. Judging by the agreement obtained between the time-dependent strains generated by Analysis 1 and the measured values for the instrumented segments, it would appear that for the particular structure under consideration herein, this effect was not of great importance on the calculated strains for the instrumented segments. Some of the effects of

starting the creep and shrinkage tests at the correct time may be illustrated by referring to Sect. 2.2.3.2 where it was pointed out that Hernandez and Gamble (28) found that the expected creep and shrinkage curves resulting from outdoor stored specimens could be satisfactorily approximated by using 50 percent relative humidity for creep and 80 percent relative humidity for shrinkage in conjunction with the C.E.B. recommendations. This was found not to be entirely true for the creep and shrinkage curves obtained from the outdoor specimens reported in the present study (see Figures 2.9 and 2.10). One important difference between the tests reported in Ref. 28 and those reported herein lies in the fact that the former tests were started during the winter while the latter ones were started during the summer. A suggestion for the possible solution to this problem would be to associate a particular shrinkage curve with the segments comprising a particular double cantilever, so that the seasonal effects are correctly accounted for in each double cantilever. It is, however, recommended that this matter be pursued in a further study.

Because the specimens used for experimentally determining creep and shrinkage curves were small when compared with the actual segments which comprise the structure, these curves had to be modified for use with Analysis 1 and Analysis 2 in order to account for the influence of size on shrinkage and creep. This effect was accounted for in the present study by multiplying the experimentally determined creep and shrinkage curves with multiplying factors. These multiplying factors were determined by making use of the C.E.B. multiplying factor K_e, which accounts for the effect of member size on creep and shrinkage (see Sect. 2.2.3 and Figures 2.5 and 2.8). For creep a value of K_e corresponding to the creep specimens and a value corresponding to the actual segments were determined. The multiplying factor used for adjusting the creep curves was subsequently found by calculating the ratio of the K_e value for the segments to the K_e value for the creep specimens. The multiplying factor applied to the shrinkage curves was determined as for the case of creep, the only difference being

that the K_e values that apply to shrinkage were used. Following the above procedure multiplying factors of 0.77 and 0.56 were derived for creep and shrinkage, respectively. These values were used for both Analysis 1 and Analysis 2. This procedure obviously only accounts for the influence of the size of the member on the magnitude of creep and shrinkage, but does not reflect the influence on the rates of creep and shrinkage. This procedure appears to be satisfactory when viewed in the light of the results of the comparisons of the total concrete strains generated by Analysis 1 and Analysis 2 with the measured strains.

For the particular case of Analysis 1, experimentally determined specific creep curves were available for only one particular age at loading, namely 28 days. This means that the method used in this analysis for evaluating creep strains reduced to the rate of creep method (see Sect. 3.2.4) for the case of Analysis 1. Because the majority of the segments were erected at least 100 days after being cast (some of the segments were substantially older than 100 days at the time of erection) it would appear reasonable to assume that the multiplying factor through which the specific creep curve was modified to introduce the influence of size on creep into the calculations should actually be interpreted as a factor that modifies the creep curve to include a combination of the effects of size as well as age at loading on creep. These remarks apply specifically to Analysis 1. As more experimentally determined specific creep curves corresponding to different ages at loading become available, the curves themselves properly reflect the effects of the age at loading on creep so that the multiplying factor, described in the previous paragraph, can be more correctly interpreted as reflecting the influence of the size of the member on creep. Analysis 2, where specific creep curves corresponding to three different ages at loading were available, is such a case. Thus, to summarize, the multiplying factor used to modify the experimentally determined specific creep curves used in the analysis should be interpreted as reflecting not only the influence of the size and shape of the member on creep but also the influence of the age at loading on creep. This will

depend on the number of experimentally determined specific creep curves available for the analysis as well as the differences between the ages at which the segments were erected and the ages at loading corresponding to the available specific creep curves.

Because of the substantial differences in the material properties used in the three analyses it is difficult to comment meaningfully on the relative merits of the procedure proposed in Sect. 3.2.4 for the calculation of creep strain in a situation where the concrete stress continually varies. On the basis of the comparison of the measured strains with the total concrete strains calculated in Analysis 2, where the proposed procedure was used in conjunction with three specific creep curves, it may be said that this procedure performed satisfactorily. It is, furthermore, of interest to note that the rate of creep method used with Analysis 1, as explained above, also yielded satisfactory results. In the case of Analysis 3 the method of superposition was used to calculate creep strains. When considering the time-dependent strains, it should be kept in mind that the creep strains calculated by each of the above-mentioned analyses inherently reflected the biases present in each of these methods, depending on whether the concrete stress was increasing or decreasing (see Sect. 3.2).

In conclusion, it would thus appear that the influence of the variable environment on creep and shrinkage had a profound effect on the long-time behavior of the structure. Indeed, for the structure under consideration here, it is imperative that the seasonal variations of the shrinkage strain be correctly included in the analysis in order to correctly forecast the time-dependent strains of the structure. If the structure is considered by the analysis as a filter that modifies the input parameters to yield the structural response, it is clear that the quality of the calculated response will directly reflect the quality of the input parameters. For the Kishwaukee River Bridge the relative importance of shrinkage in a variable environment was most probably amplified by the fact that the segments were old when erected so that the creep potential of the concrete was somewhat reduced.

4.3 Measured and Analytically Obtained Transverse Deflections

In addition to recording the concrete strains at segments SB1-N1, SB1-N9 and SB1-N16, measurements of the transverse deflection at each of these segments as well as at the corresponding segments in the opposite cantilever were taken. Ball-shaped reference points for level readings were installed on the underside of the top flange so that for each of the above-mentioned segments deflections could be measured at the centre of the cross-section and at 66 in. (1.676 m) off center. The pier segment was chosen as a fixed reference to which all measurements of deflection were referred.

The deflected shapes of the instrumented cantilever as generated by Analysis 1 at various stages of construction are presented in Figure 4.30. These deflected shapes serve to illustrate the opposing effects of the prestressing force and the self-weight of the structure on the deflection. For the cantilever the effect of the prestressing force is to produce an upward deflection while the effect of the self-weight is to produce a downward deflection. Judging by the deflected shapes presented in Figure 4.30, the prestressing force has the dominant effect during the initial construction stages, as indicated by the upward deflection of the cantilever. During the later construction stages the self-weight has the dominant effect on the deflected shape, as indicated by the net downward deflection of the cantilever for these stages of construction. These trends are to be expected when consideration is given to the increased moment due to the increased lever arm, and the decreased prestressing force due to a decreased number of tendons, during the later construction stages of the cantilever.

When segments were erected metal shims were used to correct alignments. This procedure may be expected to induce discontinuities in the slope of the cantilever at the interface of adjacent segments and, as such, induce vertical deflections. These components of deflection are of a rigid body nature and cannot be expected to induce any stresses in the structure. Since the magnitude of these corrections were unknown, they could not be included in the calculation of the deflected shapes given in Figure 4.30.

It would, however, be a simple matter to include these deflections in the calculated results if their magnitudes were known so that a direct comparison with measured deflections would be possible. No measurements of deflection were taken during the period of construction of the instrumented cantilever due to the tight construction schedule. Initial deflection measurements were started after completion of this cantilever.

The changes in the downward deflection of segment SB1-N16 which took place after the time of completion of the final structure as predicted by all three analyses are presented in Figure 4.31. For this figure the origin of the time scale coincides with the time at which the tendons which establish continuity of the final structure were stressed. The measured changes in deflection of segment SB1-N16 since the time of completion of the final structure are listed in Table 4.2. It is important to note that it is the change in transverse deflection that is being considered here and not the total deflection.

It should be pointed out that once a double cantilever was joined to an intermediate structure and the support released, this double cantilever was placed on permanent bearings at the prescribed elevation. This operation in general involved a transverse deflection of unknown magnitude. If the resulting intermediate structure was statically indeterminate this operation may be expected to modify the stresses in the structure to some extent. However, since the magnitude of these displacements were unknown it was not possible to account for these effects. In view of the excellent agreement that exists between the concrete strains generated by Analysis 1 and the measured strains it seems reasonable to assume that the effects of these operations were not very important. It should be realized that because of the unknown magnitude of the deflections induced in the structure by the corrections in alignment during construction of the cantilever, as well as by the seating of the double cantilevers on permanent bearings, the calculated deflections cannot be directly compared to the actual deflections of the structure. Because no construction activities took place once the final structure was completed, the calculated change in transverse deflection

which took place during this time period may be compared to the change in measured deflection.

Before the measured and calculated deflections are compared it is first necessary to mention the failure of a number of joints between the segments of the completed structure. The failure of these joints were discovered just after completion of the final structure and was evidently due to the fact that the epoxy in the joints between the affected segments did not properly harden (16). One of the results of this problem with the epoxy was that it could not have been counted on to transfer much shear force from one segment to the adjacent segment so that the shear was transferred primarily by the shear keys. Because these shear keys were reportedly designed to resist shear forces during erection only and not the total shear force after completion of the structure, it is not surprising that this weakness of the epoxy manifested itself in severe cracking and spalling of the concrete in the webs of the pier segments of double cantilever SB1. The joints affected by the defective epoxy included the instrumented segments. Evidently one corner of the bottom slab of segment SB1-N1 dropped 5/8 in. (15.9 mm) relative to the bottom slab of the pier segment SB1-N0 (16). The final structure was subsequently repaired by inserting stainless steel pins in the webs of the segments at the affected joints so that these pins acted as shear keys (16). Checks of the instrumentation in the bridge as carried out by the P.C.A. staff indicated that the Carlson strain meters were unaffected by the cracking which resulted from the failure of the joints, so that the measurements of concrete strain as obtained from these meters in the affected regions were still valid. It is, however, not reasonable to expect that the transverse deflections were unaffected by the failure of the joints.

For the first 91 days after completion of the final structure, the measured values of transverse deflection indicate that the downward deflection of segment SB1-N16 increased by 0.78 in. (19.8 mm) during this

time period (see Table 4.2). The results of Analysis 1 indicate an increase in the downward deflection of segment SB1-N16 of approximately 0.04 in. (1.0 mm) during this time period (see Figure 4.31). Since the time period considered above includes the time at which the failure of the joints were discovered, it seems reasonable to assume that the discrepancy in the measured and calculated change in the downward deflection of segment SB1-N16 during this time period is primarily due to the failure of the joints. For the following 200 days the values of the measured deflection indicate an increase in the downward deflection of segment SB1-N16 of 0.07 in. (1.8 mm) which compares rather well with the increase of approximately 0.05 in. (1.3 mm) as predicted by Analysis 1 for this time period (see Figure 4.31 and Table 4.2).

During the time period defined by 288 and 538 days after completion of the final structure the measured values of deflection indicate a net increase in the downward deflection of segment SB1-N16 of 0.53 in. (13.5 mm) (see Table 4.2). The results of Analysis 1 indicate an increase in the downward deflection of segment SB1-N16 of approximately 0.05 in. (1.3 mm) for the same time period (see Figure 4.31). Some preliminary calculations have indicated that this discrepancy between the measured and calculated change in deflection cannot be entirely explained in terms of the effects of the differential temperature distribution through the depth of the superstructure of the bridge. It, however, appears as if the measurements of deflection were taken under extremely adverse conditions and, as a result, cannot be expected to be as reliable as the measurements of concrete strain. Some of the sources to be blamed for the far from ideal conditions under which measurements of deflection were made appear to have been the poor light (measurements were taken inside the box girder) as well as the effects on the precise level of vibrations set up in the structure by the movement of heavy equipment across the bridge while measurements were taken.

Comparison of the magnitude of the changes of deflection of segment SB1-N16 as predicted by the three analyses for the time period associated with the final structure clearly illustrates that the magnitude of the deflections predicted by Analysis 3 is substantially smaller than those

predicted by the other two analyses (see Figure 4.31). This observation is in accordance with the relative magnitudes of the concrete strains predicted by the three analyses (see Sect. 4.2.1).

The curvatures at each of the instrumented segments as predicted by all three analyses are presented in Figures 4.32 through 4.34. A curvature corresponding to sagging is taken as positive. The small changes in curvature at the instrumented segments for the time period associated with the final structure serve to illustrate that a large portion of the time-dependent strain induced only an axial shortening of the final structure. The small change in transverse deflection in the final structure as predicted by all three analyses is the result of these small changes in curvature.

5. CALCULATED FORCES AND STRESSES OF THE KISHWAUKEE RIVER BRIDGE

5.1 Introduction

The deformations of a prestressed concrete member due to the time-dependent material properties of the concrete and steel will in general lead to a loss of prestressing force. These time-dependent strains will also tend to induce a time-dependent redistribution of bending moment for the specific case of a bridge constructed by the cantilever method. These time-dependent changes in prestressing force and bending moment will, in turn, combine to modify the concrete stresses in the structure. It should thus be clear that the prestressing force, concrete stresses and bending moments may be expected to change with time for the case of a prestressed concrete bridge built by the cantilever method. It should be pointed out that the time-dependent redistribution of bending moment will take place only after the structure becomes statically indeterminate.

The importance of having a knowledge of how these above-mentioned quantities change with time should be obvious. Consequently, the total prestressing force, concrete stresses and bending moments as predicted by Analysis 1, Analysis 2 and Analysis 3 (see Section 4.1) are presented and discussed in the following sections. As before, the results of Analysis 1 and Analysis 2 may be contrasted with each other in order to illustrate some of the effects of the variable outdoor environment on the time-dependent behavior of the structure. A comparison of the results of Analysis 2 and Analysis 3 may be used to illustrate the relative quality of the results which may be expected when the C.E.B. recommendations (11) instead of experimentally obtained data from laboratory stored specimens are used to predict the time-dependent material properties of the concrete.

The majority of the results presented herein apply to the instrumented segments, SB1-N1, SB1-N9 and SB1-N16.

During the course of the construction process of segmentally erected bridges a very strong possibility always exists that construction loads may be imposed on the structure. Indeed, for the case of the Kishwaukee River Bridge the launching girder was positioned in such a manner during the winter construction shutdown so as to impose loads on the uncompleted structure. These loads thus acted on the uncompleted structure for a time period of approximately 5 months. In order to illustrate some of the effects of the application and subsequent removal of the construction loads the structure was analyzed so as to include the application and removal of these loads. The material properties of concrete obtained experimentally from the outdoor stored specimens were used for the purposes of this analysis. This particular analysis was designated Analysis 4. The results predicted by Analysis 1 and Analysis 4 are compared in Sect. 5.5 in order to illustrate some of the effects on the time-dependent behavior of the structure of the construction loads.

Unless explicitly indicated otherwise, the origins of the time scales for each of the plots that apply to this chapter were taken as the day of erection of the particular segment to which the plot being considered applies. In order to identify the time periods associated with intermediate structure 9 and the final structure for segments SB1-N1, SB1-N9 and SB1-N16 reference should be made to Figures 4.3, 4.6 and 4.9, respectively. Appendix B also contains information about ages at time of erection.

5.2 Prestressing Force

As pointed out before, the general effect of the time-dependent concrete strain on the prestressing force in a prestressed concrete structure

is to reduce the prestressing force. There is a further loss of prestressing force associated with the stress relaxation of the steel which takes place in the absence of strain. Since the stress field that primarily resists the loads applied to a prestressed concrete structure is provided by the presence of the prestressing force, it is of importance to predict the total prestressing force with reasonable accuracy. In what follows the total prestressing forces predicted by the three analyses are presented and discussed. It should be pointed out that in addition to these time-dependent losses of prestressing force the immediate losses due to the effects of friction and anchor-set, as well as the elastic shortening of the member, were included in the analysis process. In this section, however, attention is focused primarily on the time-dependent character of the prestressing force.

Table 5.1 summarizes the time-dependent components of the prestress losses as predicted by each analysis for the time period from the time when the tendons which establish continuity of intermediate structure 9 were stressed, up to the last time interval considered. These losses are expressed as a percentage of the total prestressing force existing at the particular segment being considered just after the tendons that established continuity of intermediate structure 9 were stressed. Most of the time-dependent losses appear to have taken place during the time period described above. Clearly, the magnitude of the time-dependent component of the loss of prestressing force is very small. It should, however, be emphasized that the values presented in Table 5.1 only represent the time-dependent component of the prestress loss and that the instantaneous losses due to elastic shortening and friction losses are excluded. Time-dependent losses which occurred before continuity was established are also excluded. These losses were, of course, included in the analytical process and are consequently reflected in the magnitude of the predicted values of total prestressing force. The losses predicted by Analysis 1 are the largest while those predicted by Analysis 3 are the smallest at the segments considered. Furthermore, the losses predicted by Analysis 1 and Analysis

2 do not differ greatly while the losses predicted by Analysis 3 differ somewhat more significantly from those predicted by the other two analyses. These trends were to be more or less expected since they are consistent with the relative magnitudes of the concrete strains predicted by the three analyses.

It is, however, not the loss of prestressing force, per se, that is of importance in design practice but rather the total remaining prestressing force. As illustrated by Figures 5.1 through 5.3 as well as Table 5.1, the total remaining prestressing forces predicted by the three analyses do not differ significantly. The final values of prestressing force referred to in Table 5.1 are the predicted values at the time up to which the analyses were carried. This observation is rather significant, especially when viewed in the light of the substantial differences in the values of predicted concrete strain, especially for the case of Analysis 3. The reason for this apparent insensitivity of the total prestressing force to the concrete material properties most probably lies in the rather small loss of prestress exhibited by the structure. Even large differences in this small loss will reflect as small differences in the total prestressing force.

The shapes of the prestressing force versus time curves closely reflect the shapes of the concrete strain versus time curves. These trends are especially apparent in the results of Analysis 1 due to the degree of the fluctuations present in the concrete strain versus time curves generated by this particular analysis. The time-dependent strains generated by Analysis 1 are characterized by a period during which the strains develop at a reduced rate followed by a period during which the rate is substantially increased (see Figures 4.3 through 4.11). These trends take place during the first 250 days after erection of the instrumented segments. Inspection of Figures 5.1 through 5.3 will reveal that the period of reduced strain

is accompanied by a reduced rate of loss of prestress while the period of increased rate of strain is accompanied by an increased loss of prestress. As for the case of the total concrete strains, the observation that the magnitude of these fluctuations are increased for sections further from the pier is also applicable to the results of total prestressing force. The shapes of the curves of prestressing force versus time as predicted by Analysis 2 and Analysis 3 are smooth as are the curves of total concrete strain generated by these analyses. The fluctuations present in the curves of concrete strain versus time as generated by Analysis 2 (see Figures 4.12 through 4.20) are also properly reflected by the total prestressing force curves determined by this analysis. These observations serve to emphasize the inability of the analyses that do not make use of the concrete material properties obtained from outdoor stored specimens to predict the time-dependent behavior of the structure correctly. It should be kept in mind that, as mentioned before, the total prestressing forces predicted by the three analyses do not differ significantly, primarily due to the fact that the time-dependent loss of prestress is small.

The time-dependent behavior of concrete will induce a loss of prestressing force due to the resulting strain as distinguished from the effects of relaxation of the prestressing steel reinforcement, which will induce a loss of prestressing force in the absence of strain. The instantaneous elastic strains due to later applications of load, such as the erection of segments and the stressing of tendons, will also induce a change in the total prestressing force. It is thus clear that the time-dependent strains will to a large extent control the amount of prestress loss. It is important to realize that the magnitude of these time-dependent strains are in turn dependent on the prestress loss. The prestress loss induced in the first place by the time-dependent concrete strain will lead to a change of concrete stress. This change in concrete stress will in turn affect the rate at which creep of the concrete takes place, thus affecting the overall rate at which the time-dependent concrete strain

proceeds. A similar interaction exists between the development of the time-dependent concrete strains and the stress relaxation of the steel. These complex interactions are approximately accounted for in the analysis by discretising the analysis in the time domain and following the relevant basic assumptions outlined in Sect. 3.6.

The prestress losses due to the various time-dependent effects as predicted by the three analyses are summarized for each of the instrumented segments in Table 5.2. The losses presented in this table represent the total losses from erection of each segment due to each of the time-dependent effects including the corrections due to elastic recovery of the concrete. The effects of the moment redistribution due to each of these time-dependent effects on the prestressing force, although accounted for in the analytical procedure, are not included in these values.

Comparison of the time-dependent losses predicted by Analysis 2 with those predicted by Analysis 3 reveals that the sum of the losses due to shrinkage and creep are larger for the case of Analysis 2 while the losses due to relaxation are larger for the case of Analysis 3. This trend applies to all three segments considered and is most probably due to the fact that the higher losses due to creep and shrinkage as predicted by Analysis 2 led to lower steel stresses which in turn led to lower relaxation losses as compared to the values predicted by Analysis 3. The higher value of the concrete modulus of elasticity used for Analysis 3 also possibly contributed to this trend because it is associated with smaller concrete strains for instantaneous elastic effects which will lead to higher steel stresses and consequently higher relaxation losses. It is important to note that the total prestressing force, and consequently the steel stress, predicted by Analysis 2 is consistently lower than those predicted by Analysis 3 at all times. This may be verified by inspection of Figures 5.1 through 5.3.

A similar comparison of the prestress losses predicted by Analysis 1 with those predicted by Analysis 2 yields the somewhat surprising result that although the sum of the creep and shrinkage losses predicted by Analysis 1 are larger than those predicted by Analysis 2, the relaxation losses predicted by Analysis 1 are also larger. This trend, which applies to all three of the instrumented segments, apparently contradicts the trend established by the comparison of the results of Analysis 2 with those of Analysis 3. The explanation lies in the manner in which the prestress losses developed. Inspection of Figures 5.1 through 5.3 reveals that during the initial period under load the total predicted loss of prestressing force is somewhat less for the case of Analysis 1. This means that during this initial time period the steel stresses predicted by Analysis 1 were higher and consequently the predicted losses due to relaxation proceeded at a higher rate than for the case of Analysis 2. Because the greatest part of the expected relaxation loss takes place during the initial time period under load, it appears that the diminished rate at which the predicted prestress losses developed for the case of Analysis 1 was a prime contributor to the trend described above. It is of interest to note that since the reduced rate at which the predicted prestress losses developed for the case of Analysis 1 may be related to the manner in which the rheological properties of the concrete (specifically shrinkage) are affected by the varying outdoor environment to which the structure was actually subjected, the trends described above serve to illustrate some of the effects of the complex interaction of creep, shrinkage and relaxation on the time-dependent behavior of the structure. Although the differences in the predicted values of relaxation loss referred to above are small, the trends established by the comparisons are useful in explaining some of the aspects of the time-dependent losses of prestressing force.

5.3 Bending Moment

One of the features that characterizes the behavior of segmental prestressed concrete bridges built by the cantilever method is the time-dependent redistribution of bending moment. References (41) and (46) point out that for the case of a continuous prestressed concrete bridge cast in-situ on falsework creep will not induce any time-dependent redistribution of bending moment because the creep strains in the structure are allowed to develop in a stress field that corresponds to the original boundary conditions of the structure. In general, this statement is true only when the restraining effect of the steel reinforcement is ignored. In the present study this restraining effect is accounted for by the procedure followed to account for the effects of elastic recovery. For the case of bridges built by the cantilever method the stress field set up by the self-weight of the structure obeys the boundary conditions that correspond to a cantilever. When adjacent cantilevers are joined to form new intermediate structures the original boundary conditions are altered so that creep will then develop under a stress field that does not correspond to the original boundary conditions. The resulting creep deflections must, however, satisfy the current boundary conditions. In order to meet this requirement in statically indeterminate intermediate structures, bending moments are generally induced in the structure. The same reasoning may be applied to the explanation of the development of the time-dependent redistribution of bending moment due to creep resulting from stresses induced in the structure by loads applied to intermediate structures that do not constitute the final structure. Examples of such loads are the secondary moments due to stressing of continuity tendons of statically indeterminate intermediate structures and the change in moment resulting from the release of supports.

In the above, the creep effects due to different causes were artificially separated for purposes of illustration. In the real structure these effects take place simultaneously and interact with one another. The

effects of shrinkage and relaxation will also in general induce a time-dependent redistribution of bending moment. Once again, it should be kept in mind that creep, shrinkage and relaxation interact with one another with regard to the development of the redistribution of bending moment.

The structural mechanism whereby the change in bending moment due to the time-dependent effects develops may readily be illustrated as follows. Assume that the time-dependent concrete strains of a statically indeterminate intermediate structure develops independently of the boundary conditions. The structure is then rendered statically determinate by artifically removing all the interior supports so that the boundary conditions correspond to those of a simply supported beam. Using these boundary conditions and the time-dependent strains described above, the deflected shape of the structure may be determined. In general, the deflection of this statically determinate structure at the positions of the various interior supports will not be zero so that point loads must be applied at these positions to restore the geometric boundary conditions. The total bending moments induced in the equivalent statically determinate structure by these point loads constitute the change in bending moment due to the time-dependent effects.

Inspection of Figures 5.4 through 5.9 will reveal that the effect of the time-dependent properties of concrete and steel is to induce time-dependent changes in bending moment that are positive everywhere in the structure. That is, the magnitudes of the negative bending moments decrease with time while the magnitudes of the positive bending moments increase with time. The bending moments at the interior supports and in the mid-span regions of the interior spans at the time at which the final structure was completed and at the last time interval of these analyses are summarized in Tables 5.3 and 5.4. These tables also present the percentage change in predicted bending moment that takes place during the time period defined by the times at which the bending moments are presented. The percentage change

was based on the value of bending moment existing at the time at which the final structure was completed. It should be noted that the total values of bending moment include the secondary moments due to the stressing of the continuity tendons of statically indeterminate intermediate structures.

The results of all three analyses indicate that the percentage changes in bending moment in the support regions are small when compared to the percentage changes that take place in the mid-span regions. The results of Analysis 1 indicate an 11 percent decrease in moment at pier 1 and a 42 percent increase in the mid-span moment of span 2. It is of interest to note that for each analysis the bending moments at the different piers tend to more or less the same value with the passage of time. A similar trend may be observed for the mid-span moments of the interior spans. Percentage-wise, the largest change in support moment takes place at pier 1 and the largest change in positive moment occurs in span 2. The trend is consistently established by the results of all three analyses. Tables 5.3 and 5.4 as well as Figures 5.7 through 5.9 clearly show that at the time of completion of the final structure the negative bending moment at pier 1 is larger than those at the remaining piers and that the positive mid-span moment of span 2 is less than those of the other interior spans.

Seen in the light of the tendency of the time-dependent redistribution of bending moment to equalize the negative bending moments at the piers and to equalize the positive mid-span moments of the interior spans, as well as the tendency to induce changes of moment that are positive everywhere in the structure, it may be expected that the greatest change in bending moment would take place in the regions identified above for the time period under consideration. It should be realized that prior to the time at which the final structure was completed the bending moments in the component structures constituting intermediate structure 9 were subjected to redistribution.

It should be noted that up to the time that the continuity of intermediate structure 9 was established, all three analyses predict the same value of bending moment at each of the three instrumented segments and no redistribution of moment was predicted during this time period (see Figures 5.4 through 5.6). These results are due to the fact that during this time period the instrumented segments formed part of the double cantilever SB1, a structure that is statically determinate. Further inspection of Figures 5.4 through 5.6 will also reveal that for the time period during which the instrumented segments formed part of intermediate structure 9 the rate of change of bending moment was somewhat less than that associated with the time period during which the segments formed part of the final structure. This observation is generally true for the results generated by all three analyses. Because this trend is somewhat contrary to what may be expected when the shapes of the specific creep and shrinkage curves as well as the rate at which relaxation proceeds are considered, the explanation for this trend should in part be sought in the change of boundary conditions of the structure associated with the construction procedure. The manner in which the time-dependent bending moment varies along the structure is also of importance in this regard.

At a particular point in time the time-dependent change in bending moment must vary linearly along each span in order to satisfy the conditions of static equilibrium. Thus for the side-spans the time-dependent change in moment varies linearly from a non-zero positive value at the interior support to zero at the outer support. For the interior spans the time-dependent change in moment varies linearly from a positive value at one support to another positive value at the other support. It should thus be clear that since the change in moment does not approach zero anywhere along an interior span as for the case of a side-span, the change in moments at sections along an interior span should be larger than those for sections along a side-span, especially as the section considered approaches the outer

support where no change in moment takes place. This is substantiated by inspection of the bending moment diagrams presented in Figures 5.7 through 5.9. For intermediate structure 9 the instrumented segments formed part of a side-span while for the final structure they were contained in an interior span so that during the time period associated with intermediate structure 9 the time-dependent changes of bending moment at the instrumented segments were smaller than those that took place during the time period associated with the final structure. This argument is supported by the observation that the above-mentioned trend becomes more pronounced as the segment considered is located closer to pier 1 (see Figures 5.4 through 5.6). Specifically for the case of segment SB1-N1, which is located very close to pier 1, a negligible amount of moment redistribution was predicted for the time period associated with intermediate structure 9 (see Figure 5.4). From a designer's point of view it is of interest to note that the greatest time-dependent change in shear force most probably takes place in the side-spans due to the fact that the greatest variation of the time-dependent change in moment with distance appears to take place within these spans.

The time-dependent change of bending moment predicted by Analysis 1 was consistently larger than the changes predicted by the other two analyses for the time period associated with the final structure. Comparing the total negative bending moments at pier 1 at the time up to which the analyses were carried, Analysis 2 and Analysis 3 yielded values that were 3.5 and 2.2 percent larger than the value predicted by Analysis 1, respectively. A similar comparison of the mid-span moment of span 2 shows that Analysis 2 and Analysis 3 yielded values that were 9.8 and 9.5 percent smaller than the values predicted by Analysis 1, respectively. Bearing in mind the large difference in the values of total concrete strain predicted by Analysis 3 as compared to the results of the other two analyses, the differences in the bending moments at the supports predicted by the three

analyses are very small. It is, however, important to note that for the case of the positive mid-span moments the differences in the values predicted by Analysis 1 as compared to the values predicted by Analysis 2 and Analysis 3 are not negligible. For purposes of design it is the growth of positive moment that is of prime importance when accounting for the effects of the time-dependent moment redistribution so that it would appear that the effects of the outdoor environment on the time-dependent material properties of concrete are of some importance as far as the time-dependent increase of positive moment is concerned.

Inspection of Tables 5.3 and 5.4 reveals that for the time period associated with the final structure the percentage change in bending moment predicted by Analysis 3 was greater than the change predicted by Analysis 2 for the support as well as the mid-span regions. This trend is also present in the instrumented segments as illustrated by Figures 5.4 through 5.6. In fact, for segments SB1-N1 and SB1-N9 the total negative bending moments at the time up to which the analyses were carried as predicted by Analysis 2 are larger than those predicted by Analysis 3. The positive bending moment at segment SB1-N16 as predicted by Analysis 2 is less than the value predicted by Analysis 3. These observations are surprising, especially when viewed in the light of the substantially greater time-dependent concrete strains predicted by Analysis 2 as compared to the magnitude of the strains predicted by Analysis 3. Bearing in mind the structural mechanism whereby the change in bending moment due to the time-dependent effects develop, it is clear that the magnitude of this change in bending moment is dependent not only on the time-dependent deformations but also on the modulus of elasticity of the concrete. For given time-dependent deformations a higher value of the modulus of elasticity of the concrete will lead to greater time-dependent changes in bending moment. As previously indicated, the value of the modulus of elasticity of the concrete used with Analysis 3 was substantially greater than the value used with

Analysis 2. It would, therefore, appear that as far as the time-dependent redistribution of bending moment is concerned, the effects of the greater time-dependent concrete strains predicted by Analysis 2 was offset by the effects of the lower value used for the modulus of elasticity of concrete, as compared to the case of Analysis 3.

It should be pointed out that the explanation given above belies the extremely complicated nature of the various interactions that influence the development of the time-dependent change in bending moment. The changes in bending moment induce changes in concrete and steel stress which, in turn, influence the rate at which the time-dependent strains develop. Bearing in mind that it was these time-dependent strains which originally induced the change in bending moment it should be clear that these interactions are not simple and do not readily lend themselves to a simple explanation of observed behavior.

The time-dependent redistribution of bending moment is of importance in the design of prestressed concrete bridges constructed in segments by the cantilever method. Specifically, the relatively large increase of the positive moments in the mid-span regions is important. In the quarter-span regions the sense of the bending moment may even change (see Figures 5.7 through 5.9). It is necessary to account for these effects in the design of the type of structure under consideration herein by providing either tensioned or non-tensioned reinforcement to resist the increase of positive bending moment, otherwise, unwanted cracking may develop in the affected regions. Such cracks have, in fact, been found to develop in structures similar to the one under consideration herein, where no provision was made for the substantial time-dependent increase in positive bending moment (41).

5.4 Concrete Stress

The effect of the time-dependent material properties of the concrete and steel is to induce a loss in prestressing force as well as a redistribution of bending moment in the structure. Generally, these effects lead

directly to a time-dependent change in concrete stress in the structure. In this section the concrete stresses predicted by the three analyses are presented and discussed. Unless explicitly stated otherwise, all stresses referred to herein are compressive concrete stresses.

The stress histories for the extreme top and bottom fibers of each of the instrumented segments as predicted by each of the three analyses are presented in Figures 5.10 through 5.15. The concrete stresses at each of the instrumented segments at the time at which the final structure was completed and at the time up to which the analyses were carried are presented in Table 5.5. The percentage change of these stresses, based on the value of stress at the time of completion of the final structure, that took place during the time period associated with the final structure is also summarized.

The general trends indicated by the figures and table referred to above are that the stresses in the top fibers increase with time while the stresses in the bottom fibers decrease with time. The only exception to these trends is to be found in the stress history of segment SB1-N1 for the time period corresponding to intermediate structure 9, during which the top fiber stress decreases with time and no significant change in the bottom fiber stress takes place.

In order to explain these observed trends it is necessary to indicate how the time-dependent changes in prestressing force and bending moment each affect the stress in the extreme fibers of a particular segment. Because the effect of the time-dependent redistribution of bending moment is to induce a change in moment that is positive everywhere in the structure (see Sect. 5.3), the effect of the time-dependent change in bending moment will be to increase the compressive stresses in the top fibers and to decrease the compressive stresses in the bottom fibers. Furthermore, a given change in bending moment at a particular section will tend to induce a change in stress of greater magnitude in the bottom fiber than in the top fiber. The reason for this lies in the fact that the bottom fiber of all the

sections in the bridge being analyzed is located at a greater distance from the centroid of the section than the top fiber. According to beam theory, the magnitude of the stress at any fiber due to an applied moment is linearly related to the distance of the fiber to the centroid of the section.

Within the realm of ordinary beam theory the total change of stress due to a loss of prestressing force may be considered as the superposition of the changes of stress due to two effects. The first effect is associated with the change in axial thrust. This stress is uniformly distributed through the depth of the section and corresponds to the stress resulting from a force of magnitude equal to the change in prestressing force applied at the centroid of the section. The second effect accounts for the location of the tendons relative to the centroid of the section. This stress is linearly distributed through the depth of the section and corresponds to the stress resulting from a moment applied at the centroid of the section. The magnitude of this moment is equal to the product of the change in prestressing force and the eccentricity of the tendons measured from the centroid of the section. When these two stress distributions are superimposed it should be clear that for the extreme fiber on one side of the section centroid they will be additive while for the extreme fiber on the opposite side of the centroid they will oppose each other so that the sense of the resulting stress will depend on the relative magnitudes of the stresses set up by the thrust and moment effects.

Since the three instrumented segments were not similarly reinforced, it is necessary to consider the effects of the loss of prestressing force on the extreme fiber stresses separately for each segment. For the case of segment SB1-N1 the majority of the tendons were located in the top flange so that a loss of prestressing force would be accompanied by a decrease in the top fiber stress and a much smaller decrease in bottom fiber stress. The change in bottom fiber stress could possibly have been an increase in stress depending on the relative magnitudes of the stresses due to the thrust and moment effects, as explained above. For the case of

segment SB1-N16 the majority of the tendons were located in the bottom flange so that the effects of the loss of prestressing force at this segment may be expected to be opposite to those associated with segment SB1-N1. Thus, at segment SB1-N16 the loss of prestressing force may be expected to induce a decrease in the bottom fiber stress. Depending on the relative magnitudes of the stresses due to the thrust and moment effects, the associated change of the top fiber stress will be a smaller decrease in stress than for the case of the bottom fiber, or may even be an increase in stress. At segment SB1-N9 the tendons are divided between the top and bottom flanges in such a manner that an equal loss of prestressing force in each tendon will lead to a more or less equal decrease in stress in the top and bottom fibers. It is, however, not reasonable to expect that the magnitude of the loss of prestressing force in each tendon will be the same so that the decrease in stress at the extreme fibers due to loss of prestress are most probably not equal. The difference in the change of extreme fiber stresses is most probably smaller for the case of segment SB1-N9 than for the case of either segment SB1-N1 or segment SB1-N16 so that segment SB1-N9 represents an intermediate case relative to the other two segments.

The combined effects of the time-dependent change in bending moment and loss of prestressing force on the extreme fiber concrete stresses may best be illustrated by consideration of the appropriate stress histories of segment SB1-N1 (see Figures 5.10 and 5.11). For this particular segment the stresses due to the loss in prestressing force tend to oppose those due to the change in bending moment. For the time period associated with intermediate structure 9, segment SB1-N1 was located close to the outer support of a side-span so that no significant time-dependent change in bending moment may be expected to have taken place at this segment during this time period (see also Sect. 5.3). It would thus appear that for this time period the concrete stress at segment SB1-N1 was primarily influenced by the prestress loss. This means that the top fiber concrete stresses may be

expected to have decreased while the bottom fiber stresses may be expected not to have changed substantially during this time period. Inspection of Figures 5.10 and 5.11 will reveal that the predicted extreme fiber stresses indeed follow these trends for the time period under consideration.

For the time period associated with the final structure, segment SB1-N1 formed part of an interior span so that the time-dependent change in bending moment during this time period was no longer negligible here (see Sect. 5.3). Thus, for this time period the loss of prestressing force as well as the time-dependent change in bending moment simultaneously influence the stress at the extreme fibers of the section under consideration. Furthermore, as pointed out before, the influence of these effects will oppose each other. Figures 5.10 and 5.11 clearly indicate that for this time period the effects on the extreme fiber stresses associated with the time-dependent change in bending moment was dominant; i.e., the top fiber stress increased with time while the bottom fiber stress decreased with time. This observation is further substantiated by the fact that the magnitude of the stress change in the extreme bottom fiber is greater than that of the stress change in the extreme top fiber (for segment SB1-N1 the extreme bottom fiber is located further from the centroidal axis than the extreme top fiber).

For segments SB1-N9 and SB1-N16 the percentage increase in top fiber stress as well as the percentage decrease in bottom fiber stress for the time period associated with the final structure are both substantially larger than for the case of segment SB1-N1 (see Table 5.5). For segment SB1-N9 this trend was most probably due to the fact that the effects of the loss of prestressing force on the concrete stress were, to a greater extent than in the case of segment SB1-N1, of secondary importance relative to the effects of the time-dependent change in bending moment. In the case of segment SB1-N16 the effects of the loss of prestressing force on the concrete stress added to the effects of the time-dependent change in bending moment.

It thus seems reasonable to conclude that the effects of the time-dependent change of bending moment were of prime importance as far as the

magnitude of the concrete stress was concerned, while the effects of the loss of prestressing force were, relatively speaking, of secondary importance.

Comparing the magnitudes of the stresses predicted by each of the analyses at the time up to which they were carried, it appears as if Analysis 1 predicted the largest top fiber stresses and the smallest bottom fiber stresses. The only exception to this observation is the case of the top fiber stresses of segment SB1-N1 where Analysis 3 predicted the largest stresses (see Figures 5.10 through 5.15 and Table 5.5). This trend is most probably due to the fact that the loss of prestressing force as well as the time-dependent change in bending moment as predicted by Analysis 1 were larger than the values predicted by the other two analyses.

Comparing the final stresses predicted by Analysis 2 and Analysis 3 with the values predicted by Analysis 1, the largest percentage difference in the top fiber stresses appear to be at segment SB1-N16 where Analysis 2 and Analysis 3 both predict values that are 10 percent smaller than the value predicted by Analysis 1. A similar comparison of the predicted bottom fiber stresses indicates that the largest percentage difference for the case of Analysis 2 is at segment SB1-N9 and for the case of Analysis 3 is at segment SB1-N16 where the predicted values are 15 and 17 percent larger than the values predicted by Analysis 1, respectively. These comparisons only apply to the instrumented segments. It is furthermore of interest to note that at section SB1-N1, where the concrete stresses in both the extreme top and bottom fibers were larger than at the other instrumented segments, the final top and bottom fiber stresses predicted by Analysis 2 and Analysis 3 were less than 5.5 percent different from the values predicted by Analysis 1.

Finally, the close agreement of the concrete stresses predicted by Analysis 2 and Analysis 3 is of interest from the point of view of design, especially when viewed in the light of the substantial differences in the concrete strains predicted by these two analyses. It thus appears that for the specific case of the Kishwaukee River Bridge the concrete stresses may be satisfactorily determined by making use of the recommendations of the C.E.B.

(11) to establish the material properties of the concrete for use with the time-dependent analysis of the structure.

5.5 Influence of Construction Loads

One of the unique features of the launching girder used for the erection of the segments comprising the Kishwaukee River Bridge was that it did not normally impose significant loads on the structure. However, just after the completion of intermediate structure 9 the launching girder was placed in such a position so that it imposed major loads on the structure. The magnitude and position of these loads are indicated by Figure 5.16. The girder remained in this position until just prior to the time at which the closure segment of span 1 was cast. It thus appears that intermediate structure 9 was subjected to these construction loads for a period of approximately 5 months.

It is of some interest to study the influence of these construction loads on the time-dependent behavior of the structure. In order to achieve this aim the structure was analyzed taking into account the loads illustrated by Figure 5.16. For purposes of analysis these loads were applied at the time at which the tendons which establish continuity of intermediate structure 9 were stressed. The loads were removed at the time of casting of the closure segment of span 1. The material properties obtained experimentally from the outdoor stored specimens were assigned to the concrete. The results of this analysis, designated as Analysis 4, may therefore be directly compared to the results of Analysis 1 in order to illustrate some of the effects of the presence of the construction loads on the time-dependent behavior of the structure.

The percentage differences in the results predicted by Analysis 1 and Analysis 4 at the time up to which the analyses were carried are presented for each of the instrumented segments in Table 5.6. These percentages are based on the final values predicted by Analysis 1. Inspection of this

table will reveal that the differences in the predicted values, and consequently the effects of the construction loads on the time-dependent behavior of the structure, are of negligible importance for practical purposes. Of the quantities considered in Table 5.6 it appears as if the concrete strains are affected to the greatest extent by the presence of the construction loads, the maximum difference in predicted final concrete strain being less than 3.3 percent at the sections considered. The concrete strains in the extreme top fibers are decreased while the strains in the bottom fibers are increased by the effects of the construction loads. For the final concrete stresses at the extreme fibers this trend is reversed, i.e. the top fiber stresses are increased while the bottom fiber stresses are decreased by the presence of the construction loads. The total prestressing force is increased at segments SB1-N1 and SB1-N9, while it is decreased at segment SB1-N16 by the application and removal of the construction loads. For the case of Analysis 4 as compared with Analysis 1, the magnitude of the bending moments at the instrumented segments is greater in the negative moment region while it is less in the positive moment region. It would thus appear that the time-dependent moment redistribution was slightly inhibited by the application of the construction loads.

The development of the concrete strains at the extreme fibers of segment SB1-N1 as predicted by Analysis 1 and Analysis 4 is illustrated in Figure 5.17. For the time period associated with the application of the construction loads it appears as if the greatest part of the decrease in top fiber strain and increase in the bottom fiber strain as predicted by Analysis 4 was a result of the elastic response of the concrete to the increase in negative moment at this section caused by the application of the construction loads. However, when the construction loads are removed from the structure a residual decrease in the top fiber strains and a residual increase in bottom fiber strains are predicted by Analysis 4 relative to the results predicted by Analysis 1. For the time period during which the

construction loads were applied to the structure the presence of these loads decreased the top fiber stresses while it increased the bottom fiber stresses at segment SB1-N1 (see Figure 5.18). In the light of this behavior of the concrete stresses it appears reasonable to assume that the residual decrease in the top fiber concrete strain was primarily due to the diminished creep associated with the decreased top fiber concrete stress during this time period. Similarly, the residual increase in the bottom fiber concrete strain appears to have been primarily due to the increased creep associated with the increased bottom fiber concrete stress during this time period.

For times greater than the time at which the construction loads were removed the development of the concrete strains at both extreme fibers of segment SB1-N1 seem to have been essentially unaffected by the previous presence of the construction loads (see Figure 5.17). For this time period the only effect on the time-dependent strains appears to have been the residual strains developed during the time period during which the construction loads were applied to the structure. These observations are substantiated by the fact that for times greater than the time of removal of the construction loads the concrete strain versus time curves predicted by Analysis 1 and Analysis 4 for segment SB1-N1 are more or less parallel for both the top and bottom fiber strains (see Figure 5.17).

It should be kept in mind that both Analysis 1 and Analysis 4 made use of the rate of creep method to predict the creep of concrete under a variable state of stress because specific creep curves corresponding to only one age at loading were available for the outdoor stored specimens. It should thus be pointed out that the insensitivity of the behavior of the time-dependent strains to the previous presence of the construction loads for times beyond the time at removal of these loads should be seen partly in the light of the property of the rate of creep method to ignore the previous stress history as discussed in Sect. 3.2.2.

The concrete stresses and bending moments at segment SB1-N1 as predicted by both Analysis 1 and Analysis 4 are presented in Figures 5.18 and 5.19. These figures clearly demonstrate that the time-dependent component of the concrete stresses at both the top and bottom fibers, as well as the time-dependent component of the bending moment are essentially unaffected by the application and removal of the construction loads. Considering the extreme fiber concrete stresses and the bending moment, the only significant difference in the results predicted by Analysis 1 and Analysis 4 appears to occur during the time period during which the construction loads were applied to the structure. The decrease in top fiber stress and the increase in bottom fiber stress at segment SB1-N1, due to the application of the construction loads, are consistent with the increase in negative moment here, due to these loads. Once the construction loads are removed, the results predicted by Analysis 1 and Analysis 4 are the same for all practical purposes.

It is of some interest to investigate some of the effects of the application of the construction loads on the vertical deflection of the structure. The downward transverse deflections of the free cantilever tip (segment SB1-S17) of intermediate structure 9 as predicted by Analysis 1 and Analysis 4 at the times of application and removal of the construction loads are presented in Table 5.7. This cantilever eventually formed part of span 1 of the final structure. It should be pointed out that these deflections cannot be directly compared to the actual deformations of the structure due to the unknown magnitude of the corrections in vertical alignment that were made during the construction process. The differences in the deflections at the time of application of the construction loads and at the time of removal of these loads may, however, be expected to be comparable to the change in actual deflection that took place during this time period.

Considering the change in downward deflection of the free cantilever tip of intermediate structure 9 for the time period during which the construction loads were applied to the structure, Analysis 1 predicted a

change in downward deflection of 1.609 in. (40.9 mm) while Analysis 4 predicted a change in deflection of 2.005 in. (50.9 mm). It may thus be concluded that the effect of the application of the construction loads on the downward deflection of the free cantilever tip for the time period described above is to increase this deflection by 0.396 in. (10.0 mm). A similar comparison of the deflections of segment SB1-N16 as predicted by Analysis 1 and Analysis 4 reveals that for the time period during which the construction loads were applied to the structure the upward deflection of this segment was increased by 0.073 in. (1.9 mm) by the presence of these loads. It is of interest to note that for the time period associated with the final structure the previous application and removal of the construction loads appear to have decreased the downward change in deflection of segment SB1-N16 that takes place during this time period by 0.07 percent.

In conclusion, it would thus appear, that as far as the time-dependent components of the concrete stresses, prestressing force and bending moments are concerned, the effects of the presence of the construction loads are negligible for practical purposes. The concrete strains and, consequently, the transverse deflections seem to be affected to a greater extent than the quantities mentioned above. It furthermore appears as if most of this effect on the deformations takes place during the time period during which the construction loads are applied to the structure and that once these loads are removed the time-dependent behavior of the deformations seems to be essentially unchanged. The elastic effects associated with the application of the construction loads are not small and should be accounted for in the design process.

6. CONCLUSIONS AND RECOMMENDATIONS FOR FURTHER STUDY

The conclusions and recommendations for further study presented in the following section are based on the results of the various analyses of the Kishwaukee River Bridge as well as the results of the comparison of measured deformations of the actual structure with computed deformations. The differences in the analyses of the Kishwaukee River Bridge lie in the material properties assigned to the concrete. Concrete material properties experimentally obtained from outdoor stored and indoor stored specimens, as well as those prescribed by the C.E.B. recommendations, were used in the different analyses. The conclusions drawn herein apply, strictly speaking, only to the Kishwaukee River Bridge so that generalizations to include other structures of a similar type should be made with the utmost care.

Based on the comparison of measured deformations of the Kishwaukee River Bridge with the analytically obtained deformations, the following conclusions and recommendations for further study may be made:

1. The analytical procedure used for the time-dependent analysis of the structure performed satisfactorily. This is particularly apparent when consideration is given to the excellent agreement of the measured and computed concrete strains for the case where the concrete material properties obtained experimentally from outdoor stored specimens were used in the analytical procedure.
2. The procedure introduced during the course of this study for the estimation of the creep of concrete subjected to a varying state of stress appears to have performed satisfactorily. In this regard it is important to note that the rate of creep method yielded satisfactory results. The proposed procedure for estimating the creep of concrete reduces to the rate of creep method where specific creep curves corresponding

to only one particular age at loading are available, as was the case for the analysis that utilized the concrete material properties obtained experimentally from outdoor stored specimens.

3. Compared with the measured strains, the analysis that made use of concrete material properties obtained experimentally from outdoor stored specimens yielded the best results. In this regard the analysis that made use of the concrete material properties as prescribed by the C.E.B. recommendations yielded results that were poor, with the predicted strains being smaller than the measured values. The magnitude of the strains predicted by the analysis that made use of the material properties obtained from the laboratory stored specimens compared well with the measured values at the time up to which the analyses were carried.
4. For the particular structure under consideration herein the development of the total time-dependent strains was governed to a large extent by the manner in which the shrinkage of concrete developed and this was partly due to the fact that the segments were relatively old when erected. Because the shrinkage curve obtained from the outdoor specimens was the only one which reflected the seasonal fluctuations that characterize the shrinkage of concrete subjected to a variable outdoor environment, the analysis which made use of the material properties obtained from outdoor stored specimens was the only one which correctly predicted the development of the total time-dependent concrete strains. This particular conclusion serves to emphasize the necessity of using material properties obtained from outdoor stored specimens in order to correctly predict the behavior of the time-dependent concrete strains for structures of the type under consideration herein. These material properties may be expected to reflect the effects of the variable outdoor

environment to which the structure is subjected on the rheological properties of the concrete.

5. For the analysis which employed the concrete material properties obtained from outdoor stored specimens the seasonal dependence of shrinkage was, strictly speaking, correctly included only for the instrumented double cantilever because the same shrinkage curve was used for all the segments. This effect, however, did not appear to significantly influence the behavior of the segments studied. It is strongly recommended that this matter be made the topic of a further study which would involve the use of different shrinkage curves each of which would be associated with a different cantilever so that the seasonal effects are correctly accounted for. It should be mentioned that it appears as if the season during which the concrete is cast has an influence on the subsequent development of shrinkage. Thus, a study such as the one mentioned above would involve a substantial experimental effort because shrinkage curves would have to be determined separately to correctly account for the seasons during which the segments for the different double cantilevers are cast. Measures should be taken to insure that the seasonal fluctuations of shrinkage are carefully recorded, especially at later ages, when determining the shrinkage curves for outdoor stored specimens.
6. The procedure used in this study to modify the experimentally obtained creep and shrinkage curves to include the effects of the size and shape of the member on creep and shrinkage performed satisfactorily. There is, however, a great need for further study in this regard especially as far as experimental work is concerned. It is strongly recommended that a study of this nature should include the effects of size and shape on the creep and shrinkage of members stored outdoors.

7. An extensive comparison of calculated and measured deflections was not possible as a result of the effects of the failure of certain joints between adjacent segments on the completed structure and the questionable reliability of the measured values due to the extremely adverse conditons under which they were taken. The sense of the time-dependent changes of deflection at the instrumented segments were the same for both the measured and calculated values. The magnitudes of the time-dependent changes in transverse deflection of the completed structure are extremely small while the relative magnitudes of the time-dependent change in deflection as predicted by the three analyses are consistent with the relative magnitudes of the predicted concrete strains. In order to predict the actual deflections of the structure correctly, it is necessary to account for deflections induced in the structure by certain construction activities such as alignment corrections and the seating of the double cantilevers on permanent bearings. It appears as if a major portion of the time-dependent strain induced an axial shortening of the completed structure.

Based on a consideration of the prestressing force, bending moments and concrete stresses predicted by the analyses of the Kishwaukee River Bridge the following conclusions may be drawn:

8. The magnitude of the total time-dependent loss of prestressing force is small and the development of this loss of prestressing force with time closely reflects the manner in which the total time-dependent concrete strains develop. The total loss of prestress due to relaxation is slightly less than that due to creep, while the loss due to shrinkage is substantially less than the losses due to either creep or relaxation. The relatively small time-dependent loss of prestressing force is in part due to the reduced time-dependent concrete strain which goes hand-in-hand with the relatively great age at which the segments were erected.

9. The time-dependent redistribution of bending moment tends to reduce the magnitude of the negative bending moments and to increase the magnitude of the positive bending moments in the structure. The tendency is for the negative bending moments at the interior supports to approach the same value. A similar tendency is exhibited by the positive mid-span bending moments of the interior spans. The percentage change of the negative bending moments at the interior supports are relatively small when compared with the large percentage change of the positive mid-span bending moments of the interior spans. This large change in positive bending moment is important and must be accounted for in the design of the type of structure under consideration herein. The rate at which the time-dependent change of bending moment proceeds at a particular section of the structure depends on the construction sequence.
10. The effect of the time-dependent behavior of the concrete and steel on the extreme fiber concrete stresses in the completed structure is to increase the top fiber compressive stresses and to decrease the bottom fiber compressive stresses with time. The magnitude of the decrease in bottom fiber stress is greater than the magnitude of the increase in top fiber stress. Both the loss of prestressing force and the time-dependent change of bending moment induce changes of concrete stress. Of the two contributory effects, the time-dependent change in bending moment seems to be the more important. When the intermediate structure being considered is statically determinate no time-dependent change of bending moment takes place and consequently the time-dependent change of concrete stress for this case is governed by the loss of prestressing force. A similar situation arises in a statically indeterminate intermediate structure when the segment considered is located close to an outer support.

11. Generally the magnitudes of the total prestressing force, bending moments and concrete stresses as predicted by the analyses that make use of the concrete material properties obtained experimentally from laboratory stored specimens and those prescribed by the C.E.B. recommendations do not differ significantly. This conclusion is of significance when viewed in the light of the great difference that exists in the magnitude of the concrete strains predicted by these two analyses. The predicted deformations of the structure thus seem to be much more sensitive to the material properties assigned to the concrete than the predicted prestressing force, bending moments and concrete stresses. Since approximate procedures for determining the rheological properties of concrete are usually used in the design of these structures and since the time-dependent behavior of these structures is primarily a problem of serviceability, it is suggested that the time-dependent deformations of the structure be emphasized as a design criterion when considering the serviceability requirements of the structure.
12. The final magnitudes of the prestressing force, bending moments and concrete stresses as predicted by the analysis that makes use of the concrete material properties obtained experimentally from the outdoor stored specimens differ somewhat from the values predicted by the other two analyses.

Based on the analysis that includes the effects of the construction loads applied to the structure, the following conclusions may be drawn:

13. The time-dependent deformations of the structure are influenced to a much greater extent than the stresses and forces by the presence of the construction loads. This influence is, however, very small and appears to take place during the time of application of the loads. Once the loads are removed, the

time-dependent component of the behavior of the structure remains essentially unaffected. The effects of the construction loads on the time-dependent behavior of the prestressing force, bending moments and concrete stresses are, for practical purposes, negligible. Most of the effects of the construction loads on the structure are elastic in nature. These elastic effects are not small and should be accounted for in the design process.

The following general conclusions and recommendations may be made:

14. Generalizations in the type of bridge under consideration herein are very difficult because of the dependence of the time-dependent response of these structures on the construction history. A parametric study is, nonetheless, recommended. It is suggested that a simpler structure be considered for such a study.

15. The continuation of obtaining field data in terms of both measurements of the deformations of actual structures as well as obtaining material properties of concrete from outdoor stored specimens is strongly recommended.

LIST OF REFERENCES

1. ACI Committee 209, Subcommittee I, "Effects of Concrete Constituents, Environment, and Stress on Creep and Shrinkage of Concrete," ACI SP-27, Designing for Effects of Creep, Shrinkage, and Temperature in Concrete Structures, Detroit, 1971, pp. 1-42.

2. ACI Committee 209, Subcommittee II, "Prediction of Creep, Shrinkage and Temperature Effects in Concrete Structures," ACI SP-27, Designing for Effects of Creep, Shrinkage, and Temperature in Concrete Structures, Detroit, 1971, pp. 51-93.

3. Ali, I., and Kesler, C. E., "Mechanics of Creep in Concrete," ACI SP-9, Symposium on Creep of Concrete, Houston, 1964, pp. 35-57.

4. Anderson, T. C., Houdeshell, D. M., and Gamble, W. L., "Construction and Long Term Behaviour of 1/8th Scale Prestressed Concrete Bridge Components," Structural Research Series No. 384, Civil Engineering Studies, University of Illinois, Urbana, October 1972.

5. Ballinger, C. A., Podolny, W., and Abrahams, M. J., "A Report on the Design and Construction of Segmental Prestressed Concrete Bridges in Western Europe - 1977," U. S. Department of Transportation, Federal Highway Administration, Report No. FHWA-RD-78-44, July 1978.

6. Bazant, Z. P., "Prediction of Concrete Creep Effects using Age-Adjusted Effective Modulus Method," ACI Journal, Proc., Vol. 69, April 1972, pp. 212-217.

7. Belmain, M., and Le Bourdelles, Y., "Etude du Retrait et des Deformations de Flange dans un Pont en Beton Precontraint Construit par Encorbellement," Annales des Ponts et Chaussees, No. II, 1971, pp. 81-103.

8. Bennett, E. W., and Loat, D. R., "Shrinkage and Creep of Concrete as Affected by the Fineness of Portland Cement," Magazine of Concrete Research, Vol. 22, No. 71, June 1970, pp. 69-78.

9. Breen, J. E., Cooper, R. L., and Gallaway, T. M., "Minimizing Construction Problems in Segmentally Precast Box Girder Bridges," Research Report 121-6F, Center for Highway Research, University of Texas at Austin, Aug. 1975.

10. Brown, R. C., Burns, N. H., and Breen, J. E., "Computer Analysis of Segmentally Erected Precast Prestressed Box Girder Bridges," Research Report 121-4, Center for Highway Research, University of Texas at Austin, Nov. 1974.

11. C. E. B. (European Concrete Committee), "International Recommendations for the Design and Construction of Concrete Structures, Principles and Recommendations," June 1970.

12. Danon, J. R., and Gamble, W. L., "Time-Dependent Deformations and Losses in Concrete Bridges Built by the Cantilever Method," Structural Research Series No. 437, Civil Engineering Studies, University of Illinois, Urbana, January 1977.

13. Davies, R. D., "Some Experiments on the Applicability of the Principle of Superposition to the Strains of Concrete Subjected to Changes of Stress, with Particular Reference to Prestressed Concrete," Magazine of Concrete Research, Vol. 9, No. 27, Nov. 1957, pp. 161-172.

14. Davis, R. E., Davis, H. E., and Brown, E. H., "Plastic Flow and Volume Changes of Concrete," Proceedings, ASTM 37, 1937, Part II, pp. 317-330.

15. Dilger, W., Ghali, A., Kountouris, C., "Time Dependent Forces Induced by Settlement in Continuous Prestressed Concrete Structures," Symposium, International Association for Bridge and Structural Engineering, Madrid, 1970, pp. 89-98.

16. Engineering News Record, "Twin box girder bridges develop cracks in joints," 31 May 1979, pp. 8-9; "Epoxy blamed for crack in bridge," 26 July 1979, p. 13; "Cracked bridge cured by pins through joints," 22 May 1980, p. 41.

17. England, G. L., and Ross, A. D., "Reinforced Concrete under Thermal Gradients," Magazine of Concrete Research, Vol. 14, No. 40, March 1962, pp. 2-12.

18. Fadl, A. I., and Gamble, W. L., "Time-Dependent Behavior of Noncomposite and Composite Post-Tensioned Concrete Girder Bridges," Structural Research Series No. 430, Civil Engineering Studies, University of Illinois, Urbana, October 1976.

19. Ghali, A., Neville, A. M., and Jha, P. C., "Effects of Elastic and Creep Recoveries of Concrete on Loss of Prestress," ACI Journal, Proc., Vol. 64, No. 12, Dec. 1967, pp. 802-810.

20. Ghali, A., Sisodiya, R. G., and Tadros, G. S., "Computer Program for Displacements and Losses in Multi-Stage Prestressed Members," Research Report, Civil Engineering Department, The University of Calgary, Calgary, Alberta, Canada, 1973.

21. Ghali, A., Sisodiya, R. G., and Tadros, G. S., "Displacements and Losses in Multistage Prestressed Members," Proc. ASCE, Journal of the Structural Division, Vol. 100, No. ST11, Nov. 1974, pp. 2307-2322.

22. Glodowski, R. J., and Lorenzetti, J. J., "A Method for Predicting Prestress Losses in a Prestressed Concrete Structure," PCI Journal, Vol. 17, No. 2, March/April 1972, pp. 17-31.

23. Godden, W. G., "Numerical Analysis of Beam and Column Structures," Prentice Hall Inc., London, 1965.

24. Greenspan, D., "Introduction to Numerical Analysis and Applications," Markham Publishing Company, Chicago, 1971.

25. Guyon, Y., "Limit State Design of Prestressed Concrete," Vol. 2, Halsted Press and John Wiley and Sons, 1974.

26. Hansen, T. C., and Mattock, A. H., "Influence of Size and Shape of Member on the Shrinkage and Creep of Concrete," ACI Journal, Proc., Vol. 63, No. 2, Feb. 1966, pp. 267-290.

27. Henneberger, W., and Breen, J. E., "First Segmental Bridge in the U. S.," Civil Engineering Magazine, ASCE, June 1974, pp. 54-57.

28. Hernandez, H. D., and Gamble, W. L., "Time-Dependent Prestress Losses in Pretensioned Concrete Construction," Structural Research Series No. 417, Civil Engineering Studies, University of Illinois, Urbana, May 1975.

29. Huang, T., "Anchorage Take-up Loss in Post-Tensioned Members," PCI Journal, Vol. 14, No. 8, Aug. 1969, pp. 30-35.

30. Illinois Department of Transportation, "Private Communication to W. L. Gamble and V. Marshall," March 1980, Aug. 1980, Sept. 1980 and Nov. 1980.

31. Illston, J. M., "The Delayed Elastic Deformation of Concrete as a Composite Material," International Conference on the Structure of Concrete, London, Cement and Concrete Association, 1965, pp. 24-36.

32. Kabir, A. F., "Nonlinear Analysis of Reinforced Concrete Panels, Slabs and Shells for Time-Dependent Effects," Report No. UC SESM 76-6, University of California at Berkeley, Dec. 1976.

33. Kashima, S., and Breen, J. E., "Construction and Load Tests of a Segmental Precast Box Girder Bridge Model," Research Report 121-5, Center for Highway Research, University of Texas at Austin, Feb. 1975.

34. Keijer, U., "Long-Term Deflections of Cantilever Prestressed Bridges," Sympoisum, International Association for Bridge and Structural Engineering, Madrid, 1970, pp. 27-34.

35. Khachaturian, N., and Gurfinkel, G., "Prestressed Concrete," McGraw-Hill Book Company, 1969.

36. Khalil, M. S. A., "Time-Dependent Non-Linear Analysis of Prestressed Concrete Cable-Stayed Girders and Other Concrete Structures," Ph.D. Thesis, University of Calgary, Calgary, Alberta, Canada, 1979.

37. Kokubu, M., Goto, Y., Ozaka, Y., Okamura, H., and Momoshima, S., "Measurements of Creep and Shrinkage in Actual Prestressed Concrete Bridges," Symposium, International Association for Bridge and Structural Engineering, Madrid, 1970, pp. 19-26.

38. Lacey, G. C., and Breen, J. E., "Long Span Prestressed Concrete Bridges of Segmental Construction, State of the Art," Research Report 121-1, Center for Highway Research, University of Texas at Austin, May 1969.

39. Lacey, G. C., and Breen, J. E., "The Design and Optimization of Segmentally Precast Prestressed Box Girder Bridges," Research Report 121-3, Center for Highway Research, University of Texas at Austin, Aug. 1975.

40. Leonhardt, F., "Prestressed Concrete: Design and Construction," W. Ernst, Berlin, 1964.

41. Libby, J. R., "Segmental Box Girder Bridge Superstructure Design," ACI Journal, Proc., Vol. 73, No. 5, May 1976, pp. 279-290.

42. Magura, D. D., Sozen, M. A., and Siess, C. P., "A Study of Stress Relaxation in Prestressing Reinforcement," PCI Journal, Vol. 9, No. 2, April 1964, pp. 13-57.

43. McHenry, D., "A New Aspect of Creep in Concrete and its Application to Design," Proc., ASTM, Vol. 43, 1943, pp. 1069-1084.

44. Mossiossian, V., "Mechanisms of Creep and Shrinkage in Plain, Reinforced and Prestressed Concrete," Department of Civil Engineering, University of Illinois, Urbana, May 1970.

45. Mossiossian, V., and Gamble, W. L., "Time-Dependent Behavior of Noncomposite and Composite Prestressed Concrete Structures under Field and Laboratory Conditions," Structural Research Series No. 385, Civil Engineering Studies, University of Illinois, Urbana, May 1972.

46. Muller, J., "Long-Span Precast Prestressed Concrete Bridges Built in Cantilever," ACI SP-23, First International Symposium on Concrete Bridge Design, 1969, pp. 705-740.

47. Muller, J., "Ten Years of Experience in Precast Segmental Construction," PCI Journal, Vol. 20, No. 1, Jan./Feb. 1975, pp. 28-61.

48. Nasser, K. W., and Neville, A. M., "Creep of Concrete at Elevated Temperatures," ACI Journal, Proc., Vol. 62, No. 12, Dec. 1965, pp. 1567-1579.

49. Neville, A. M., and Meyers, B. L., "Creep of Concrete: Influencing Factors and Prediction," ACI SP-9, Symposium on Creep of Concrete, Houston, 1964, pp. 1-31.

50. Neville, A. M., "Creep of Concrete: Plain, Reinforced, and Prestressed," North-Holland Publishing Company, Amsterdam, 1970.

51. Neville, A. M., "Properties of Concrete," 2nd Edition, Pitman Publishing Company, 1977.

52. Portland Cement Association, "Private Communication to W. L. Gamble," June 1979, May 1980, May 1980, Sept. 1980, Oct. 1980, and Nov. 1980.

53. Ross, A. D., "Creep of Concrete Under Variable Stress," ACI Journal, Proc., Vol. 54, No. 9, March 1958, pp. 739-758.

54. Shiu, K. N., Russel, H. G., Marshall, V., and Gamble, W. L., "Time-Dependent Behaviour of Segmental Cantilever Concrete Bridges," Portland Cement Association Report to State of Illinois, Department of Transportation, Oct. 1979 (limited circulation).

55. "Standard Method of Test for Creep of Concrete in Compression," C512-69, American Society for Testing and Materials, Philadelphia, Pa.

56. "Standard Test Method for Compressive Strength of Cylindrical Concrete Specimens," C39-72, American Society for Testing and Materials, Philadelphia, Pa.

57. Troxell, G. E., Raphael, J. M., and Davis, R. E., "Long-Time Creep and Shrinkage Tests of Plain and Reinforced Concrete," Proceedings, ASTM 58, 1958, pp. 1101-1120.

58. van Zyl, S. F., "Analysis of Curved Segmentally Erected Prestressed Concrete Box Girder Bridges," Report No. UC SESM78-2, University of California at Berkeley, Jan. 1978.

59. Zienkiewicz, O. C., and Watson, M., "Some Creep Effects in Stress Analysis with Particular Reference to Concrete Pressure Vessels," Nuclear Engineering and Design, No. 4, 1966, pp. 406-412.

Table 4.1: Comparison of the Time-Dependent Change of Concrete Strain Predicted by the Three Analyses

Segment	Position of Fiber	Analysis 1	Analysis 2	Analysis 3
SB1-N1	Top	1	0.77	0.55
	Bottom	1	0.83	0.53
SB1-N9	Top	1	0.88	0.61
	Bottom	1	0.93	0.58
SB1-N16	Top	1	1.02	0.67
	Bottom	1	0.98	0.64

Note: The time period considered above corresponds to the time period defined by the time at which continuity of intermediate structure 9 was established up to the time up to which the analyses were carried.

All changes of strain are expressed as fractions of the changes predicted by Analysis 1.

Table 4.2: Measured Change in Deflection of Segment SB1-N16

Time (Days)	Deflection of Segment SB1-N16 (in.)
0	0
13	0.40
91	0.78
174	0.72
260	0.84
288	0.85
538	1.38

Note: All changes in deflection are taken relative to the deflection at day 0.

Day 0 corresponds to the time at which the final structure was completed.

The failure of the joints between the segments was discovered just prior to day 13.

1 in. = 25.4 mm.

Table 5.1: Total Prestressing Force and Prestress Loss as Predicted by Analysis 1, Analysis 2 and Analysis 3

Segment	Analysis	Prestress Loss (%)	Final Prestress Force as a Fraction of the Value Calculated by Analysis 1	
SB1-N1	1	8.7	1	(11,068 kips)*
	2	7.1	1.01	
	3	5.6	1.04	
SB1-N9	1	8.6	1	(6,020 kips)*
	2	7.9	1.01	
	3	6.1	1.03	
SB1-N16	1	9.6	1	(5,628 kips)*
	2	9.4	1.00	
	3	7.4	1.03	

Note: The prestress losses refer to the time-dependent component of prestress loss that occurred during the time period defined by the time at which the continuity tendons for intermediate structure 9 were stressed up to the time up to which the analyses were carried. These losses are expressed as percentages of the values that existed just after the continuity tendons for intermediate structure 9 were stressed.

The final values of prestressing force refer to the values existing at the time up to which the analyses were carried.

* Final Force from Analysis 1.

1 kip = 4.448 kN.

Table 5.2: Total Prestress Losses Due to Shrinkage, Creep and Relaxation

Segment	Analysis	Prestress Loss Due To:		
		Shrinkage (kips)	Creep (kips)	Relaxation (kips)
SB1-N1	1	183	587	403
	2	241	440	398
	3	143	303	418
SB1-N9	1	100	292	223
	2	137	226	219
	3	80	157	226
SB1-N16	1	80	374	208
	2	123	308	203
	3	73	213	214

Note: 1 kip = 4.448 kN

Table 5.3: Redistribution of Support Moments for the Time Period Corresponding to the Final Structure

Pier	Analysis	Bending Moment (k-ft)		Change in Bending Moment (%)
		Time at Completion of Final Structure	Time up to which Analysis was Carried	
1	1	81,352	72,394	11.0
	2	81,247	74,926	7.8
	3	81,125	73,957	8.8
2	1	76,880	72,459	5.8
	2	76,724	74,371	3.1
	3	79,130	75,205	5.0
3	1	78,461	73,095	6.8
	2	77,776	74,975	3.6
	3	79,582	75,360	5.3
4	1	76,520	72,105	5.8
	2	77,402	74,958	3.2
	3	78,779	75,059	4.7

Note: The analysis was continued for 600 days after the final structure was completed.

1 k-ft = 1.356 kN-m

Table 5.4: Redistribution of Mid-Span Moments for the Interior Spans for the Time Period Corresponding to the Final Structure

Span	Analysis	Bending Moment (k-ft)		Change in Bending Moment (%)
		Time at Completion of Final Structure	Time up to which Analysis was Carried	
2	1	15,994	22,706	42.0
	2	16,124	20,478	27.0
	3	14,982	20,547	37.1
3	1	17,441	22,328	28.0
	2	17,864	20,435	14.4
	3	15,753	19,823	25.8
4	1	17,605	22,509	27.9
	2	17,505	20,135	15.0
	3	15,910	19,891	25.0

Note: The analysis was continued for 600 days after the final structure was completed.

1 k-ft = 1.356 kN-m

Table 5.5: Change of Concrete Stress for the Time Period Corresponding to the Final Structure

Segment	Analysis	Concrete Stress (ksi)				Change in Stress (%)	
		Time at Completion of Final Structure		Time up to which Analysis was Carried		Top Fiber	Bottom Fiber
		Top Fiber	Bottom Fiber	Top Fiber	Bottom Fiber		
SB1-N1	1	0.49	1.36	0.55	1.17	12.2	14.0
	2	0.47	1.36	0.52	1.23	10.6	9.6
	3	0.51	1.35	0.58	1.20	13.7	11.1
SB1-N9	1	0.40	0.81	0.52	0.53	30.0	34.6
	2	0.39	0.80	0.47	0.61	20.5	23.8
	3	0.39	0.82	0.50	0.60	28.2	26.8
SB1-N16	1	0.26	0.96	0.39	0.65	50.0	32.3
	2	0.26	0.93	0.35	0.73	34.6	21.5
	3	0.24	0.99	0.35	0.76	45.8	23.2

Note: All the stresses are compressive.

The analysis was continued for 600 days after the final structure was completed.

1 ksi = 6.895 N/mm^2.

Table 5.6: Percentage Difference in the Final Results Predicted by Analysis 1 and Analysis 4

Segment	Concrete Strain		Concrete Stress		Prestressing Force	Bending Moment
	Top Fiber	Bottom Fiber	Top Fiber	Bottom Fiber		
SB1-N1	- 3.28	2.45	0.73	- 0.09	0.27	- 0.06
SB1-N9	- 2.75	3.29	0.19	- 0.19	0.03	- 1.14
SB1-N16	- 0.84	0.59	0.00	- 0.15	- 0.05	- 0.01

Note: The final results refer to the predicted results at the time up to which the analyses were carried.

A negative sign indicates a decrease in the particular quantity as predicted by Analysis 4 relative to the result predicted by Analysis 1.

All percentages are based on the final values predicted by Analysis 1.

Table 5.7: Effect on Free Cantilever Tip Deflection Due to Application and Removal of Construction Loads

Time	Deflection Predicted by Analysis 1 (in.)	Deflection Predicted by Analysis 4 (in.)
Just prior to application of construction loads	1.626	1.626
Just after application of construction loads	1.626	2.272
Just prior to removal of construction loads	3.235	4.277
Just after removal of construction loads	3.235	3.607

Note: Downward deflections are taken positive.

1 in. = 25.4 mm.

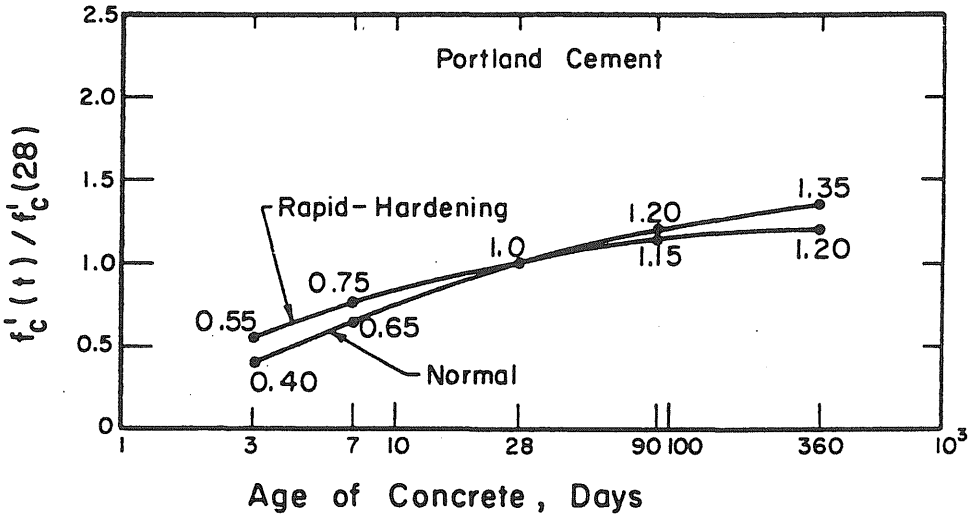

Fig. 2.1 Ratio of Compressive Strength at Age t to that at 28 Days According to European Concrete Committee

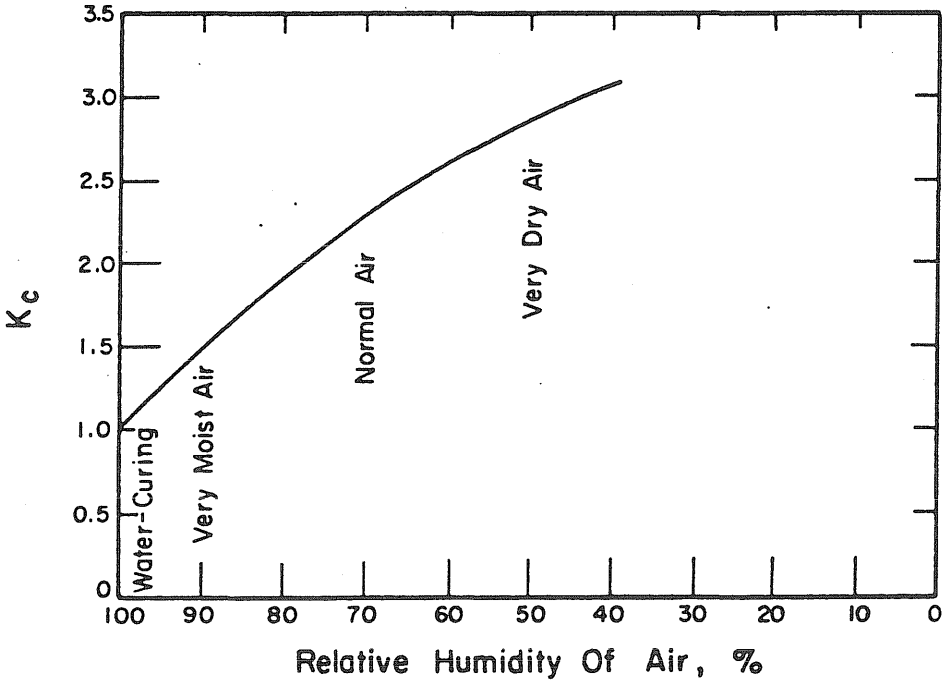

Fig. 2.2 European Concrete Committee Creep Prediction Factor Coefficient K_c vs. Relative Humidity

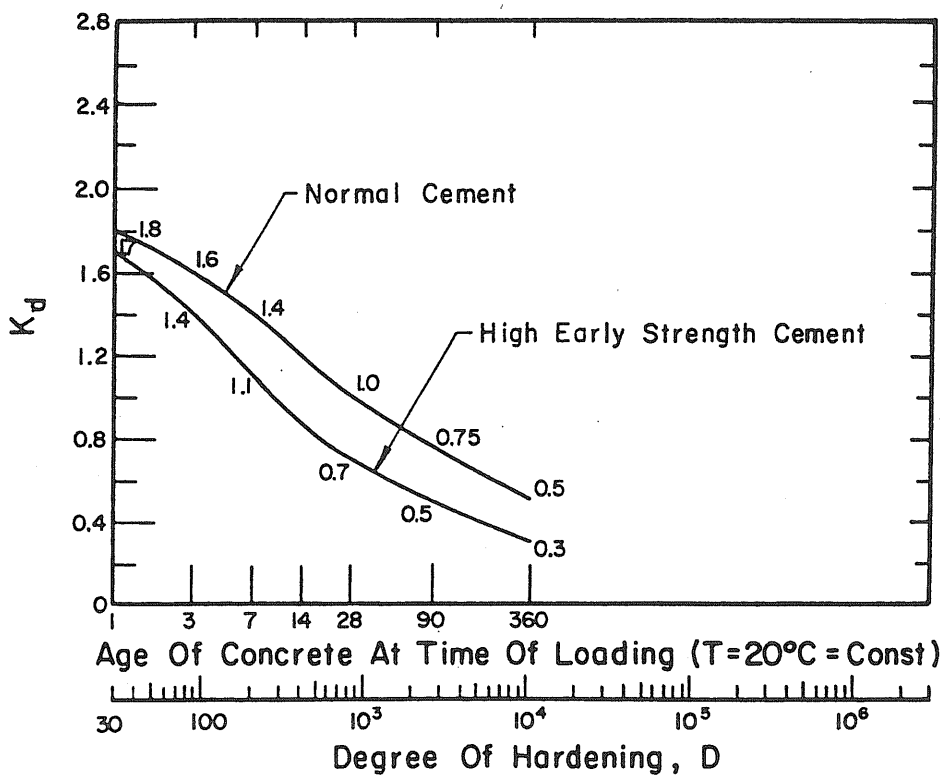

Fig. 2.3 European Concrete Committee Creep Prediction Factor Coefficient K_d vs. Age at Loading

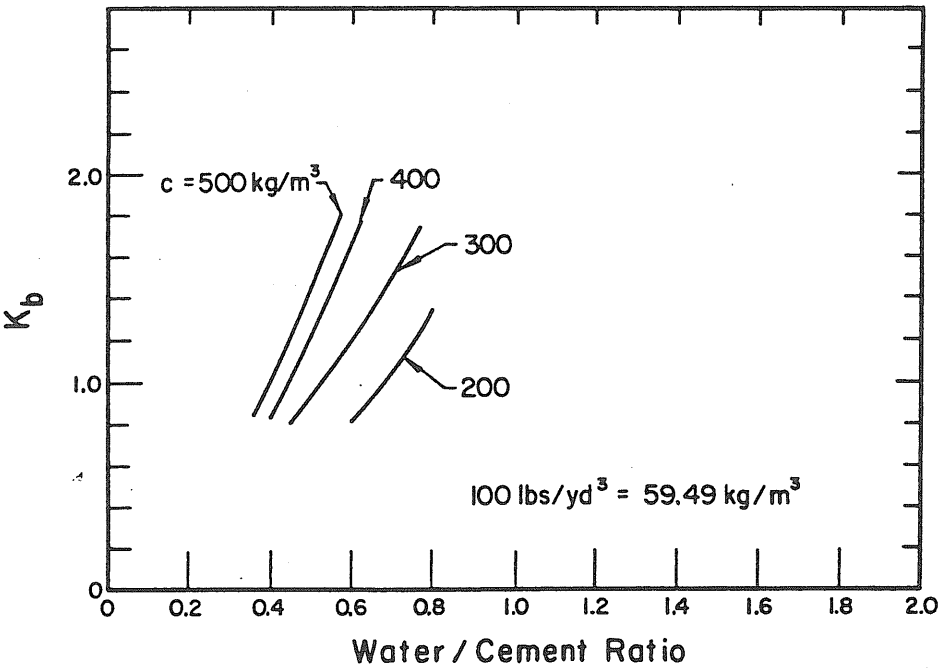

Fig. 2.4 European Concrete Committee Creep Prediction Factor Coefficient K_b vs. Mix Properties

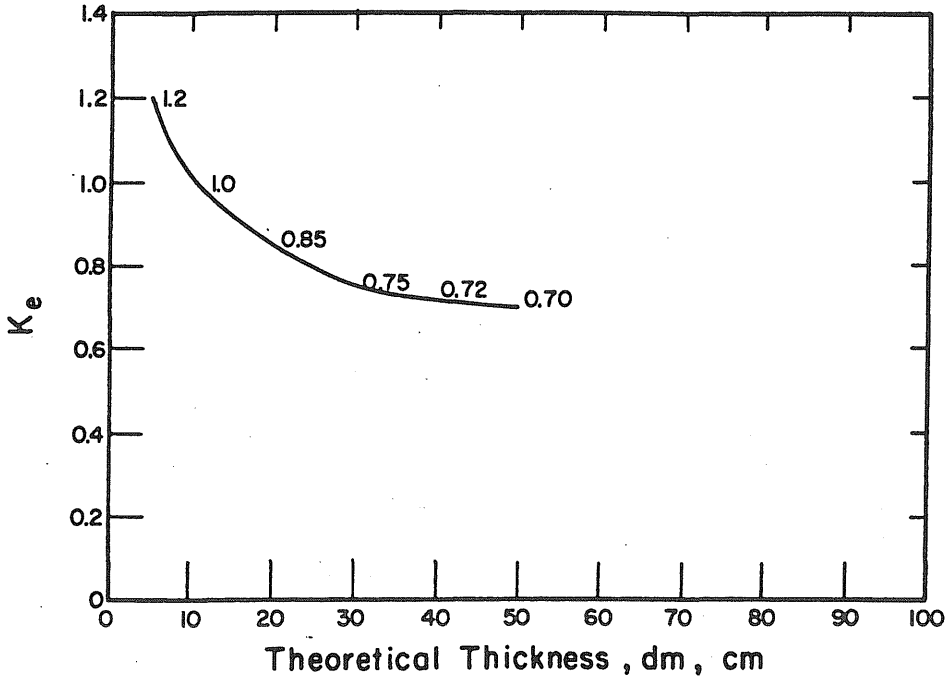

Fig. 2.5 European Concrete Committee Creep Prediction Factor Coefficient K_e vs. Theoretical Thickness

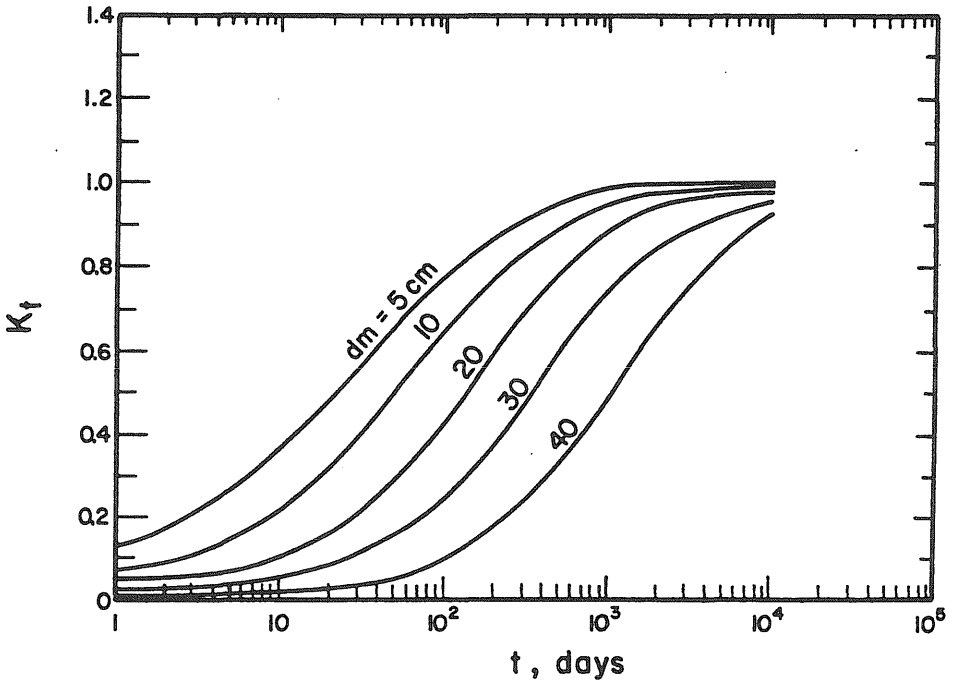

Fig. 2.6 European Concrete Committee Creep Prediction Factor Coefficient K_t vs. Time

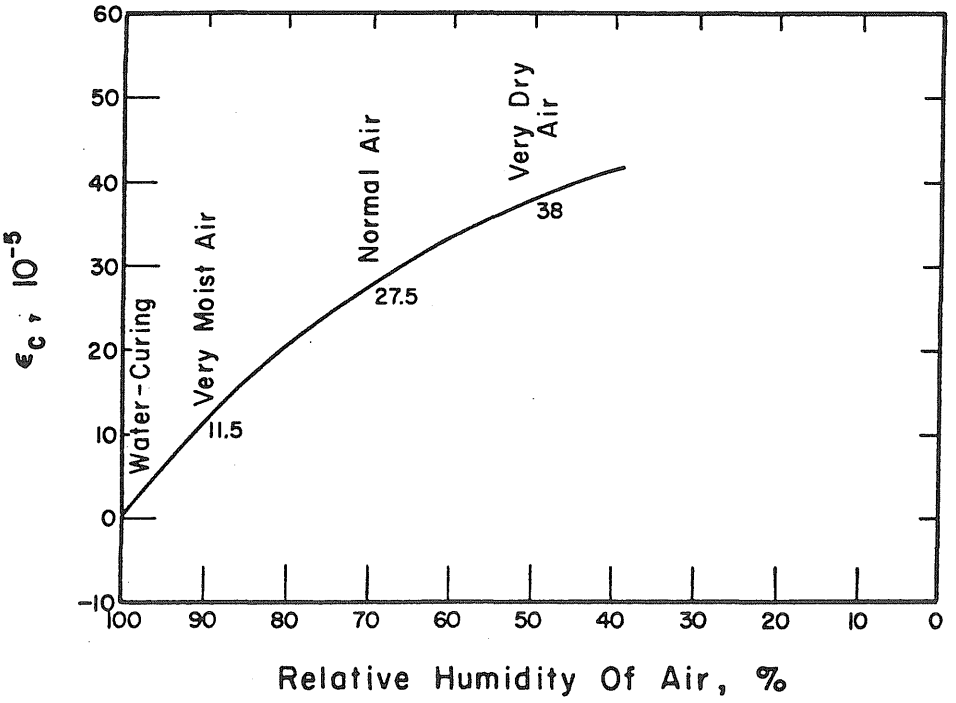

Fig. 2.7 European Concrete Committee Shrinkage Prediction Factor Coefficient ε_c vs. Relative Humidity

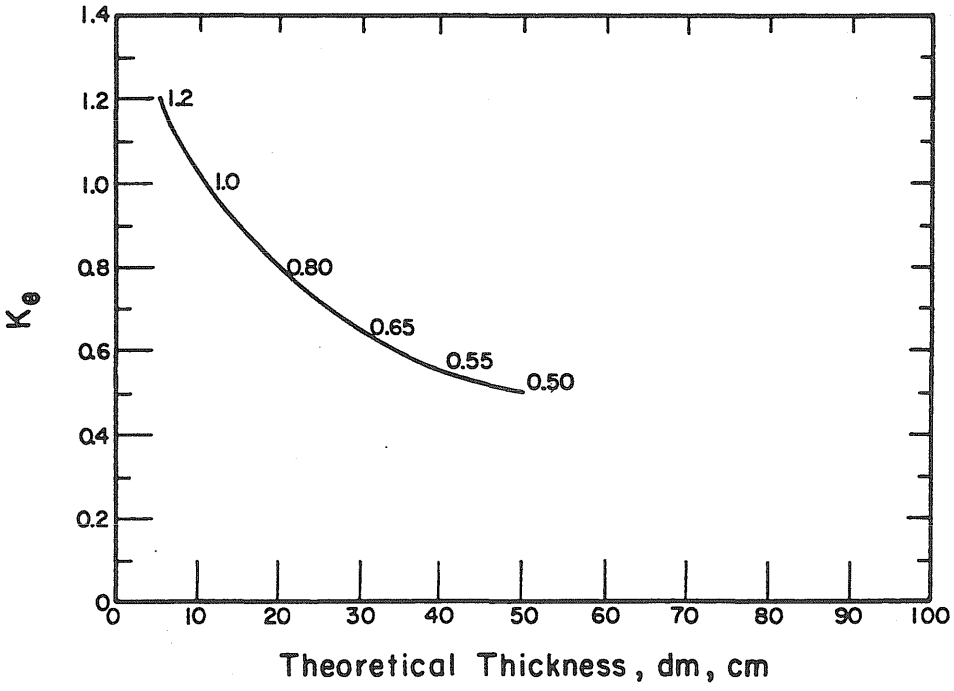

Fig. 2.8 European Concrete Committee Shrinkage Prediction Factor Coefficient K_e vs. Theoretical Thickness

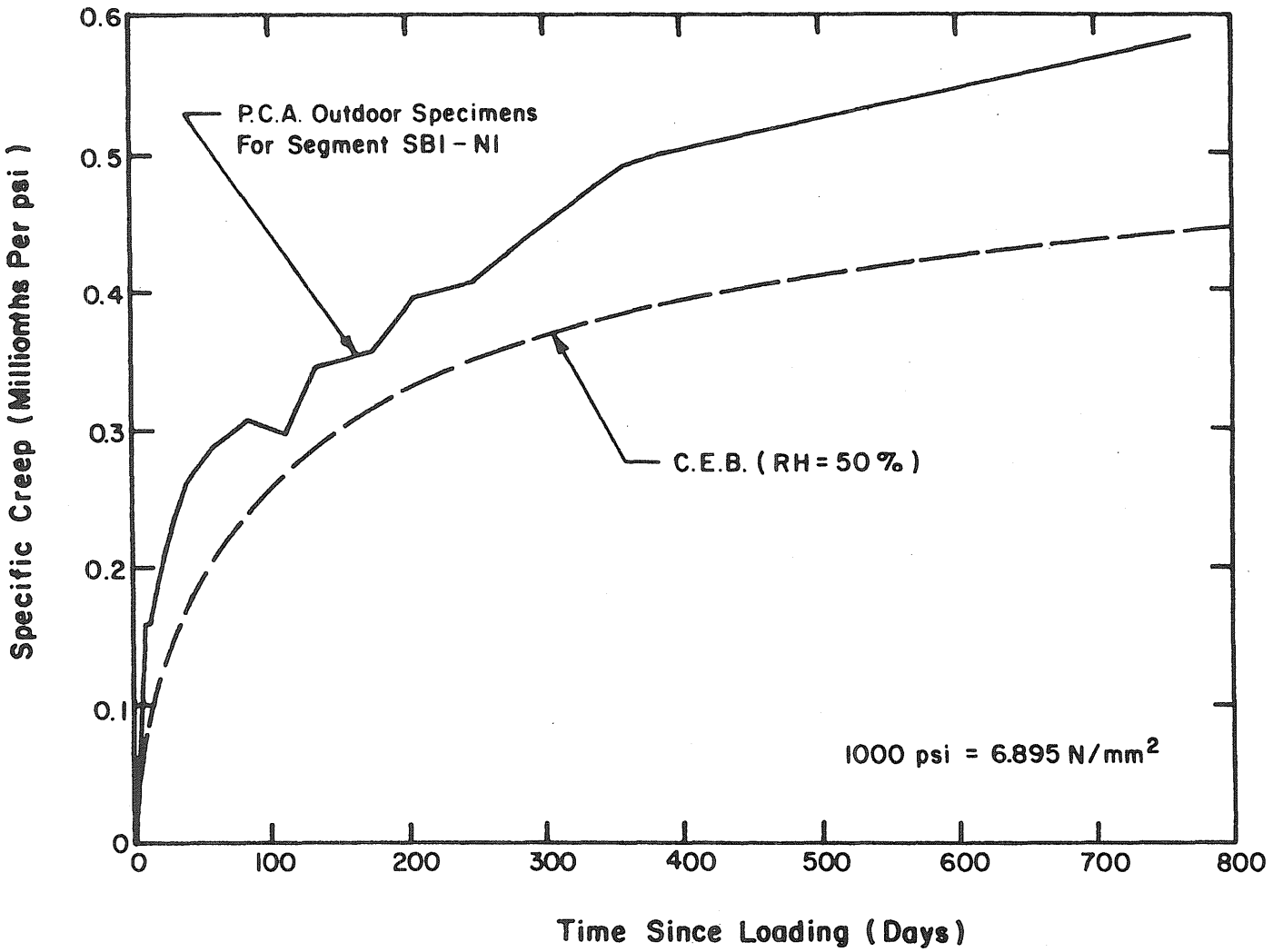

Fig. 2.9 Measured and Predicted Specific Creep Curves for Outdoor Stored Creep Specimens (Segment SB1-N1)

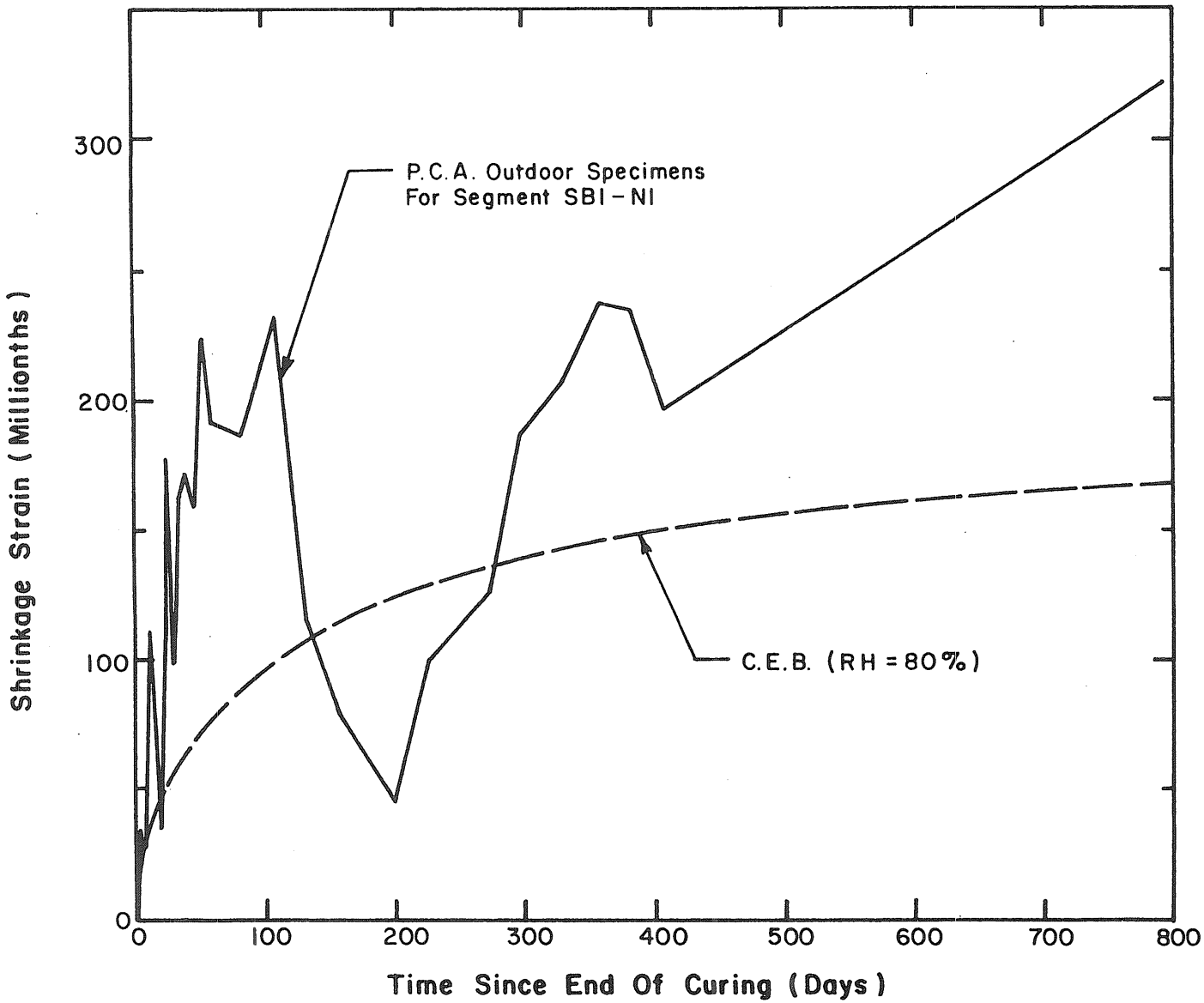

Fig. 2.10 Measured and Predicted Shrinkage Curves for Outdoor Stored Shrinkage Specimens (Segment SB1-N1)

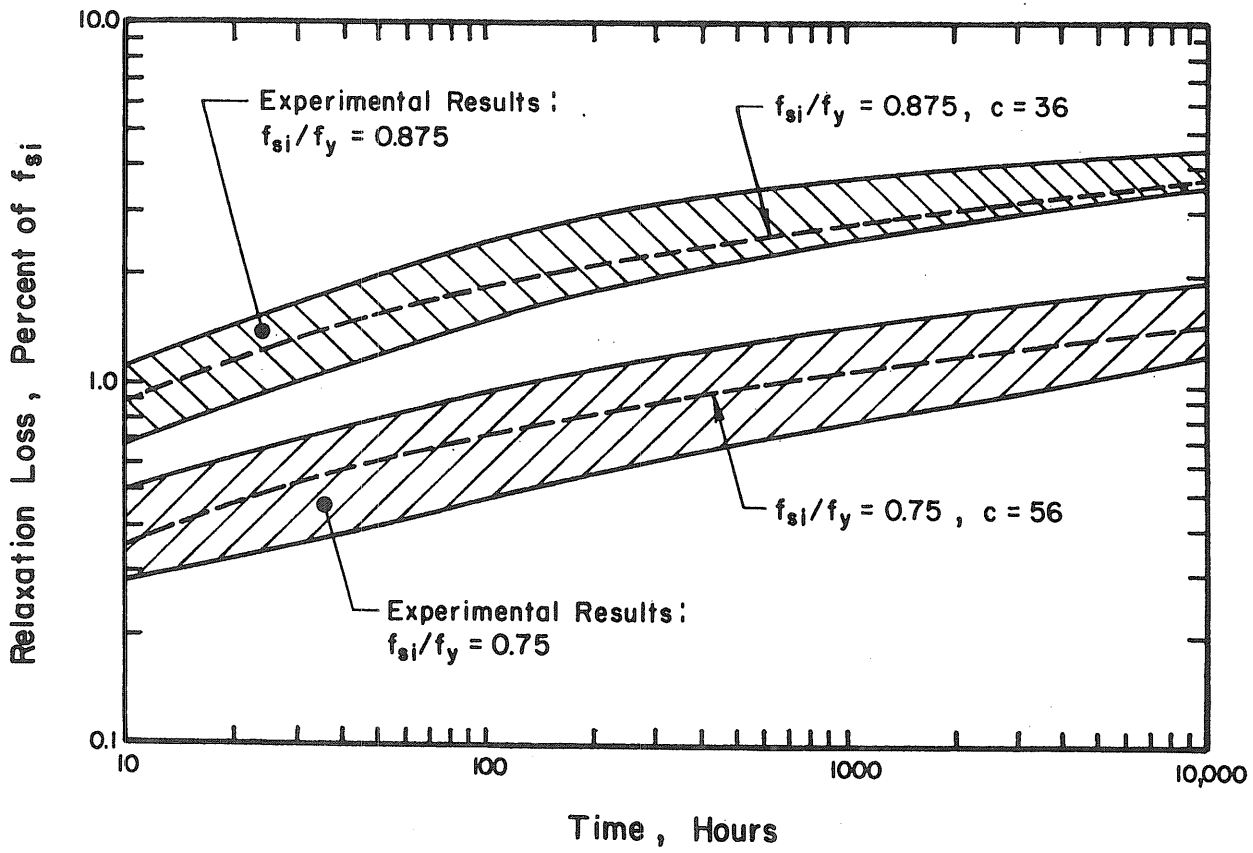

Fig. 2.11 Fit of Eq. 2.9 to Experimentally Obtained Relaxation Data for Dywidag Bars

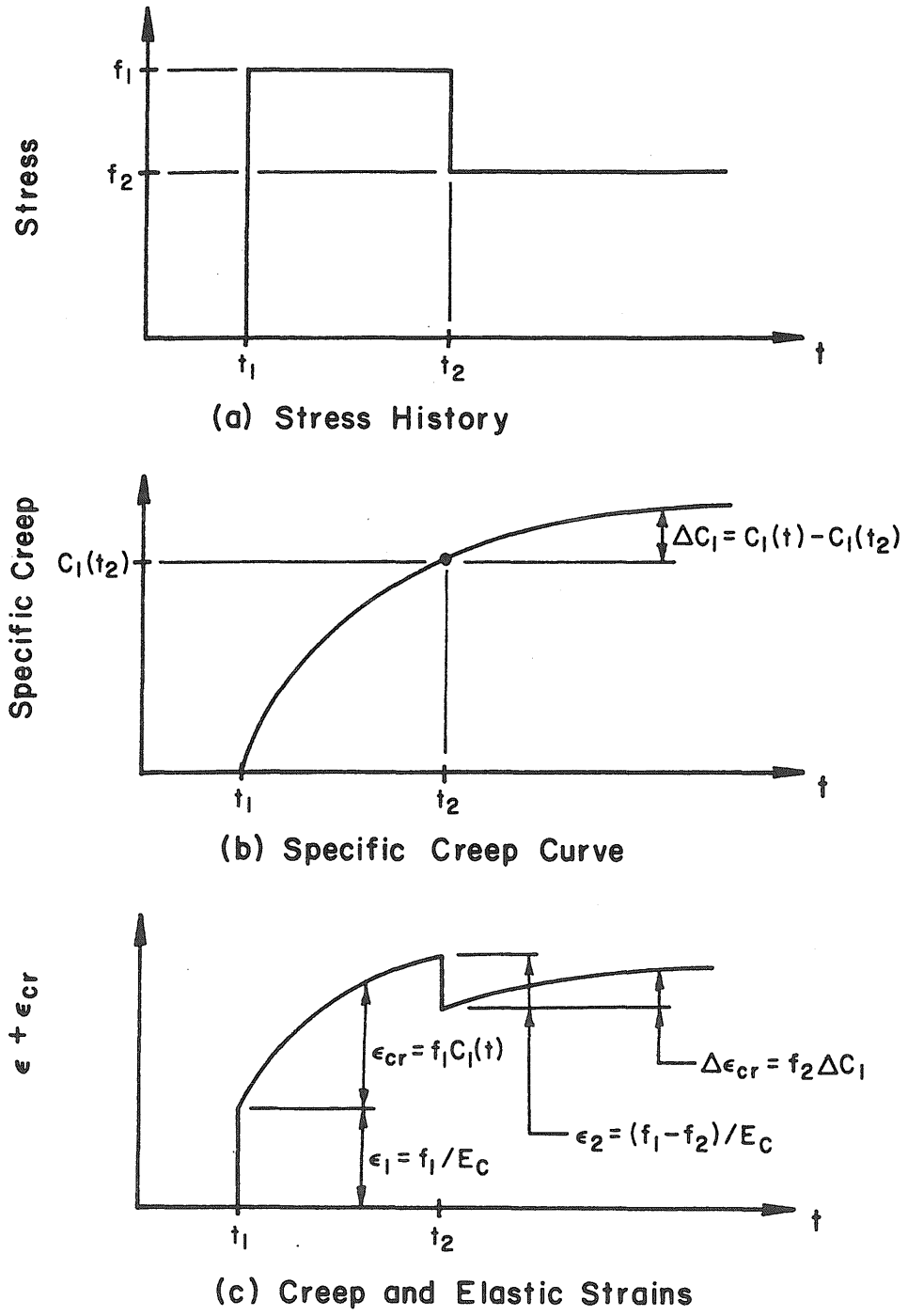

Fig. 3.1 Prediction of Creep Under Variable Stress According to the Rate of Creep Method

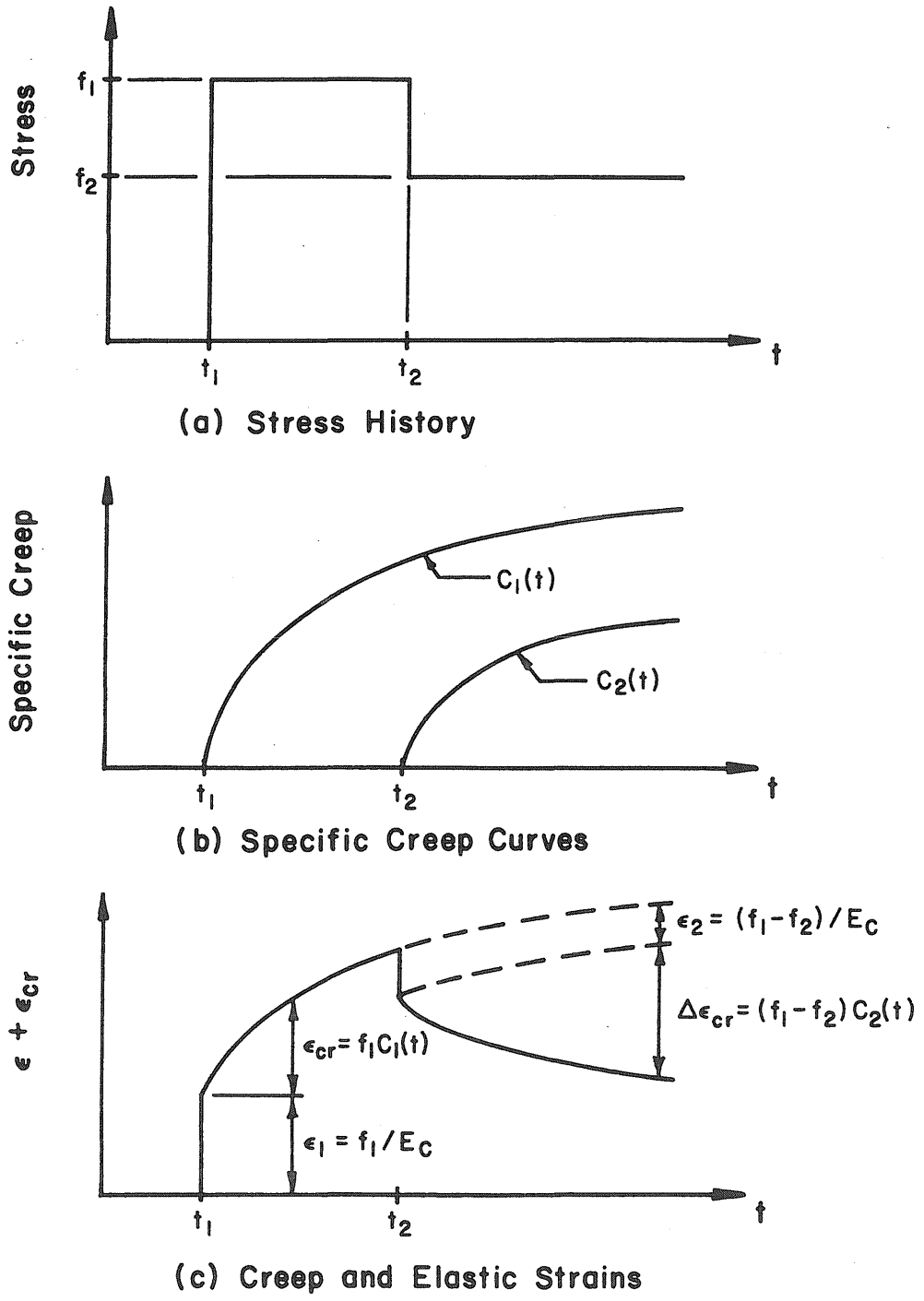

Fig. 3.2 Prediction of Creep under Variable Stress According to the Method of Superposition

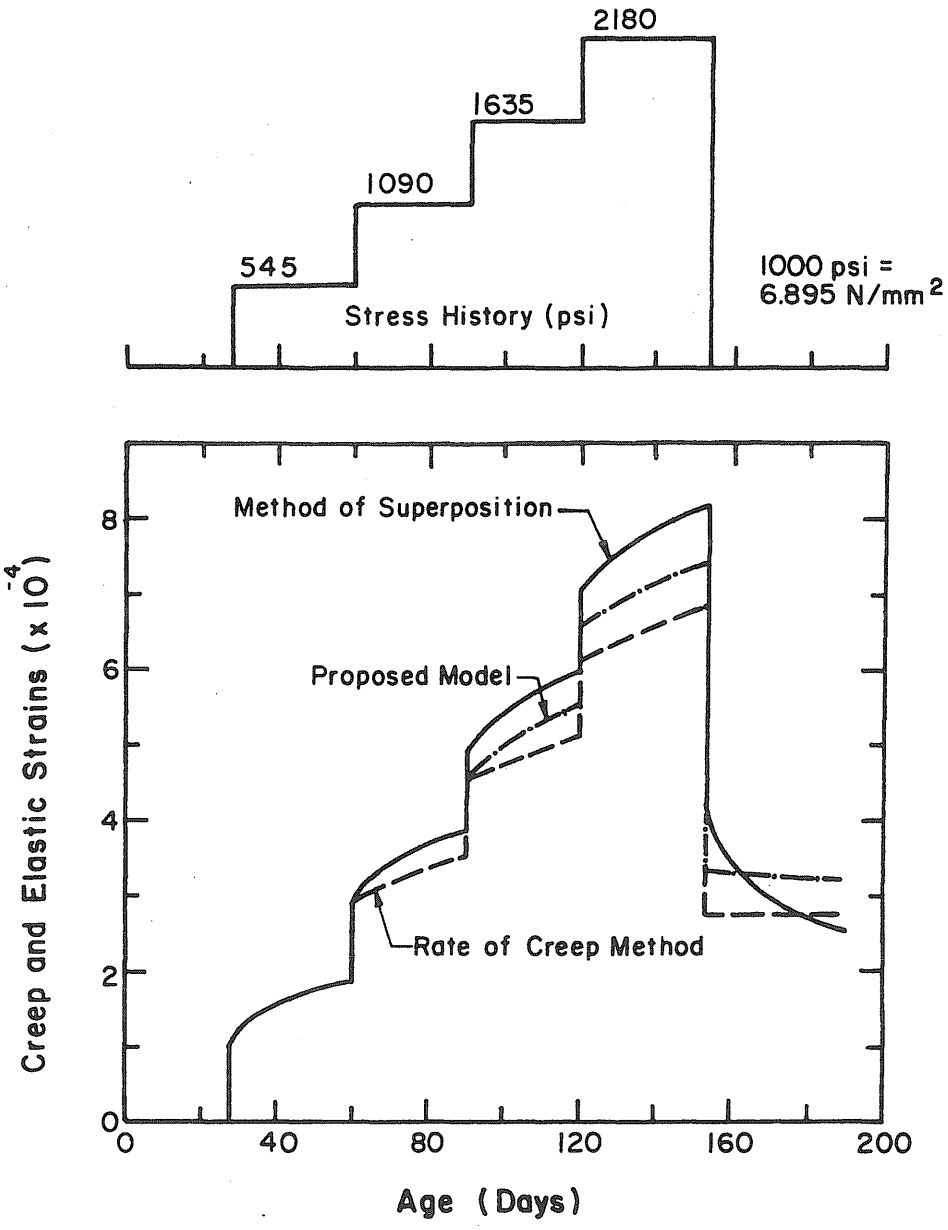

Fig. 3.4 Creep of Concrete Subjected to an Increasing Stress History as Predicted by the Rate of Creep Method, the Method of Superposition and the Method Proposed in this Study

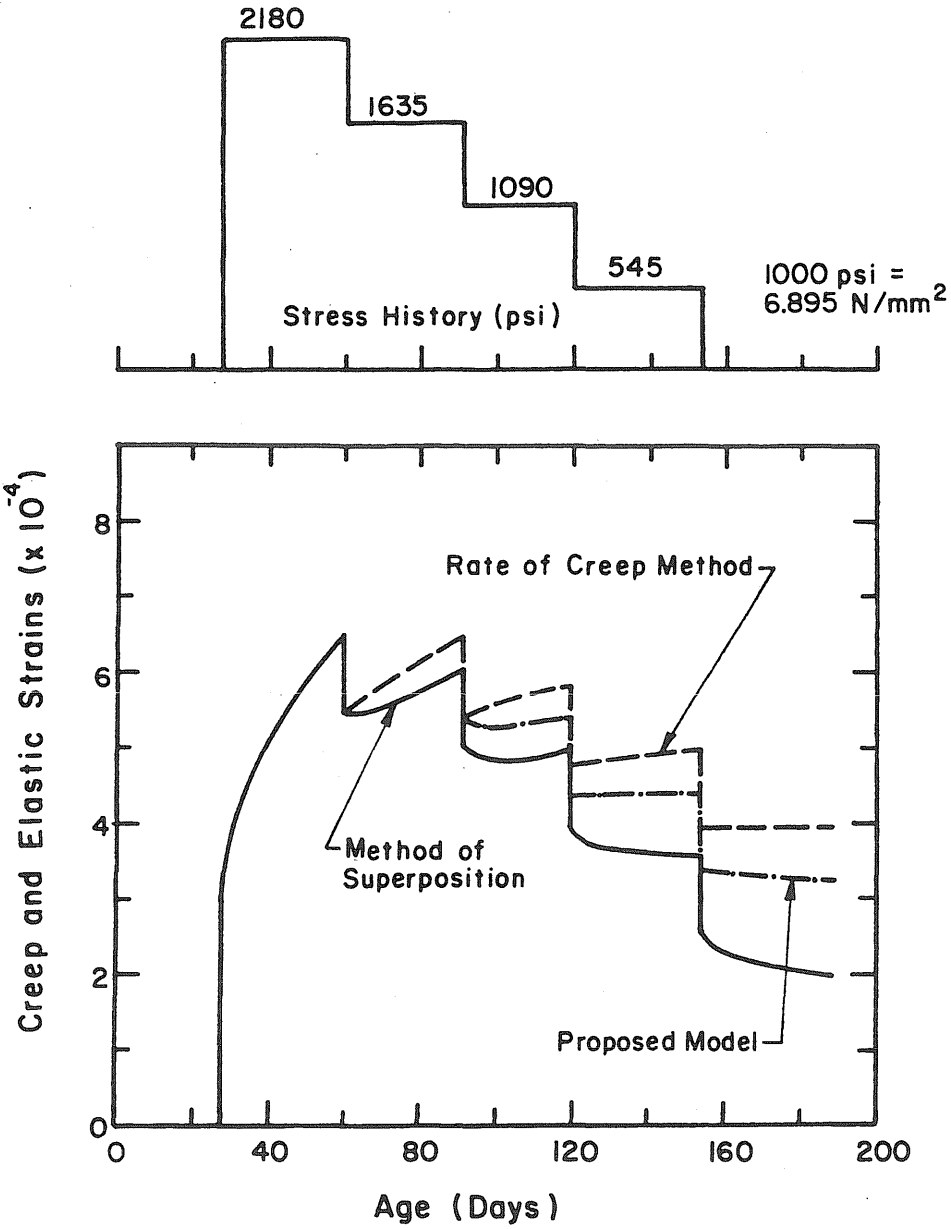

Fig. 3.5 Creep of Concrete Subjected to a Decreasing Stress History as Predicted by the Rate of Creep Method, the Method of Superposition and the Method Proposed in this Study

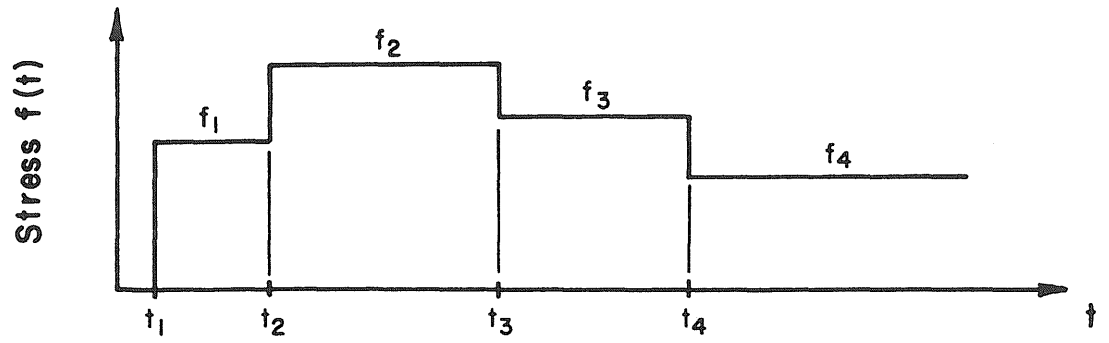

(a) Stress History

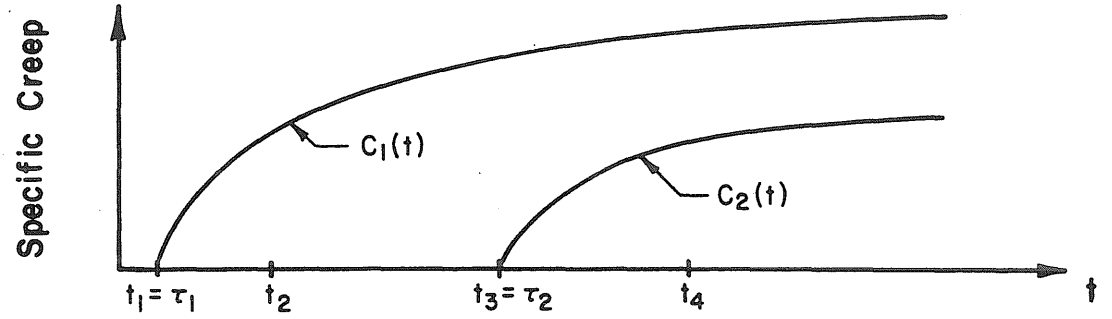

(b) Specific Creep Curves

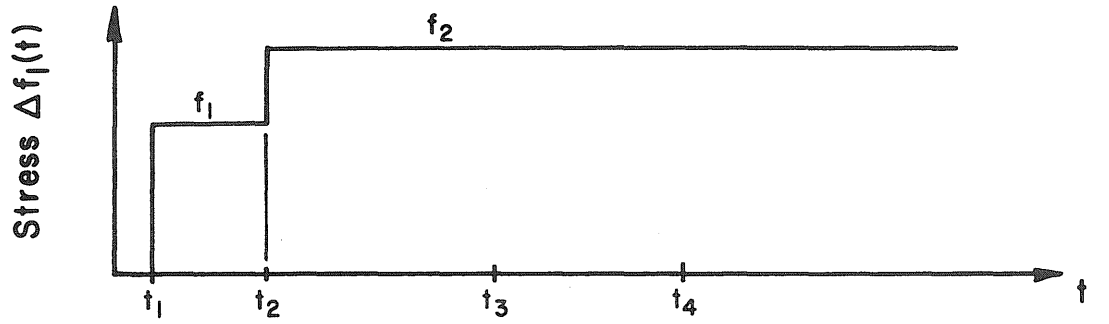

(c) Sub-History $\Delta f_1(t)$

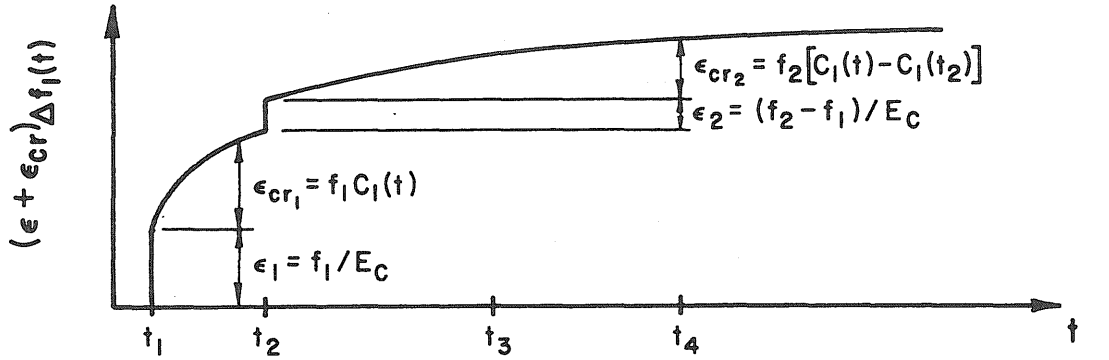

(d) Elastic and Creep Strains Due To Sub-History $\Delta f_1(t)$

Fig. 3.3 Prediction of Creep under Variable Stress According to the Method Proposed in this Study

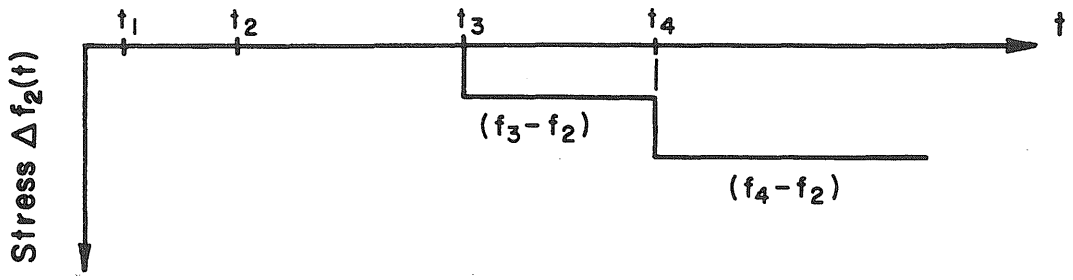

(e) Sub-History $\Delta f_2(t)$

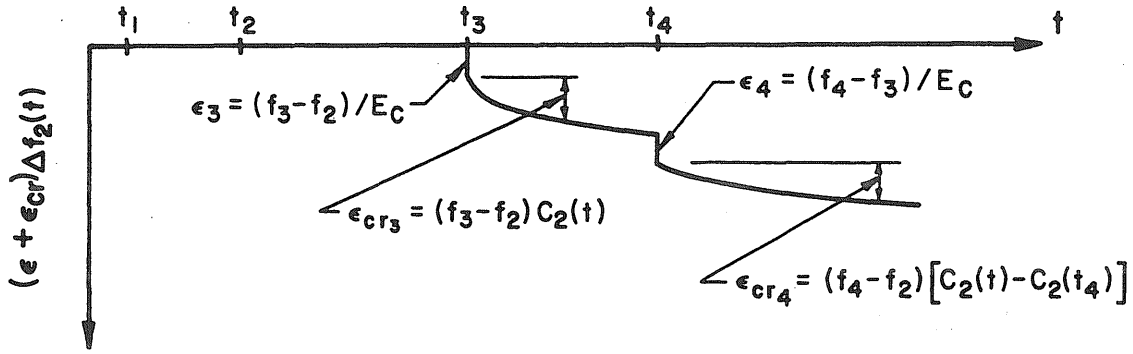

(f) Elastic and Creep Strains Due To Sub-History $\Delta f_2(t)$

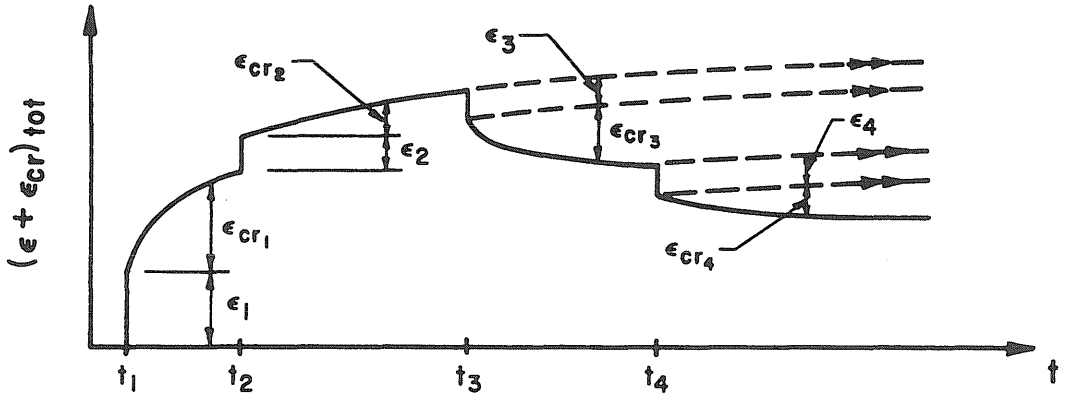

(g) Total Elastic and Creep Strains

Fig. 3.3 (Continued)

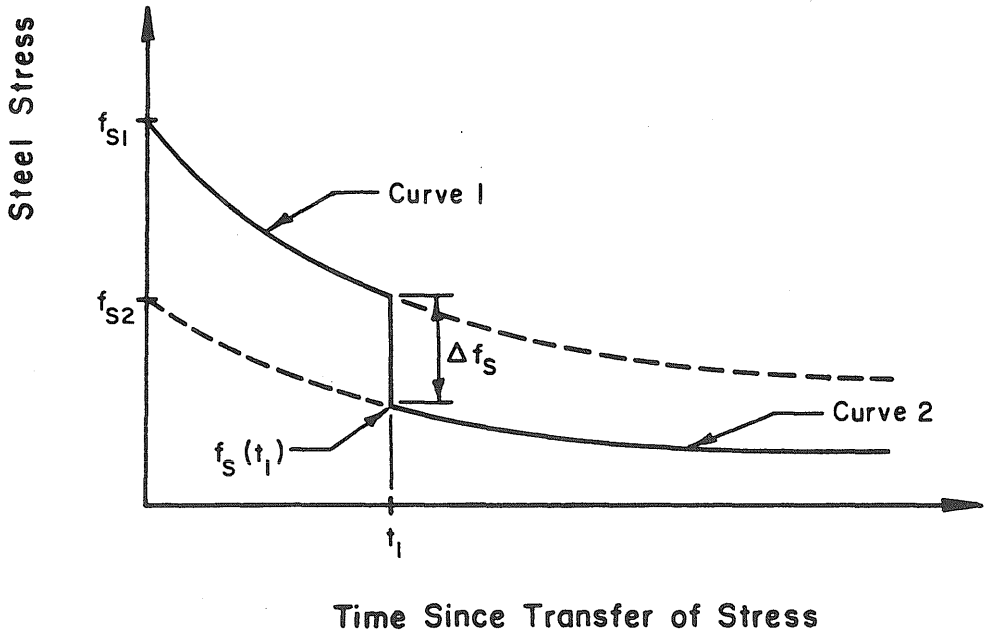

Fig. 3.6 Prediction of Steel Relaxation under a Variable State of Strain

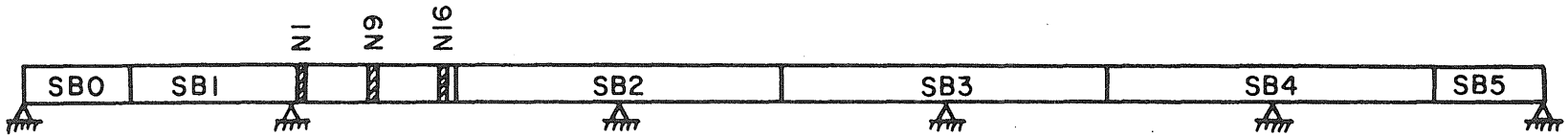

Fig. 4.1 Location of Instrumented Segments

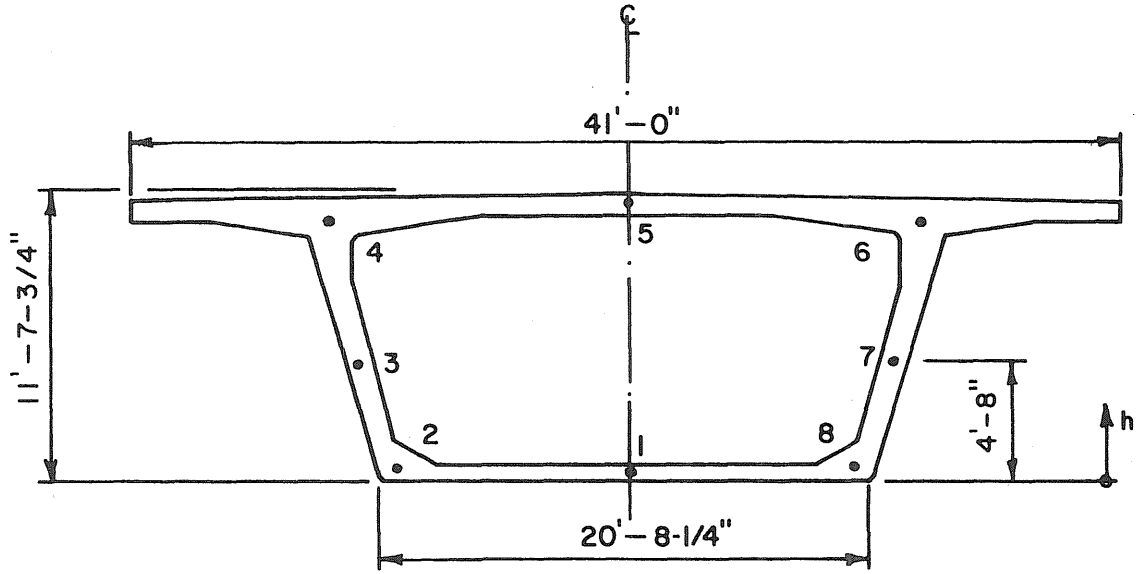

1 in. = 25.4 mm
1 ft = 304.8 mm

Fig. 4.2 Location of Carlson Strain Meters

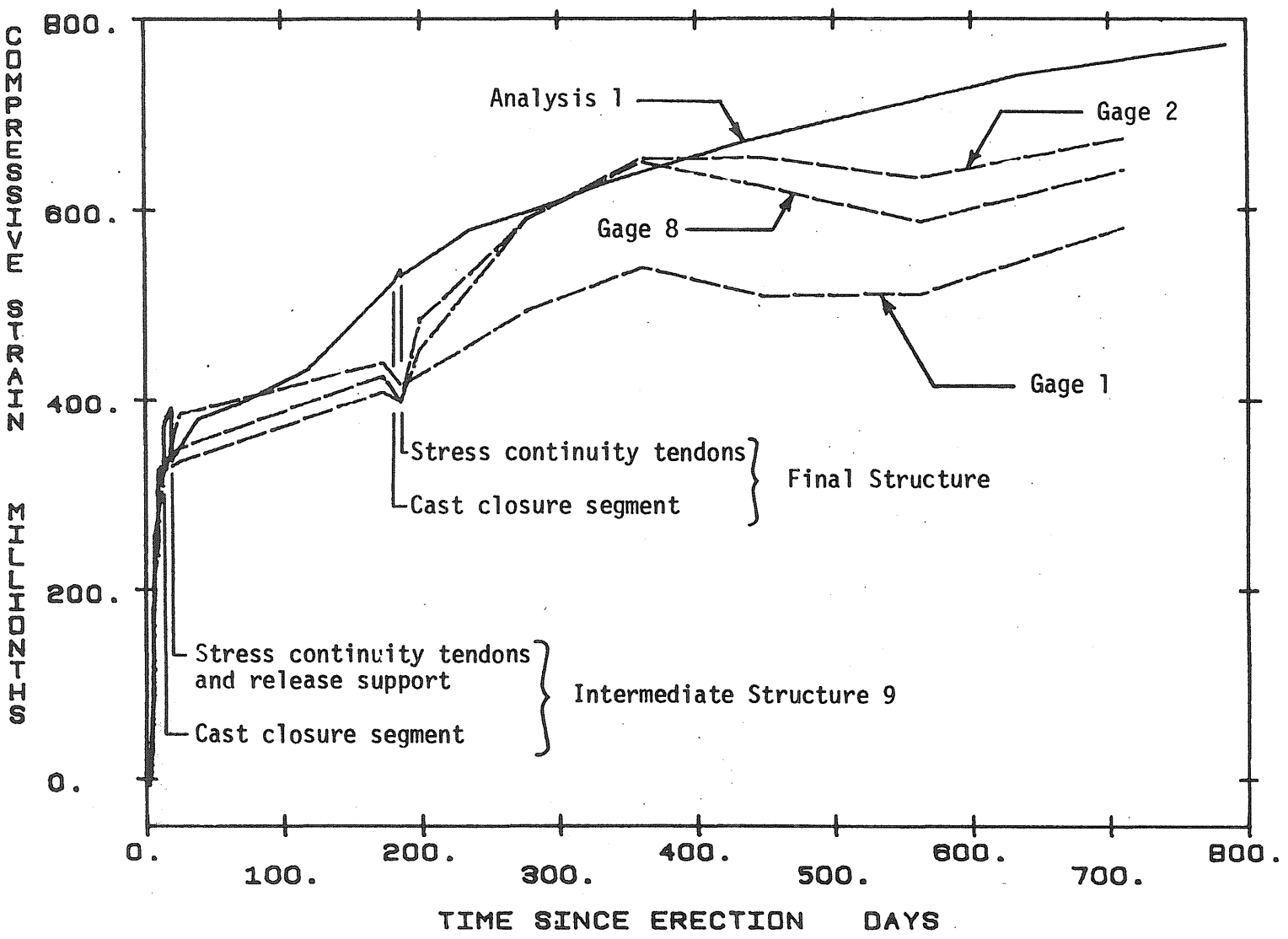

Fig. 4.3 Comparison of Measured and Calculated Concrete Strains in Bottom Flange of Segment SB1-N1 (Analysis 1, h = 8 in.)

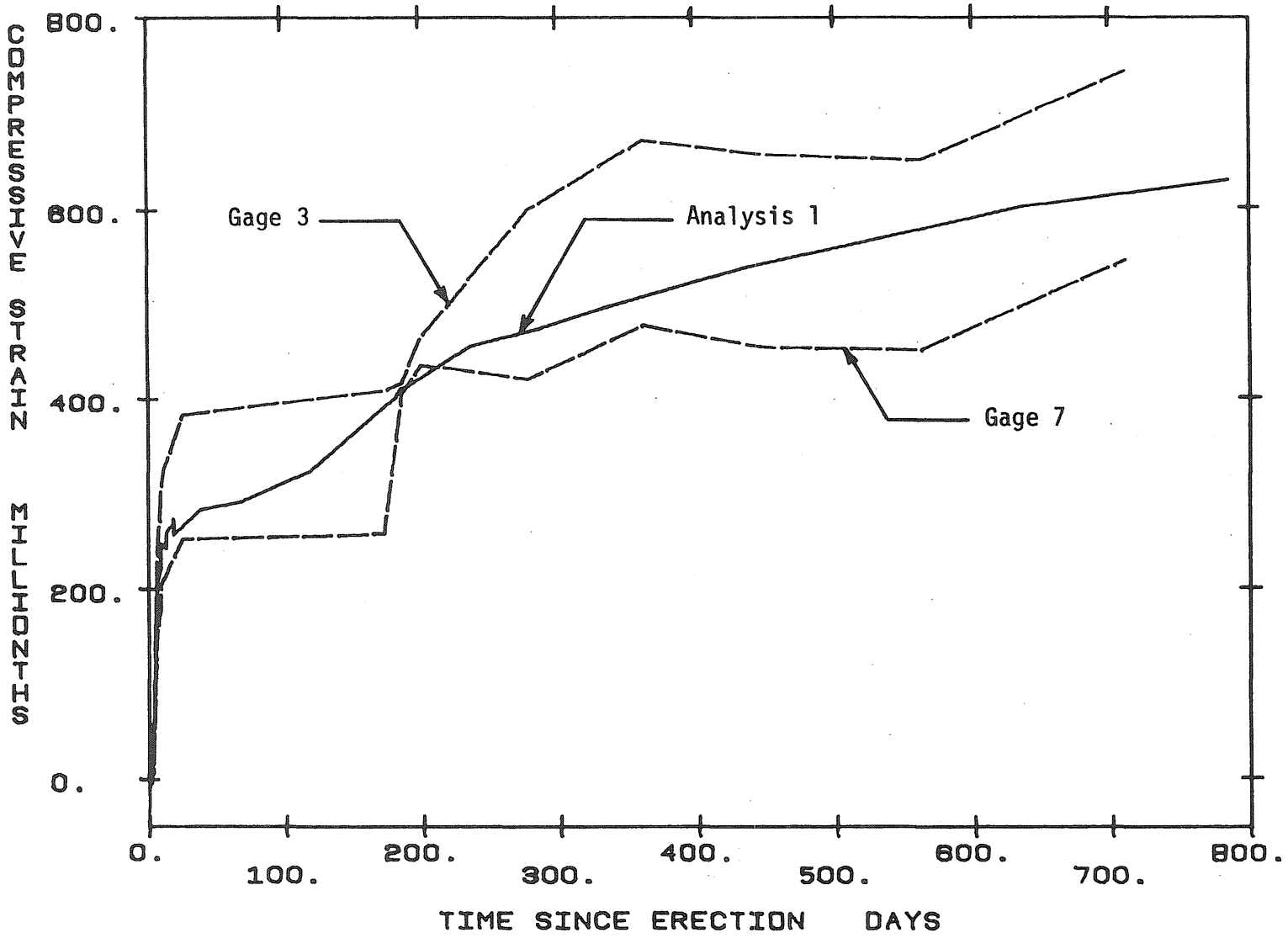

Fig. 4.4 Comparison of Measured and Calculated Concrete Strains in Webs of Segment SB1-N1 (Analysis 1, h = 56 in.)

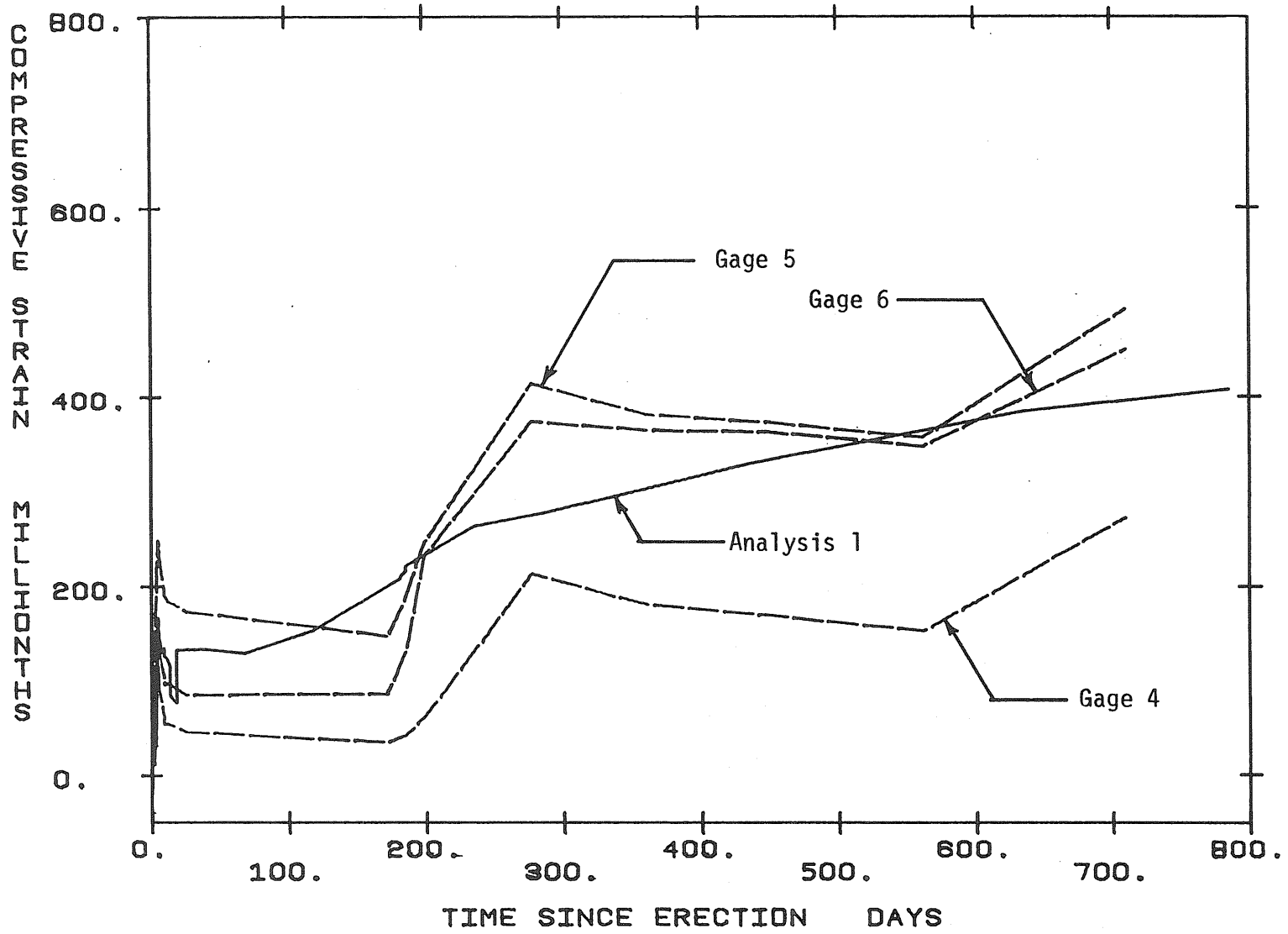

Fig. 4.5 Comparison of Measured and Calculated Concrete Strains in Top Flange of Segment SB1-N1 (Analysis 1, h = 131 in.)

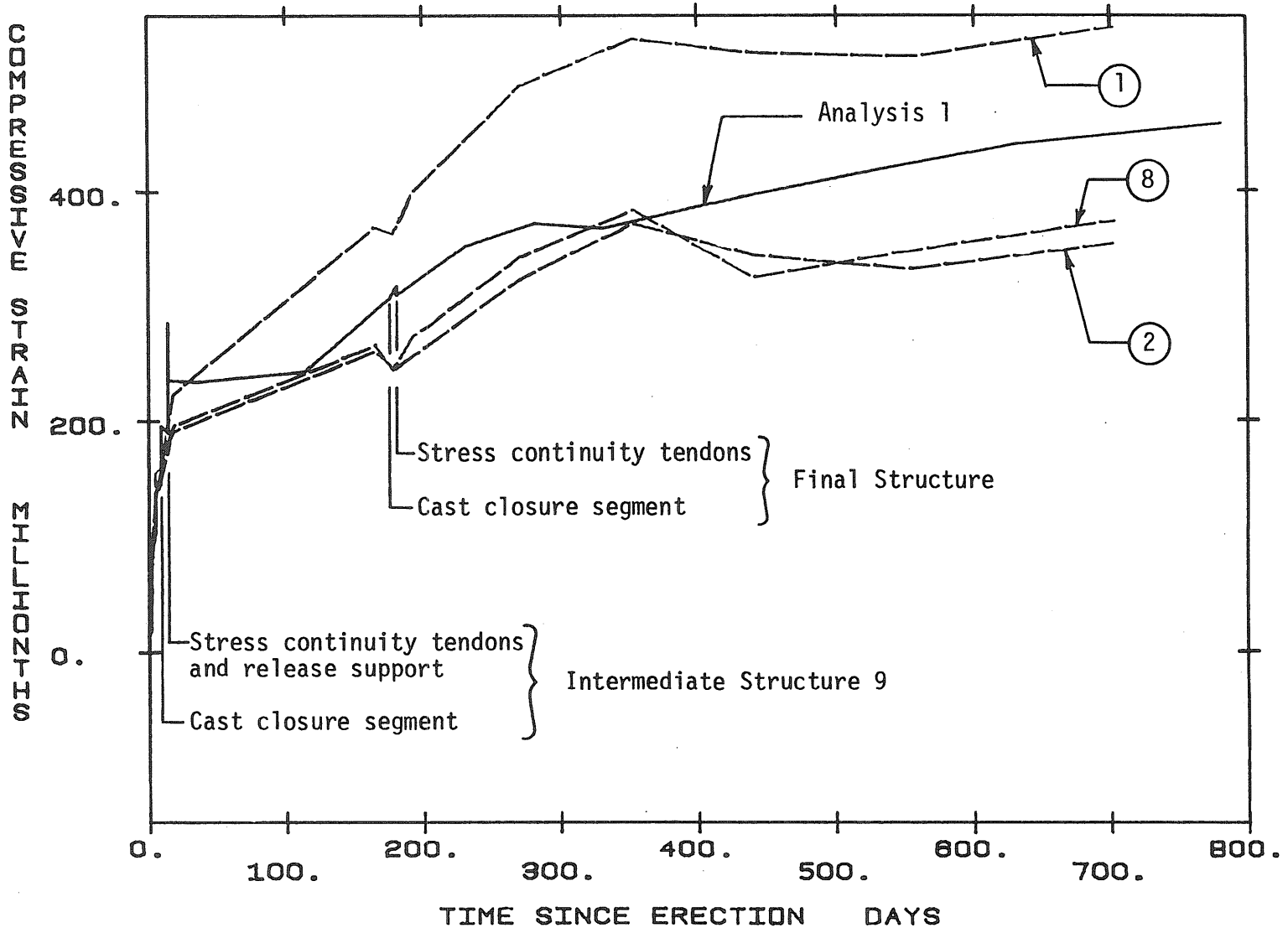

Fig. 4.6 Comparison of Measured and Calculated Concrete Strains in Bottom Flange of Segment SB1-N9 (Analysis 1, h = 8 in.)

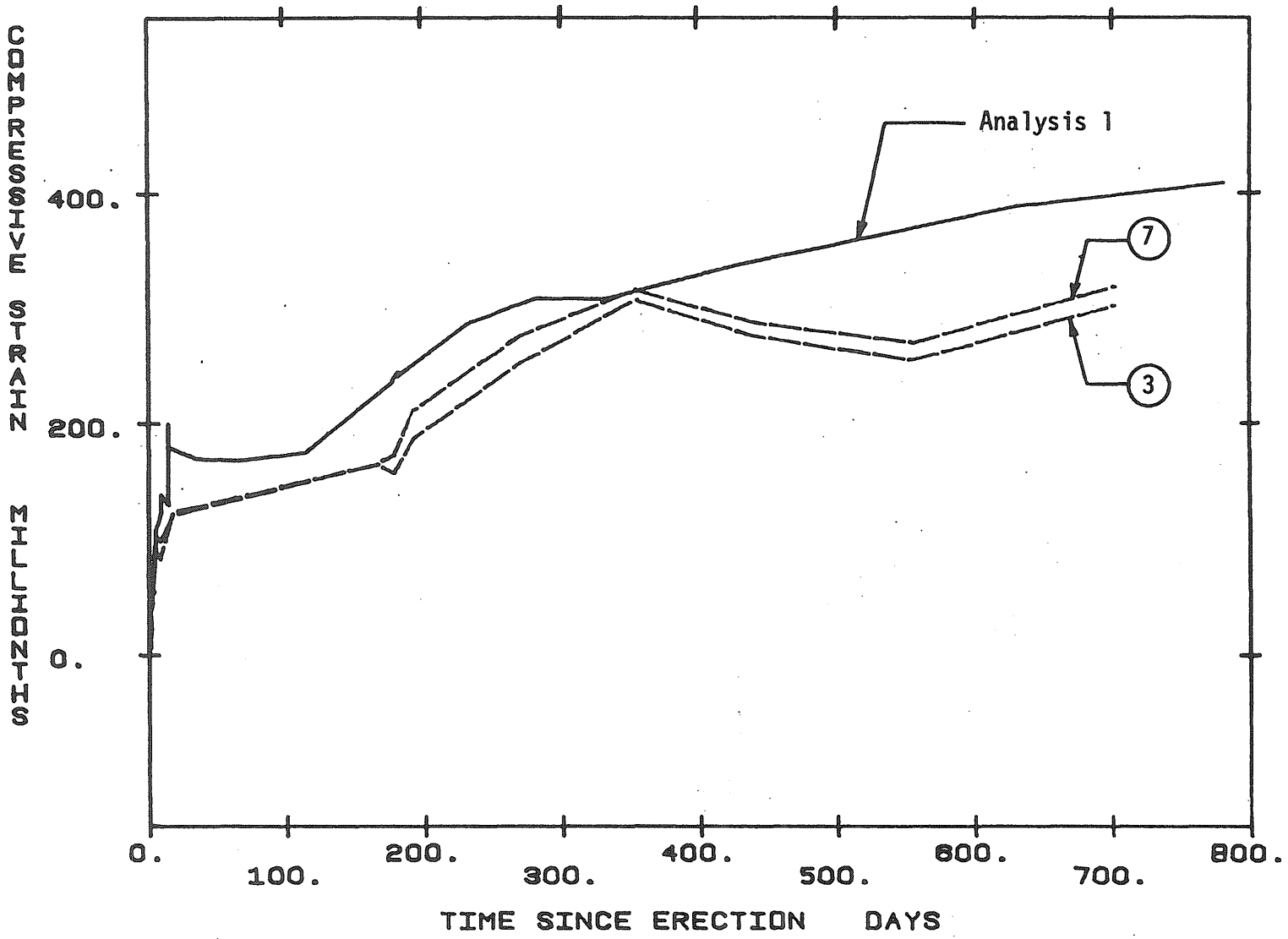

Fig. 4.7 Comparison of Measured and Calculated Concrete Strains in Webs of Segment SB1-N9 (Analysis 1, h = 56 in.)

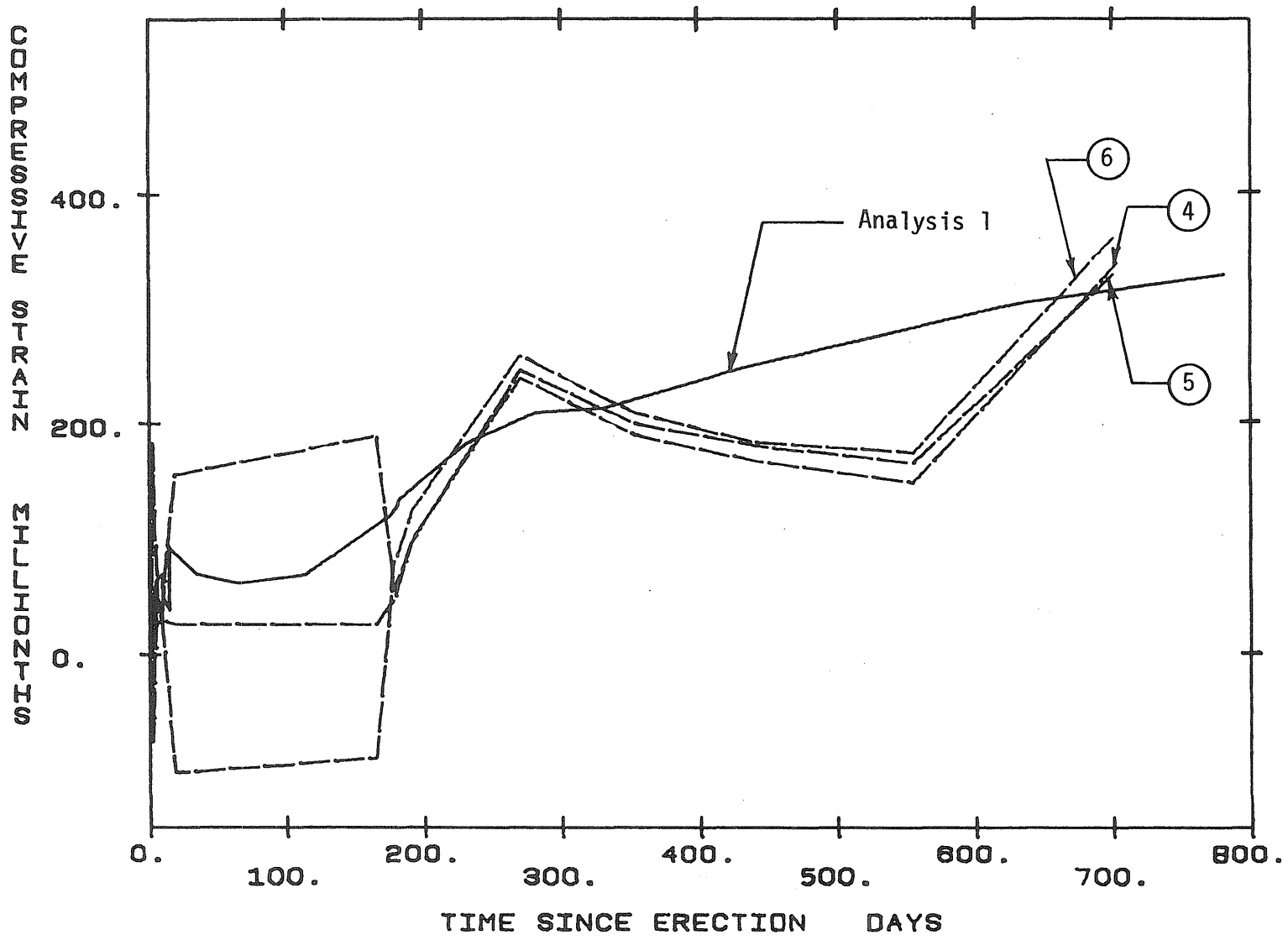

Fig. 4.8 Comparison of Measured and Calculated Concrete Strains in Top Flange of Segment SB1-N9 (Analysis 1, h = 131 in.)

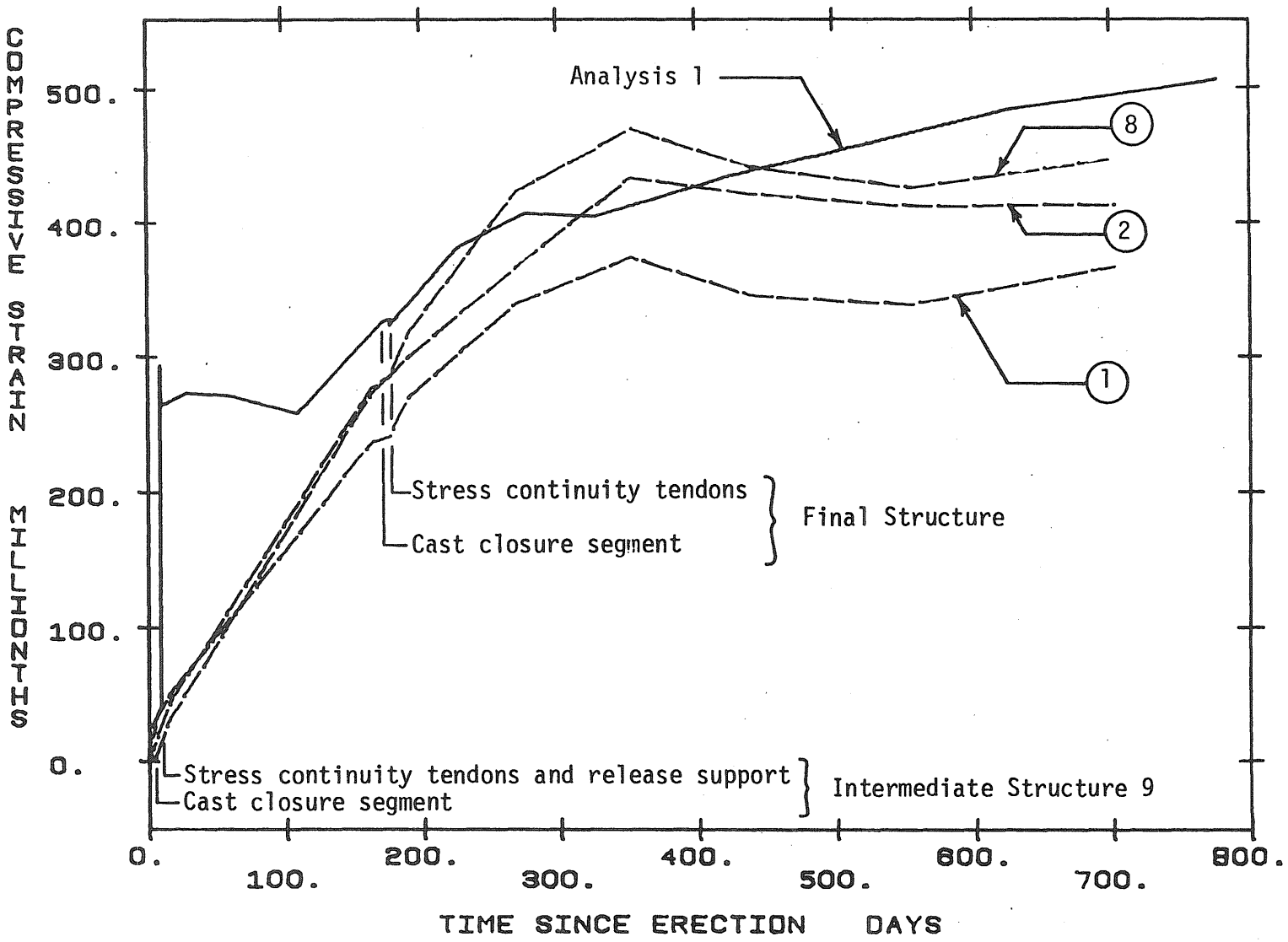

Fig. 4.9 Comparison of Measured and Calculated Concrete Strains in Bottom Flange of Segment SB1-N16 (Analysis 1, h = 8 in.)

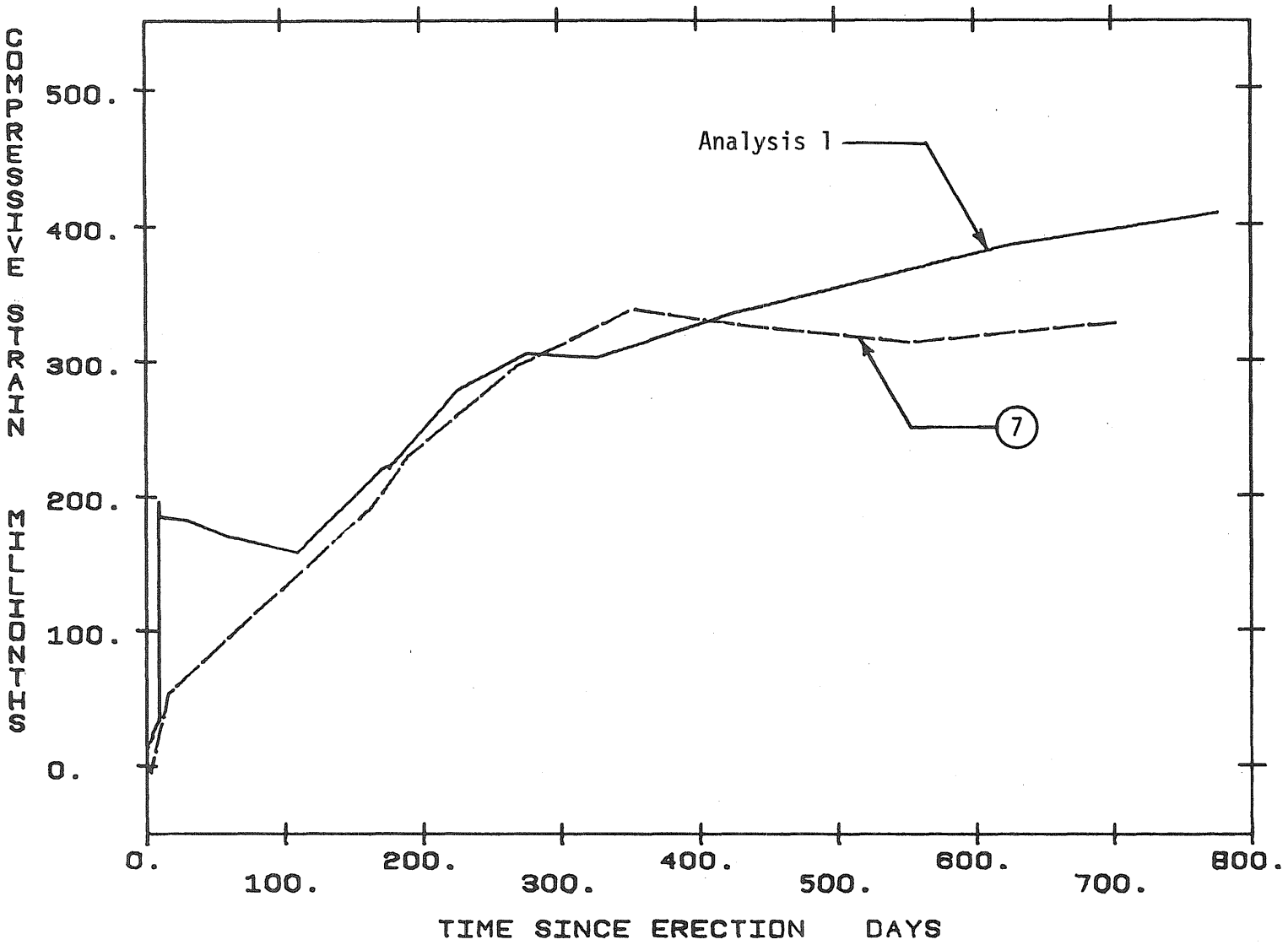

Fig. 4.10 Comparison of Measured and Calculated Concrete Strains in Webs of Segment SB1-N16 (Analysis 1, h = 56 in.)

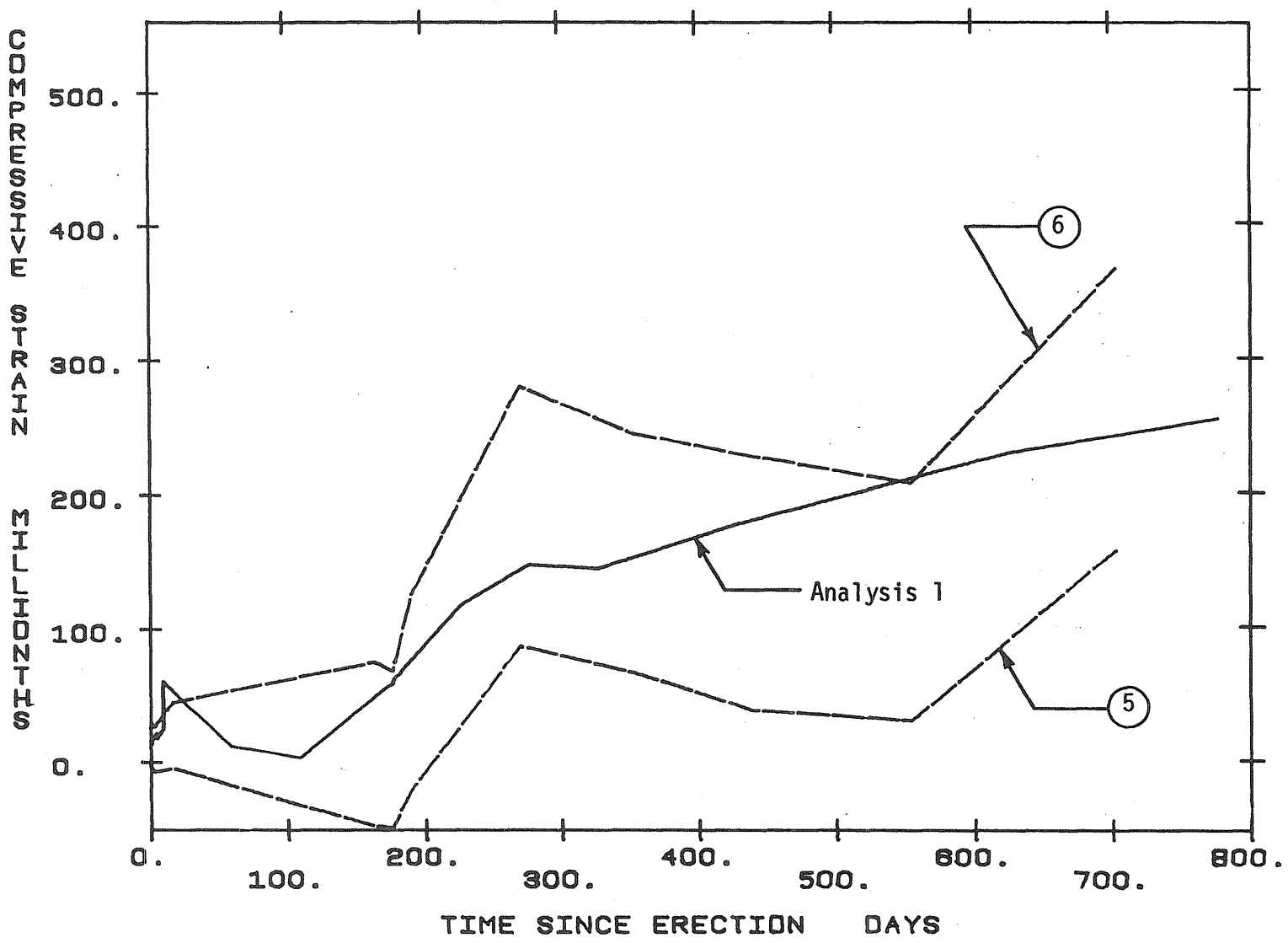

Fig. 4.11 Comparison of Measured and Calculated Concrete Strains in Top Flange of Segment SB1-N16 (Analysis 1, h = 131 in.)

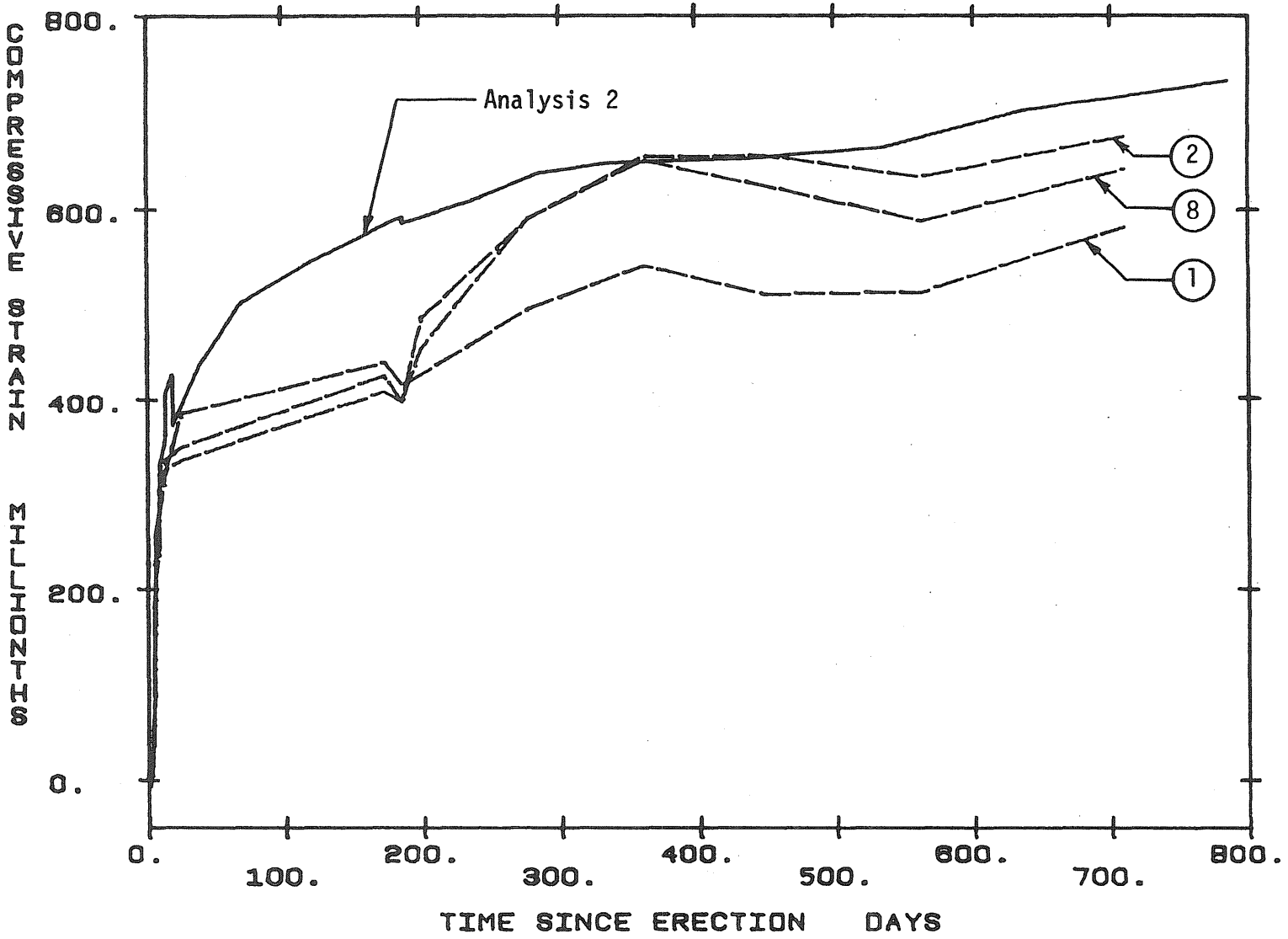

Fig. 4.12 Comparison of Measured and Calculated Concrete Strains in Bottom Flange of Segment SB1-N1 (Analysis 2, h = 8 in.)

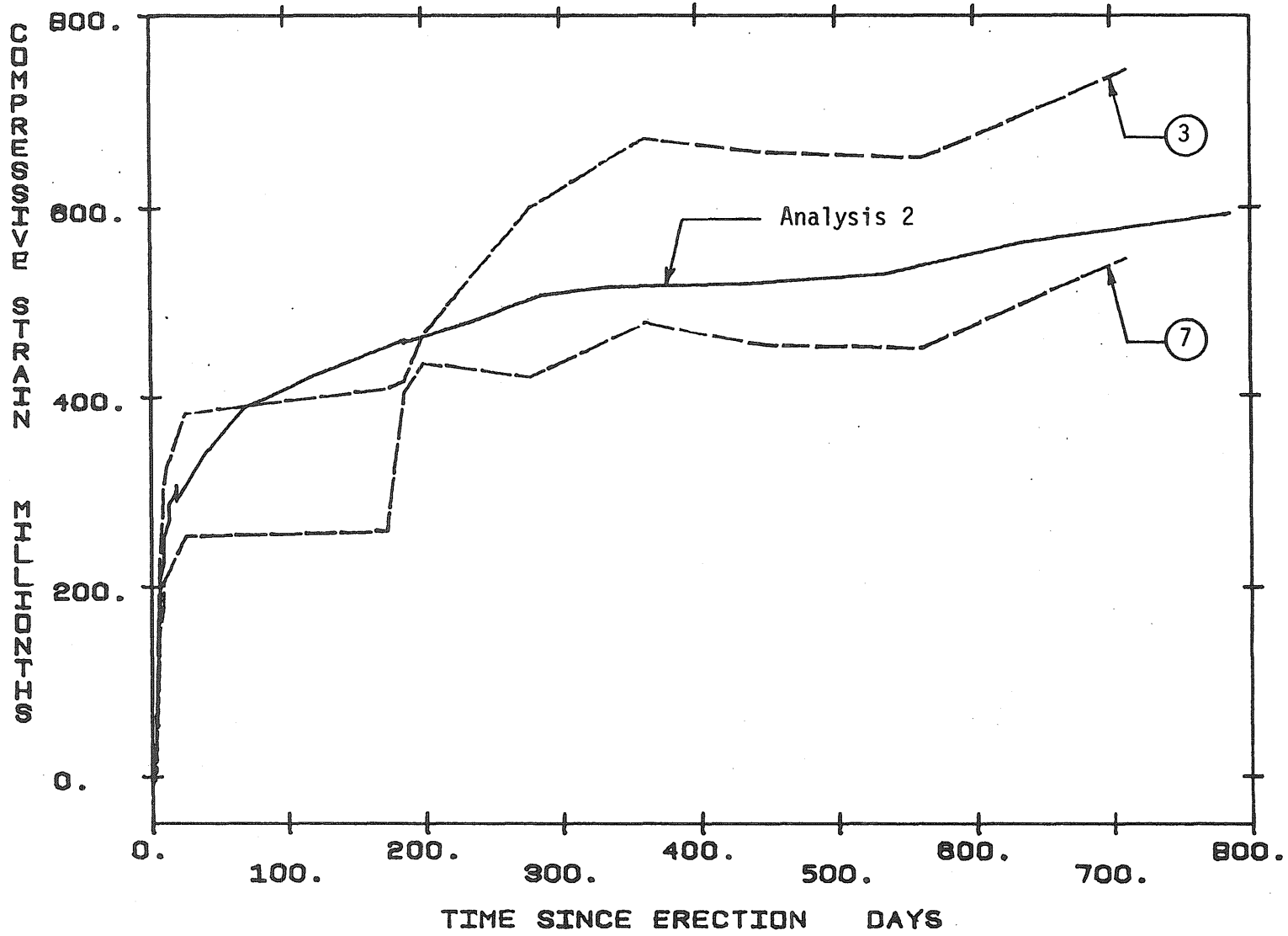

Fig. 4.13 Comparison of Measured and Calculated Concrete Strains in Webs of Segment SB1-N1 (Analysis 2, h = 56 in.)

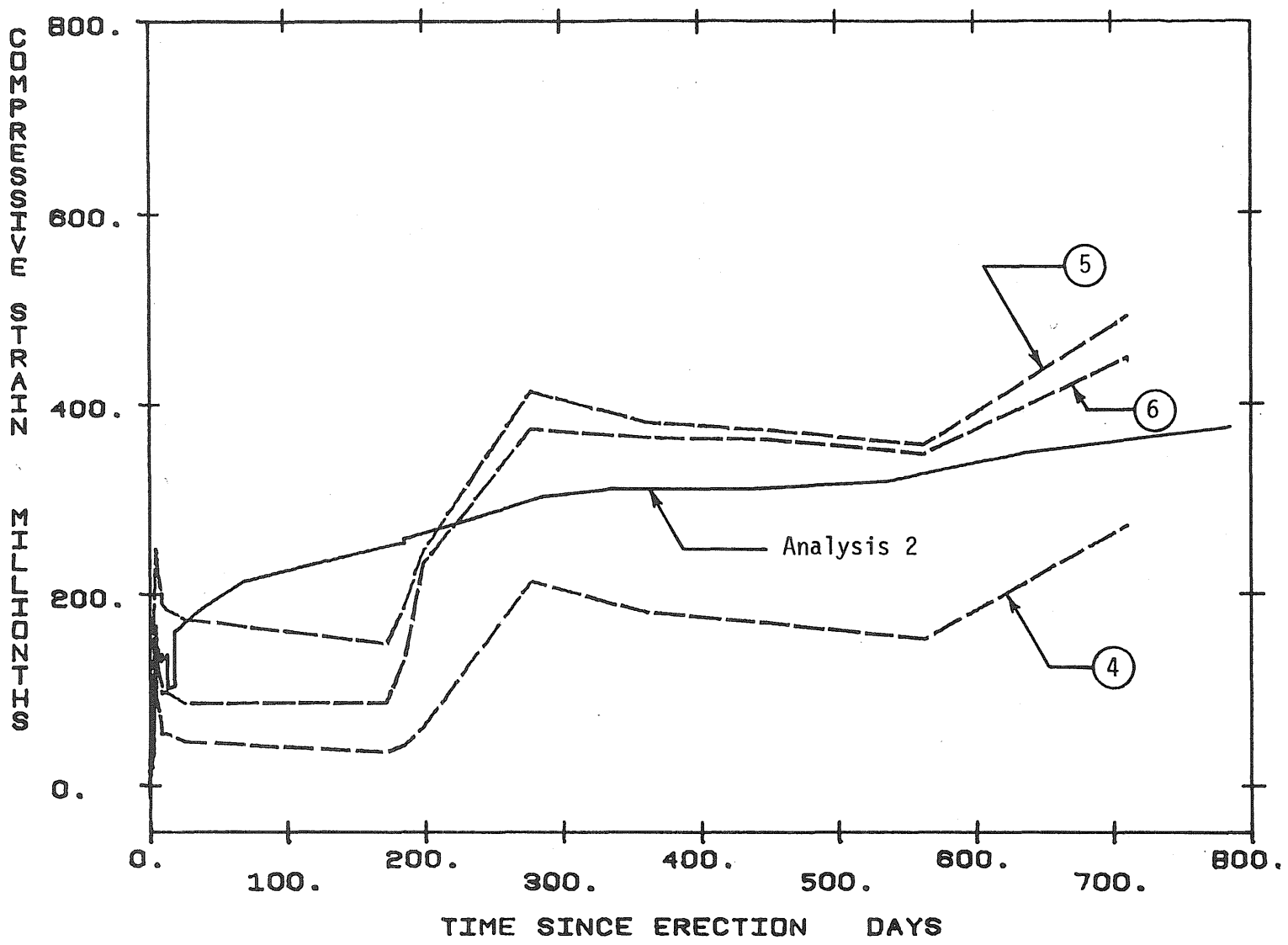

Fig. 4.14 Comparison of Measured and Calculated Concrete Strains in Top Flange of Segment SB1-N1 (Analysis 2, h = 131 in.)

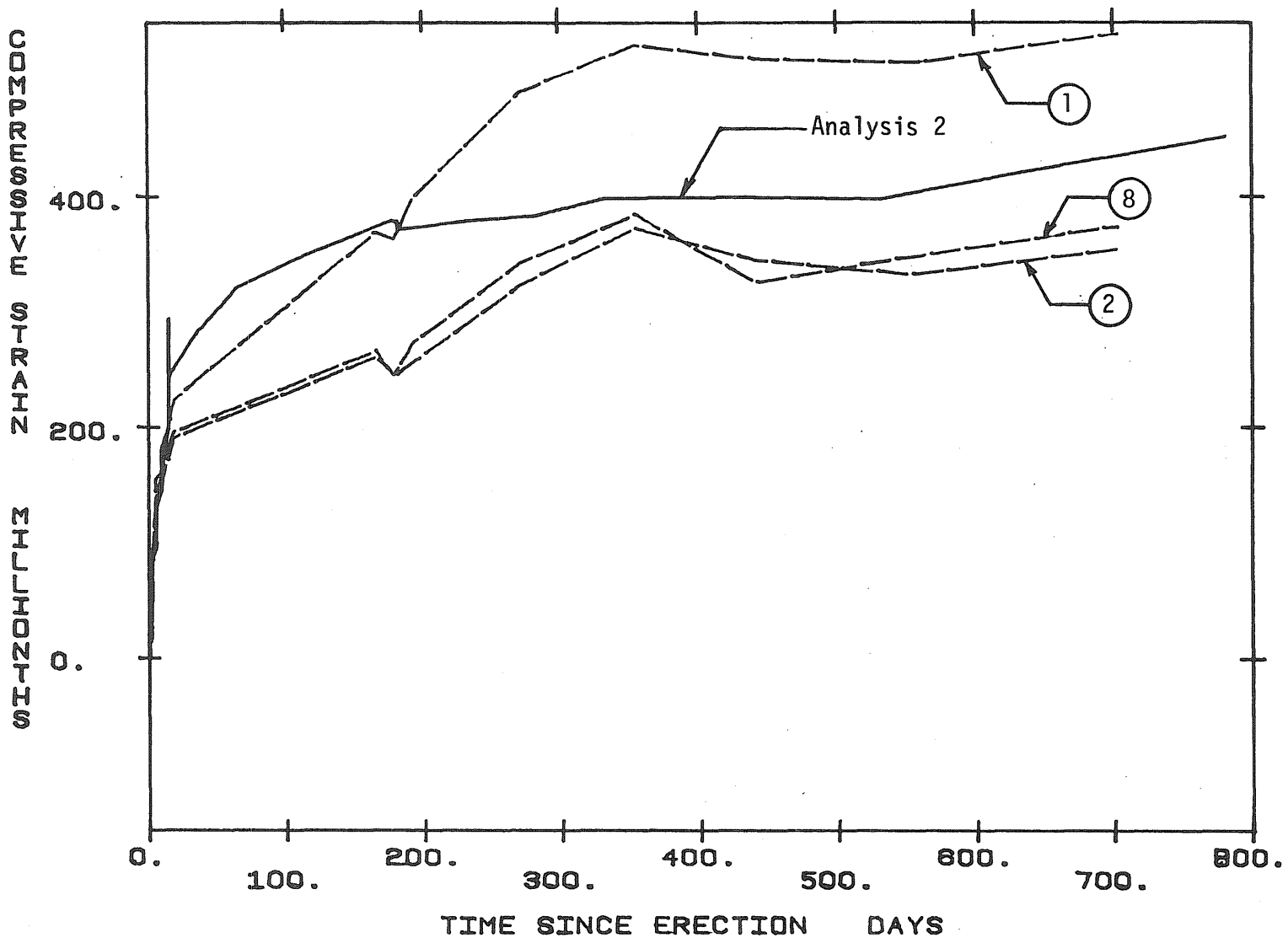

Fig. 4.15 Comparison of Measured and Calculated Concrete Strains in Bottom Flange of Segment SB1-N9 (Analysis 2, h = 8 in.)

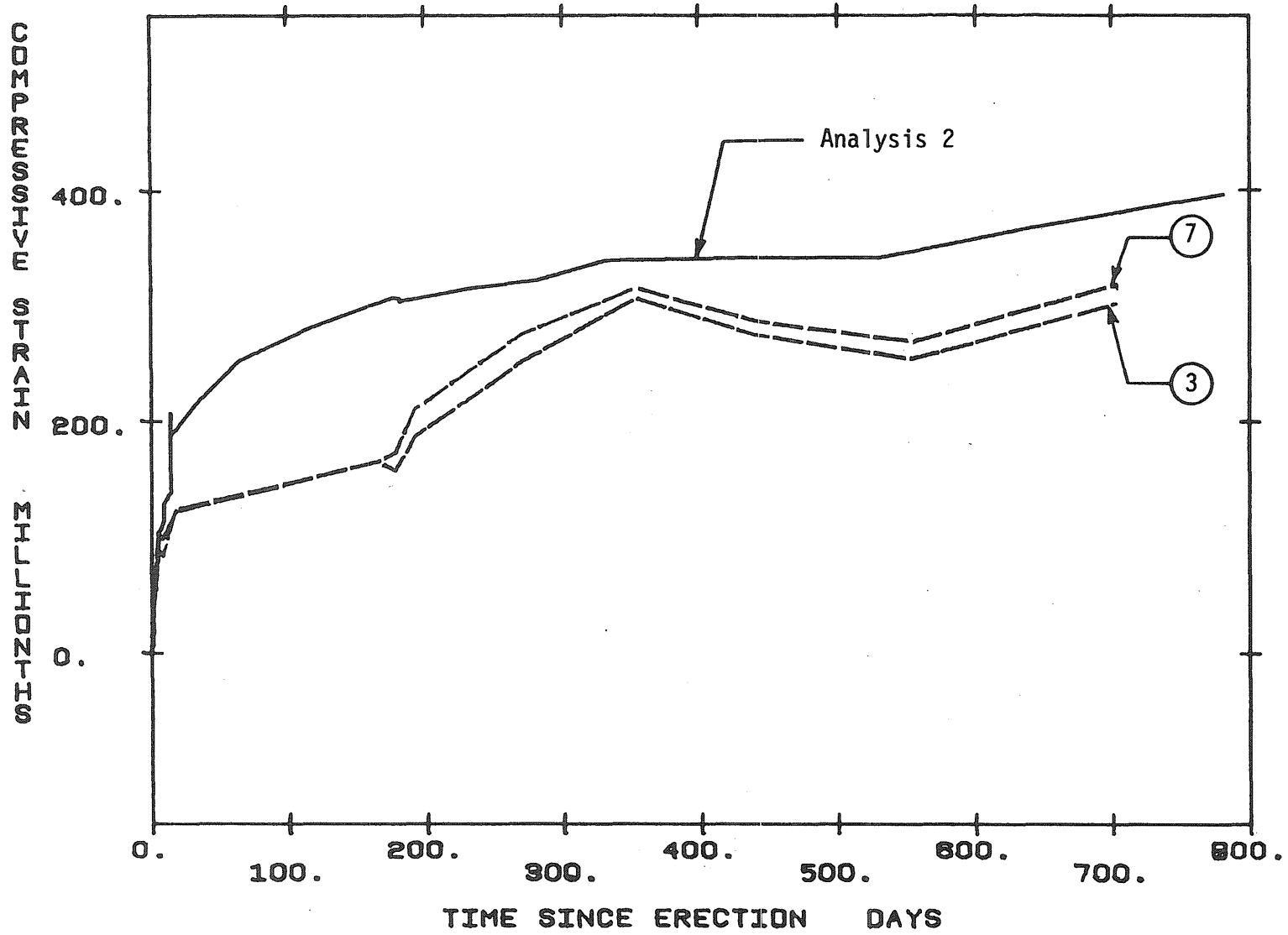

Fig. 4.16 Comparison of Measured and Calculated Concrete Strains in Webs of Segment SB1-N9 (Analysis 2, h = 56 in.)

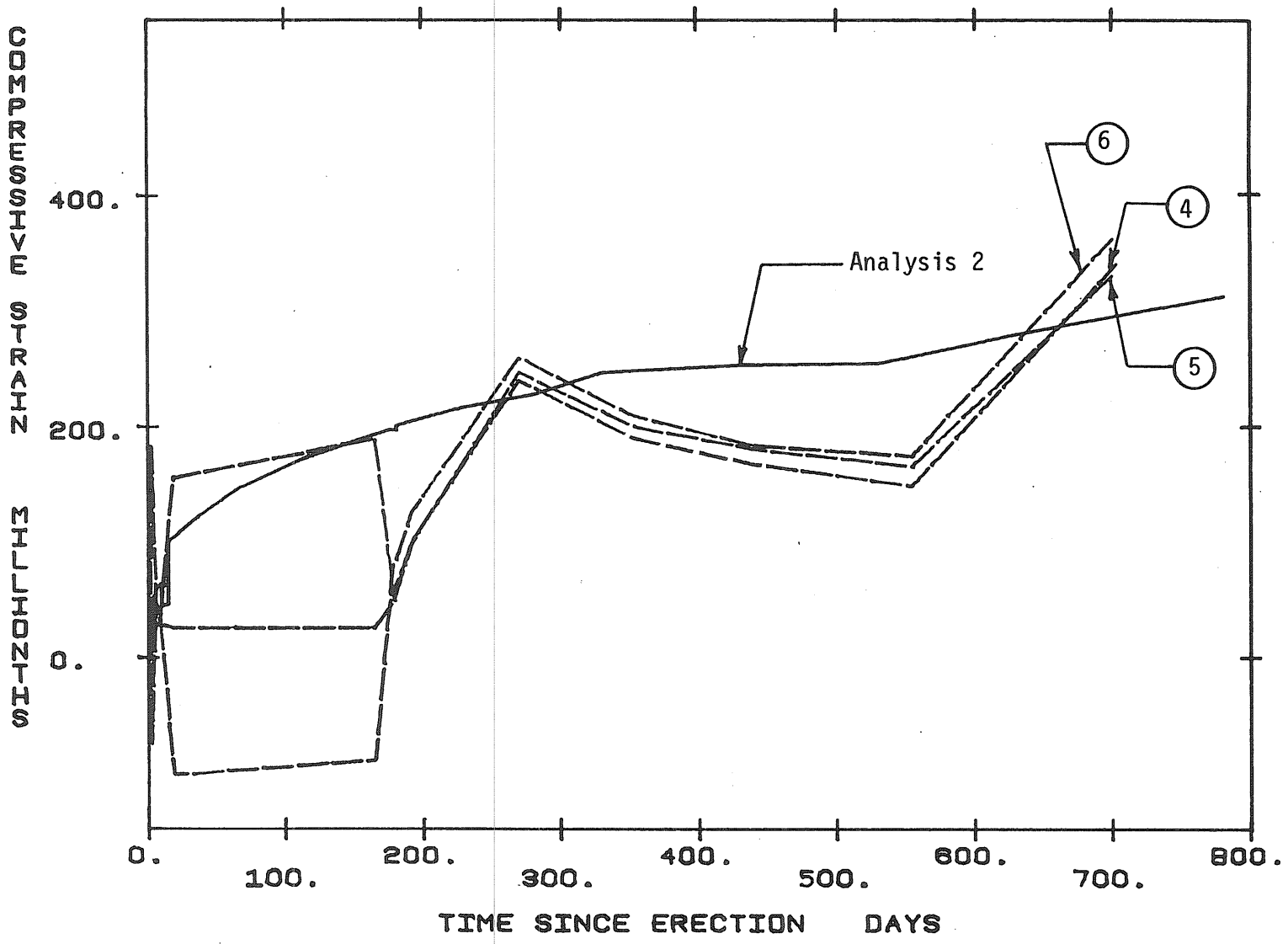

Fig. 4.17 Comparison of Measured and Calculated Concrete Strains in Top Flange of Segment SB1-N9 (Analysis 2, h = 131 in.)

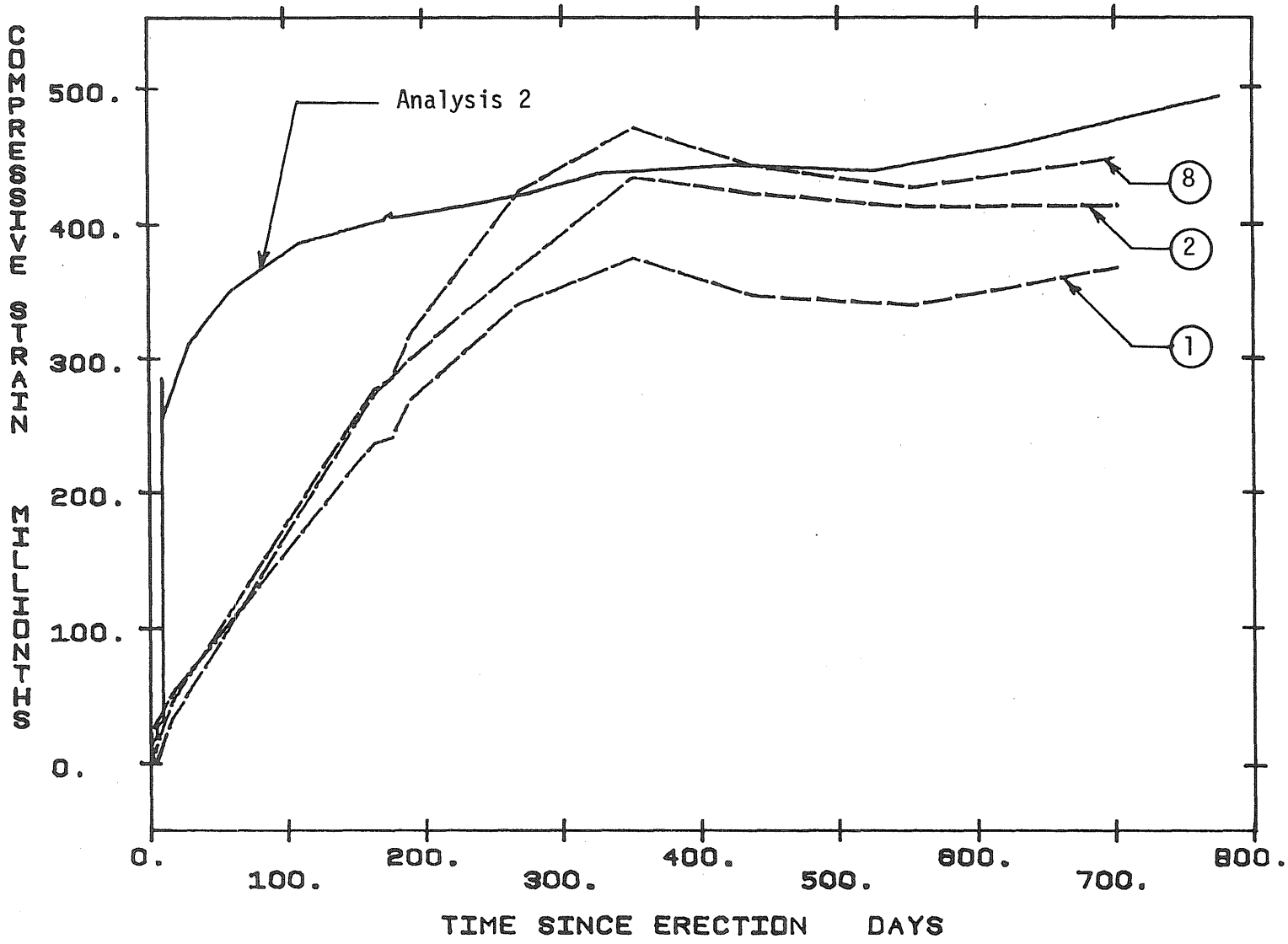

Fig. 4.18 Comparison of Measured and Calculated Concrete Strains in Bottom Flange of Segment SB1-N16 (Analysis 2, h = 8 in.)

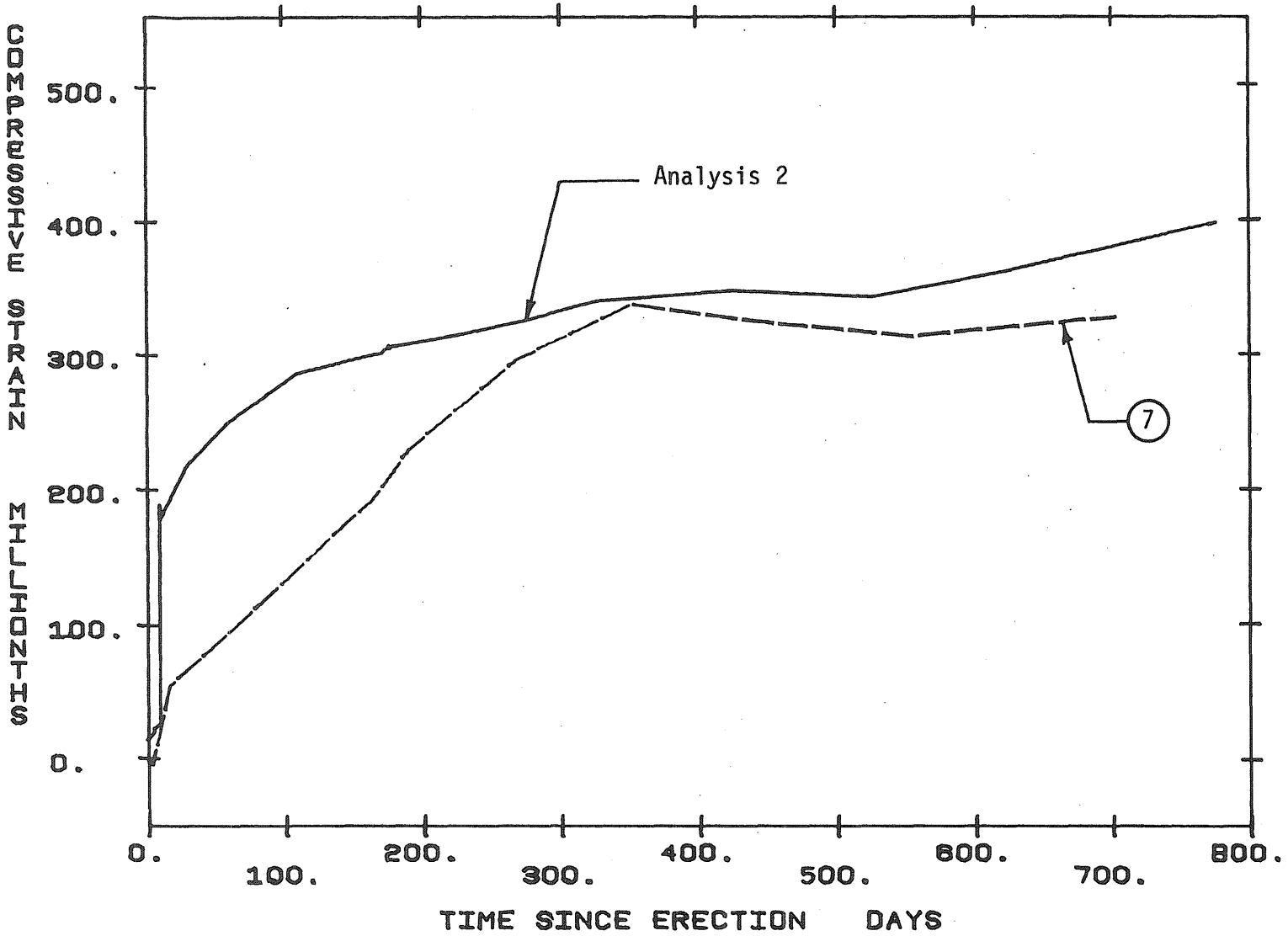

Fig. 4.19 Comparison of Measured and Calculated Concrete Strains in Webs of Segment SB1-N16 (Analysis 2, h = 56 in.)

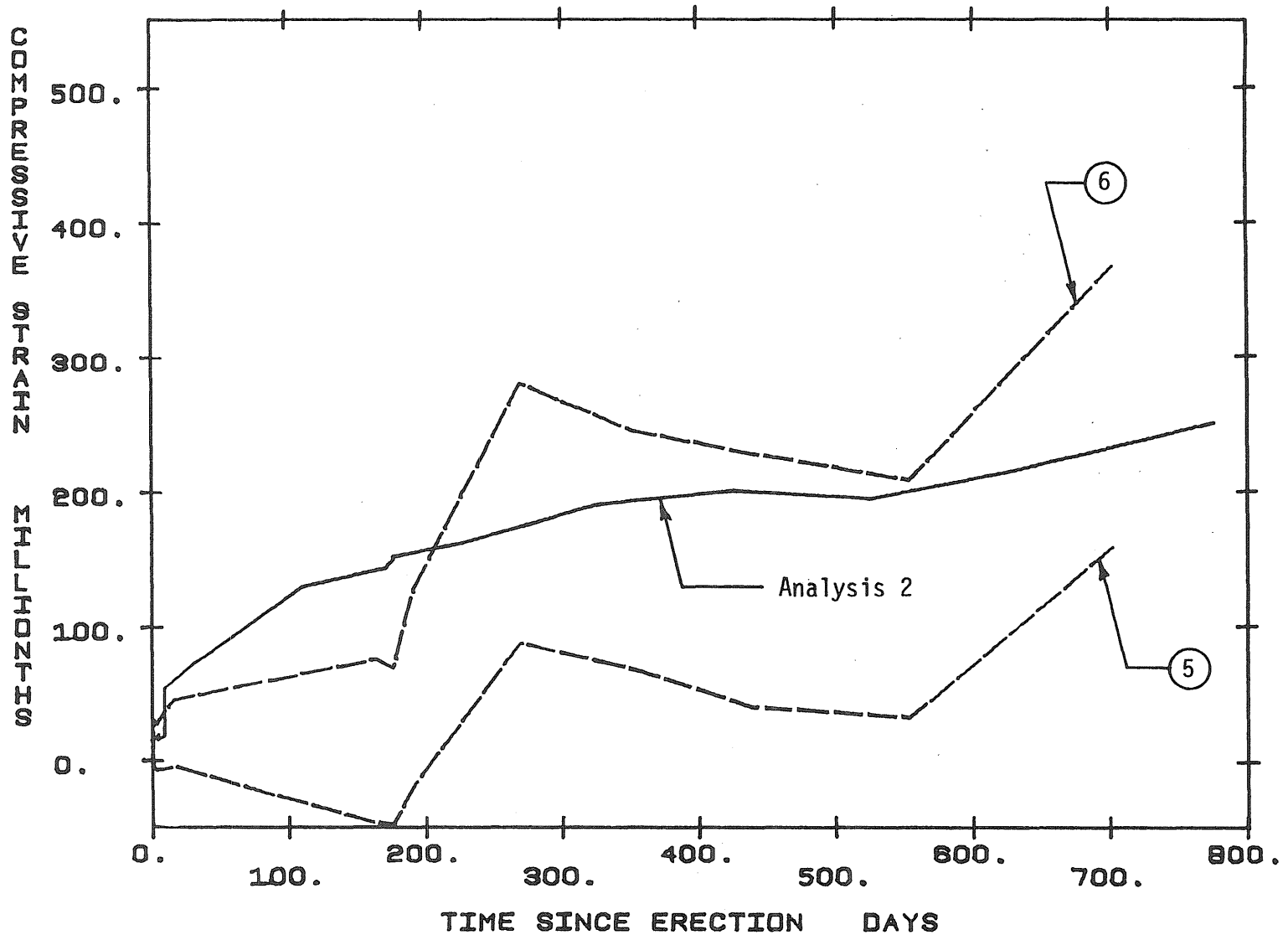

Fig. 4.20 Comparison of Measured and Calculated Concrete Strains in Top Flange of Segment SB1-N16 (Analysis 2, h = 131 in.)

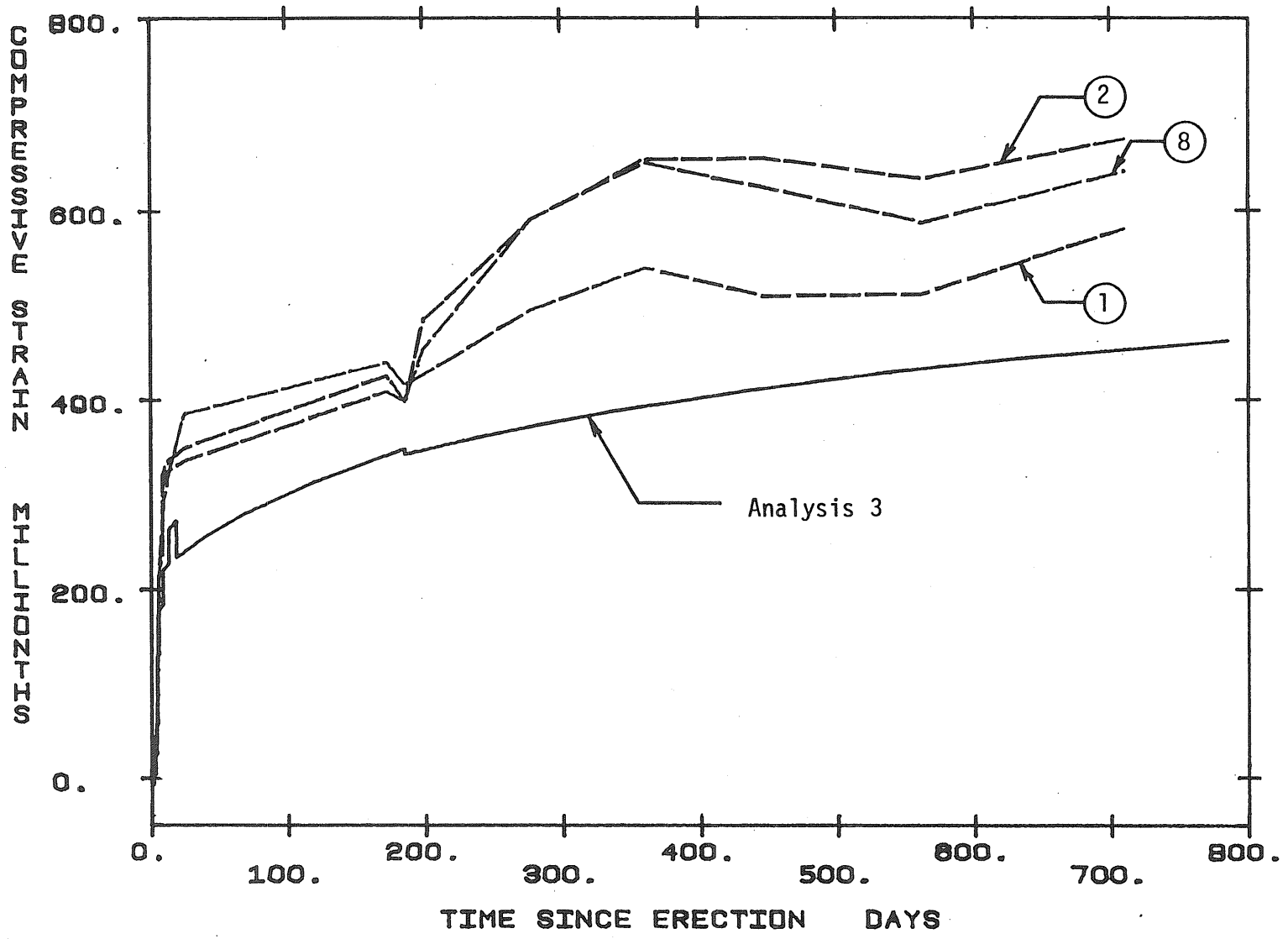

Fig. 4.21 Comparison of Measured and Calculated Concrete Strains in Bottom Flange of Segment SB1-N1 (Analysis 3, h = 8 in.)

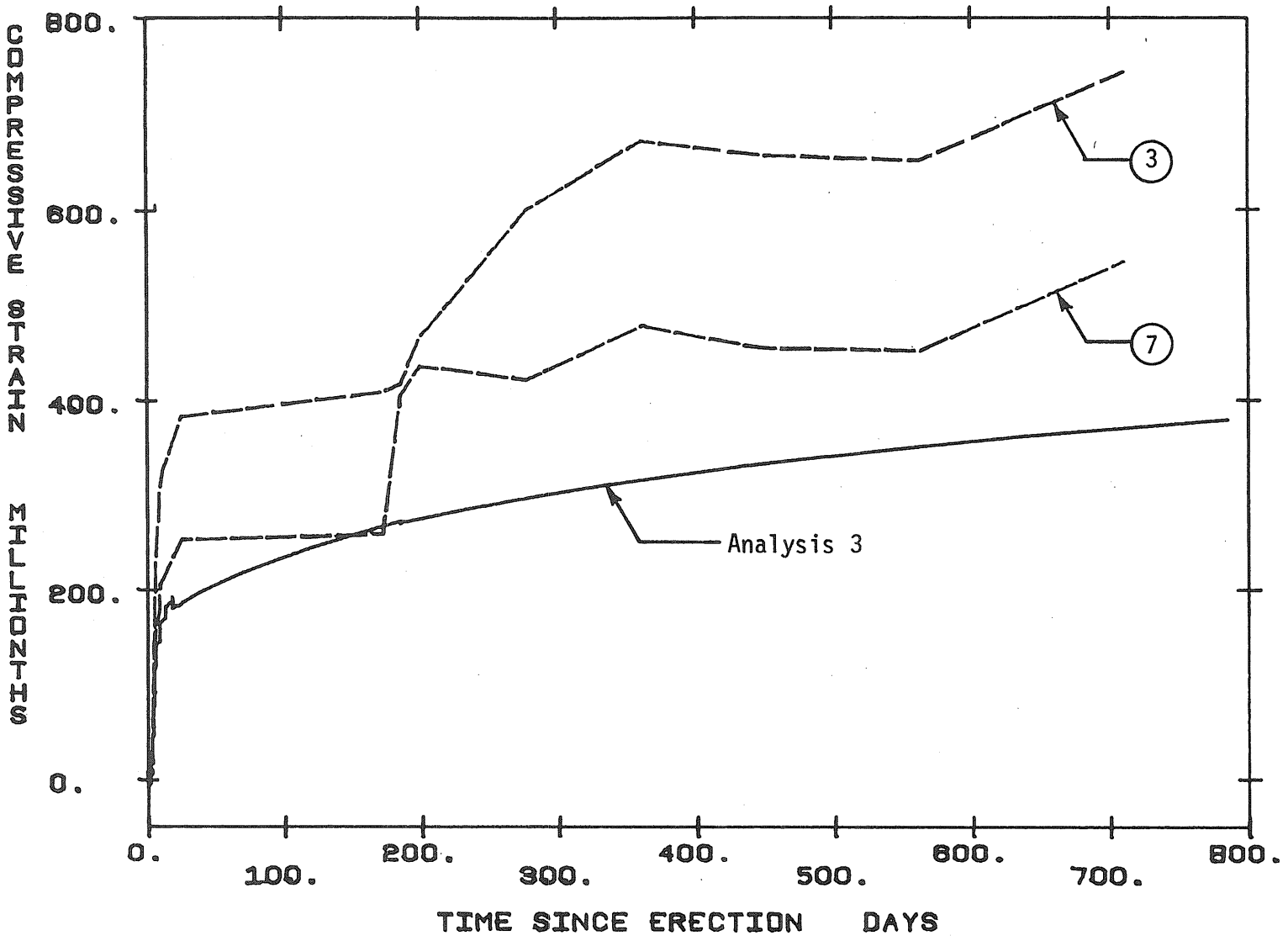

Fig. 4.22 Comparison of Measured and Calculated Concrete Strains in Webs of Segment SB1-N1 (Analysis 3, h = 56 in.)

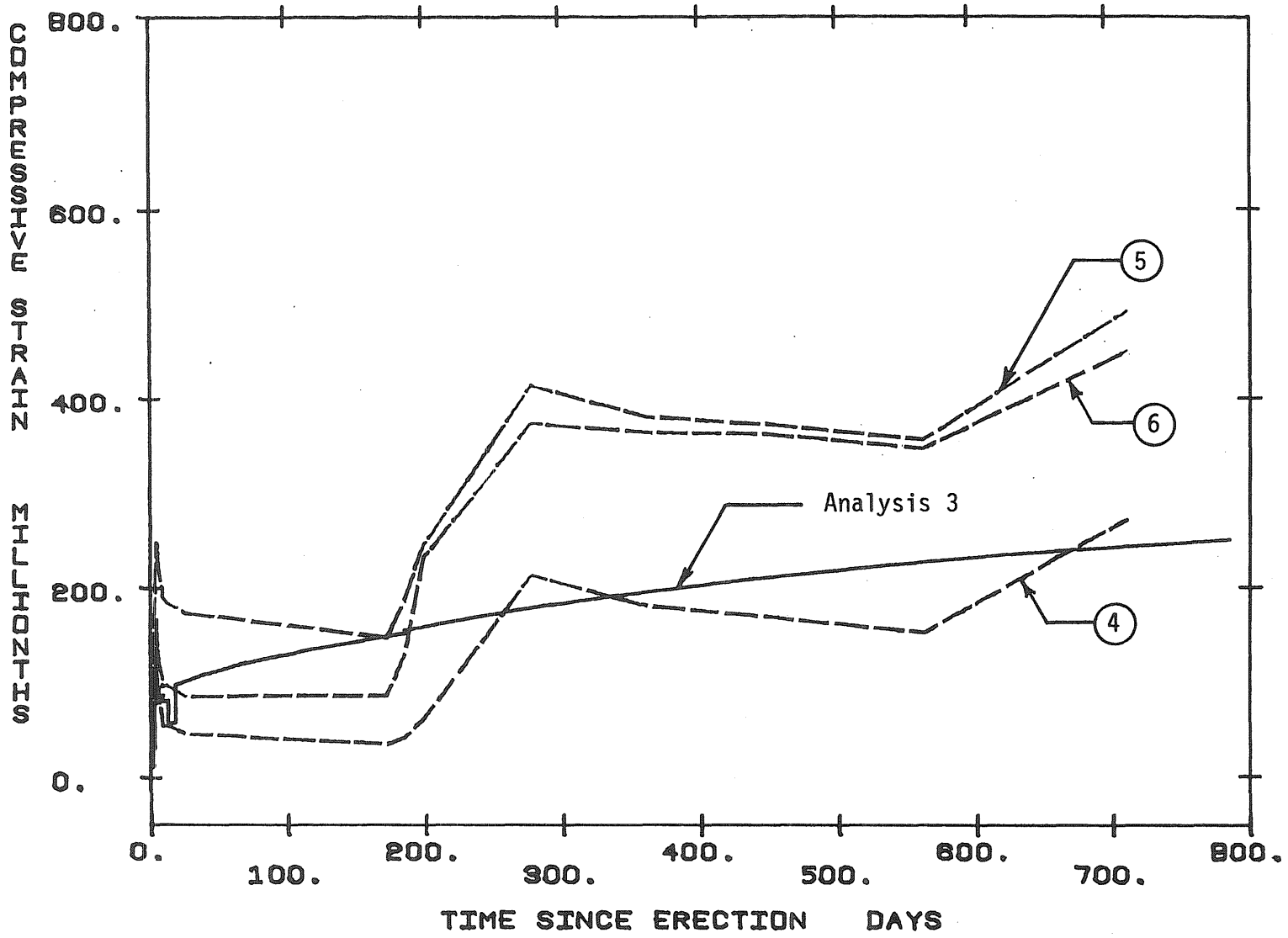

Fig. 4.23 Comparison of Measured and Calculated Concrete Strains in Top Flange of Segment SB1-N1 (Analysis 3, h = 131 in.)

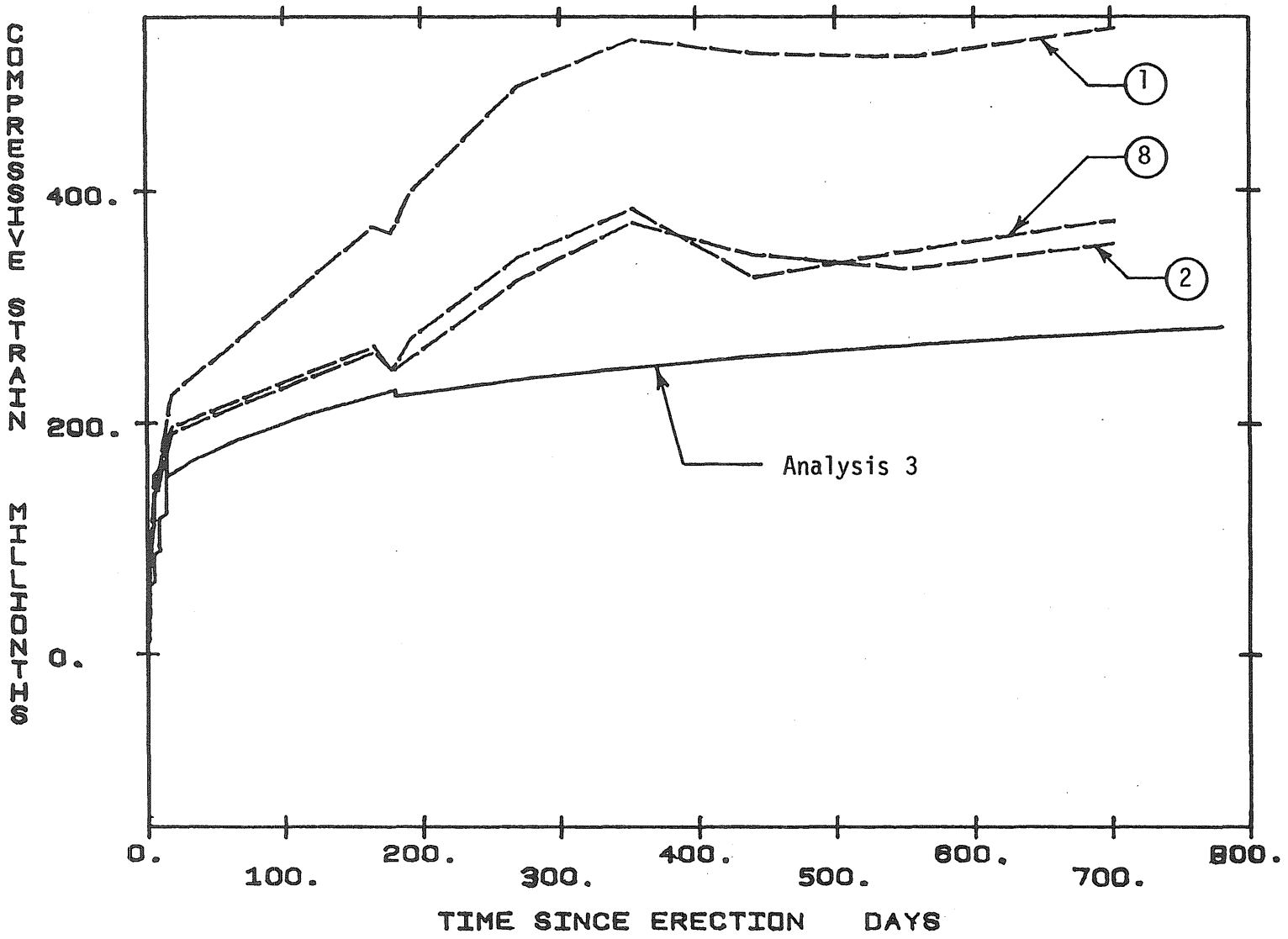

Fig. 4.24 Comparison of Measured and Calculated Concrete Strains in Bottom Flange of Segment SB1-N9 (Analysis 3, h = 8 in.)

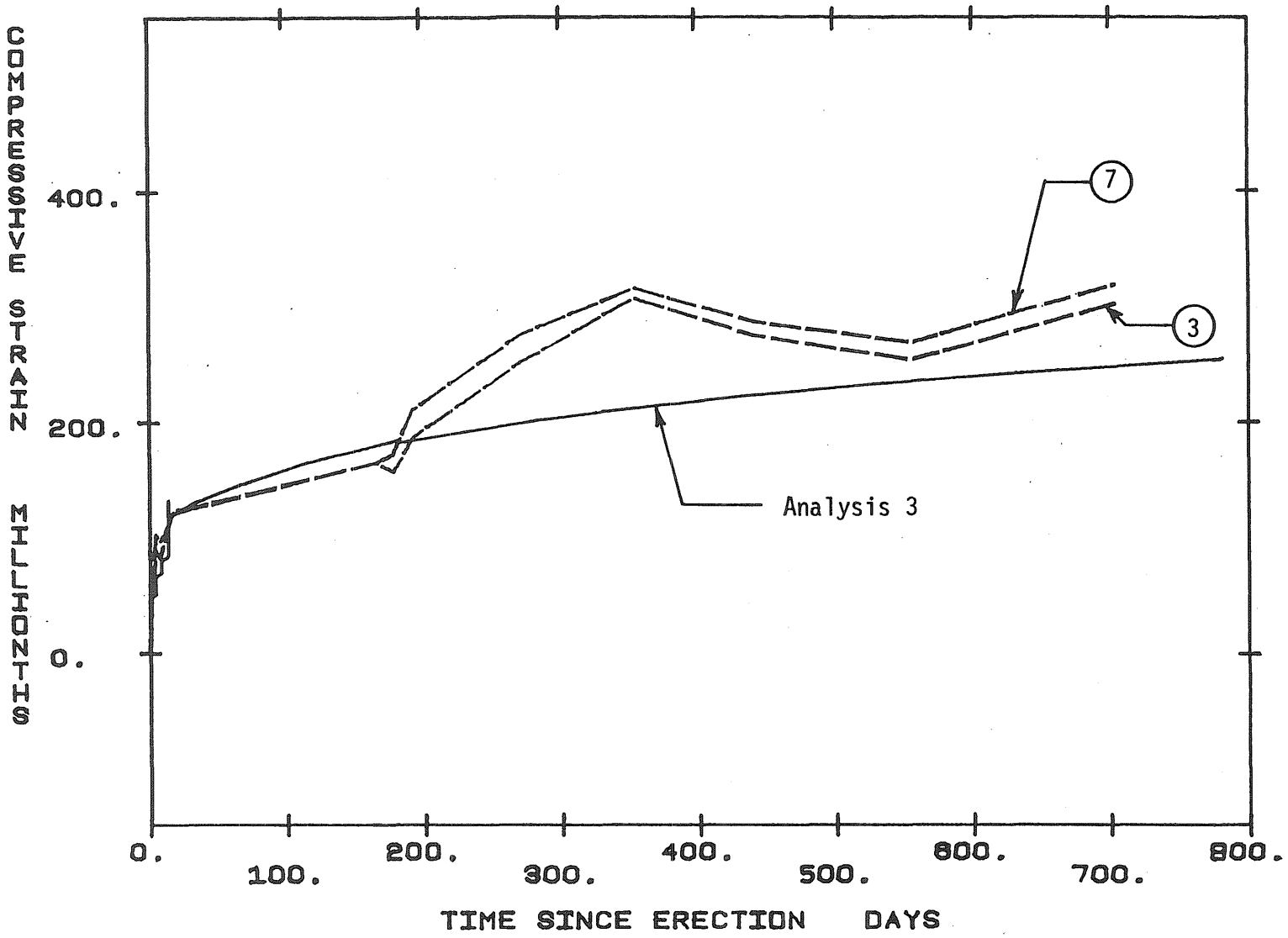

Fig. 4.25 Comparison of Measured and Calculated Concrete Strains in Webs of Segment SB1-N9 (Analysis 3, h = 56 in.)

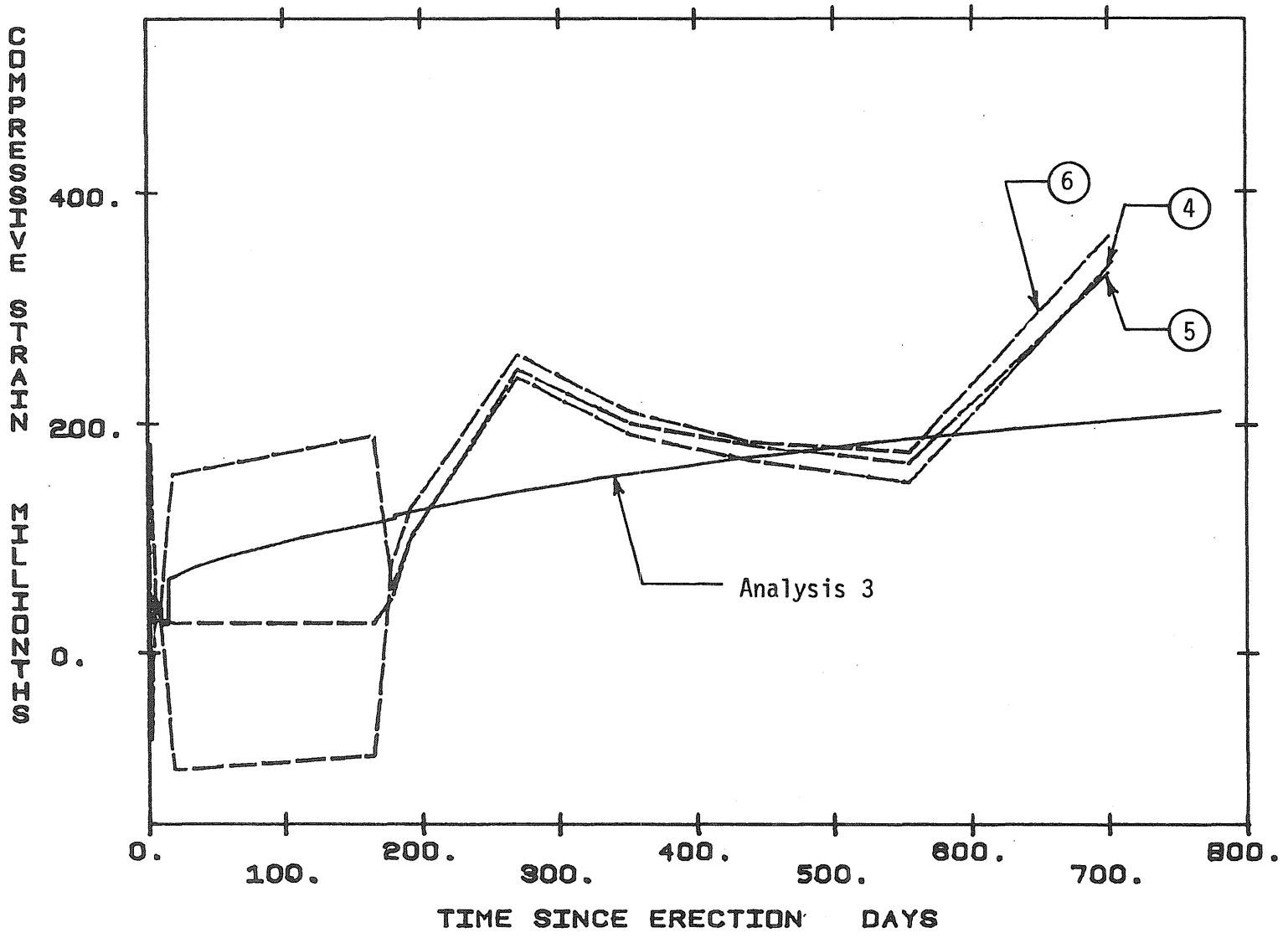

Fig. 4.26 Comparison of Measured and Calculated Concrete Strains in Top Flange of Segment SB1-N9 (Analysis 3, h = 131 in.)

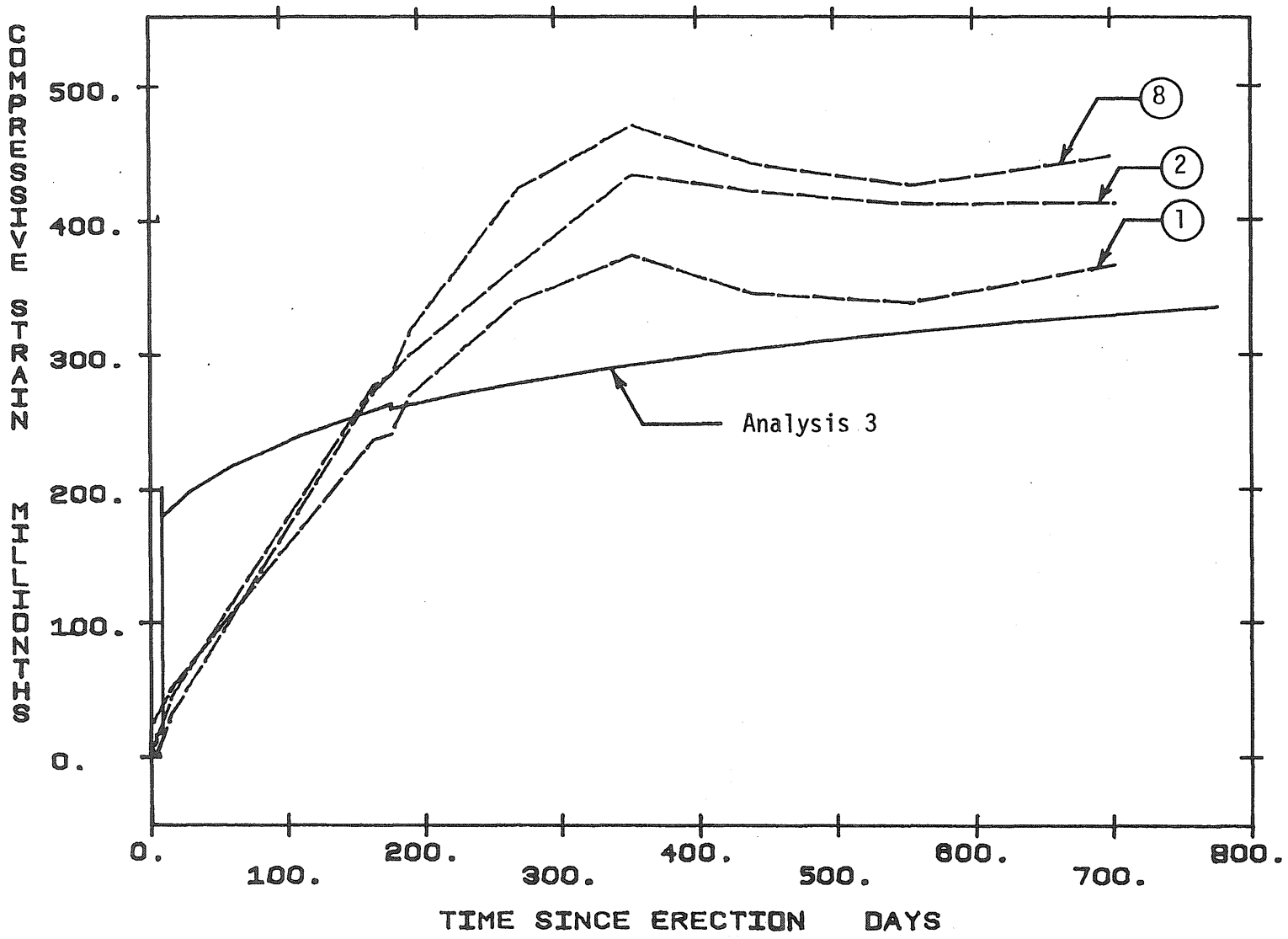

Fig. 4.27 Comparison of Measured and Calculated Concrete Strains in Bottom Flange of Segment SB1-N16 (Analysis 3, h = 8 in.)

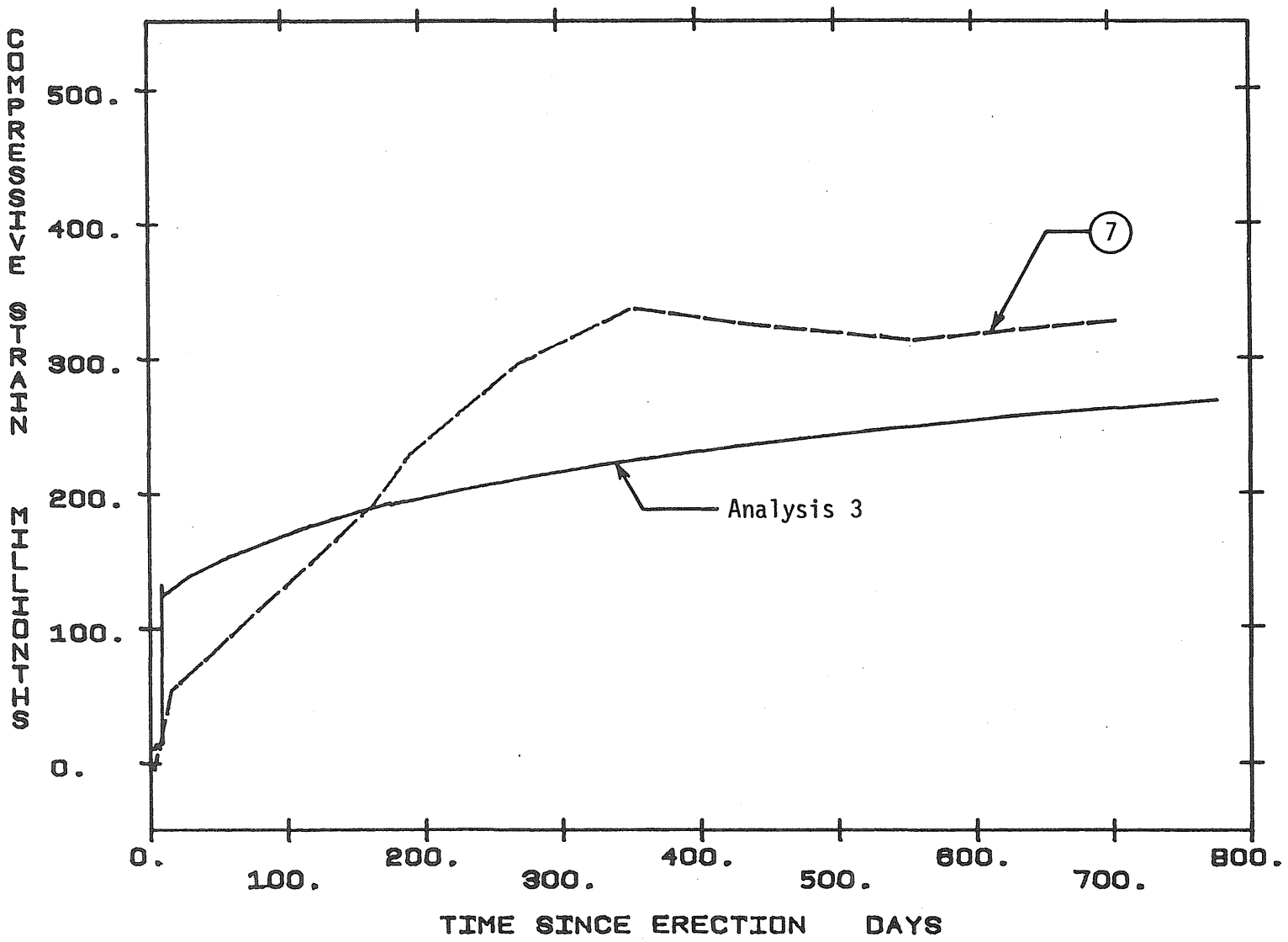

Fig. 4.28 Comparison of Measured and Calculated Concrete Strains in Webs of Segment SB1-N16 (Analysis 3, h = 56 in.)

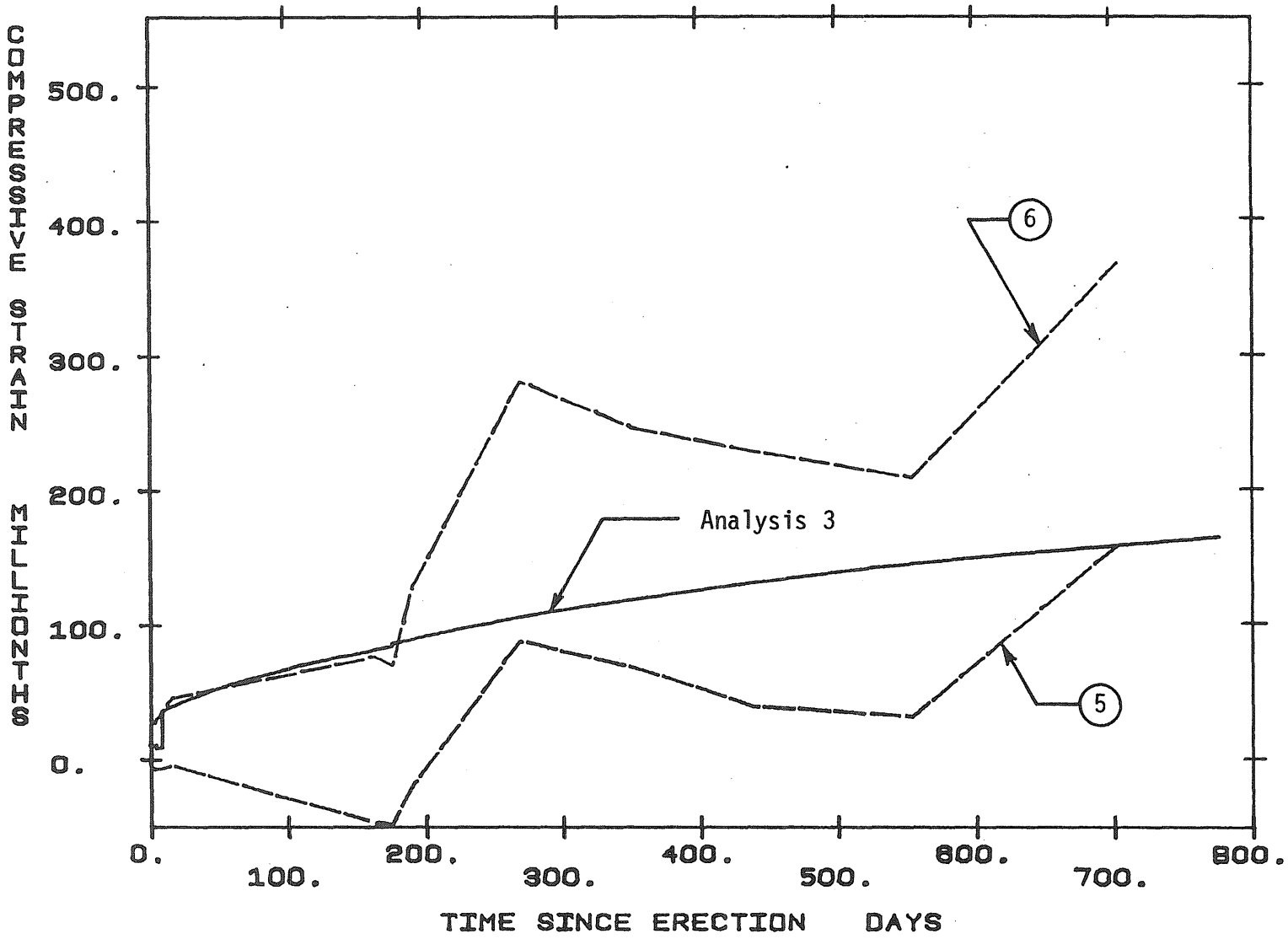

Fig. 4.29 Comparison of Measured and Calculated Concrete Strains in Top Flange of Segment SB1-N16 (Analysis 3, h = 131 in.)

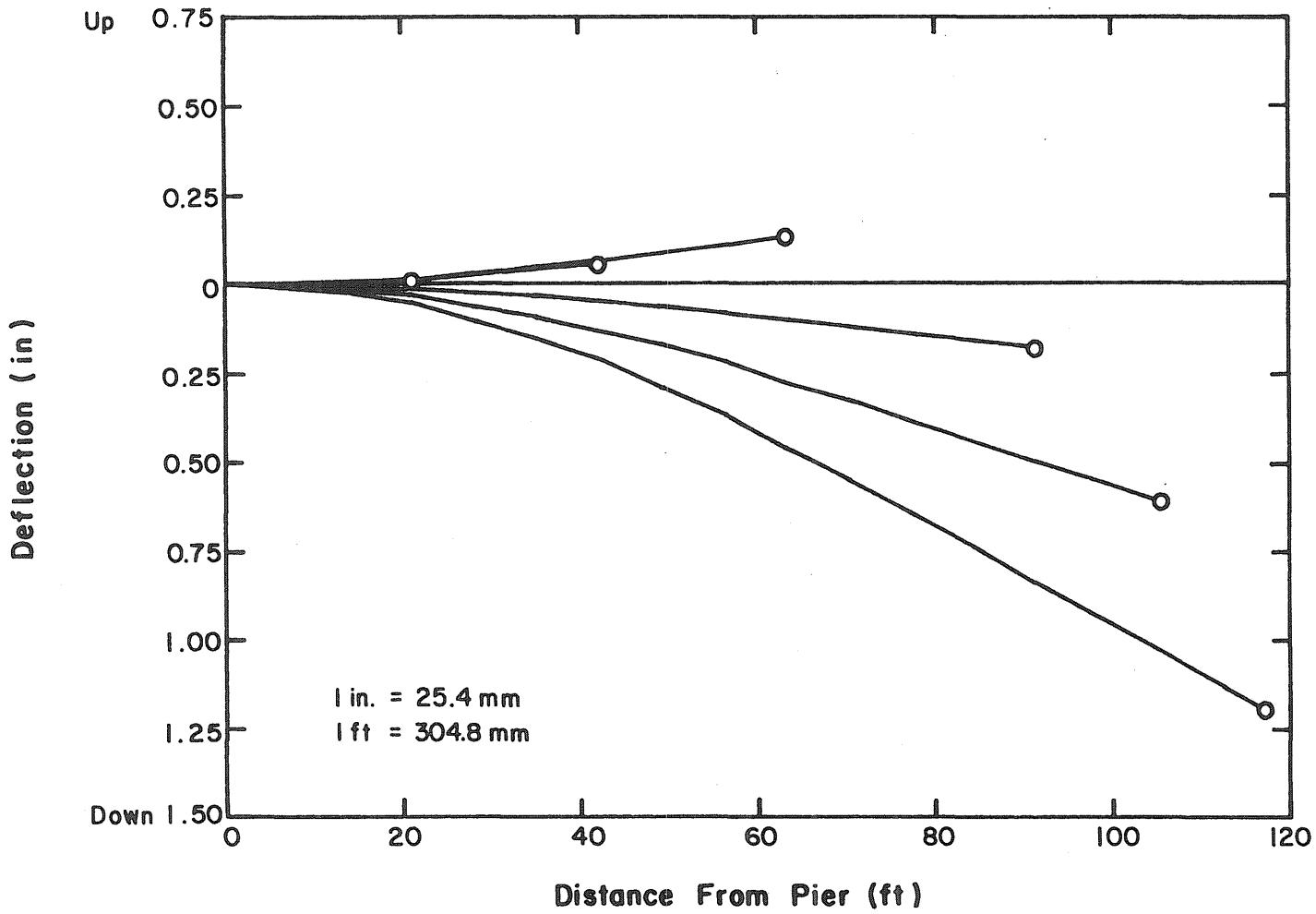

Fig. 4.30 Deflected Shape of Instrumented Cantilever During Construction as Predicted by Analysis 1

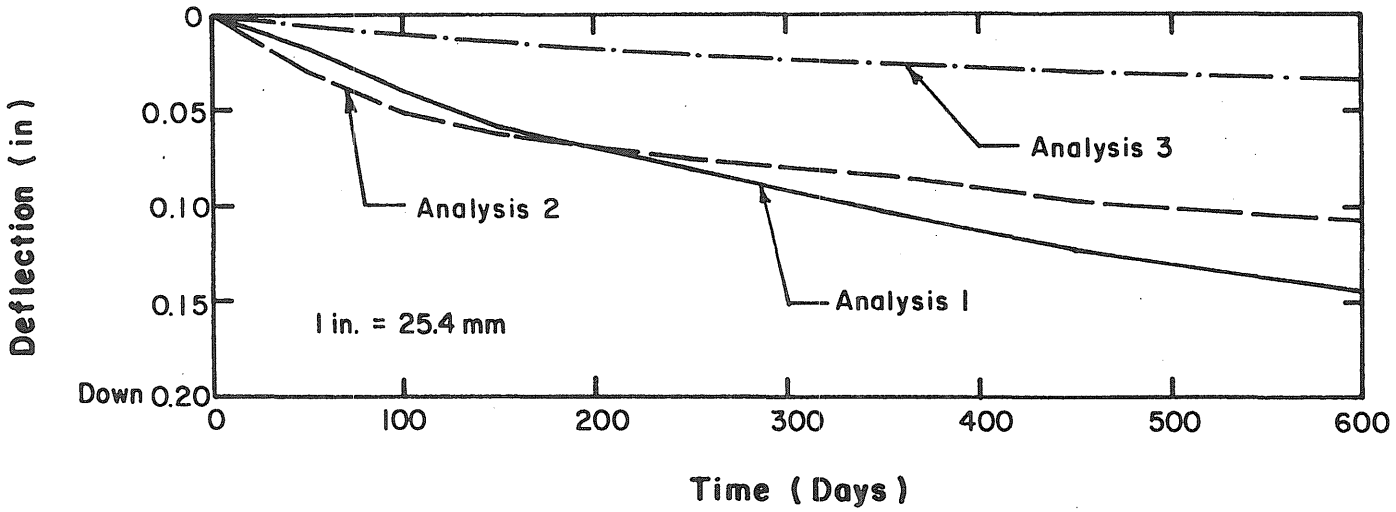

Fig. 4.31 Calculated Change in Deflection of Segment SB1-N16 Since Completion of Final Structure

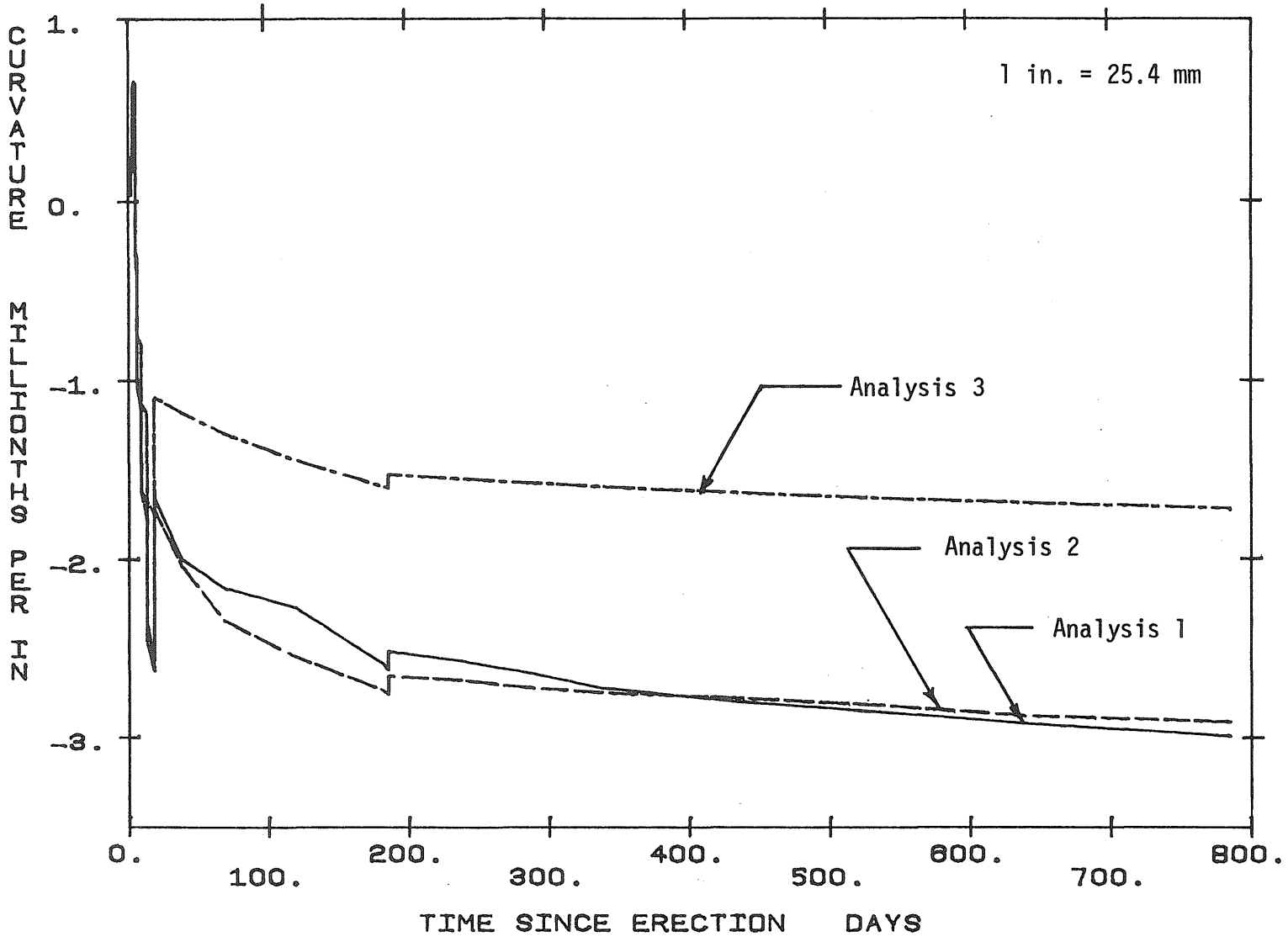

Fig. 4.32 Calculated Curvatures for Segment SB1-N1

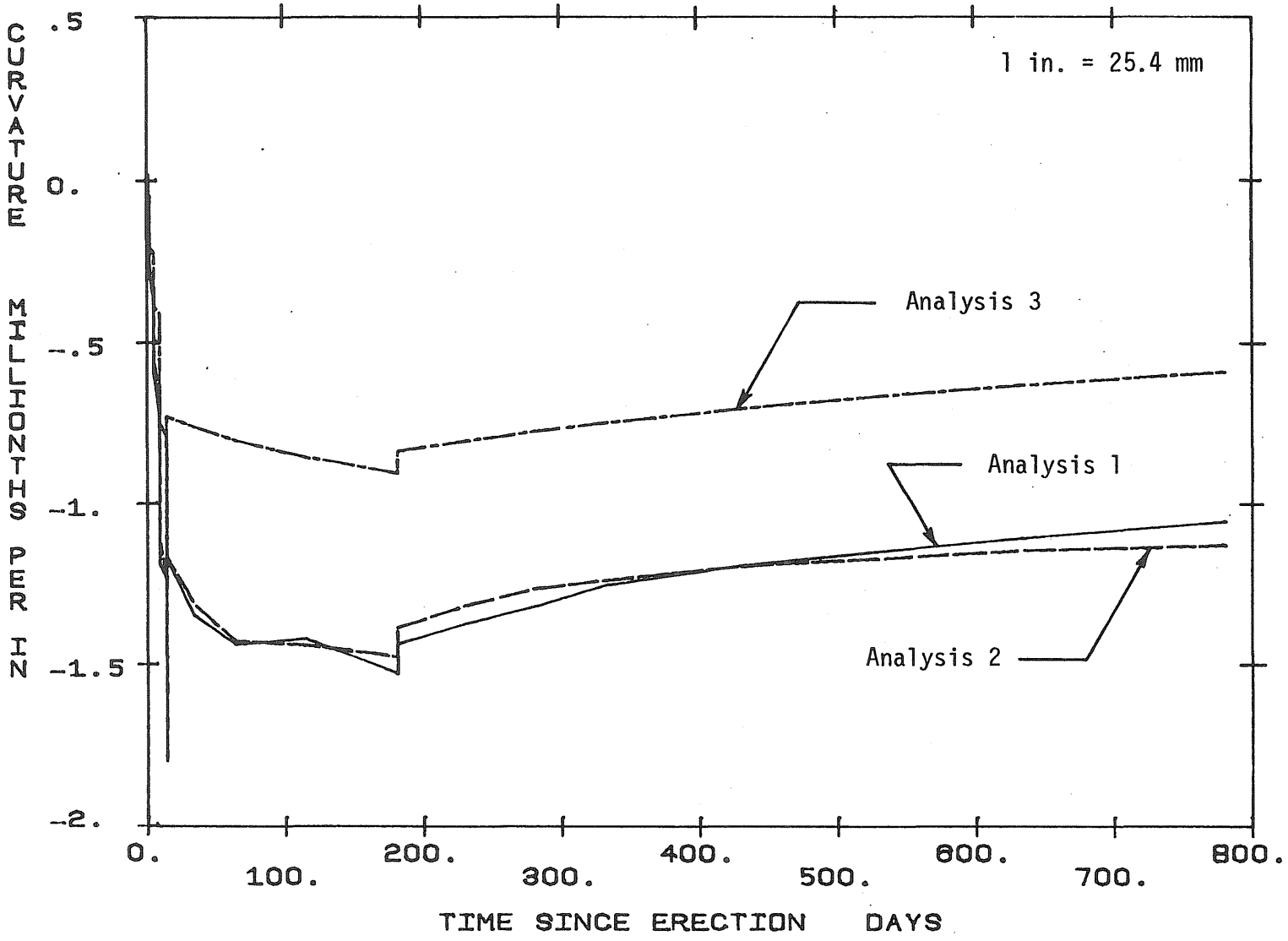

Fig. 4.33 Calculated Curvatures for Segment SB1-N9

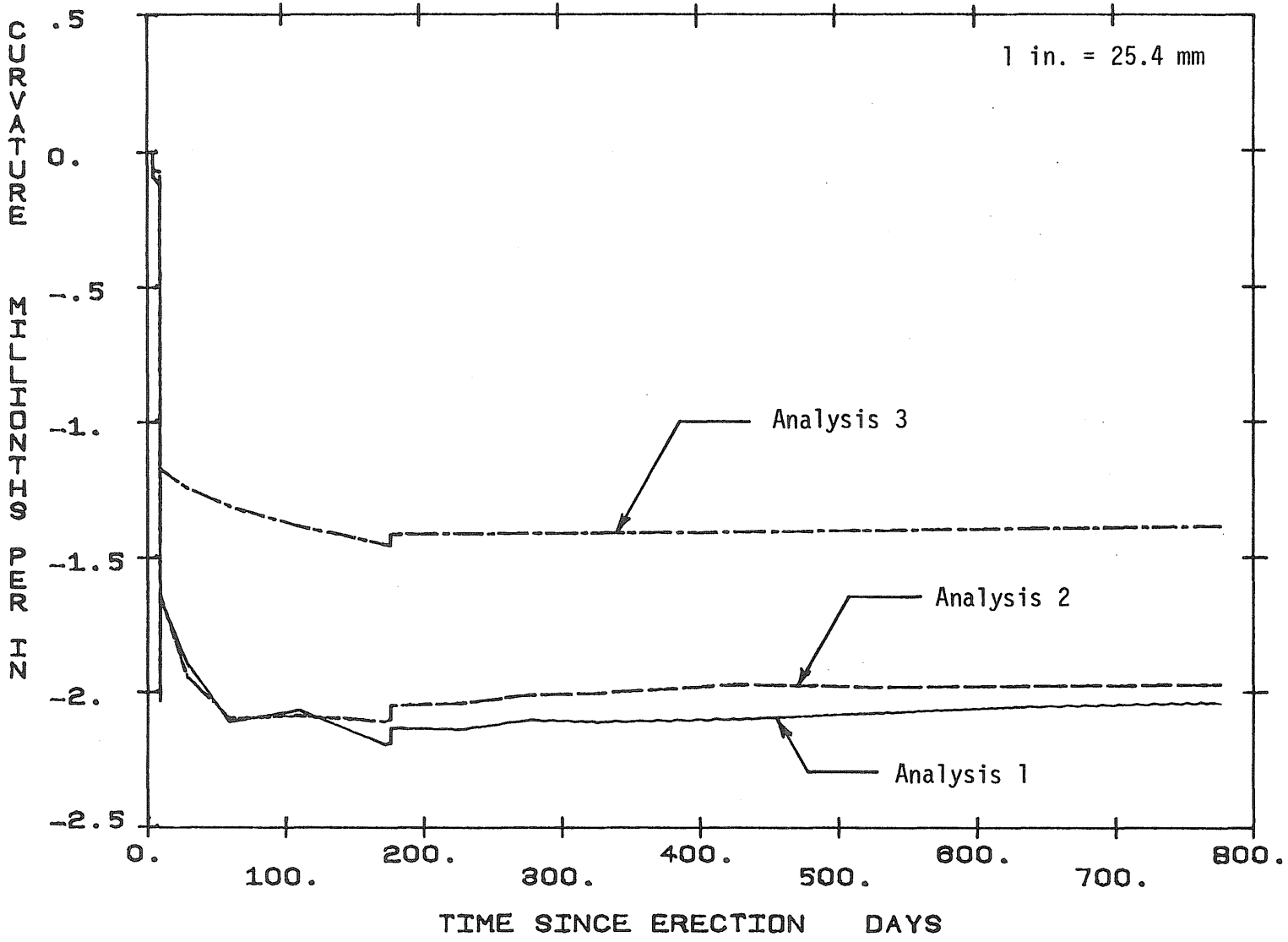

Fig. 4.34 Calculated Curvatures for Segment SB1-N16

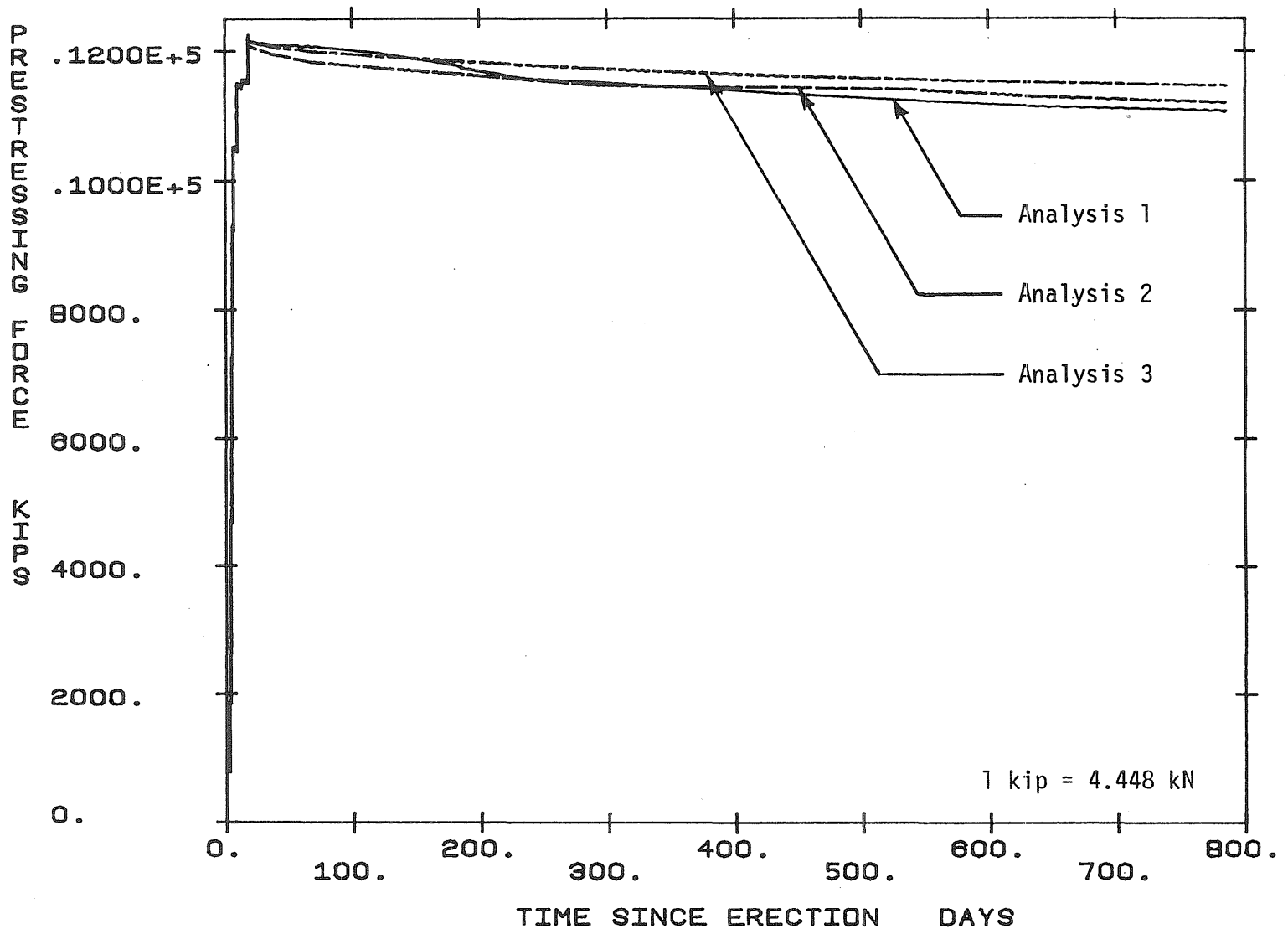

Fig. 5.1 Calculated Total Prestressing Force at Segment SB1-N1

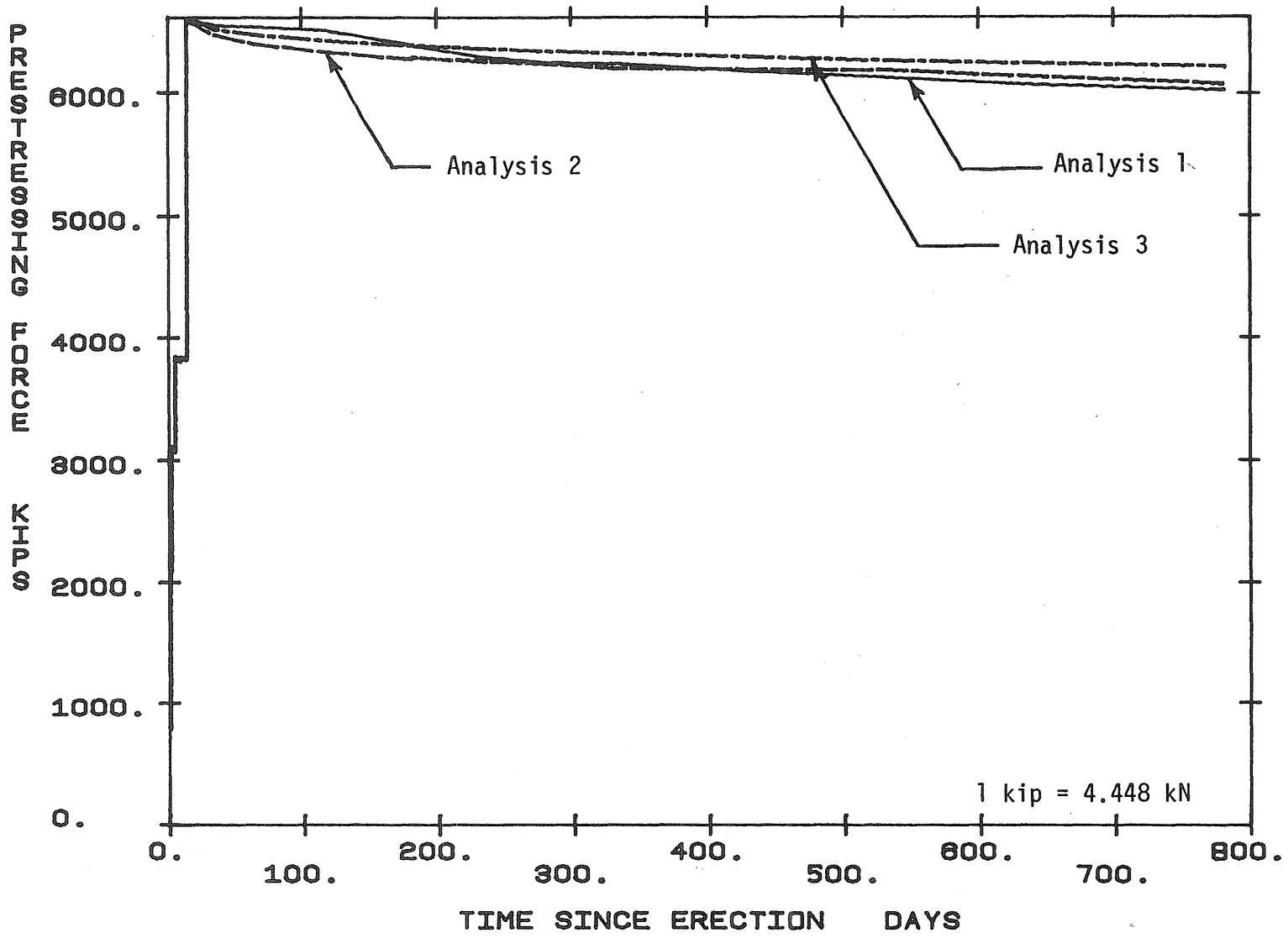

Fig. 5.2 Calculated Total Prestressing Force at Segment SB1-N9

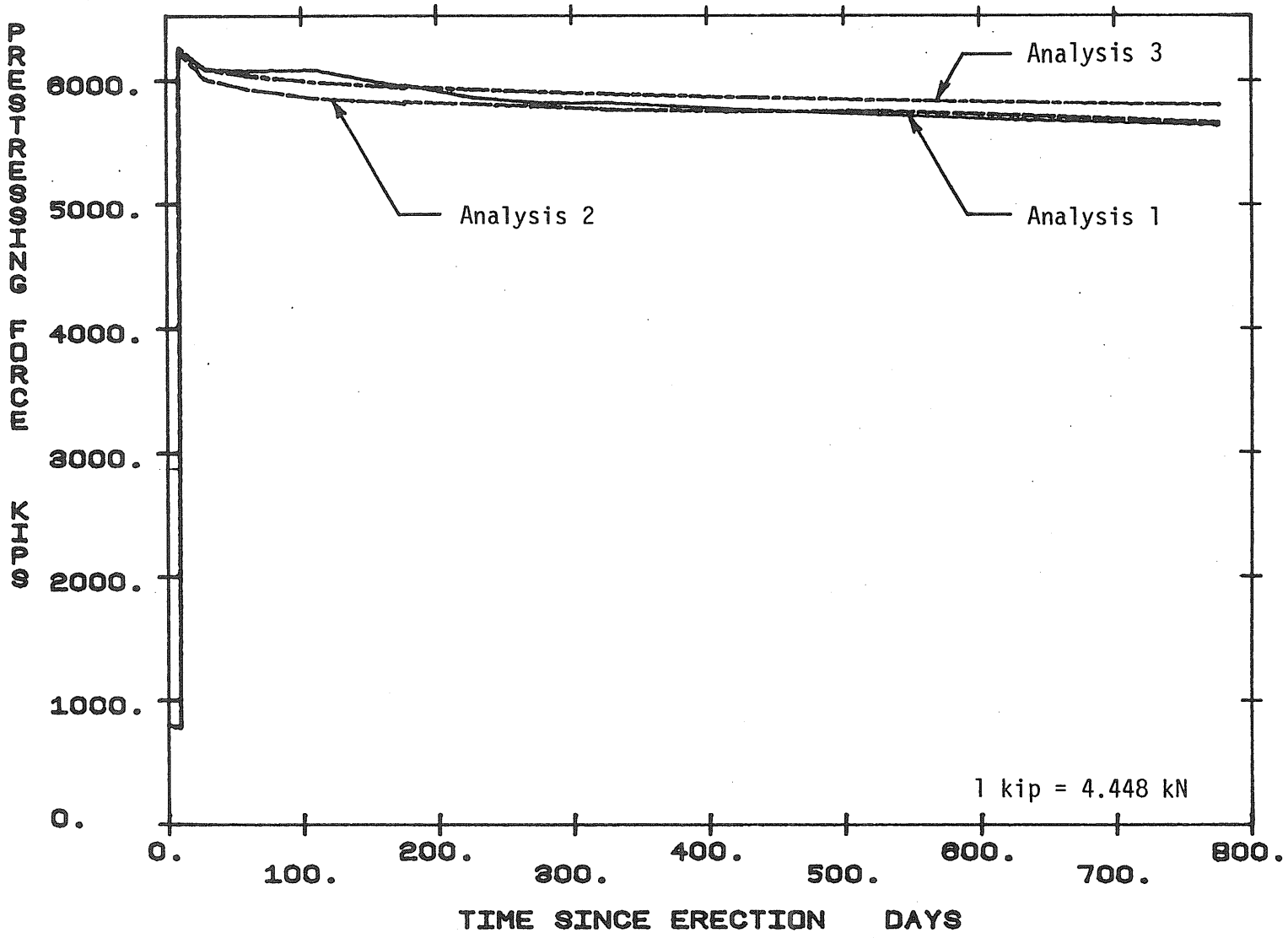

Fig. 5.3 Calculated Total Prestressing Force at Segment SB1-N16

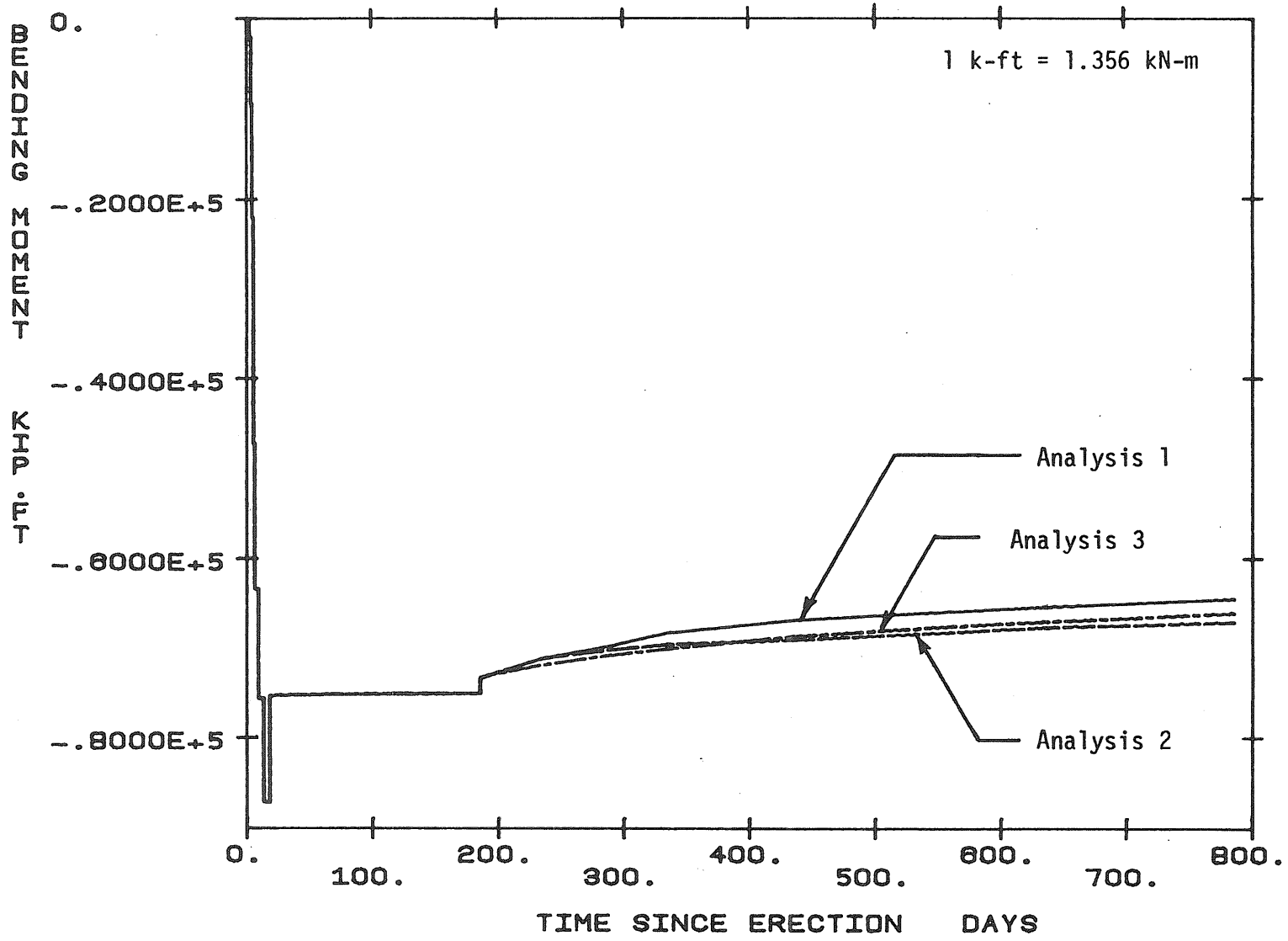

Fig. 5.4 Calculated Bending Moment at Segment SB1-N1

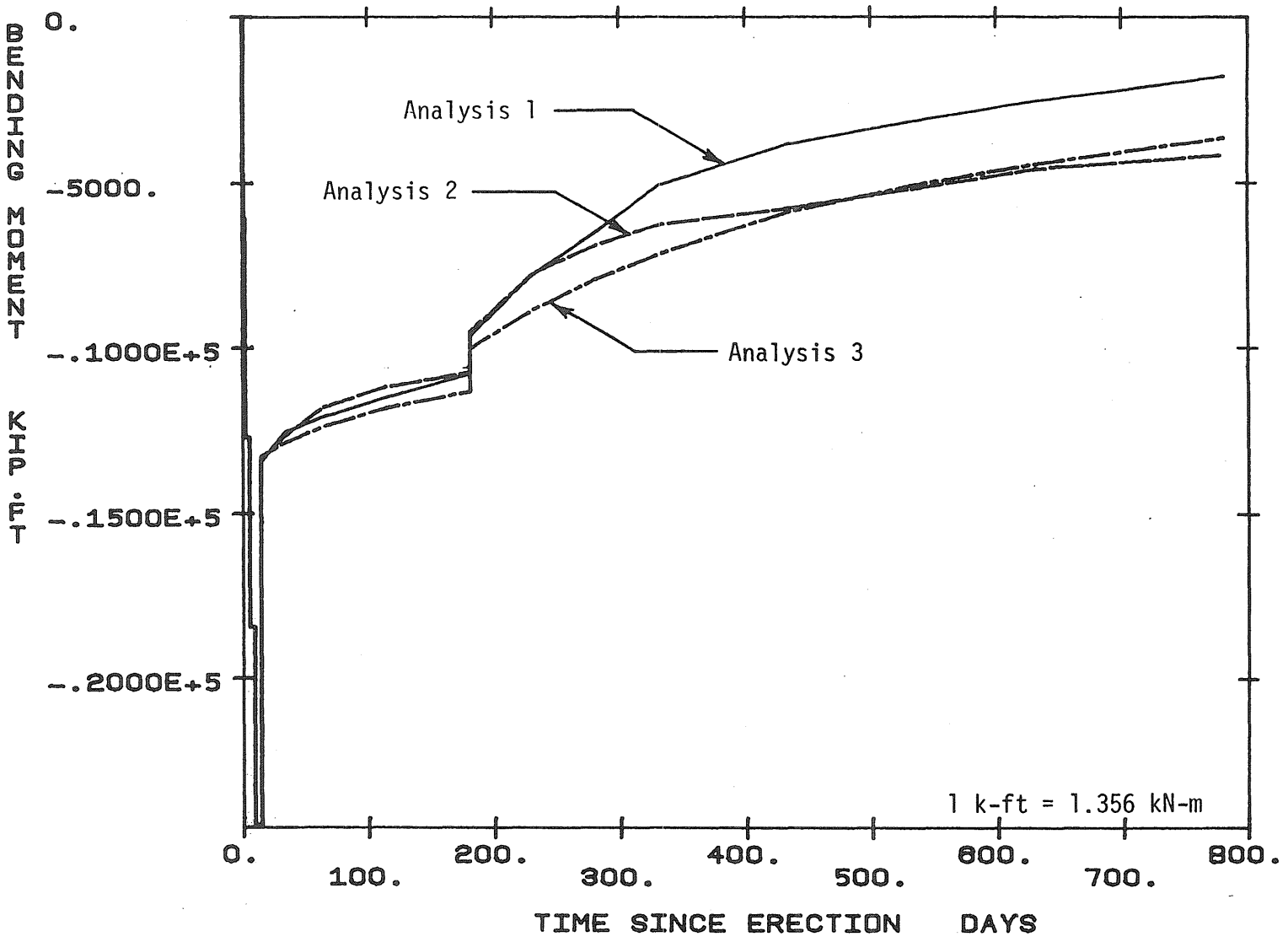

Fig. 5.5 Calculated Bending Moment at Segment SB1-N9

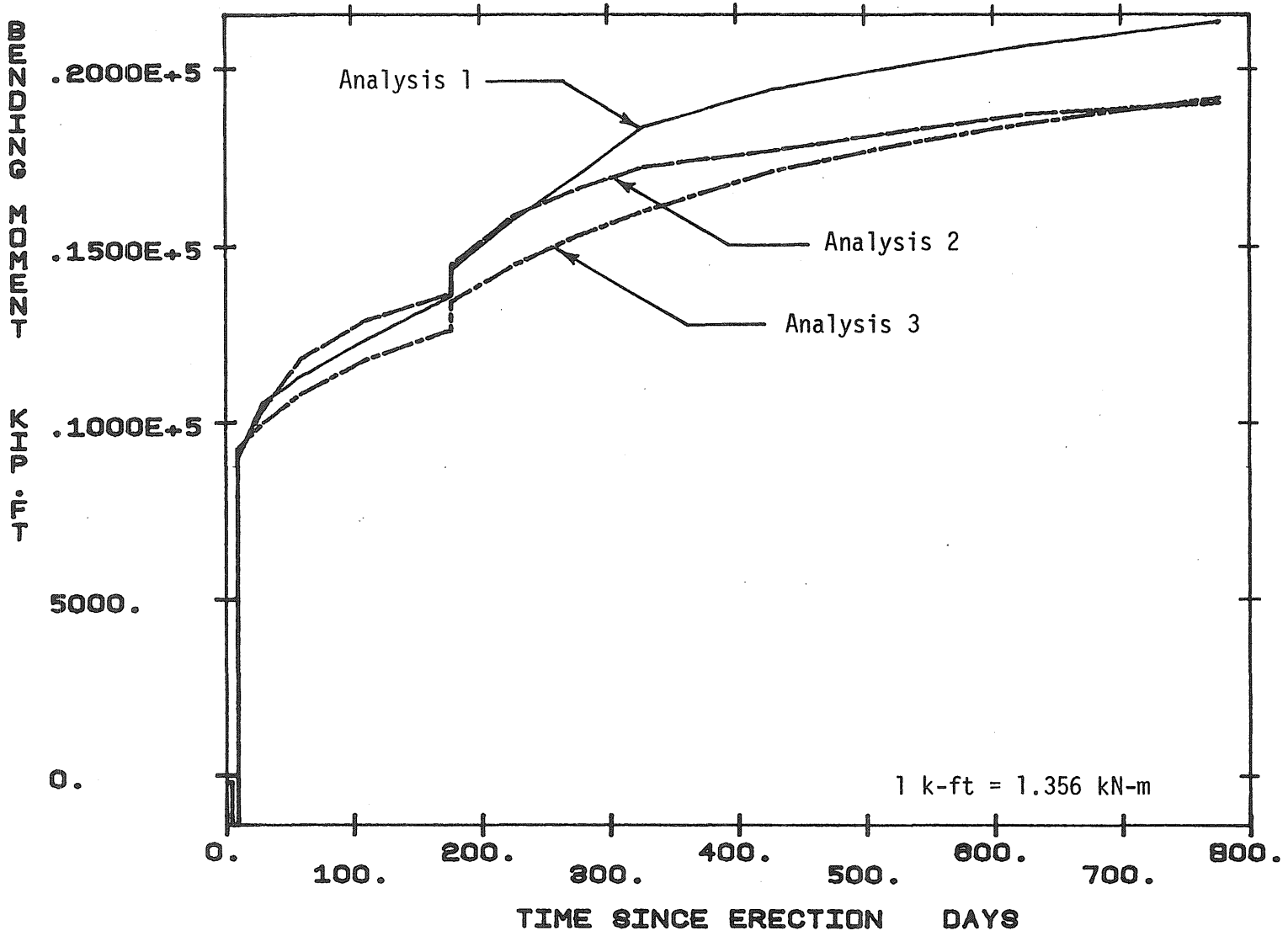

Fig. 5.6 Calculated Bending Moment at Segment SB1-N16

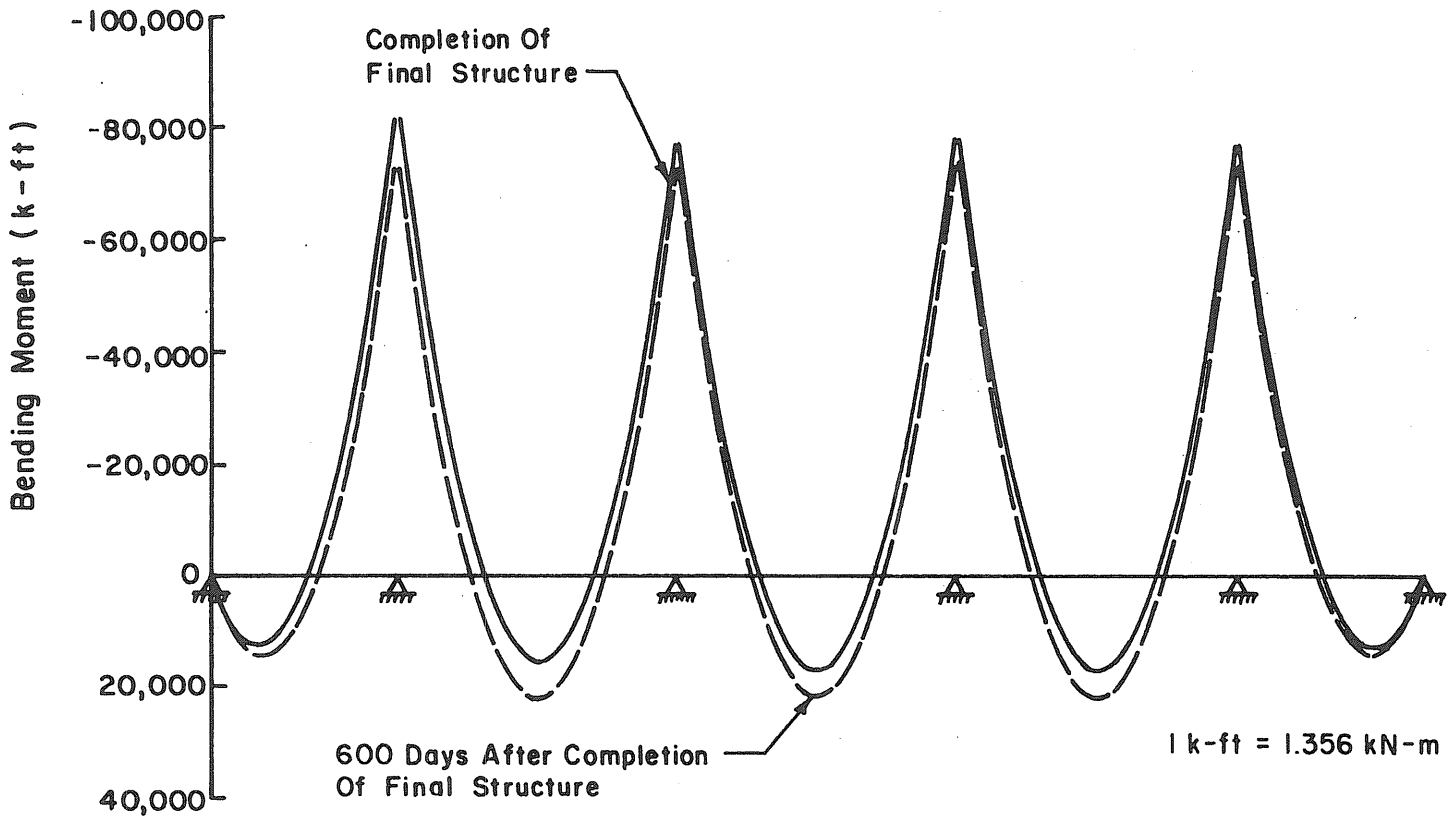

Fig. 5.7 Redistribution of Bending Moment in the Final Structure as Predicted by Analysis 1

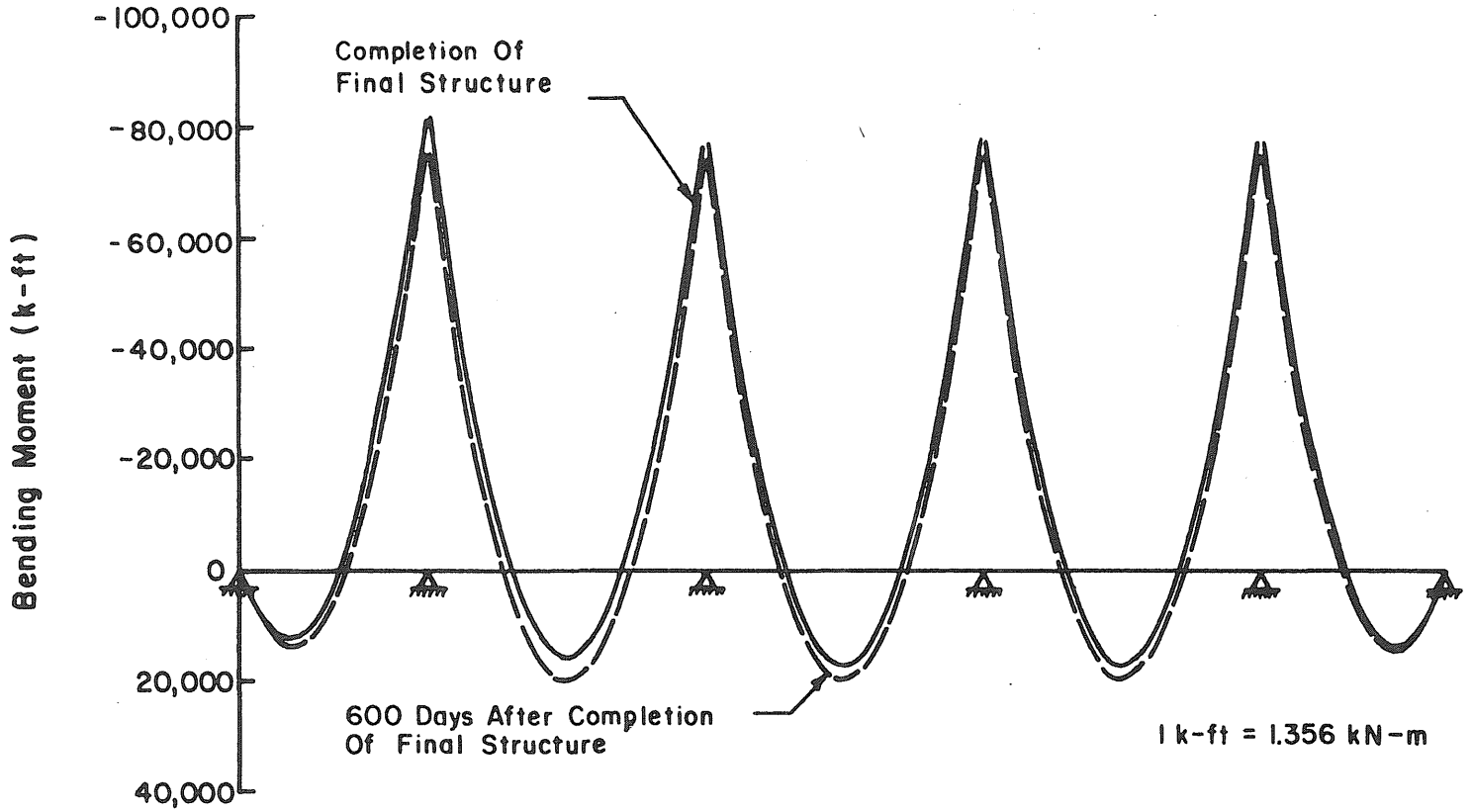

Fig. 5.8 Redistribution of Bending Moment in the Final Structure as Predicted by Analysis 2

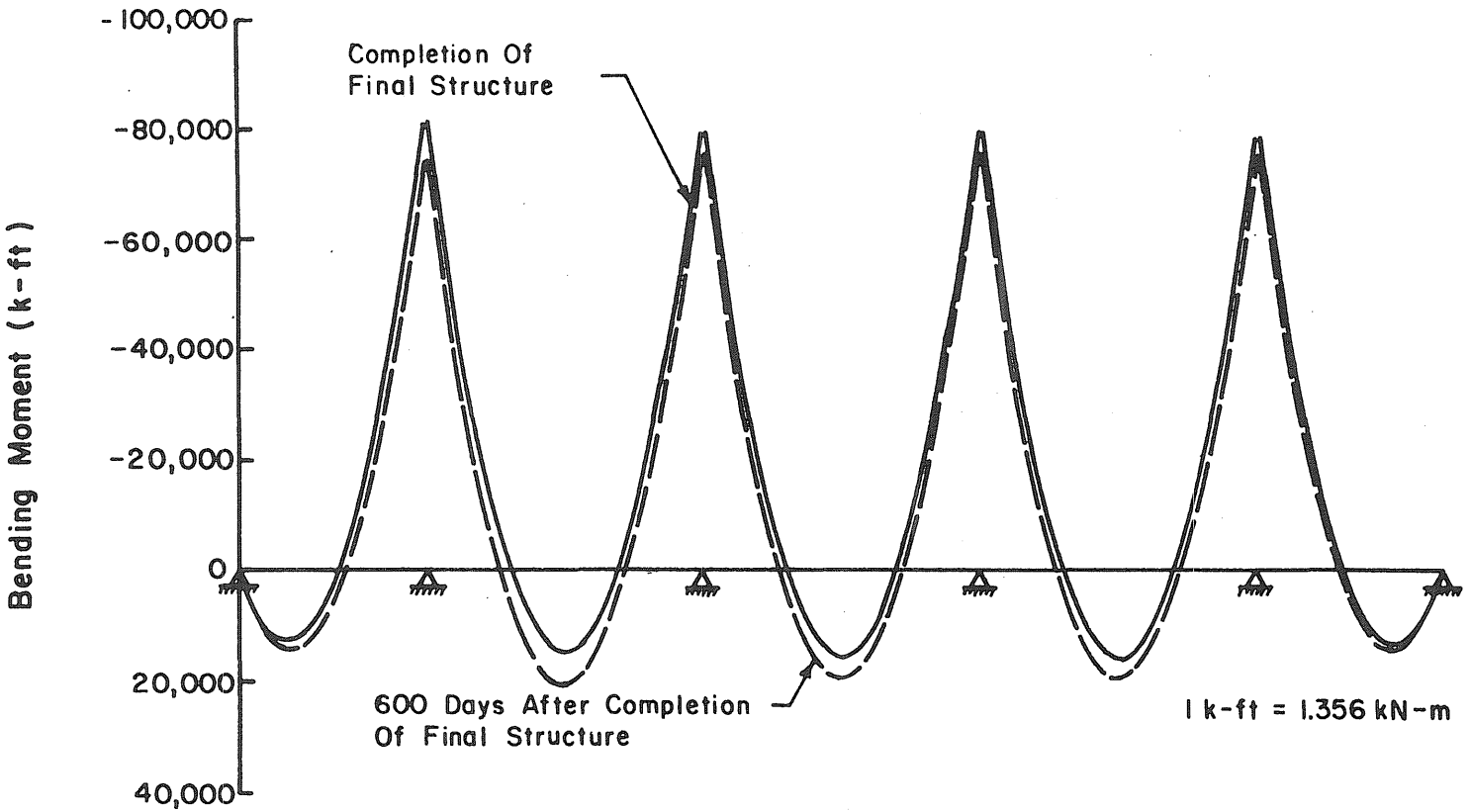

Fig. 5.9 Redistribution of Bending Moment in the Final Structure as Predicted by Analysis 3

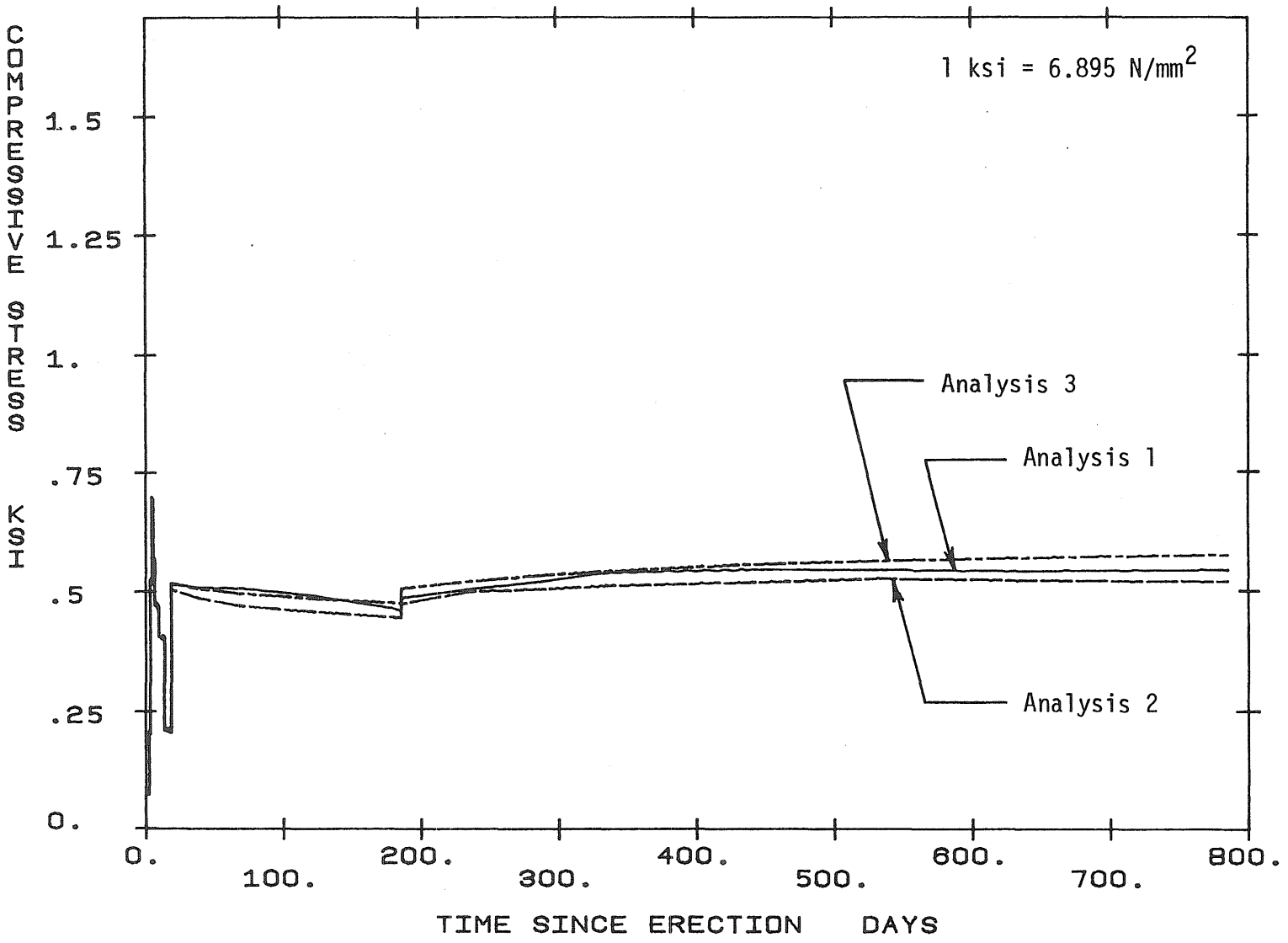

Fig. 5.10 Calculated Top Fiber Concrete Stress at Segment SB1-N1

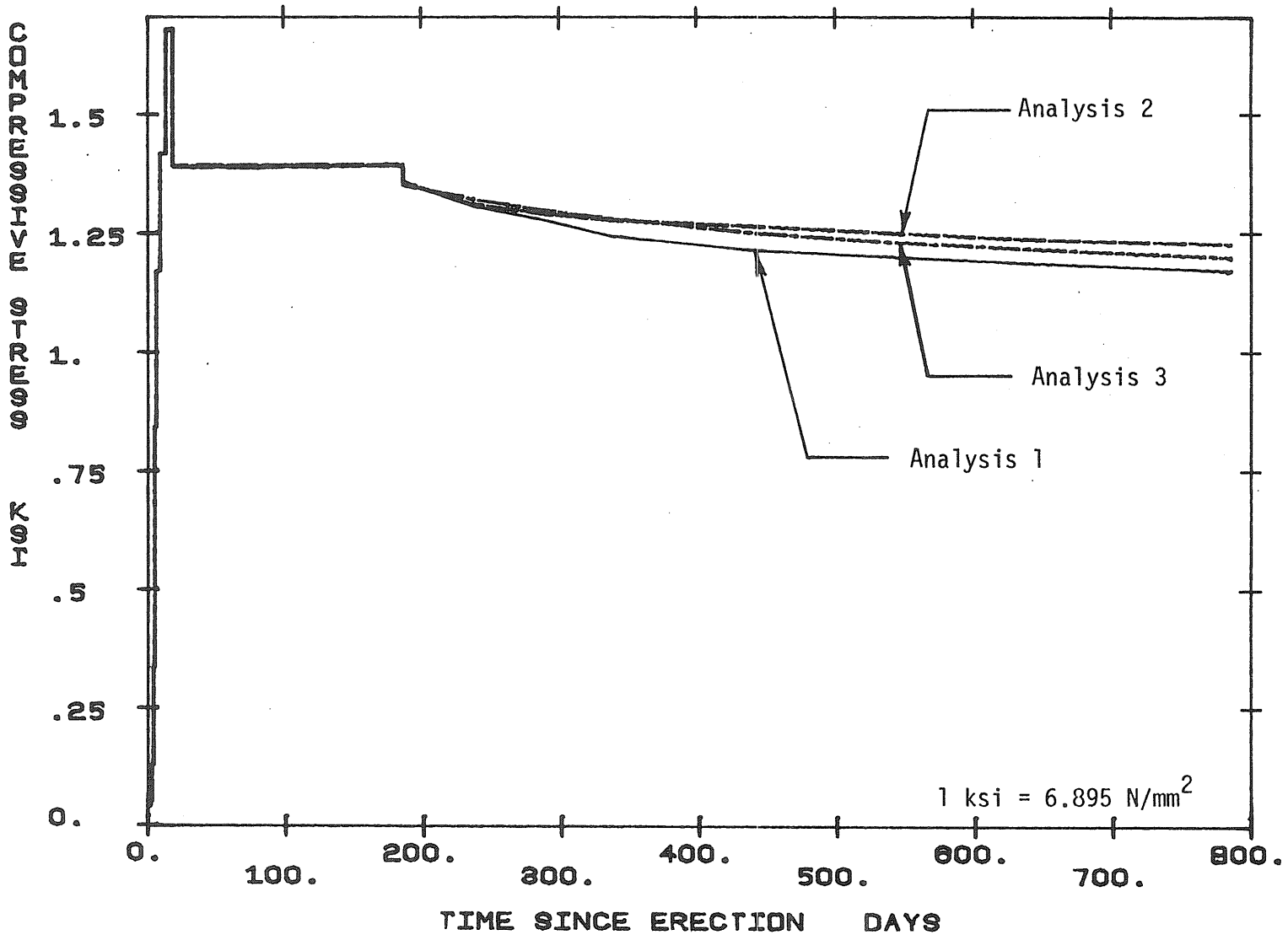

Fig. 5.11 Calculated Bottom Fiber Concrete Stress at Segment SB1-N1

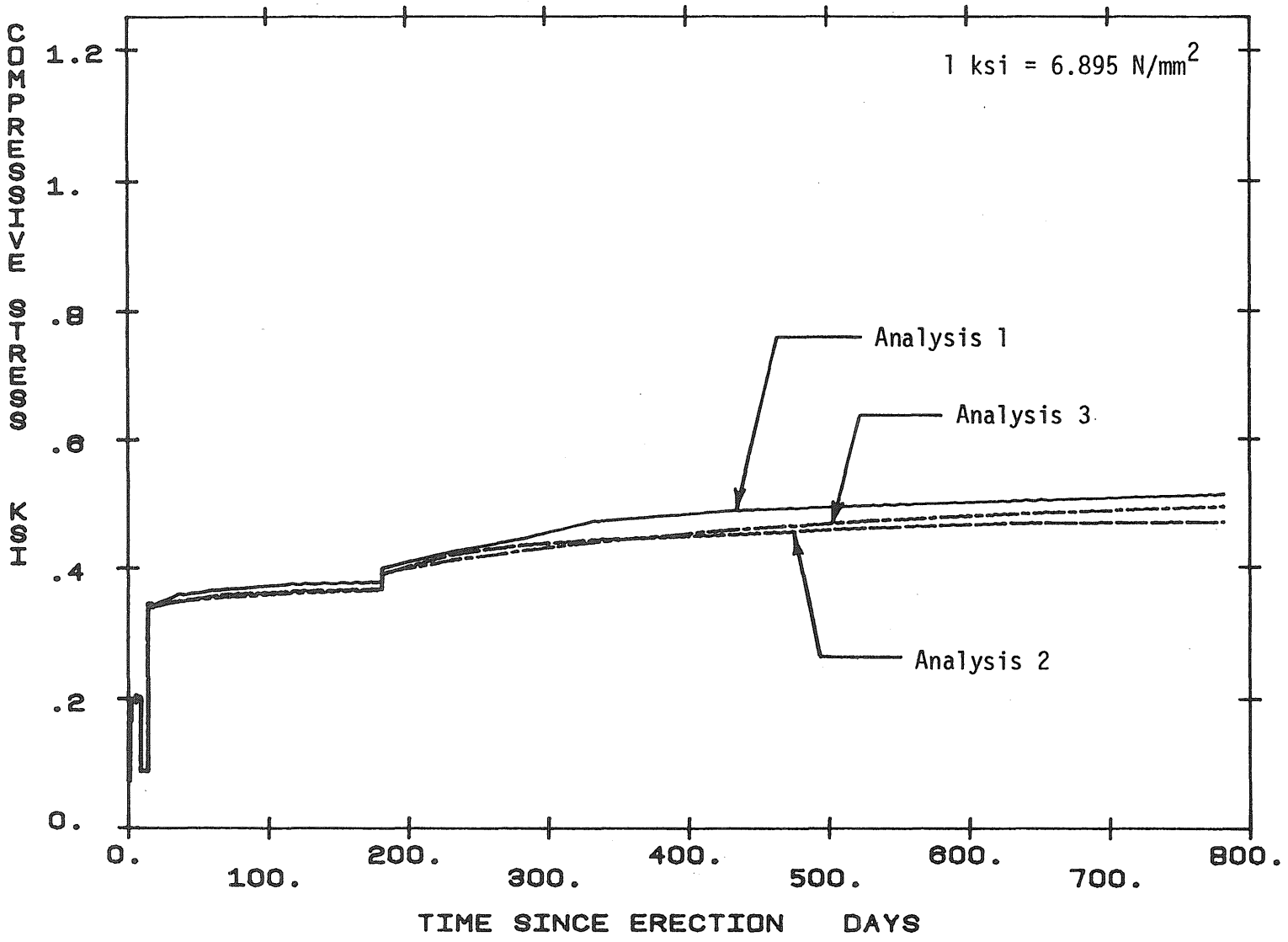

Fig. 5.12 Calculated Top Fiber Concrete Stresses at Segment SB1-N9

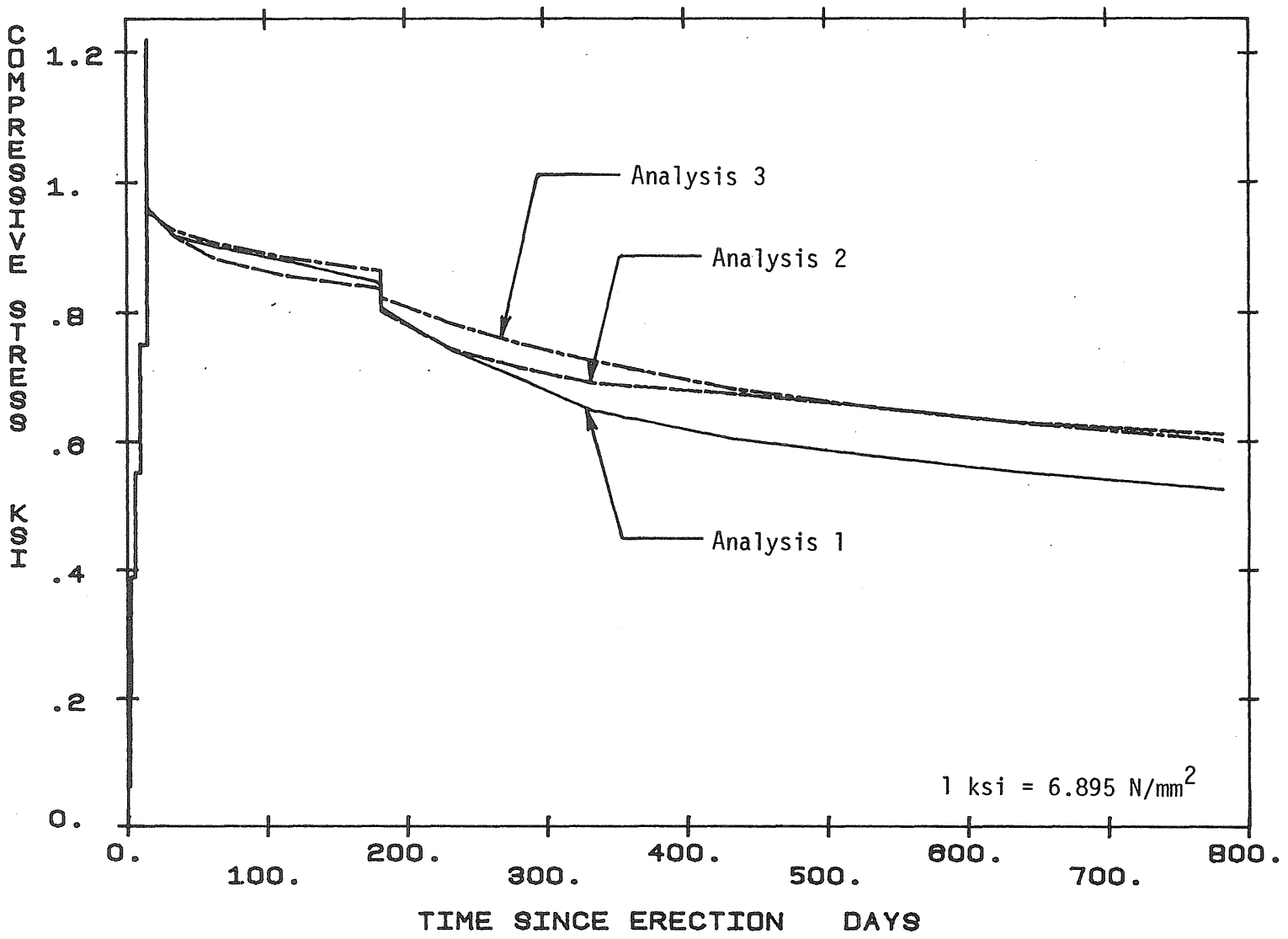

Fig. 5.13 Calculated Bottom Fiber Concrete Stresses at Segment SB1-N9

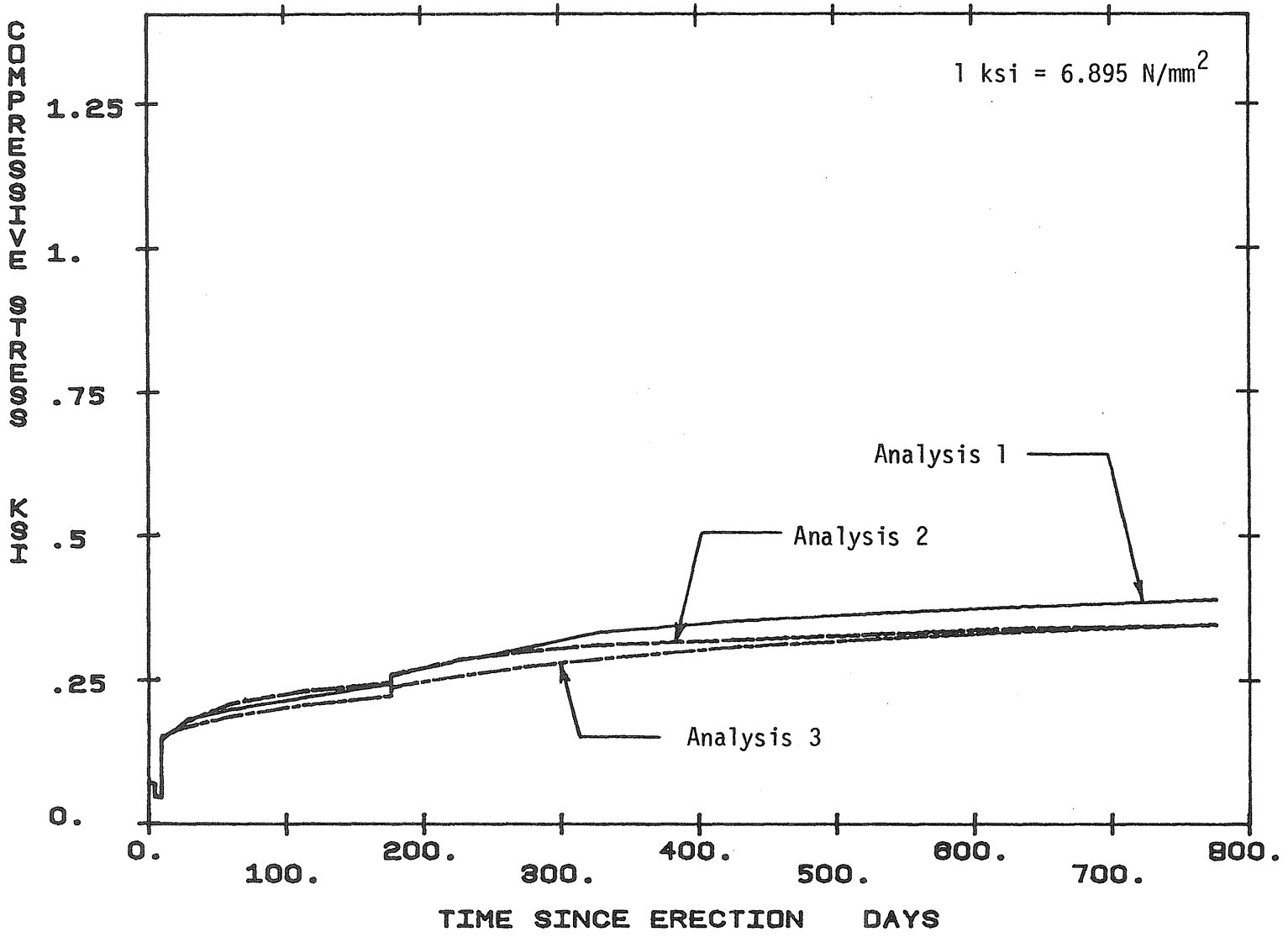

Fig. 5.14 Calculated Top Fiber Concrete Stresses at Segment SB1-N16

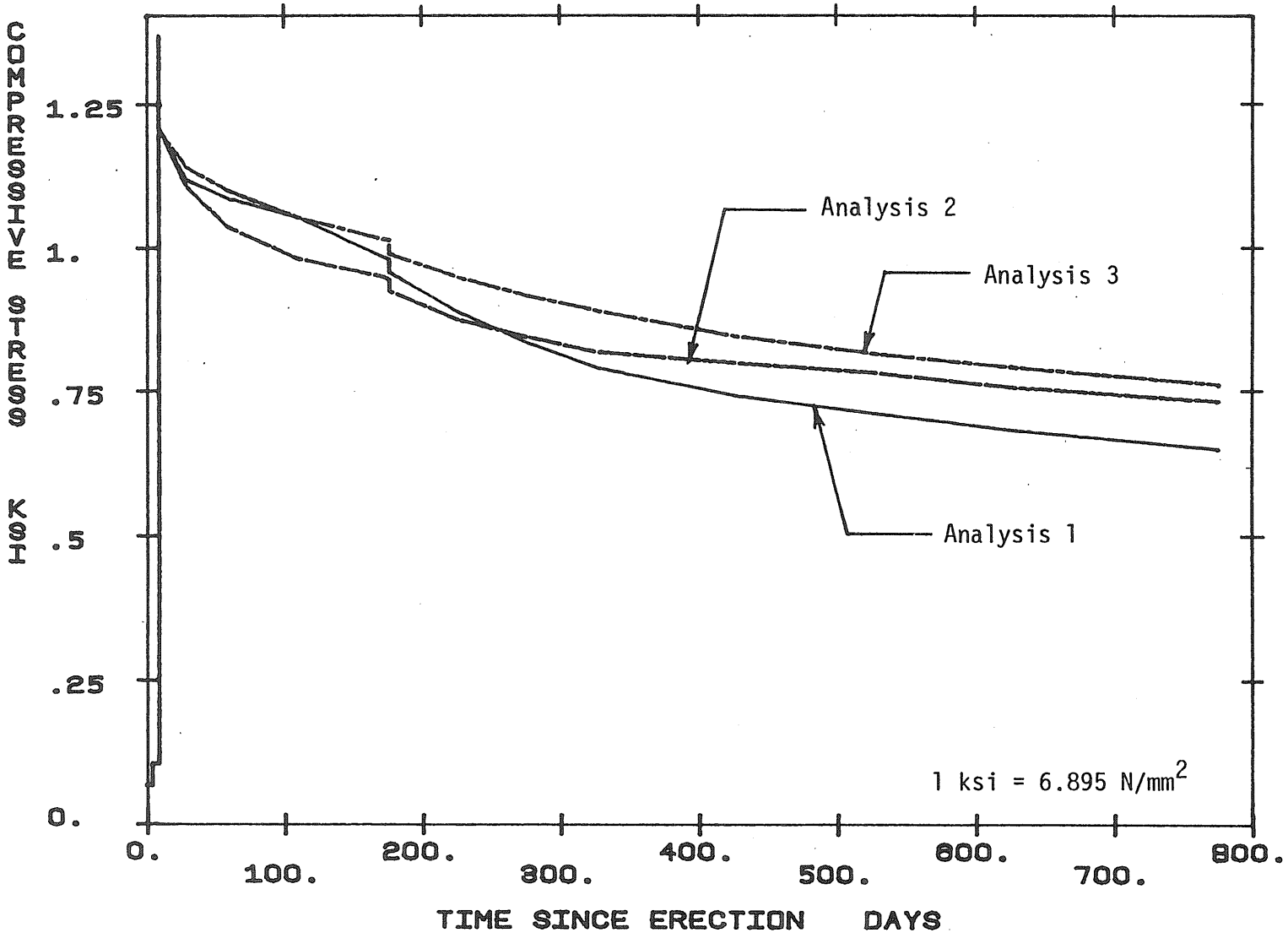

Fig. 5.15 Calculated Bottom Fiber Concrete Stresses at Segment SB1-N16

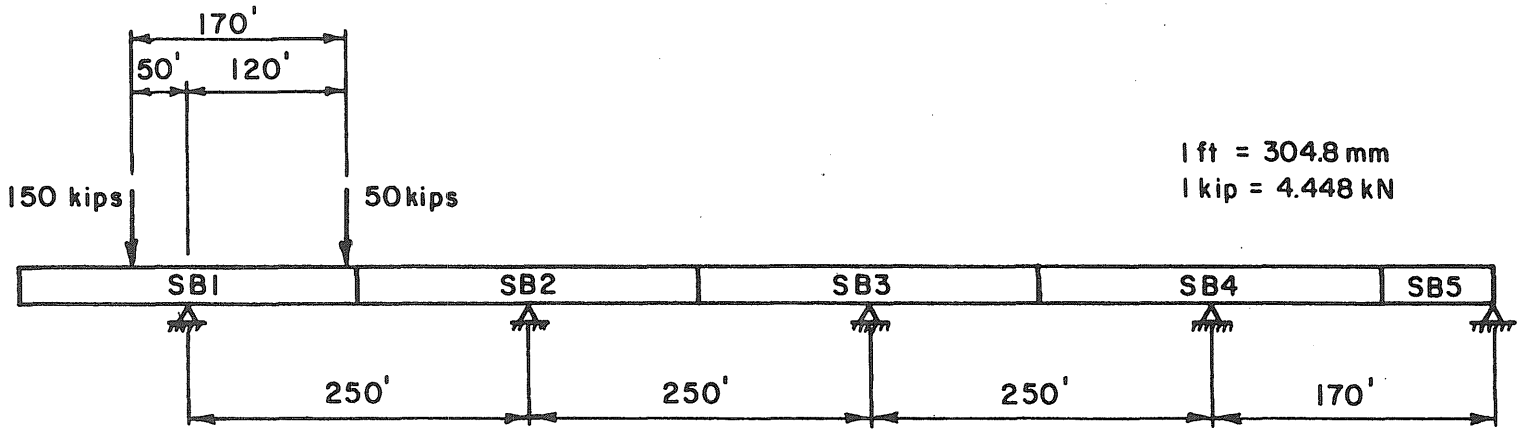

Fig. 5.16 Construction Loads Applied to Intermediate Structure 9

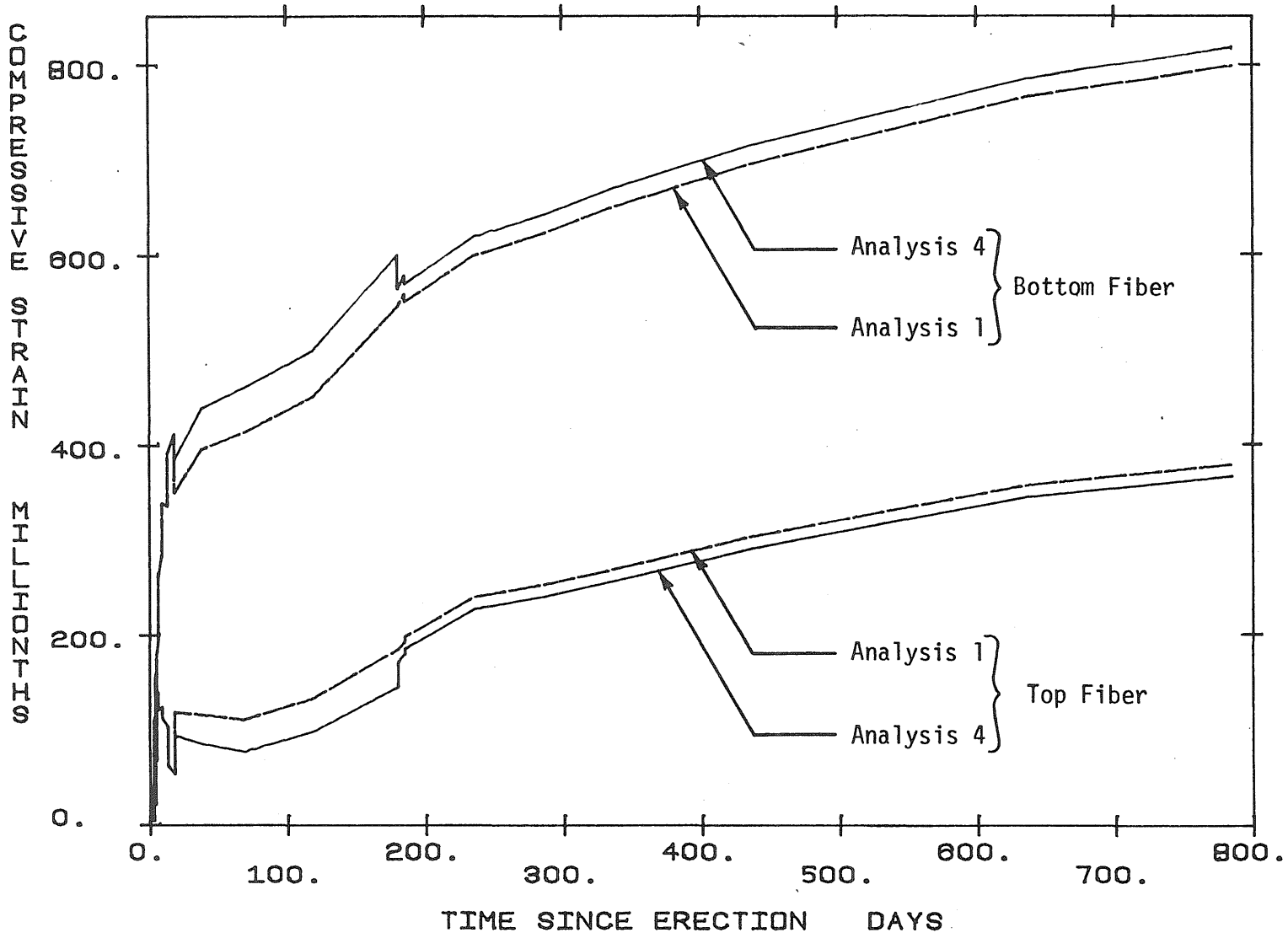

Fig. 5.17 Effects of the Construction Loads on the Extreme Fiber Concrete Strains at Segment SB1-N1

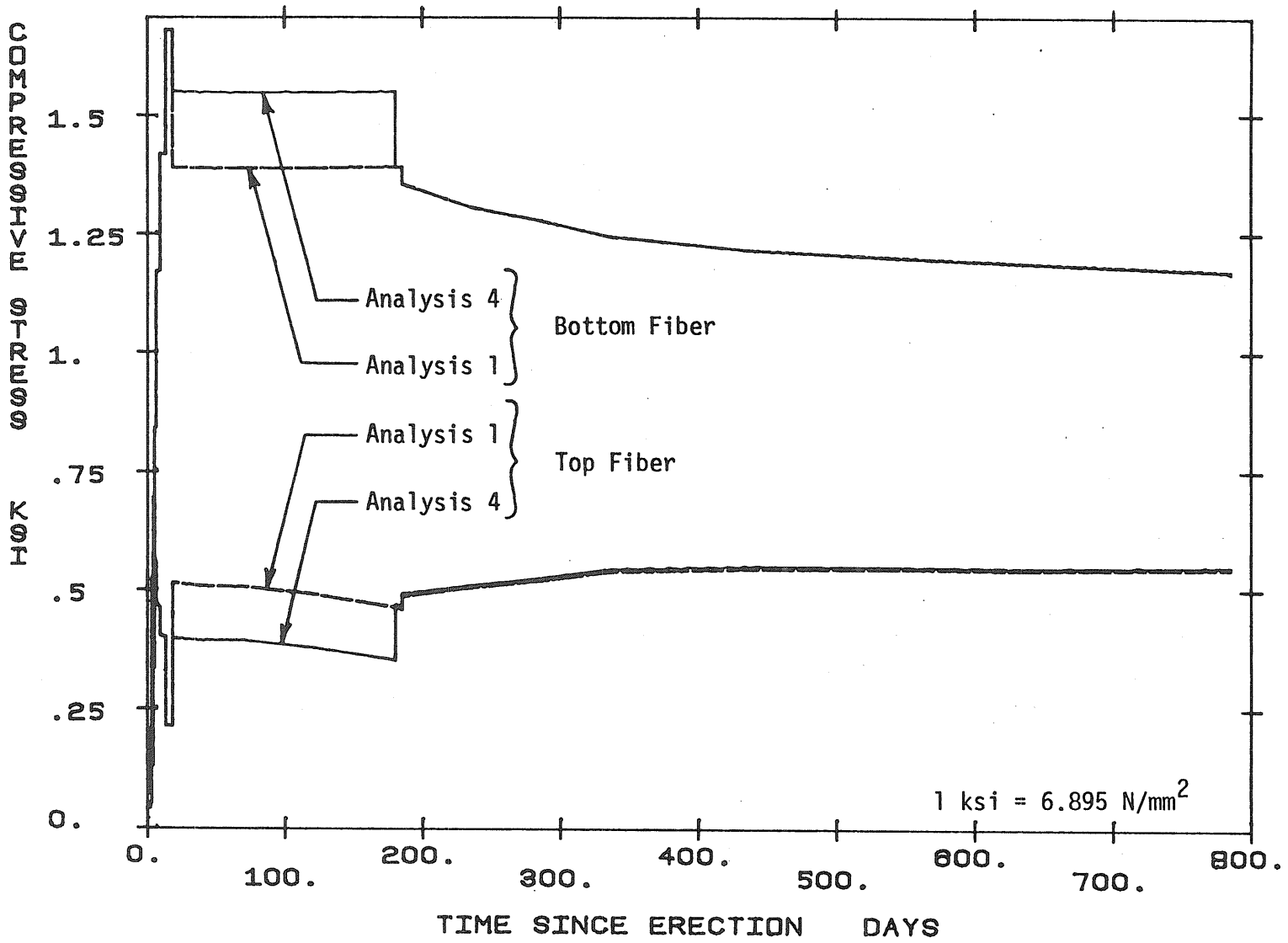

Fig. 5.18 Effects of the Construction Loads on the Extreme Fiber Concrete Stresses at Segment SB1-N1

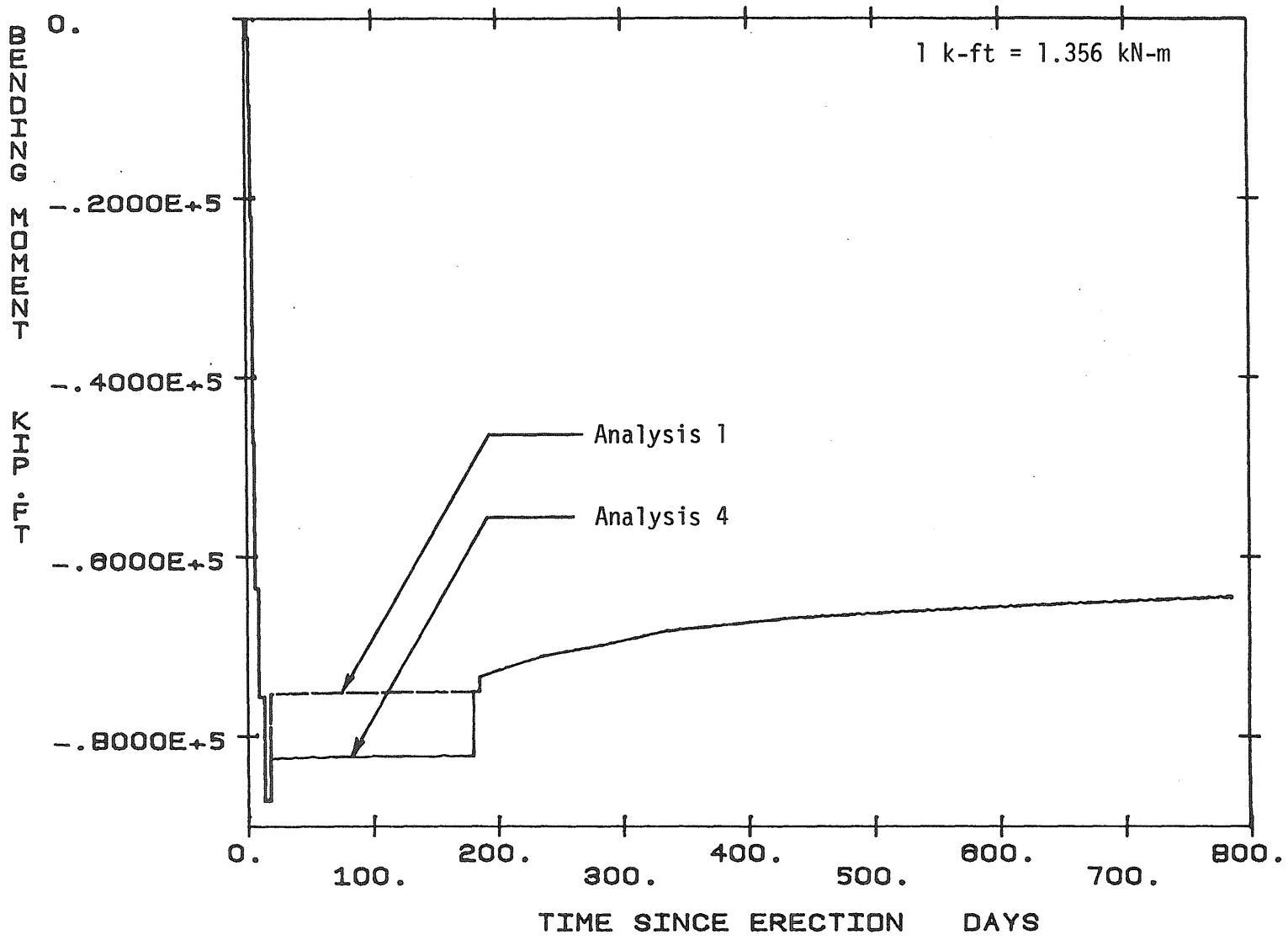

Fig. 5.19 Effects of the Construction Loads on the Bending Moment at Segment SB1-N1

APPENDIX A

DERIVATION OF EXPRESSIONS USED IN THE ANALYTICAL PROCEDURE

A.1 Creep Expressions According to the C.E.B. Recommendations

A.1.1 Expressions for C.E.B. Factors, K_t and K_d

When the time-dependent behavior of the structure was determined on the basis of creep and shrinkage properties as determined by the C.E.B. recommendations (11), the creep strains were estimated by making use of the method of superposition. For this particular case the computations were simplified by deriving mathematical expressions for the C.E.B. creep factors K_t and K_d, where K_t describes the time-dependence of creep and K_d reflects the effects of the concrete age at loading on creep. These multiplying factors are given by the C.E.B. in graphical form.

K_t was assumed to be described by the following exponential expression:

$$K_t = (1 - e^{-\alpha t^{\beta}}) \qquad (A.1.1)$$

where: t = time in days, since the concrete was initially loaded and

α and β = coefficients to be determined by fitting expression A.1.1 to the curves given by the C.E.B. recommendations for K_t.

Consideration of Fig. 2.6 reveals that K_t is also a function of theoretical thickness, d_m. A different set of values for α and β was derived for each K_t curve given by the C.E.B., i.e. for values of

d_m = 5, 10, 20, 40 and 80 cm. The values of α and β as derived by a curve fitting procedure for the above values of d_m are listed in Table A.1.

The values of α and β were determined as follows: First of all, rewrite Eq. A.1.1 as follows:

$$\ln [- \ln (1 - K_t)] = \beta \ln t + \ln \alpha \qquad (A.1.2)$$

For a particular value of d_m, the appropriate curve for K_t as given by the C.E.B. recommendations may be used to plot values of $\ln [- \ln (1 - K_t)]$ versus $\ln t$. If these values plot as a straight line then the functional form assumed by Eq. A.1.1 for K_t, is correct because Eq. A.1.2 represents the equation of a straight line in a $\ln [- \ln (1 - K_t)]$ versus $\ln t$ system of axes. Figure A.1 reveals that the above assumption was correct because the $\ln [- \ln (1 - K_t)]$ versus $\ln t$ values almost lie on a straight line. This plot applies to values of K_t for d_m = 5 cm.

The least squares fitting procedure (24) was then used to fit a straight line through these points. The intercept of this line on the $\ln [- \ln (1 - K_t)]$ axis yields $\ln \alpha$, from which α is readily determined. The slope of this line yields β.

K_d was assumed to be described by the following hyperbolic expression:

$$K_d = \frac{1}{A + B \tau^n} \qquad (A.1.3)$$

where: τ = concrete age at loading, in days and

A, B, and n = coefficients to be determined by fitting expression A.1.3 to the curves given by the C.E.B. recommendations for K_d.

Curves of K_d for normal portland cement and high early strength cement are given (see Fig. 2.3). A set of values of A, B and n had to be

derived for each curve. The same basic procedure was followed to fit Eq. A.1.3 to the curves given by the C.E.B. recommendations for K_d, as for the case of K_t:

Rewrite Eq. A.1.3 as follows:

$$\frac{1}{K_d} = B\,\tau^n + A \qquad \text{(A.1.4)}$$

The non-linear expression given by Eq. A.1.4 can be linearized by assuming a value for n. Using the least squares procedure a straight line was fitted to values of $1/K_d$ and τ^n, as determined by using the curves given by the C.E.B. recommendations. The intercept on the $1/K_d$ axis and the slope directly yield the values of B and A, respectively. Following this procedure a set of values for A and B may be determined for a particular value of n. Each of these fitted curves were then compared to the K_d values given by the C.E.B. recommendations, by finding the sum of the squares of the errors at a number of specific values of τ. The values of A, B and n corresponding to the fitted curve that yielded the smallest value of the sum of the squares of the errors, as found above, were used.

The following expressions were used for K_d:

Normal portland cement

$$K_d = \frac{1}{0.402 + 0.152\,\tau^{0.4}} \qquad \text{(A.1.5)}$$

High early strength cement

$$K_d = \frac{1}{0.309 + 0.284\,\tau^{0.4}} \qquad \text{(A.1.6)}$$

These expressions are compared to the values of K_d given by the C.E.B. recommendations in Fig. A.2.

A.1.2 Calculation of the Change in Creep Strain During a Time Interval

In what follows an expression is derived for the calculation of the change in creep strain over a time interval. This expression applies specifically to the case where the creep properties of the concrete are based on the C.E.B. recommendations. As explained before, the method of superposition was used to predict the creep response of concrete when the C.E.B. creep properties were used.

According to the C.E.B. recommendations the creep strain may be expressed as follows:

$$\varepsilon_{cr}(t) = \frac{f_c}{E_{b28}} K_c K_b K_e K_d K_t \qquad (A.1.7)$$

where: f_c = constant sustained concrete stress,

E_{b28} = secant modulus of elasticity of the concrete at 28 days and

K_c, K_b, K_e, K_d, K_t = multiplying factors that reflect the effect of intrinsic and environmental factors on the magnitude of creep (see Sect. 2.2.3.1).

This expression may be rewritten as follows:

$$\varepsilon_{cr}(t) = \frac{f_c}{E_{b28}} \xi K_d(\tau) K_t(t - \tau) \qquad (A.1.8)$$

where: $\xi = K_c K_d K_e$,

$K_d(\tau) = \frac{1}{A + B \tau^n}$,

$K_t(t-\tau) = [1 - e^{-\alpha(t-\tau)^\beta}]$ and

τ = age at which the concrete was initially loaded.

Applying the method of superposition in conjunction with Eq. A.1.8, the creep strain at time t_m is given by

$$\varepsilon_{cr}(t_m) = \frac{\xi}{E_{b28}} \left\{ \sum_{i=1}^{m-1} \Delta f_{ci} \, K_d(t_i) \, [1 - e^{-\alpha(t_m - t_i)^{\beta}}] \right\} \qquad (A.1.9)$$

where: Δf_{ci} = change in concrete stress at time t_i.

Notice that ξ/E_{b28} is written outside the summation due to the fact that this quotient is independent of time.

Similarly, the creep strain at time t_{m+1} is given by

$$\varepsilon_{cr}(t_{m+1}) = \frac{\xi}{E_{b28}} \left\{ \sum_{i=1}^{m} \Delta f_{ci} \, K_d(t_i) \, [1 - e^{-\alpha(t_{m+1} - t_i)^{\beta}}] \right\} \qquad (A.1.10)$$

The change of creep strain during the m-th time interval is given by

$$\Delta\varepsilon_{cr}(\Delta t_m) = \varepsilon_{cr}(t_{m+1}) - \varepsilon_{cr}(t_m) \qquad (A.1.11)$$

Substitution of expressions A.1.9 and A.1.10 into the above expression yields:

$$\Delta\varepsilon_{cr}(\Delta t_m) = \frac{\xi}{E_{b28}} \left\{ \sum_{i=1}^{m} \Delta f_{ci} \, K_d(t_i) \, [e^{-\alpha(t_m - t_i)^{\beta}} - e^{-\alpha(t_{m+1} - t_i)^{\beta}}] \right\} \qquad (A.1.12)$$

The above expression clearly illustrates that the calculation of creep strains at a given time requires a record of the previous stress history.

A.2 Elastic Recovery

As pointed out in Sect. 3.4, the elastic and creep recoveries associated with the change in prestressing force during the lifetime of a prestressed concrete member must be accounted for, otherwise the total prestress loss will be overestimated. Essentially, the elastic recovery of the concrete represents the effect of the restraint offered by the prestressing steel to concrete deformation. Therefore, the approach followed in deriving an expression for the estimation of elastic recovery of the concrete was based on a process of reestablishing compatibility of the strains of the concrete and steel, at the level of the steel, when a strain was imposed on the concrete cross-section. The other requirement that must always be satisfied is that of equilibrium.

In what follows, a procedure is presented for the calculation of the effects of elastic recovery of the concrete when a linearly varying strain distribution is imposed on the concrete cross-section. No restriction is placed on the number of different tendons or the positions of the individual tendons over the depth of the cross-section. It is important to note that for all the derivations that follow, stresses and strains are taken negative for compression and positive for tension.

Firstly, stiffness matrices associated with the axial strain (i.e. strain at the centroid of the section) and the curvature of the section are derived for both the concrete and steel.

For the steel:

$$[K_s] \begin{Bmatrix} \varepsilon_s \\ \phi_s \end{Bmatrix} = \begin{Bmatrix} P_s \\ M_s \end{Bmatrix} \qquad (A.2.1)$$

The stiffness matrix for the steel is given by

$$[K_s] = E_s \begin{bmatrix} \sum A_i & \sum A_i e_i \\ \sum A_i e_i & \sum A_i e_i^2 \end{bmatrix} \qquad (A.2.2)$$

where: E_s = modulus of elasticity of the steel,
A_i = cross-sectional area of tendon i,
e_i = eccentricity of tendon i measured from the centroidal axis of the section, taken positive when the tendon is below the centroidal axis, and negative when above,
ε_s = strain associated with the steel, at the centroid of the section (see Fig. A.3),
ϕ_s = curvature associated with the steel strain (see Fig. A.3),
P_s = resultant of the forces in all the tendons, applied at the centroid of the section (see Fig. A.3) and
M_s = resultant of the moments of the forces in all the tendons, about the centroid of the section (see Fig. A.3).

It is understood that the indicated summations in Eq. A.2.2 include all the tendons in the section.

For the concrete:

$$[K_c] \begin{Bmatrix} \varepsilon_c \\ \phi_c \end{Bmatrix} = \begin{Bmatrix} P_c \\ M_c \end{Bmatrix} \qquad (A.2.3)$$

The stiffness matrix for the concrete is given by

$$[K_c] = E_c \begin{bmatrix} A_c & 0 \\ 0 & I_c \end{bmatrix} \qquad (A.2.4)$$

where: E_c = modulus of elasticity of the concrete,
A_c = cross-sectional area of the concrete section,
I_c = moment of inertia of the concrete section about the centroidal axis,
ε_c = concrete axial strain (see Fig. A.4),
ϕ_c = curvature of concrete section (see Fig. A.4),
P_c = resultant force acting on the concrete section, applied at the centroid (see Fig. A.4) and
M_c = resultant moment acting on the concrete section, about the centroid (see Fig. A.4).

The elements of each column of the above stiffness matrices were evaluated by setting the degree of freedom corresponding to the particular column to unity, while the other is set to zero. The forces required for equilibrium correspond to the elements of the particular column of the stiffness matrix. This process is illustrated for steel and concrete in Figs. A.3 and A.4, respectively.

Consider the case where a linearly varying strain is imposed on the concrete section. The strain distribution is defined by the strains at the extreme top and bottom fibers of the section, $\Delta\varepsilon_t$ and $\Delta\varepsilon_b$, respectively (see Fig. A.5). This strain clearly violates the compatibility assumption, i.e. that the change of strain in the steel is equal to the change of strain in the concrete at the same level. In order to restore compatibility, forces must be applied to the steel as well as the concrete. The resultant of the steel forces, P_s, is applied at the centroid of the section. The resultant of the moments of the steel forces about the centroid is designated by M_s. The resultant concrete force, P_c, is applied at the centroid, while the resultant moment about the centroid, acting on the concrete, is designated by M_c (see Fig. A.5).

Horizontal and moment equilibrium yields:

$$\begin{Bmatrix} P_s \\ M_s \end{Bmatrix} + \begin{Bmatrix} P_c \\ M_c \end{Bmatrix} = \begin{Bmatrix} 0 \\ 0 \end{Bmatrix} \qquad \text{(A.2.5)}$$

Compatibility of strains yield:

$$\begin{aligned} \varepsilon_{st} - \varepsilon_{ct} &= \Delta\varepsilon_t \\ \varepsilon_{sb} - \varepsilon_{cb} &= \Delta\varepsilon_b \end{aligned} \qquad \text{(A.2.6)}$$

See Fig. A.5 for the definition of the strains involved in Eq. A.2.6. These above expressions may be manipulated in order to express the compatibility requirements in terms of strains at the level of the centroid of the section and curvatures:

$$\begin{aligned} \varepsilon_s - \varepsilon_c &= \Delta\varepsilon \\ \phi_s - \phi_c &= \Delta\phi \end{aligned} \qquad \text{(A.2.7)}$$

where: ε_s, ε_c and $\Delta\varepsilon$ are defined in Fig. A.5, and ϕ_s, ϕ_c and $\Delta\phi$ are the curvatures as defined by

$$\phi_s = \frac{\varepsilon_{sb} - \varepsilon_{st}}{d}$$

$$\phi_c = \frac{\varepsilon_{cb} - \varepsilon_{ct}}{d}$$

$$\Delta\phi = \frac{\Delta\varepsilon_b - \Delta\varepsilon_t}{d}$$

Substitution of Eqs. A.2.1 and A.2.3 into A.2.5 yields

$$[K_s] \begin{Bmatrix} \varepsilon_s \\ \\ \phi_s \end{Bmatrix} + [K_c] \begin{Bmatrix} \varepsilon_c \\ \\ \phi_c \end{Bmatrix} = \begin{Bmatrix} 0 \\ \\ 0 \end{Bmatrix}$$

Equations A.2.7 are used to eliminate ε_c and ϕ_c from the above expression. By performing this substitution and after rearrangement the following expression is obtained:

$$\left[[K_c]^{-1} [K_s] + [I]\right] \begin{Bmatrix} \varepsilon_s \\ \\ \phi_s \end{Bmatrix} = \begin{Bmatrix} \Delta\varepsilon \\ \\ \Delta\phi \end{Bmatrix}$$

where: I is a 2 x 2 identity matrix.

Upon substitution of the appropriate arrays and subsequent simplification

$$\begin{bmatrix} \left(1 + \dfrac{n \sum A_i}{A_c}\right) & \dfrac{n \sum A_i e_i}{A_c} \\ \\ \dfrac{n \sum A_i e_i}{I_c} & \left(1 + \dfrac{n \sum A_i e_i^2}{I_c}\right) \end{bmatrix} \begin{Bmatrix} \varepsilon_s \\ \\ \phi_s \end{Bmatrix} = \begin{Bmatrix} \Delta\varepsilon \\ \\ \Delta\phi \end{Bmatrix} \qquad \text{(A.2.8)}$$

where: $n = E_s/E_c$ = modular ratio.

Equation A.2.8 can be solved to yield ε_s and ϕ_s. Once these quantities are known, they can be used to find the change in steel force (prestressing force) associated with the imposed concrete strain, as well

as the corrections that must be applied to the imposed concrete strain to yield the final concrete strain.

The change in steel force in the i-th tendon is given by:

$$P_{si} = (\varepsilon_s + \phi_s e_i) A_i E_s \qquad \text{(A.2.9)}$$

The corrections that must be applied to the imposed concrete strains at the top and bottom fibers of the section are given by:

$$\varepsilon_{ct} = (\varepsilon_s - \phi_s y_t) - \Delta\varepsilon_t$$

$$\varepsilon_{cb} = (\varepsilon_s + \phi_s y_b) - \Delta\varepsilon_b \qquad \text{(A.2.10)}$$

where: y_t and y_b are the distances of the centroid to the extreme top and bottom fibers, respectively.

The total corrected concrete strains at the extreme top and bottom fibers of the section, are given by:

$$\varepsilon'_{ct} = \Delta\varepsilon_t + \varepsilon_{ct}$$

$$\varepsilon'_{cb} = \Delta\varepsilon_b + \varepsilon_{cb} \qquad \text{(A.2.11)}$$

The changes in concrete stress, associated with the change in steel force are obtained as follows:

$$f_{c_{top}} = \frac{P_c}{A_c} - \frac{M_c y_t}{I_c}$$

$$f_{c_{bot}} = \frac{P_c}{A_c} + \frac{M_c y_b}{I_c} \qquad \text{(A.2.12)}$$

The values to be used for P_c and M_c in Eq. A.2.12 are obtained from Eqs. A.2.1 and A.2.5:

$$\begin{Bmatrix} P_c \\ M_c \end{Bmatrix} = - \begin{Bmatrix} P_s \\ M_s \end{Bmatrix} = - [K_s] \begin{Bmatrix} \varepsilon_s \\ \phi_s \end{Bmatrix}$$

A.3 Calculation of Changes in Concrete Stress and Strain and Prestressing Force

As previously pointed out, the effects of creep, shrinkage and relaxation were assumed to be independent during a particular time interval. Thus, the effects of each of these phenomena could be determined separately during a time interval and then superimposed at the end of that time interval.

Each of these time-dependent effects as well as externally applied loads lead to a change in prestressing force, which goes hand in hand with an elastic change in concrete stress and strain. In what follows an outline is given of how the expressions given in Sect. A.2 were applied to account for the above-mentioned effects.

The change in free shrinkage strain that takes place at a particular section during a time interval may be readily determined. This strain is assumed to be uniformly distributed across the cross-section. By applying this strain distribution to the cross-section, Eq. A.2.8 may be used to find ε_s and ϕ_s. Subsequently, Eq. A.2.9 yields the change in prestressing force in each tendon and Eqs. A.2.12 yield the associated change in concrete stress, due to the change in shrinkage strain. The final corrected change in shrinkage strain for the time interval is obtained by using Eqs. A.2.11 in conjunction with Eqs. A.2.10.

The unrestrained change in creep strain during a time interval is determined at the extreme top and bottom fibers of the concrete section

using the procedure outlined in Sect. 3.2.4 or the method of superposition, depending on whether or not experimentally determined creep properties are being used. This change in creep strain is linearly distributed through the depth of the cross-section because linear creep theory is assumed to be applicable. The exact procedure outlined for the case of shrinkage is applied to the strain distribution determined above in order to find the change in prestressing force in each tendon as well as the change in concrete stress due to the change in creep strain for the time interval. This procedure simultaneously yields the final corrected change in creep strain that takes place during the time interval.

The procedure outlined in Sect. 3.3 is used to determine the change in prestressing force due to relaxation in each tendon during a particular time interval. Once these changes in prestressing force are known, beam theory may be used to calculate the associated changes in concrete stress and strain. The procedure outlined for the case of shrinkage is applied to this strain distribution to find the changes in prestressing force and concrete stress due to the elastic recovery of concrete. The corrected concrete strains thus obtained represent the final corrected change in concrete strain due to relaxation for the time interval. By adding the changes in prestressing force and concrete stress due to relaxation to the change in these quantities due to elastic recovery of concrete, as calculated above, the final corrected changes in prestressing force and concrete stress due to relaxation for the time interval are determined.

When loads are imposed on the structure, such as the effect of the self weight of a newly erected segment or the stressing of new tendons, the resulting concrete stresses and strains may be calculated at each section by making use of beam theory. The change in prestressing force and the associated change in concrete stress due to elastic recovery of the concrete are calculated by applying the procedure as outlined for the case of shrinkage to the above concrete strain distribution. The change in prestressing force, and corrected total change in strain thus obtained, represent the final values of these quantities due to application of the load.

The final corrected change in concrete stress is found by adding the change in concrete stress due to application of the load, to the change in concrete stress due to elastic recovery. For the particular case in which a new tendon is being stressed, it should be noted that this particular tendon is excluded from the calculations which account for the effects of elastic recovery.

For the case of applied loads, the concrete stresses and strains predicted by the above procedure, used in conjunction with the net section properties, will be the same as those predicted by using the transformed section properties. The general proof of this statement is rather tedious and consequently not presented here. Finally, it should be pointed out that the net concrete section properties should, in the strict sense, be used in the analytical procedure. In this study, the gross section properties were used.

A.4 Initial Prestressing Force

For post-tensioned systems, the initial prestressing force will generally vary along the length of a tendon due to instantaneous losses in force arising from friction and anchor-set. For such systems the following expression is commonly used for the estimation of friction losses (35):

$$f_s(x) = f_{so}\, e^{-(kx+\mu\alpha)} \qquad (A.4.1)$$

where: $f_s(x)$ = steel stress at a distance x from the jacking end,
f_{so} = steel stress at the jacking end,
e = base of Napierian logarithms,
k = wobble friction coefficient per unit length,
μ = curvature friction coefficient,
α = total angular change of the tendon profile measured from the jacking end to the point at a distance x from this end and

x = distance from the jacking end to the point on the tendon being considered.

It is understood that the steel stresses in Eq. A.4.1 apply to the time immediately following the stressing operation but prior to anchoring.

Methods for finding the prestress losses associated with anchor-set may be found in Refs. 18, 29 and 40. The iterative approach given by Leonhardt (40) accounts for the effects of the actual tendon profile, and furthermore makes provision for the possibility that the reverse coefficient of friction may be unequal to the coefficient of friction associated with stressing of the tendon. In general the reverse coefficient of friction is larger than the coefficient associated with stressing of the tendon. When the above approach is applied to straight tendons, closed-form expressions may be derived for the total initial prestressing force.

In what follows, expressions are developed for the calculation of the initial prestressing force in straight tendons. These expressions account for the instantaneous loss of prestressing force associated with friction and anchor-set.

Considering Fig. A.6, it may be seen that the effect of anchor-set is to reduce the steel stress from $f_s(x)$ to $f_s^*(x)$. The distance over which anchor-set affects the prestressing force extends over a distance b from the live anchor. This distance will be referred to as the slip length. Considering an element dx of the tendon situated a distance x from the jacking end, the change in its length $d\Delta$ due to anchor set may be written

$$d\Delta = \frac{1}{E_s} [f_s(x) - f_s^*(x)] \, dx \qquad (A.4.2)$$

The total change in length that takes place in the tendon over the slip length b must be equal to the amount that the tendons slip at the

anchor Δ due to anchor set. The total slip may be obtained by integration of Eq. A.4.2:

$$\Delta = \frac{1}{E_s} \int_o^b [f_s(x) - f_s^*(x)]\, dx = \frac{1}{E_s} (\text{Area ABC}) \qquad (A.4.3)$$

Thus, the area ABC is linearly related to the slip that takes place at the anchor.

Applying Eq. A.4.1 to the case of straight tendons (i.e. $\alpha = o$), $f_s(x)$ and $f_s^*(x)$ may be expressed as (see Fig. A.6):

$$f_s(x) = f_{so}\, e^{-kx} \qquad (A.4.4)$$

$$f_s^*(x) = f_{sb}\, e^{-k(b-x)} = f_{so}\, e^{-2kb}\, e^{kx} \qquad (A.4.5)$$

Substitution into Eq. A.4.3 and performing the indicated integration yields:

$$\Delta = \frac{f_{so}}{kE_s} [1 - e^{-kb}]^2 \qquad (A.4.6)$$

Eq. A.4.6 is now solved for the slip length b:

$$b = -\frac{1}{k} \ln \left[1 - \sqrt{\frac{\Delta k E_s}{f_{so}}}\right] \qquad (A.4.7)$$

where: ln = Napierian logarithm.

Once the slip length, b , is known, the initial steel stress can be calculated by using Eq. A.4.5 over the interval $0 \leq x \leq b$ and Eq. A.4.4 over the rest of the tendon. These expressions may be written in terms of prestressing force simply by replacing the steel stresses by appropriate values of steel force. It must be confirmed that the slip length, b , is less than or equal to the tendon length.

In the case of segmentally constructed post-tensioned bridges, some of the prestressing tendons may be very short. In these short tendons it is possible that the slip length may extend over the entire length of the tendon. Consideration of Fig. A.7 will reveal that knowledge of $f_s(L)$, the steel stress at the dead-end anchor, will enable one to estimate the steel stress everywhere in the tendon.

Referring to Fig. A.7:

$$f_s^*(x) = f_s(L)\, e^{-k(L-x)} \qquad (A.4.8)$$

where: L = total length of the tendon.

Eq. A.4.4 for $f_s(x)$ is, of course, still valid. Bearing in mind that the slip that takes place at the anchor is related to $1/E_s$ (Area ABCD),

$$\Delta = \frac{1}{E_s} \int_0^L [f_s(x) - f_s^*(x)]\, dx = \frac{1}{E_s} \text{(Area ABCD)} \qquad (A.4.9)$$

Substituting Eqs. A.4.4 and A.4.8 into the above expression, performing the integration and solving for $f_s(L)$, the following expression is obtained:

$$f_s(L) = f_{so} + \frac{\Delta k E_s}{(e^{-kL} - 1)} \qquad (A.4.10)$$

Once $f_s(L)$ is known, the initial steel stress in the tendon may be calculated from Eq. A.4.8.

For tendons stressed from both ends, the procedures outlined above may be followed to determine the initial prestressing force. If the slip length is less than or equal to half the tendon length, the first set of equations is used independently at both ends of the tendon. If the slip length exceeds half the tendon length, the second set of equations may be used, with L set equal to half the length of the tendon. For this particular case only one half of the tendon need be considered because the variation of prestressing force will be symmetrical about the middle of the tendon.

A.5 Effects of Static Indeterminancy

For statically indeterminate structures, the equations of equilibrium do not yield enough information to enable one to determine the stresses that arise in the structure due to the application of load. Thus, the material properties need to be included in the solution of such a problem. Furthermore, the time-dependent deformations of statically indeterminate prestressed concrete structures may be expected to lead to time-dependent changes in stress distribution. Specifically, for statically indeterminate prestressed concrete beams this means that a time-dependent redistribution of bending moment may be expected to take place due to the combined effects of shrinkage, creep and relaxation.

In this study, the effects of static indeterminancy were treated by a flexibility approach. In order to outline the approach followed, consider the beam continuous over n supports, as illustrated in Fig. A.8a. Firstly, the structure is made statically determinate by removing all the interior supports, as shown in Fig. A.8b. In general, the imposed load system or time-dependent strains, whichever is being considered, will impose non-zero deflections in the equivalent statically determinate beam at the locations of the interior supports.

From this point on the object is to find a set of point loads that will satisfy the original boundary conditions, when they are applied to the equivalent statically determinate structure at the positions of the supports. These point loads correspond to the unknown interior reactions. This objective is accomplished by calculating the deflections of the equivalent statically determinate structure at the positions of the interior supports due to a unit point load applied, in turn, at the locations of each interior support. Figure A.8c defines these deflections for the unit point load applied at support j. By making use of the principle of superposition and the fact that the vertical deflection at each support is zero, the following expressions may be written:

$$
\begin{aligned}
&R_2\delta_{22} + R_3\delta_{23} + - - - + R_{(n-1)}\delta_{2(n-1)} + \Delta_2 = 0\\
&R_2\delta_{32} + R_3\delta_{33} + - - - + R_{(n-1)}\delta_{3(n-1)} + \Delta_3 = 0\\
&\quad - \qquad - \qquad\qquad - \qquad - \qquad -\\
&\quad - \qquad - \qquad\qquad - \qquad - \qquad -\\
&\quad - \qquad - \qquad\qquad - \qquad - \qquad -\\
&R_2\delta_{(n-1)2} + R_3\delta_{(n-1)3} + - - - + R_{(n-1)}\delta_{(n-1)(n-1)} + \Delta_{(n-1)} = 0
\end{aligned}
$$

(A.5.1)

where: Δ_i = deflection of the equivalent statically determinate structure at the location of support i due to the effects of applied loads or time-dependent effects, whichever is being considered,

δ_{ij} = deflection of the equivalent statically determinate structure at the location of support i due to a unit point load applied at the location of support j and

R_i = vertical reaction at support i.

The positive directions of the above quantities are defined in Fig. A.8. Equations A.5.1 represent (n-2) simultaneous equations in (n-2) unknowns. This system of equations may be cast in matrix form as follows:

$$\begin{bmatrix} \delta_{22} & \delta_{23} & - & - & - & \delta_{2(n-1)} \\ \delta_{32} & \delta_{33} & - & - & - & \delta_{3(n-1)} \\ - & - & & & & - \\ - & - & & & & - \\ - & - & & & & - \\ \delta_{(n-1)2} & \delta_{(n-1)3} & - & - & - & \delta_{(n-1)(n-1)} \end{bmatrix} \begin{Bmatrix} R_2 \\ R_3 \\ - \\ - \\ - \\ R_{(n-1)} \end{Bmatrix} = \begin{Bmatrix} -\Delta_2 \\ -\Delta_3 \\ - \\ - \\ - \\ -\Delta_{(n-1)} \end{Bmatrix} \tag{A.5.2}$$

This expression may be represented in a more compact notation as:

$$[F]\{R\} = -\{\Delta\} \tag{A.5.3}$$

This system of equations may readily be solved to yield {R}, the unknown reactions at the interior supports. Once these reactions are known, they may be applied to the equivalent statically determinate structure as point loads and the resulting moments, stresses, strains and deflections calculated. It should be noted that for the case of a tendon being stressed, the moments thus calculated are the so-called secondary, or parasitic, moments due to prestressing. The total of the moments, stresses, strains and deflections due to the applied actions or deformations is obtained by superimposing the results obtained above on the results obtained by applying the actual action or deformations to the equivalent statically determinate structure.

In the light of the above derivation, it should be clear that the elements of a particular column of the flexibility matrix [F] may be generated by finding the deflection of the equivalent statically determinate structure at the locations of each of the interior supports, due to the application of a unit point load at the location of the support to which this particular column of the flexibility matrix applies (see Eqs. A.5.2 and A.5.3 and Fig. A.8c).

Finally, the numerical integration procedure as outlined by Godden (23) was used for the calculation of deflections in this study.

Table A.1: Coefficients for the Expression for the C.E.B. Creep and Shrinkage Factor, K_t

Theoretical Thickness (cm)	α	β
5	0.139	0.515
10	0.0709	0.574
20	0.0331	0.608
40	0.0103	0.713
80	0.00101	0.934

Note: These coefficients are for use with the following expression:

$$K_t = (1 - e^{-\alpha t^{\beta}})$$

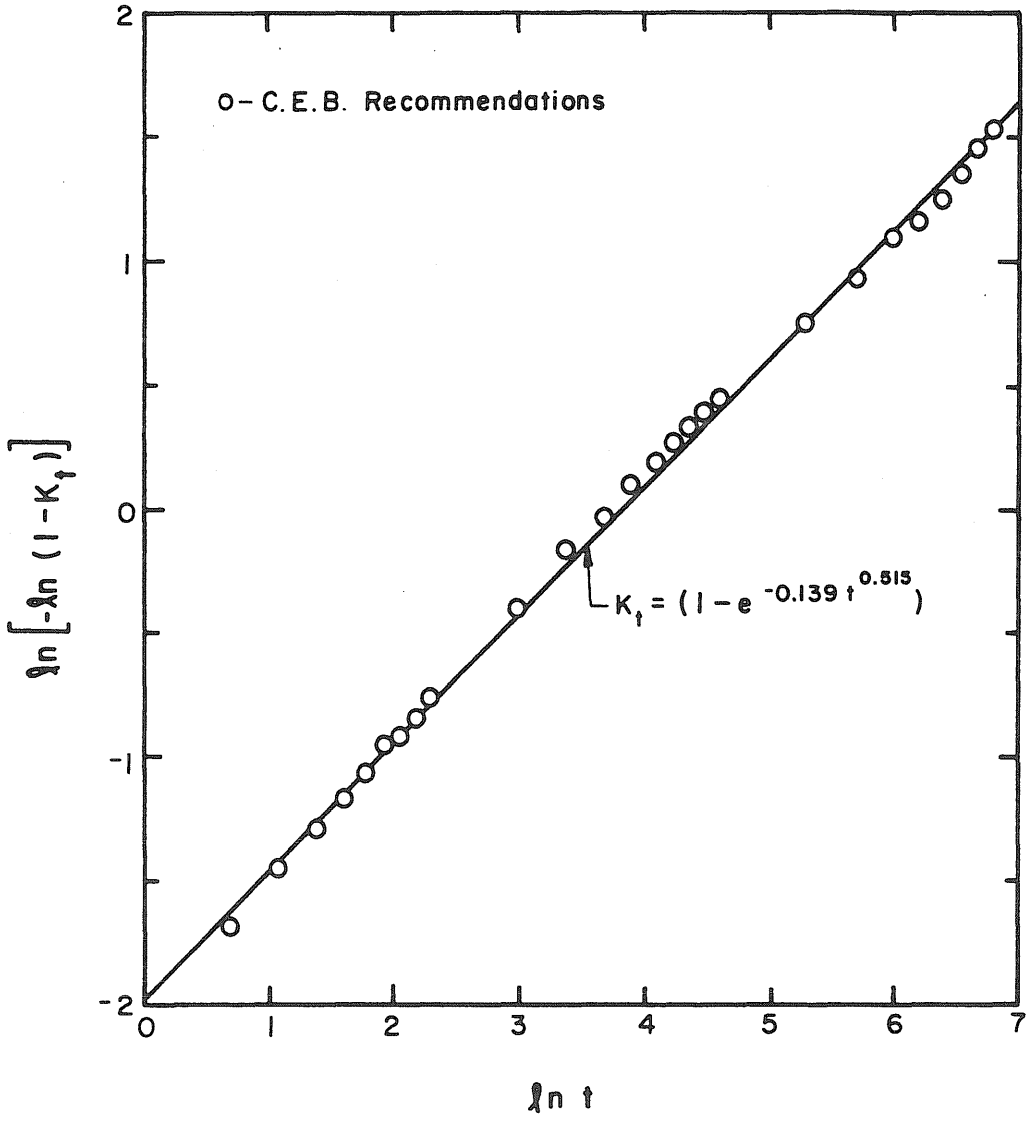

Fig. A.1 Fitted Expression for C.E.B. Creep Factor K_t, Theoretical Thickness = 5 cm

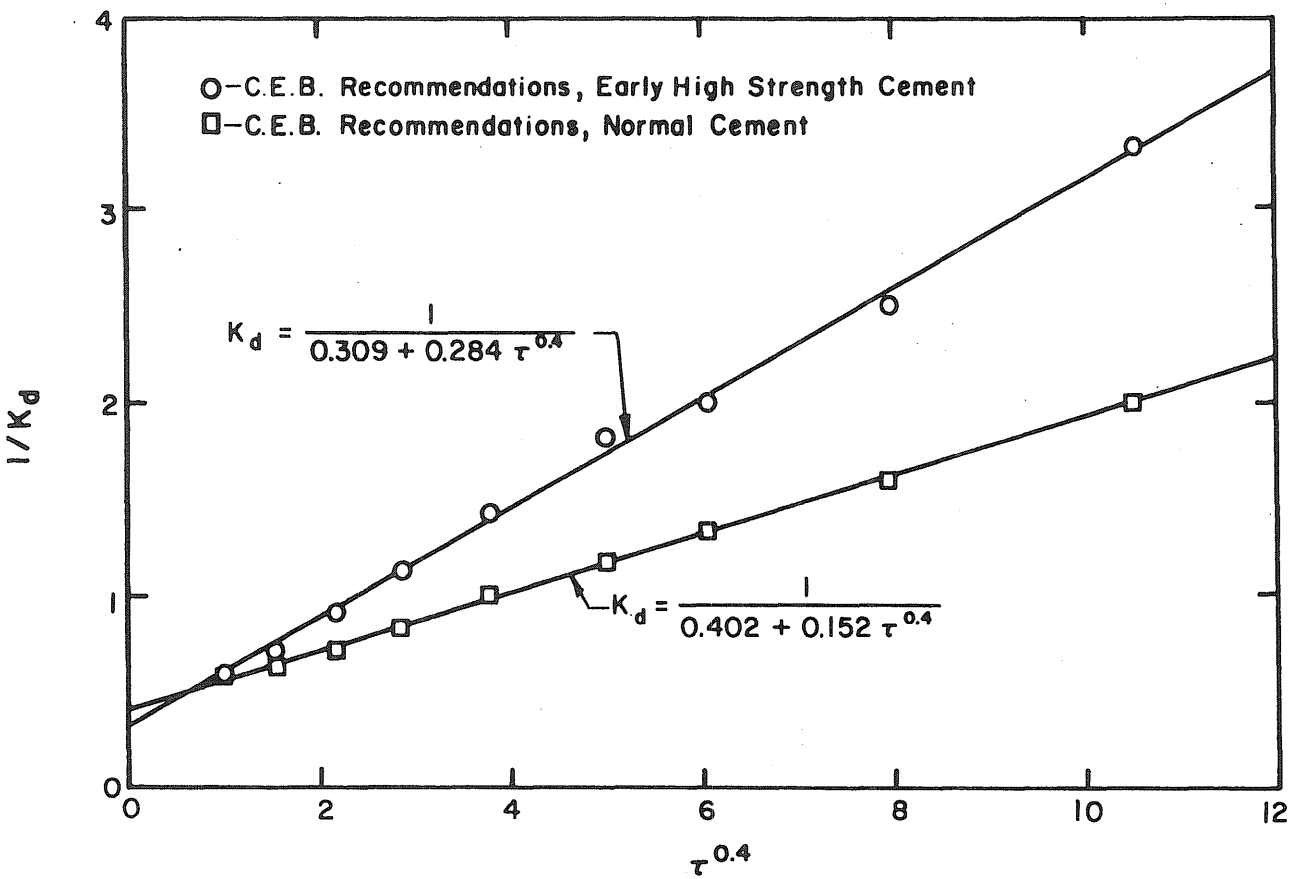

Fig. A.2 Fitted Expressions for C.E.B. Creep Factor K_d

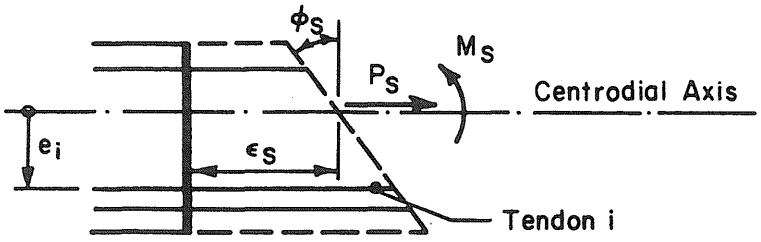

(a) Degrees of Freedom and Associated Forces

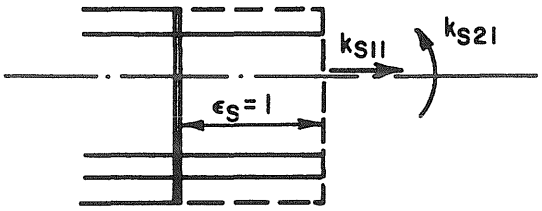

$k_{S11} = E_S \Sigma A_i$

$k_{S21} = E_S \Sigma A_i e_i$

(b) First Column of Stiffness Matrix ($\epsilon_S = 1$ and $\phi_S = 0$)

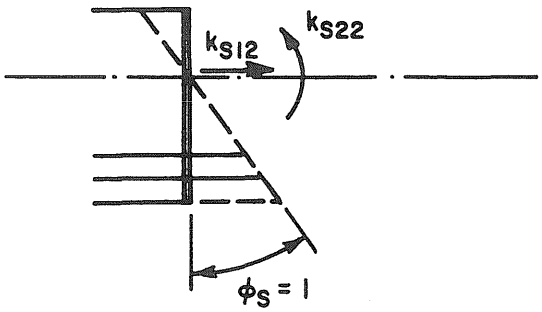

$k_{S12} = E_S \Sigma A_i e_i$

$k_{S22} = E_S \Sigma A_i e_i^2$

(c) Second Column of Stiffness Matrix ($\epsilon_S = 0$ and $\phi_S = 1$)

Fig. A.3 Derivation of the Stiffness Matrix Corresponding to the Prestressing Steel Reinforcement at a Section

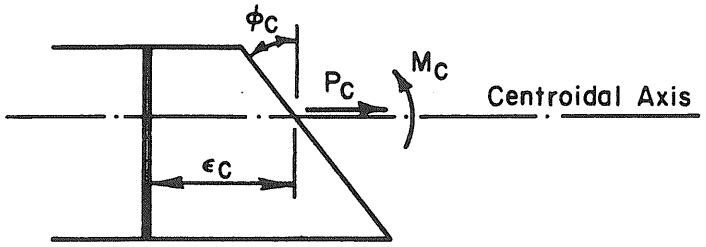

(a) Degrees of Freedom and Associated Forces

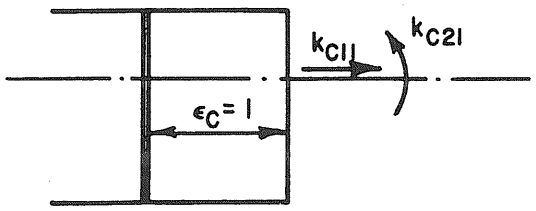

$k_{C11} = E_C A_C$

$k_{C21} = 0$

(b) First Column of Stiffness Matrix ($\epsilon_C = 1$ and $\phi_C = 0$)

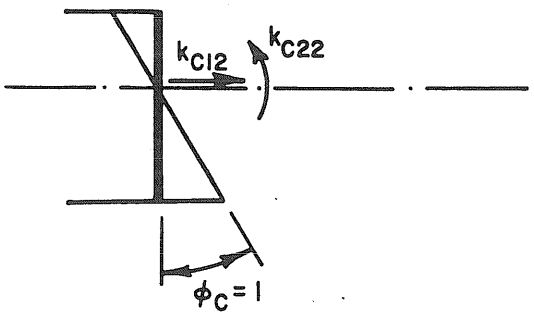

$k_{C12} = 0$

$k_{C22} = E_C I_C$

(c) Second Column of Stiffness Matrix ($\epsilon_C = 0$ and $\phi_C = 1$)

Fig. A.4 Derivation of the Stiffness Matrix Corresponding to the Concrete Section

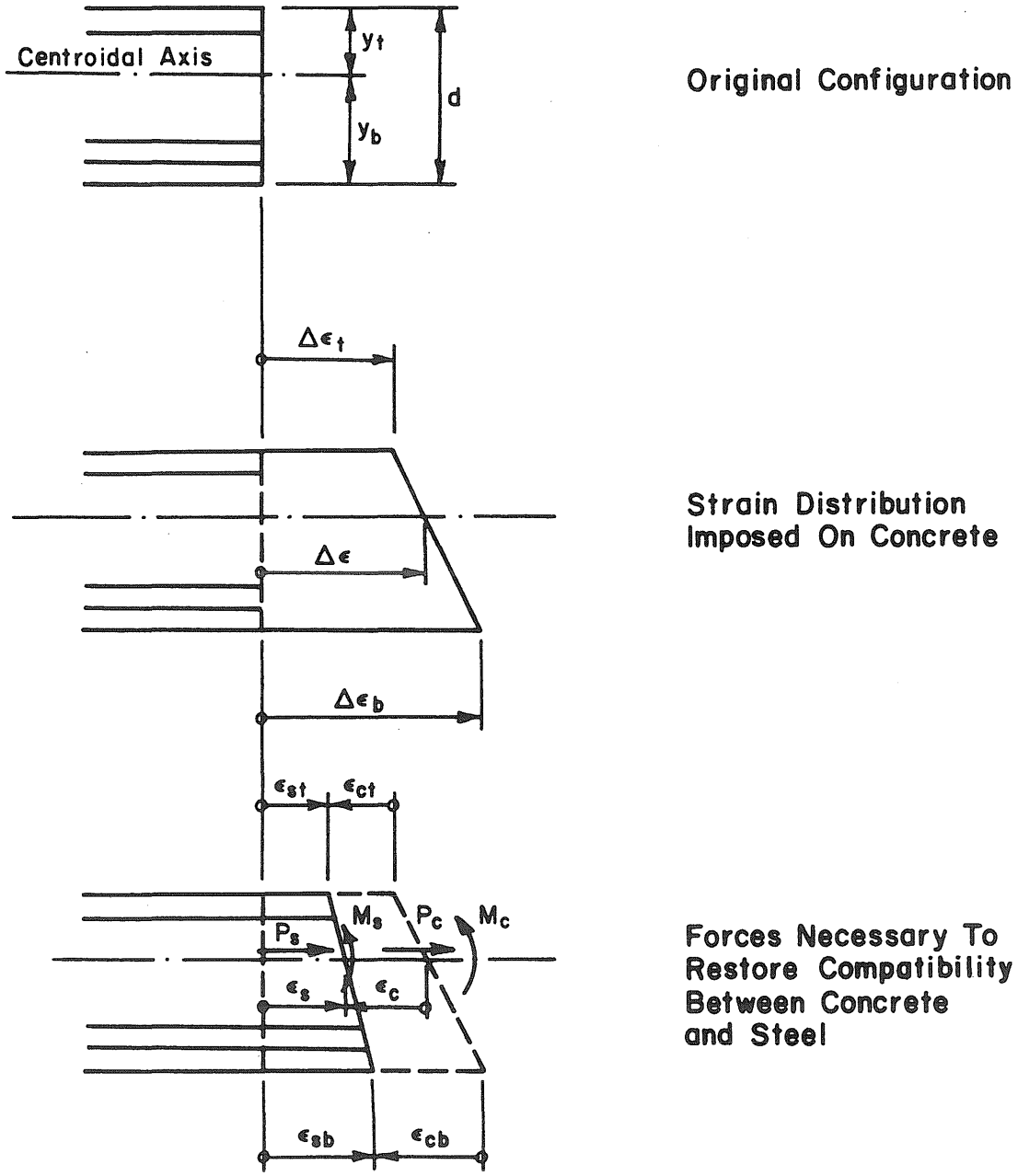

Fig. A.5 Calculation of Elastic Recovery Resulting from a Linear Strain Distribution Applied to the Concrete at a Section

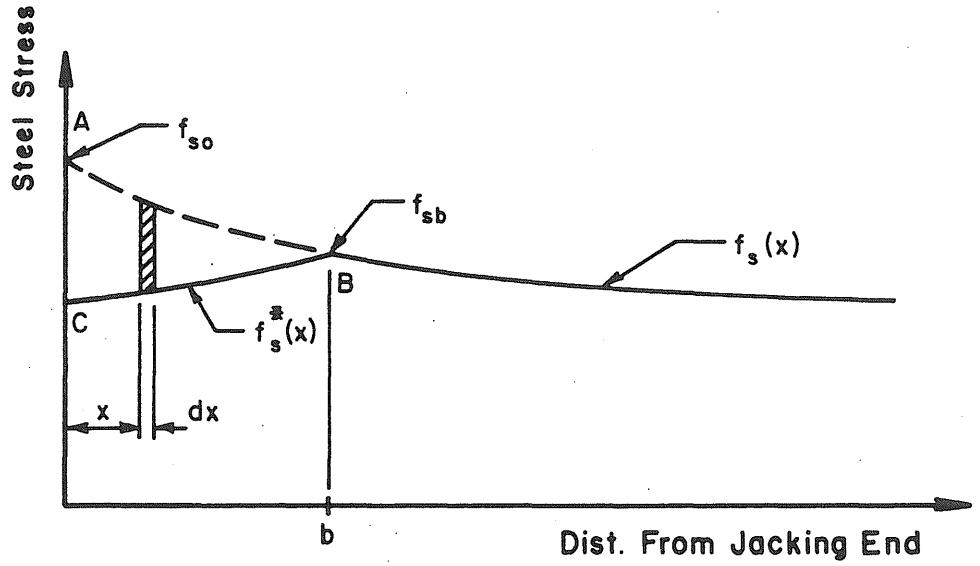

Fig. A.6 Variation of Initial Steel Stress Along Tendon when Slip Length is Less than Tendon Length

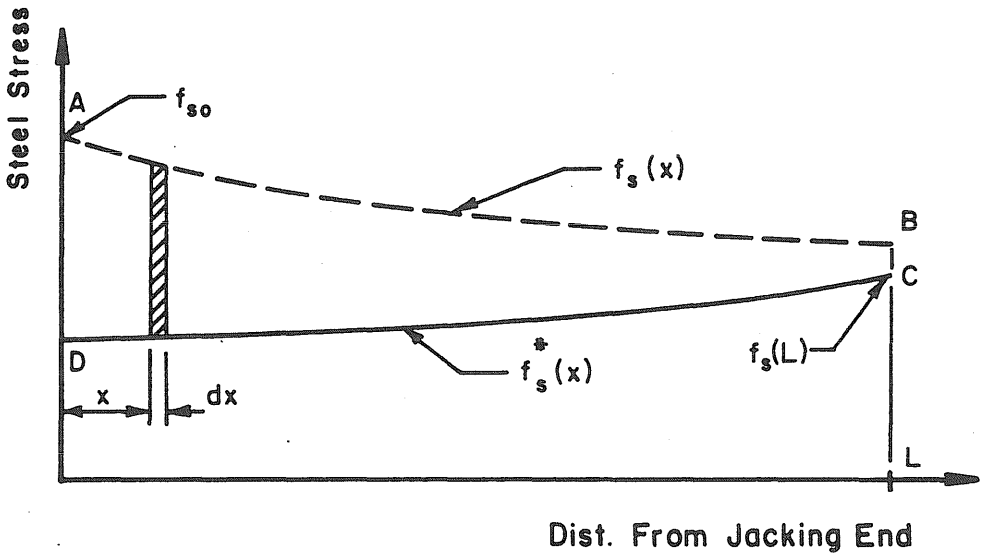

Fig. A.7 Variation of Initial Steel Stress Along Tendon when Slip Length is Equal to Tendon Length

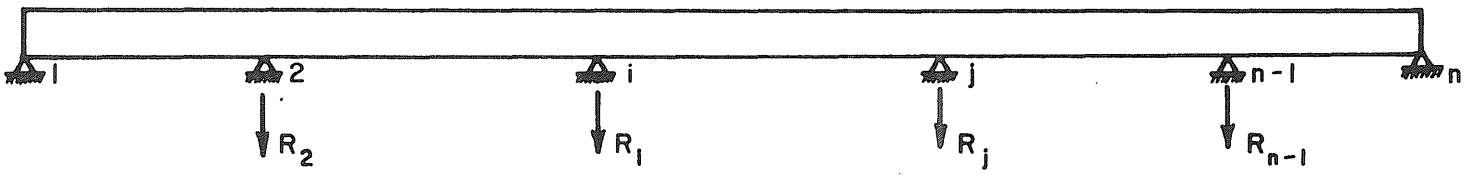

(a) Original Structure

(b) Equivalent Statically Determinate Structure

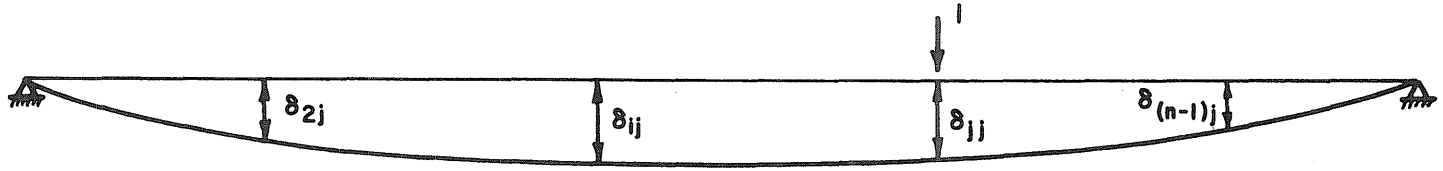

(c) Structure and Loading System For Generating
The i-th Column Of The Flexibility Matrix

Fig. A.8 Derivation of Flexibility Matrix for Statically Indeterminate Intermediate Structures

APPENDIX B

THE KISHWAUKEE RIVER BRIDGE AND EXPERIMENTALLY DETERMINED CONCRETE MATERIAL PROPERTIES

The Kishwaukee River Bridge is located in Winnebago County, about four miles south of Rockford, Illinois. The structure spans over the heavily wooded Kishwaukee River Valley and, consequently, one of the primary considerations for selecting a particular construction procedure was the preservation of the environment. In order to achieve this aim the segmental cantilever construction procedure was a natural choice because this method eliminates the use of heavy construction false-work and temporary supports.

The contents of this Appendix are devoted to a description of the structure itself as well as a presentation of the experimentally determined material properties of the concrete used in the bridge. These material properties were determined by tests conducted at the laboratories of the Portland Cement Association (P.C.A.). All the information presented in this Appendix was supplied by either the P.C.A. or the Illinois Department of Transportation (30,52).

It is important to note that the origin of the time scale which is used to define the points in time at which each construction activity took place has arbitrarily been chosen as the day prior to which the first segment was cast. Thus, the day on which the first segment was cast is designated as day one.

B.1 The Kishwaukee River Bridge

B.1.1 General Description

The Kishwaukee River Bridge comprises two identical parallel bridges, each bridge having three 250 ft (76.2 m) interior spans and two 170 ft (51.8 m) side spans for an overall length of 1090 ft (332.2 m). The final structure is continuous over all five spans. An elevation of the structure as well as the designation assigned to each segment is shown in Figure B.1a. Each double cantilever is made up of 34 precast segments, while the side-span ends each comprise 6 segments. Adjacent double cantilevers are joined to each other by means of a cast in-situ closure segment (see Figure B.1b).

Typically each segment has a constant depth of 11 ft 4 in (3.454 m), a top width of 41 ft (12.50 m), and a length of 7 ft (2.134 m). The overall dimensions of such a segment is given in Figure B.2. Note that, in a double cantilever, the bottom flange thickness varies continually from 8 in. to 18 in. (0.203 m to 0.457 m) over the first six segments on each side of the pier (see Figure B.1b). The section properties of each particular segment to be found in a double cantilever or side-span end are listed in Tables B.1 and B.2, respectively. The pier segments were each provided with a diaphragm, the effect of which was ignored in the analytical procedure. The instrumented segments are designated SB1-N1, SB1-N9 and SB1-N16.

B.1.2 Erection Sequence

The bridge was erected by the segmental cantilever construction procedure. Following this procedure, a double cantilever was progressively constructed by adding segments to each side of the pier. Once the erection of a particular double cantilever was completed, it was joined to an adjacent double cantilever by providing a cast in-situ closure segment. Continuity between the two structures was finally established by stressing the so-called continuity prestressing tendons.

In order to restrict to a minimum the unbalanced moment that will

occur at the pier during the construction of a double cantilever, segments were added alternately to cantilevers on opposite sides of the pier. Vertical prestressing and suitably placed flat jacks were provided at the pier to resist the unbalanced moment. Once the double cantilever was joined to the rest of the structure and the continuity tendons stressed, the moment resisting part of the support was destroyed by releasing the vertical prestressing tendons at the pier and placing the double cantilever on the bearings. From that time onward, the support functions as a simple support. This operation is termed release of the support.

Segments were erected by making use of a steel launching girder. After the segment to be erected was in position, epoxy was applied to mating surfaces and the segment subsequently post-tensioned to the cantilever. During this erection procedure metal shims were used to correct alignments as needed. This operation is of importance when interpreting the measured vertical deflection of the bridge. In order to insure that adjacent segments match properly, the segments were precast using the short-line method of match-casting.

The casting and erection times of each segment are given in Tables B.3 and B.4, respectively. Each of the precast segments was assumed to have been cured for 2 days, while the in-situ closure segments were cured for 7 days. It should be noted that for the purposes of analysis the actual erection sequence was used for the instrumented double cantilever, SB1. In order to save some computational time, the erection sequences used for the purposes of the analysis of the other double cantilevers were somewhat modified by erecting more segments at fewer time steps than was the case for the actual structure. This step is justified by the relatively great age at which these segments were erected. It should also be mentioned that the modifications to the actual erection sequence were minimal. The actual casting sequence of all the segments was used by the analysis.

The sequence in which the double cantilevers and side-span ends were joined to each other is given in Figure B.3. This figure also gives the

times at which each of the in-situ closure segments was cast as well as the times at which the different sets of continuity tendons were stressed to their final value. It should be mentioned that prior to being stressed to this final value, the continuity tendons were stressed to 40 percent of the final value one day after the closure segment was cast.

For the purposes of the analysis it was assumed that the interior supports were released at the times at which the continuity tendons were stressed. In the actual structure this operation usually took place two days after these tendons were stressed. It was, however, felt that the discrepancy introduced into the calculation of creep strain would be negligible due to the relatively great age of most of the segments by the time this operation was performed. For this very reason it was assumed that the continuity tendons were directly stressed to their final value at the times given in Figure B.3.

It should be noted that both side-span ends were erected on falsework.

B.1.3 Prestressing Details

During the construction of each double cantilever, tendons were provided primarily to resist the negative moments induced by the self-weight of the structure. These tendons were located in the top flange of the beam. Two tendons were provided in the bottom flange to facilitate the erection of segments. The tendons that established continuity of two adjacent cantilevers were primarily located in the bottom flange of the beam in order to provide some measure of positive moment resistance. The locations of the tendons in the top and bottom flanges are indicated by Figure B.2.

All prestressing tendons used in the Kishwaukee River Bridge were 1¼ in. (31.8 mm) diameter Dywidag-Threadbar. Each of these tendons were stressed to 145 kips (645 kN) and anchored at 136 kips (605 kN). All

tendon profiles were straight. The variation of the number of tendons along the bridge is summarized in Figure B.4.

For the construction of a double cantilever the times at which the tendons were stressed were dictated by the erection sequence of the segments. The stressing times of the continuity tendons are summarized in Figure B.3.

For the purposes of analysis a wobble coefficient of 0.0007/ft (0.0023/m) and an anchor-set of 0.01 in. (0.25 mm) was assumed.

B.2 Material Properties of the Concrete

At the time that each of the instrumented segments were cast, thirty-five 6 x 12 in. (150 x 300 mm) concrete cylinders, per segment, were prepared in the precasting plant. These cylinders were steam cured for several hours and then shipped to the P.C.A. laboratories in Skokie, Illinois, for testing. Some of the cylinders were cured in the laboratories under constant environmental conditions at $73^{o}F$ ($23^{o}C$) and 50 percent relative humidity, while others were subjected to the outdoor environment. It was felt that the exposed specimens would be subjected to about the same environmental conditions as the bridge itself. In what follows, a brief description of the concrete material properties as determined by tests on these specimens is given. A more extensive report will be published in the near future.

The variation of the concrete compressive strength and the modulus of elasticity was determined by conducting tests which conform to the ASTM Specification C-39 (56). These properties of the concrete at different ages are summarized in Table B.5.

Shrinkage measurements on both the indoor and outdoor specimens were started 7 days after casting. There were three sets of laboratory stored creep specimens, each set being loaded at a different age. The ages at loading were 28, 90 and 180 days. All the outdoor creep specimens were loaded at an age of 28 days. All creep tests were conducted in

compliance with the ASTM Specification C-512 (55), each specimen being subjected to a constant stress of 2000 psi (13.8 N/mm^2). The experimentally obtained specific creep curves for the different ages at loading as well as the shrinkage curves for all three of the instrumented segments are given in Figures B.5 through B.8 for the laboratory stored specimens, and in Figures B.9 and B.10 for the outdoor specimens.

For the purposes of the analytical procedure followed in this study, the material properties were assumed to be the same for each segment. Thus, the values of compressive strength and modulus of elasticity used in the analysis were obtained by taking the average of the appropriate quantities at each age. The specific creep and shrinkage curves used by the analysis procedure were not obtained by averaging appropriate curves, but rather by selecting curves corresponding to particular segments. The specific creep curves as well as the shrinkage curves used in the analysis are listed in Table B.6.

For the particular case where the recommendations of the C.E.B. (11) were used to generate the material properties of the concrete, the average 28-day compressive strengths for the outdoor specimens were used in the analysis. The creep and shrinkage multiplying factor reflecting the dependence of these phenomena on the composition of the concrete, K_b, deserves some special attention here (see Sect. 2.2.3.1). During the course of the casting of the prefabricated segments the mix proportions of the concrete were changed several times. The water-cement ratio and the cement content used in three different mixes are listed in Table B.7. Each of these combinations yielded a different value for K_b. These values of K_b were then averaged and the result used in the analysis.

Table B.1: Section Properties of Segments in the Double Cantilevers

Segment	Length (in.)	Cross-Sectional Area ($in.^2$)	Moment of Inertia ($in.^4$)	Distance of Top Fiber to Centroidal Axis (in.)	Distance of Bottom Fiber to Centroidal Axis (in.)	Weight (k/ft)
S0 and N0	42.000	13,692	42,115,000	62.762	76.988	14.263
S1 and N1	84.625	13,465	41,297,000	61.758	77.992	14.026
S2 and N2	84.625	13,022	39,537,000	59.650	80.100	13.565
S3 and N3	84.625	12,595	37,607,000	57.408	82.342	13.120
S4 and N4	84.625	12,183	35,502,000	55.031	84.719	12.691
S5 and N5	84.625	11,787	33,216,000	52.521	87.229	12.278
S6 through S16 N6 through N16	84.625	11,595	32,005,000	51.216	88.534	12.078
S17 and N17	28.625	11,595	32,005,000	51.216	88.534	12.078
Closure Segment	150.750	14,845	45,510,000	67.150	72.600	15.464

Note: 1 in. = 25.4 mm

1 k/ft = 14.594 kN/m

Table B.2: Section Properties of Segments in the Side-Span Ends

Segment	Length (in.)	Cross-Sectional Area ($in.^2$)	Moment of Inertia ($in.^4$)	Distance of Top Fiber to Centroidal Axis (in.)	Distance of Bottom Fiber to Centroidal Axis (in.)	Weight (k/ft)
S0 and N0	36.000	11,595	32,005,000	51.216	88.534	12.078
S1 through S4 N1 through N4	90.000	11,595	32,005,000	51.216	88.534	12.078
S5 and N5	51.313	11,595	32,005,000	51.216	88.534	12.078

Note: 1 in. = 25.4 mm

1 k/ft = 14.594 kN/m

Table B.3: Casting Times of the Segments
Days after 6 August 1977

Segment	Double Cantilever				Side-Span Ends SB0 and SB5
	SB1	SB2	SB3	SB4	
S17	446	298	244	189	-
S16	445	294	243	187	-
S15	444	293	242	185	-
S14	441	292	241	181	-
S13	440	290	238	179	-
S12	439	290	237	173	-
S11	438	287	236	164	-
S10	437	287	235	161	-
S9	434	285	230	154	-
S8	433	284	229	152	-
S7	432	283	228	147	-
S6	432	280	227	138	-
S5	370	279	224	133	70
S4	369	278	223	130	67
S3	368	277	222	122	62
S2	367	276	221	119	60
S1	364	272	220	116	55
S0	322	7	19	22	42
N0	311	1	11	14	319
N1	339	248	193	76	322
N2	341	249	195	82	326
N3	342	250	196	85	327
N4	343	251	199	88	328
N5	346	252	201	90	322
N6	347	255	202	91	-
N7	348	256	203	94	-
N8	349	256	206	95	-
N9	350	258	207	96	-
N10	353	259	208	97	-
N11	355	262	209	98	-
N12	355	263	210	101	-
N13	356	264	213	102	-
N14	357	265	214	103	-
N15	360	266	215	104	-
N16	361	269	216	105	-
N17	362	270	217	110	-

Note: Day 1 corresponds to the day on which the first segment was cast.

Table B.4: Erection Times of the Segments
Days after 6 August 1977

Segment	Double Cantilevers				Side-Span Ends SB0 and SB5
	SB1	SB2	SB3	SB4	
S17	458	437	412	362	-
S16	458	437	412	361	-
S15	455	437	411	361	-
S14	455	435	411	360	-
S13	455	434	411	360	-
S12	454	434	410	357	-
S11	454	434	410	357	-
S10	454	433	409	356	-
S9	453	433	409	356	-
S8	453	432	406	355	-
S7	453	432	406	354	-
S6	453	432	406	354	-
S5	452	431	402	353	94
S4	452	431	402	353	91
S3	452	431	399	349	91
S2	451	430	398	348	91
S1	449	428	397	347	90
S0	448	427	392	340	63
N0	448	427	396	341	468
N1	449	428	397	346	615
N2	451	430	398	348	615
N3	451	430	399	349	615
N4	452	431	399	350	615
N5	452	431	402	353	615
N6	452	432	402	353	-
N7	453	432	406	354	-
N8	453	432	406	354	-
N9	453	432	409	355	-
N10	454	433	409	356	-
N11	454	433	410	356	-
N12	454	434	410	357	-
N13	454	434	410	360	-
N14	455	434	411	360	-
N15	455	435	411	361	-
N16	458	437	412	361	-
N17	458	437	412	362	-

Note: Day 1 corresponds to the day on which the first segment was cast.

Table B.5: Compressive Strength and Modulus of Elasticity of Concrete

Segment	Curing Environment	Age (Days)	Compressive Strength (psi)	Modulus of Elasticity (ksi)
SB1-N1	Controlled	28	5680	4320
		180	6240	4490
	Outdoor	28	5750	4200
		180	6460	4530
SB1-N9	Controlled	28	6190	4470
		90	6070	4630
		180	6450	4760
	Outdoor	28	6080	4620
		90	6510	4720
		180	6450	4580
SB1-N16	Controlled	28	5740	4420
		90	6130	4750
		180	6290	4410
	Outdoor	28	4670	4190
		180	6200	4240

Note: 1 ksi = 6.895 N/mm^2

1 ksi = 1000 psi

Table B.6: Specific Creep and Shrinkage Curves Used in the Analyses

Curing Environment	Specific Creep Age at Loading (Days)			Shrinkage
	28	90	180	
Controlled	SB1-N1	SB1-N9	SB1-N1	SB1-N1
Outdoor	SB1-N1	-	-	SB1-N1

Table B.7: Cement Content and Water-Cement Ratios for Different Concrete Mixes

Cement Content (lbs/yd^3)	Water-Cement Ratio
658	0.46
658	0.44
705	0.44

Note: 1 lb/yd^3 = 0.593 kg/m^3

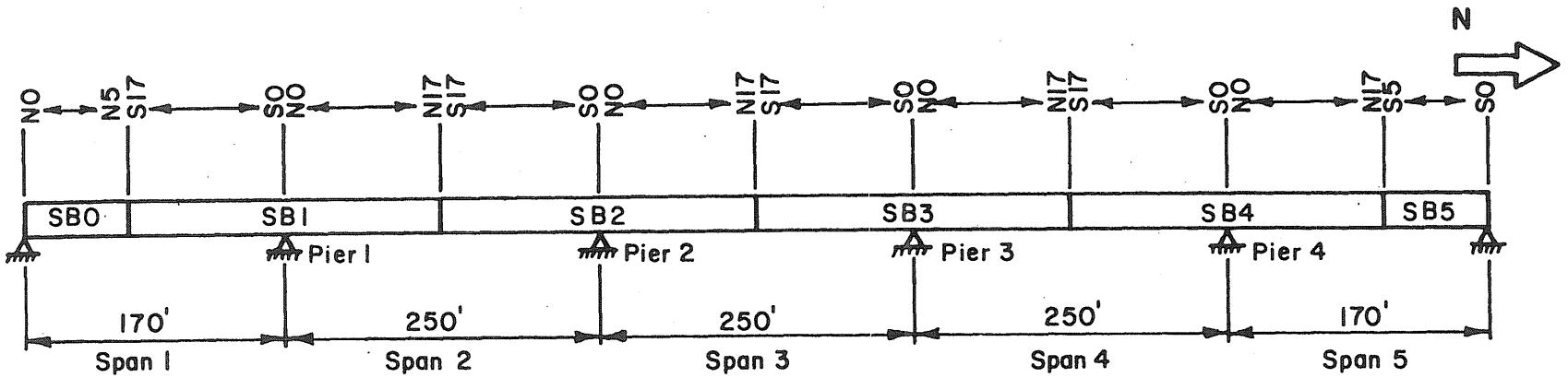

(a) Elevation

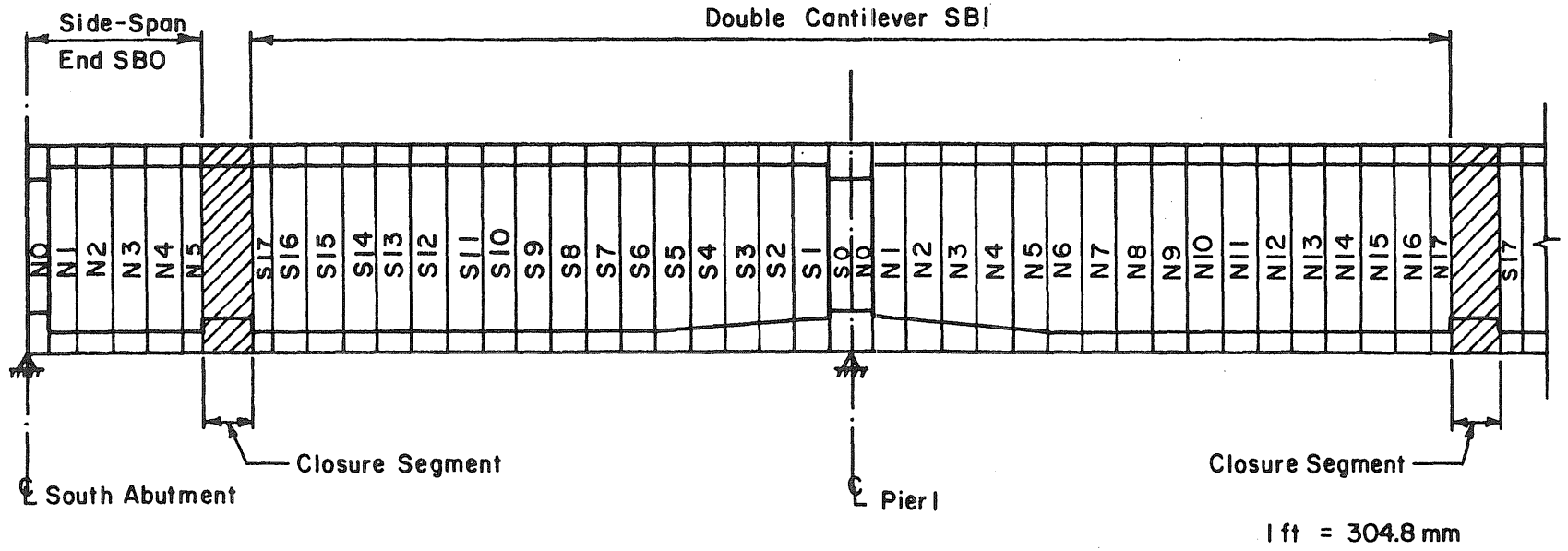

(b) Longitudinal Section

Fig. B.1 Elevation and Designation of the Various Segments of the Kishwaukee River Bridge

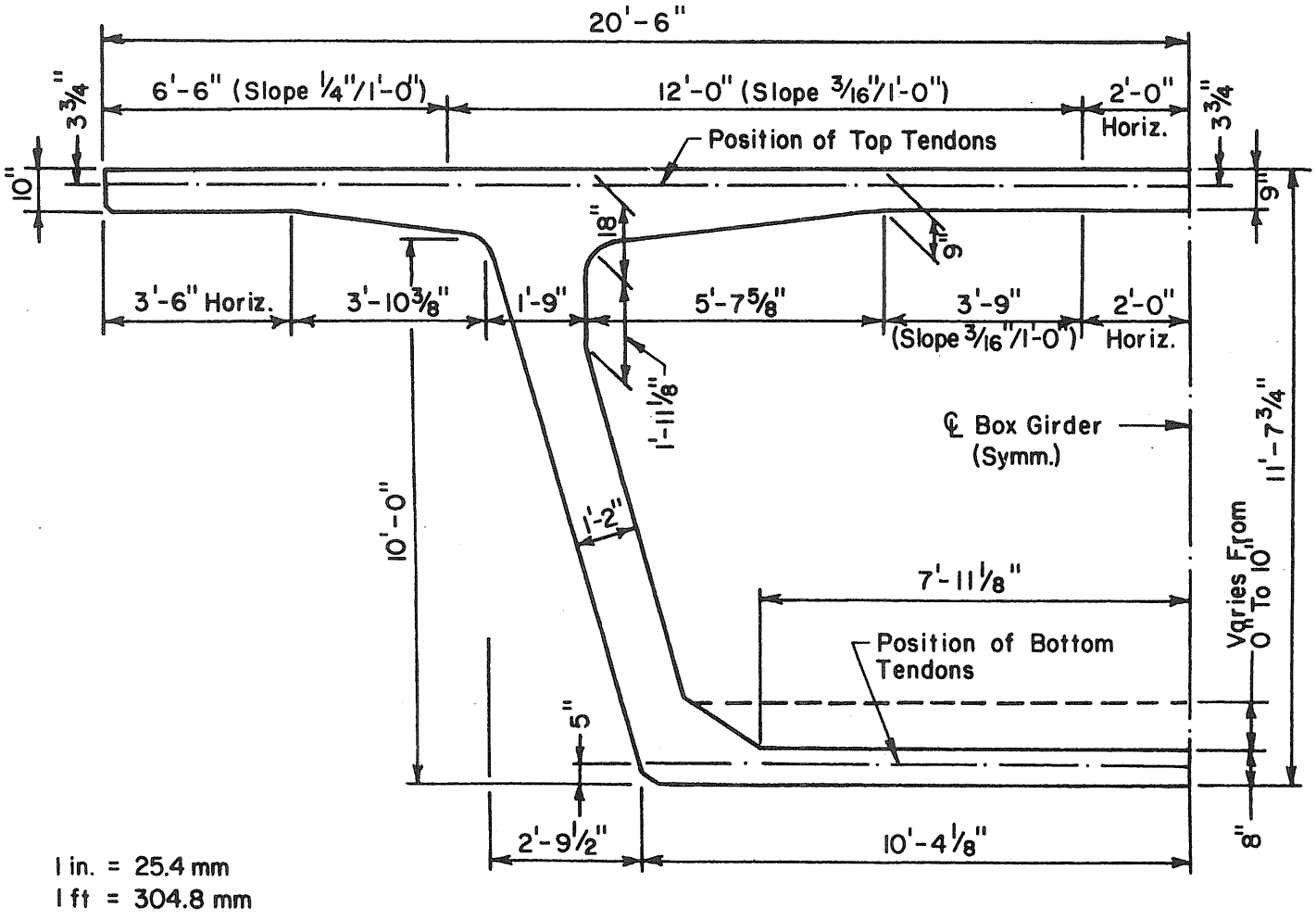

Fig. B.2 Cross-Section of a Typical Segment

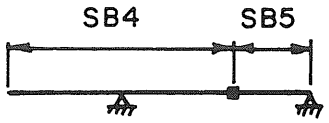

(a) Intermediate Structure 6

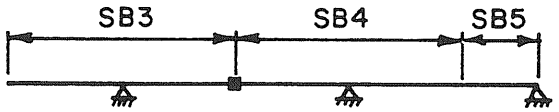

(b) Intermediate Structure 7

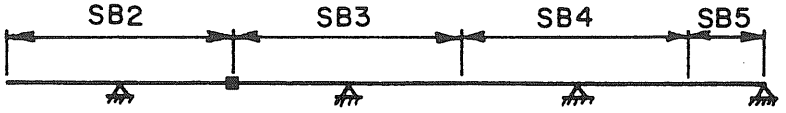

(c) Intermediate Structure 8

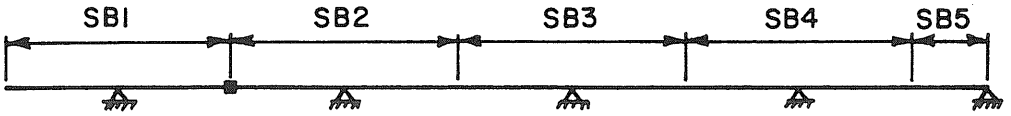

(d) Intermediate Structure 9

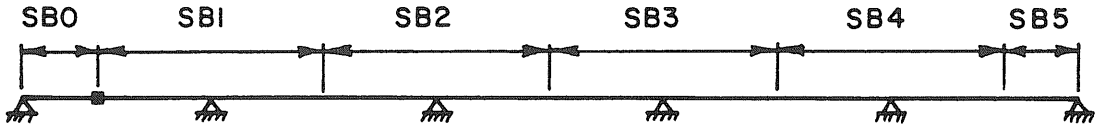

(e) Final Structure

Substructure	Time At Which Closure Segment Is Cast	Time At Which Continuity Tendons Are Stressed
6	382	387
7	419	424
8	441	446
9	462	467
10	629	634

Note : Times Are In Days Since 6 Aug. 1977

Fig. B.3 Sequence in which Double Cantilevers were Joined to Form Final Structure

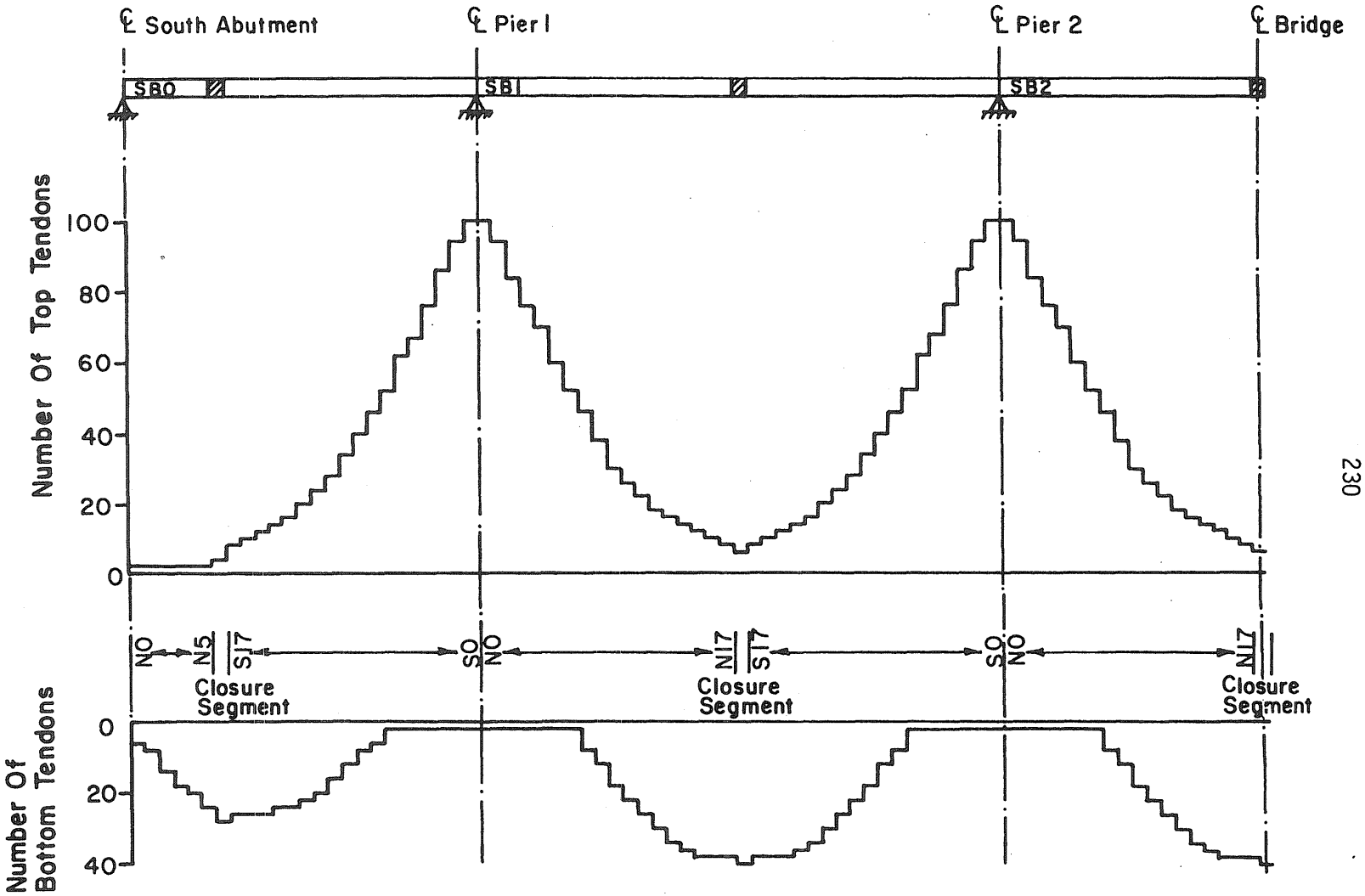

Fig. B.4 Distribution of Prestressing Tendons along the Bridge

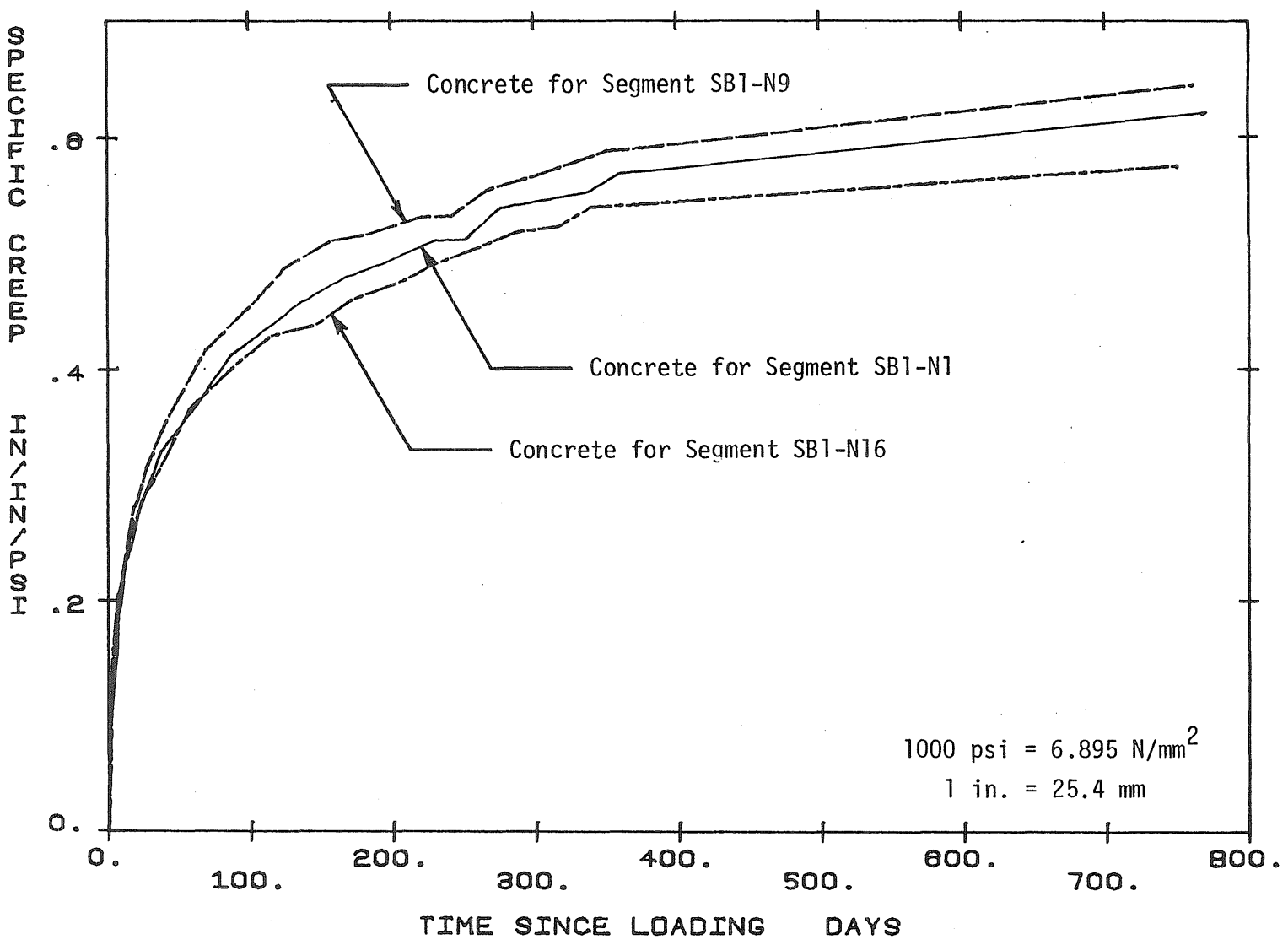

Fig. B.5 Specific Creep Curves for Laboratory Stored Specimens Loaded at an Age of 28 Days

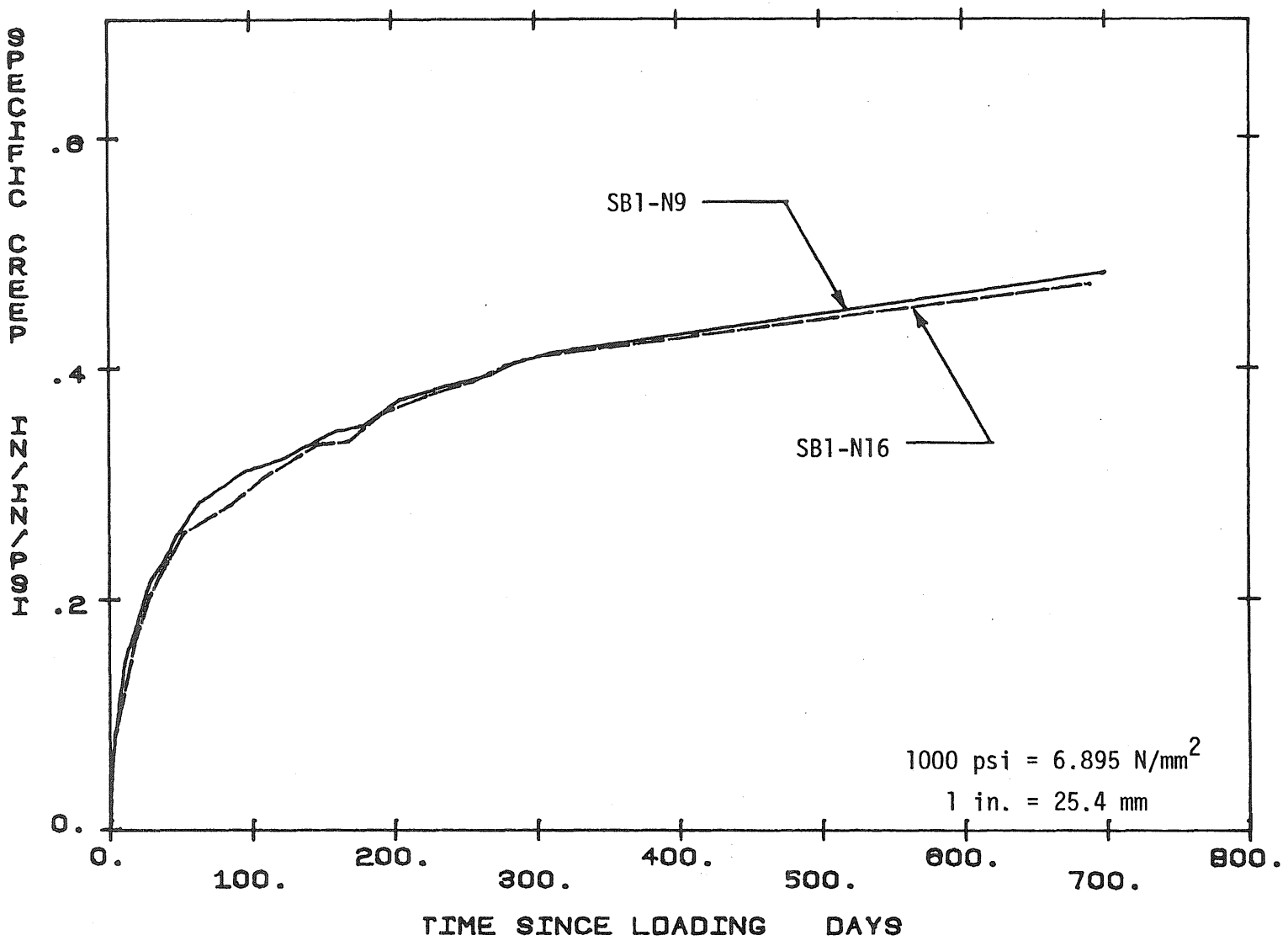

Fig. B.6 Specific Creep Curves for Laboratory Stored Specimens Loaded at an Age of 90 Days

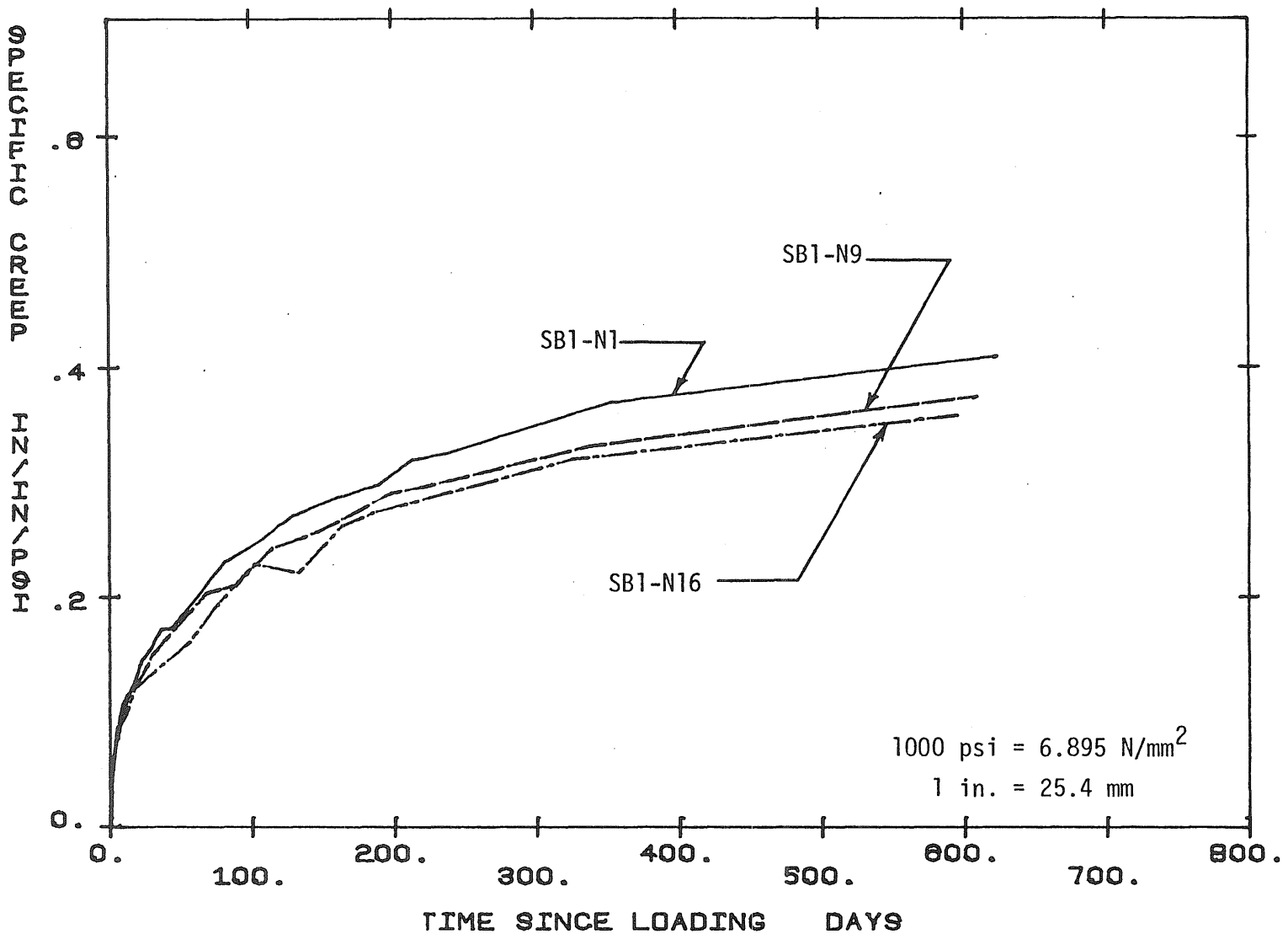

Fig. B.7 Specific Creep Curves for Laboratory Stored Specimens Loaded at an Age of 180 Days

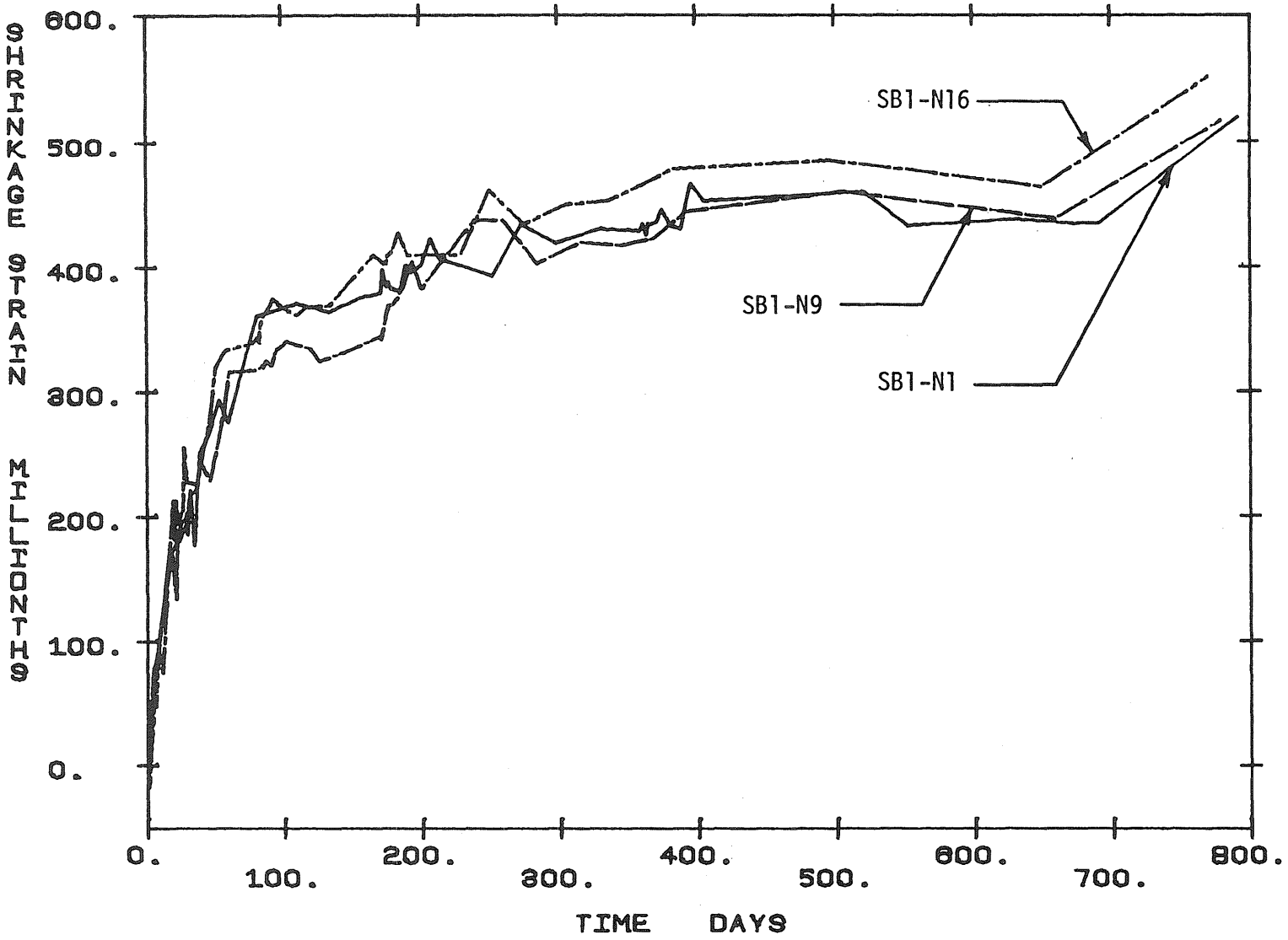

Fig. B.8 Shrinkage Curves for Laboratory Stored Specimens

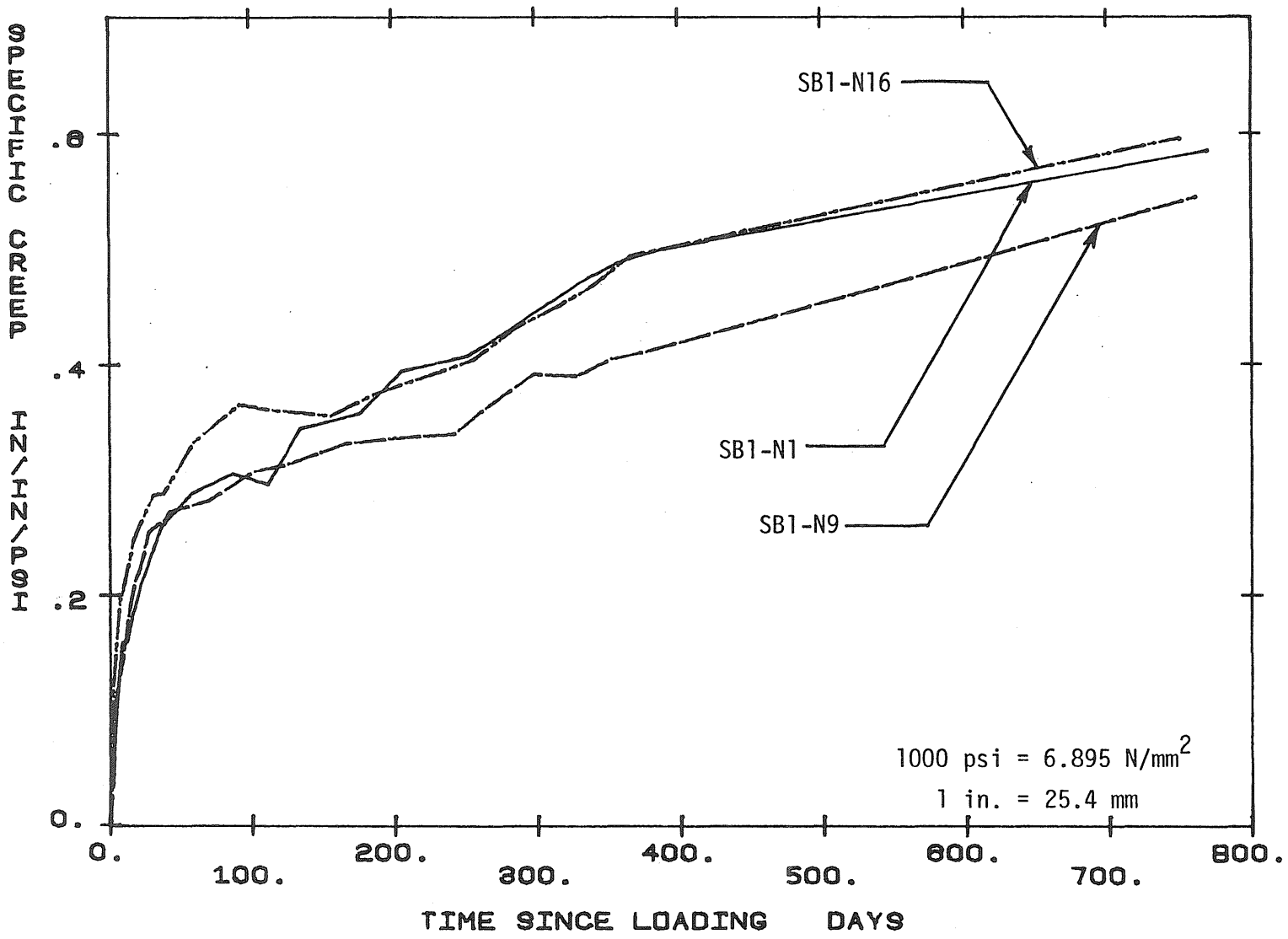

Fig. B.9 Specific Creep Curves for Outdoor Stored Specimens Loaded at an Age of 28 Days

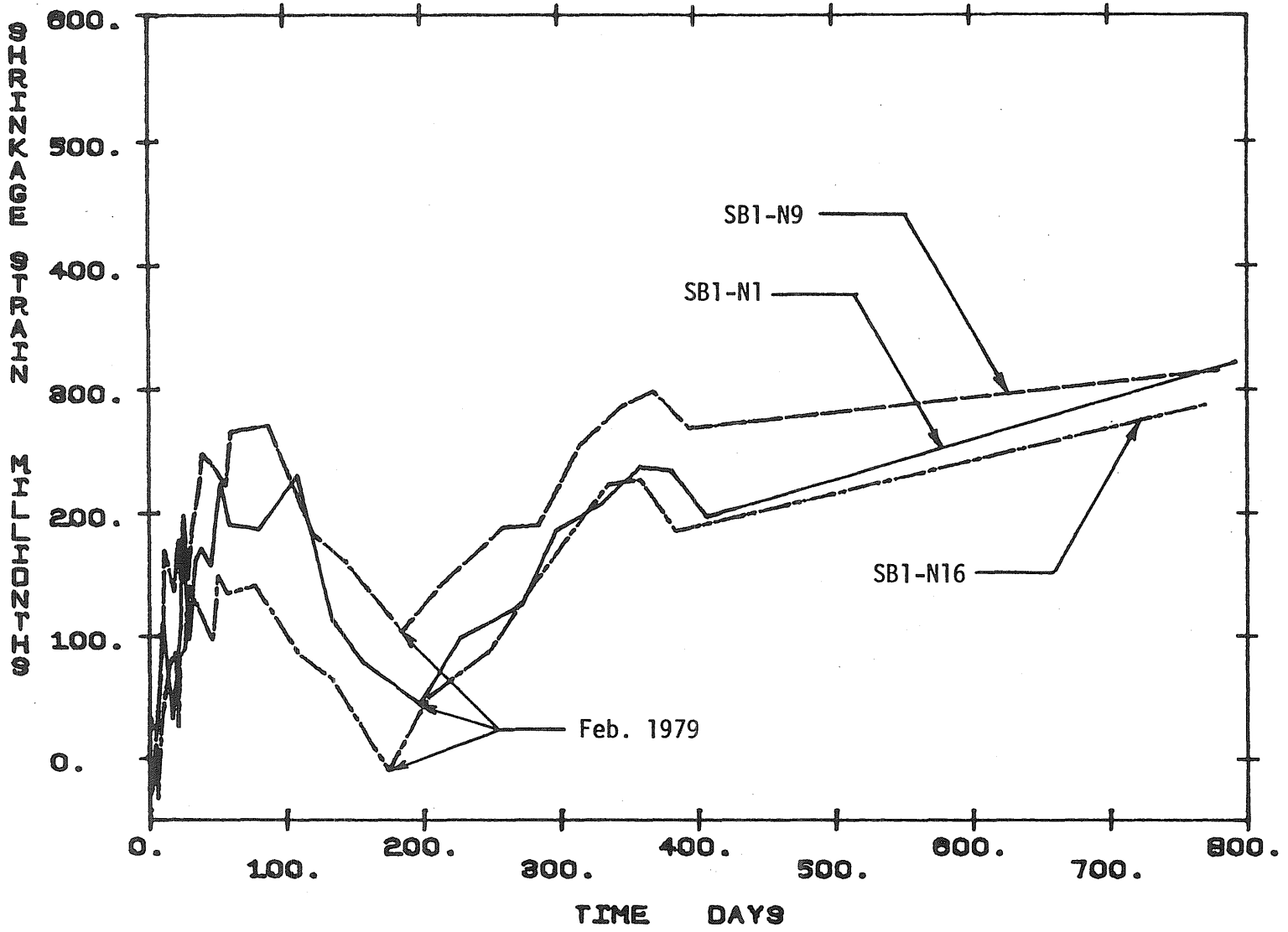

Fig. B.10 Shrinkage Curves for Outdoor Stored Specimens

APPENDIX C

NOTATION

The symbols used throughout this study are defined as they first appear. For convenience they are summarized in what follows:

$a_i(\tau)$	=	aging parameters, for use with the Dirichlet series representation of specific creep
A	=	coefficient used in the expression for K_d, as given in Appendix A, Sect. A.1.1
A_c	=	cross-sectional area of the concrete section
A_i	=	cross-sectional area of tendon i
b	=	distance over which anchor-set affects the prestressing force, measured from the jacking end
B	=	coefficient used in the expression for K_d, as given in Appendix A, Sect. A.1.1
c	=	relaxation constant, depending on the type of prestressing strand
$C_i(t)$	=	specific creep at time t, for concrete loaded at age t_i
$C_r(t_i)$	=	specific creep at time t_i, for concrete initially loaded at age τ_r
$C_\tau(t)$	=	specific creep at time t, for concrete initially loaded at age τ
d_m	=	theoretical thickness of member, as defined by the C.E.B. recommendations
D	=	degree of hardening of the concrete at the time of loading

e_i = eccentricity of tendon i measured from the centroidal axis of the section, taken positive when the tendon is below the centroidal axis, and negative when above

E_{b28} = secant modulus of elasticity of the concrete at an age of 28 days

E_c, $E_c(t)$ = modulus of elasticity of the concrete at time t

$E'_c(t)$ = effective modulus of the concrete at time t, as defined in Sect. 3.2.1

E_s = modulus of elasticity of the steel

f_c = constant sustained concrete stress

$f_c(t)$ = concrete stress as a function of time

f_i, $f(t_i)$ = concrete stress at time t_i

$f_{c_{top}}$ = concrete stress in extreme top fiber of cross-section

$f_{c_{bot}}$ = concrete stress in extreme bottom fiber of cross-section

$f'_c(t)$ = cylinder compressive strength of concrete as a function of time since casting

$f_s(t)$ = steel stress at time t

f_{si} = initial steel stress

f_{so} = steel stress at the jacking end, just prior to anchoring of the tendon

$f_s(x)$ = steel stress at a distance x from the jacking end, just prior to anchoring of the tendon

f_y = yield stress of steel, measured at an offset strain of 0.001

[F] = flexibility matrix, as defined in Appendix A, Sect. A.5

I_c = moment of inertia of the concrete section about the centroidal axis

k = wobble friction coefficient, per unit length

K_b = factor expressing the dependence of creep and shrinkage on the composition of the concrete mix, defined in Sect. 2.2.3.1

K_c = factor expressing the dependence of creep on relative humidity, defined in Sect. 2.2.3.1

K_d = factor expressing the dependence of creep on the concrete age at the time of loading, defined in Sect. 2.2.3.1

K_e = factor expressing the dependence of creep and shrinkage on the member size and shape, defined in Sect. 2.2.3.1 and Sect. 2.2.3.2

K_p = factor including the restraining effect of the longitudinal reinforcement on shrinkage, defined in Sect. 2.2.3.2

K_t = factor expressing the time dependence of creep and shrinkage, defined in Sect. 2.2.3.1

$[K_c]$ = stiffness matrix for the concrete cross-section, associated with the axial strain and curvature of the section

$[K_s]$ = stiffness matrix for the prestressing steel, associated with the axial strain and curvature of the section

ln = natural or Napierian logarithm

log = logarithm to the base 10

L = tendon length

M_c = resultant moment of the concrete force about the section centroid necessary to restore compatibility of steel and concrete strains when a strain is imposed on the cross-section

M_s = resultant moment of the steel forces about the section centroid necessary to restore compatibility of steel and concrete strains when a strain is imposed on the cross-section

n = E_s/E_c, modular ratio; also used as a coefficient in the expression for K_d, as given in Appendix A, Sect. A.1.1

p = percentage longitudinal steel

P_c = resultant concrete force necessary to restore compatibility of steel and concrete strains when a strain is imposed on the cross-section

P_s = resultant steel force necessary to restore compatibility of steel and concrete strains when a strain is imposed on the cross-section

P_{si} = change in force in the i-th tendon due to the effects of elastic recovery

R = ratio of specific creep recovery to specific creep

R_i = vertical reaction at support i of an intermediate structure

$\{R\}$ = column vector containing the reactions at the interior supports of a statically indeterminate intermediate structure

t, t_i = time

T = temperature

x = distance from the jacking end to the point on the tendon being considered

y_b = distance of the section centroid to the extreme bottom fiber of the section

y_t = distance of the section centroid to the extreme top fiber of the section

α = coefficient used in the expression for K_t, as given in Appendix A, Sect. A.1.1; elsewhere it represents the total angular change of the tendon profile between the jacking end and any point x along the span, in radians

β = coefficient used in the expression for K_t, as given in Appendix A, Sect. A.1.1

δ_{ij} = deflection of the equivalent statically determinate structure, as defined in Appendix A, Sect. A.5, at the location of support i due to a unit point load applied at the location of support j

Δ = anchor set

Δ_i = deflection of the equivalent statically determinate structure, as defined in Appendix A, Sect. A.5, at the location of support i due to the effects of applied loads or time-dependent effects

Δ_t = number of days at which hardening of the concrete took place at T°C

$\{\Delta\}$ = column vector containing the Δ_i's which apply to the interior supports of a statically indeterminate intermediate structure

Δf_{ci}, $\Delta f(t_i)$ = change in concrete stress at time t_i

Δf_s = change in steel stress due to causes other than relaxation

$\Delta\varepsilon$ = imposed axial strain on concrete cross-section, defined in Appendix A, Sect. A.2

$\Delta\varepsilon_b$ = imposed strain in extreme bottom fiber of concrete cross-section, defined in Appendix A, Sect. A.2

$\Delta\varepsilon_{cr}(\Delta t_m)$ = change of creep strain during the m-th time interval

$\Delta\varepsilon_t$ = imposed strain in extreme top fiber of concrete cross-section, defined in Appendix A, Sect. A.2

$\Delta\phi$ = imposed curvature of concrete cross-section, defined in Appendix A, Sect. A.2

ε = instantaneous elastic strain

ε_c = basic shrinkage strain as a function of relative humidity, defined in Sect. 2.2.3.2; also used as axial strain of the concrete section as defined in Appendix A, Sect. A.2

ε_{cb}, ε_{ct} = concrete strains involved in the calculation of the effects of elastic recovery, defined in Appendix A, Sect. A.2

ε_{cr}, $\varepsilon_{cr}(t)$ = total creep strain at time t

ε_s = strain associated with the steel, at the centroid of the section, defined in Appendix A, Sect. A.2

ε_{sb}, ε_{st} = hypothetical steel strains involved in the calculation of the effects of elastic recovery, defined in Appendix A, Sect. A.2

ε_{sh} = shrinkage strain at time t

ε'_{cb} = concrete strain in the extreme bottom fiber corrected for the effects of elastic recovery

ε'_{ct} = concrete strain in the extreme top fiber corrected for the effects of elastic recovery

λ_i = retardation times, for use with the Dirichlet series representation of specific creep

μ = curvature friction coefficient

ξ = creep coefficient independent of time and concrete age at loading, defined in Appendix A, Sect. A.1.2

τ = concrete age at loading

τ_i = concrete age at loading corresponding to the i-th specific creep curve

$\phi(T)$ = temperature shift function, for use with the Dirichlet series representation of specific creep

ϕ_c = curvature of concrete section as defined in Appendix A, Sect. A.2

ϕ_s = curvature associated with the steel strain as defined in Appendix A, Sect. A.2

ϕ_t = creep coefficient, expressed as the product of five partial factors